Iranian National Institute for Oceanography and Atmospheric Science

United Nations Educational, Scientific and Cultural Organization

Intergovernmental Oceanographic Commission

Proceedings

Volume 2

RCOWA

2nd International Conference on Oceanography for West Asia 2020

دومین کنفرانس بین المللی اقیانوس شناسی غرب آسیا

16 - 17 Sep. 2020 ۲۶ و ۲۷ شهریور ۱۳۹۹

بسم الله الرحمن الرحیم

Dear colleagues, experts, and students

With the development and spread of scientific publications and documentaries, mass media, and virtual space, today's world increasingly realizes the importance of the sea and the ocean in human life. Even though the oceans play a role in all aspects of life, from the air we breathe to the food production, we know very little about the oceans, and most of our knowledge of the seas is limited to shallow waters.

For exploration in marine and oceanic sciences, we need to organize and plan, including detailed observations and documentation from biological, chemical, physical, geological, and other aspects. Therefore, research in these areas needs to provide the necessary information and database for sustainable resource management and blue economy development.

Our region West Asia, as the cradle of civilizations, enjoys a long history of maritime in the North West Indian Ocean and connected seas. The region encompasses states that many of them are emerging as marine nations.

Several marine-related associations are active in the Indian Ocean, such as IOARA, RCOWA, and ROPME. The Regional Education and Research Center on Oceanography for West Asia has been operating as a UNESCO Category II Center alongside the Iranian National Institute for Oceanography and Atmospheric Science since 2015. Its activities focused on realizing a role in line with global trends in marine and oceanic sciences and promoting oceanography in Iran and neighboring countries in the Persian Gulf, the Oman Sea, and the North Indian Ocean. Another mission of the center is to draw people and managers' attention to the marine environment and anthropogenic changes in the marine ecosystem.

The mentioned conference was an important scientific event that the RCOWA has been planning for about two years, with the Governing Board's approval. It scheduled to take place on June 8-9, 2020 coinciding with World Ocean Day. But with the COVID19 pandemic and its continuation a few weeks before the mentioned time, we postponed it, hoping for the pandemic ending in September. The situation became such that it was neither possible to hold as regular, nor to wait for it again. So we decided to have it as a web conference. Accordingly, we decided to make the conference more fruitful in scientific and educational impact by conducting four workshops on the four oceanic subjects: coral reefs, Ocean pollution and microplastics, climate change, and tsunami early warning system. As a new initiative, we uploaded the video of the presentations on the exclusive channel in the most famous Iranian video sharing system "apparat". It makes them accessible forever.

We all know the positives and negatives of web conferences: personal and face-to-face communication between experts is weaker in this situation. Internet systems fluctuate due to the heavy traffic caused by schools and universities in the current times. Some attendees may not yet be sufficiently adapted to the online presentation, and so on. The advantages of this method must be mentioned, such as the possibility of more people attending the conference from different parts of the country and the world. Also, avoiding human dangers and environmental consequences that trips create, reducing costs, and perhaps the convenience of attending the conference when we are sitting comfortably at home.

I hope that the Second Conference on Oceanography for West Asia, which was one of our initial but essential experiences in holding an online scientific meeting, achieved expected goals, and more and less fulfilled the audience's expectations. In this conference, we had more than one hundred scientific research results in different branches of oceanography. Conference attendees from more than 12 countries were online. The lectures were divided into seven thematic sections, each of which was divided into three specialized panels. Sections began with a keynote speech with presenters often from outside Iran. Each panel was managed online by a scientist inside the institute and another colleague outside.

We are at the beginning of the ocean decade realized by UNESCO/IOC. I wish the two-day conference was a step forward for learning the ocean decade goals and having a healthy ocean.

In the end, I think I have to express my respect to all pioneers of oceanography in I.R. of Iran, cherish the memory of Professors B. Mokhayer, and H. Zomorodian, the founder and first director of our institute.

All the best

B. Abtahi

Prof. in Marine Ecology SBU, INIOAS

Proceedings

RCOWA

2nd International Conference on Oceanography for West Asia 2020

Conference Organization Chart

Second International Conference on Oceanography for West Asia

Chair	Prof. Behrooz Abtahi
Scientific Secretary	Dr. Hamid Alizadeh Lahijani
Executive Secretary	Dr. Mohammad Hossein Kazeminezhad
Head of Scientific Secretariat	Dr. Gholamreza Mohammadpour
Public Affairs	Dr. Babak Moradi

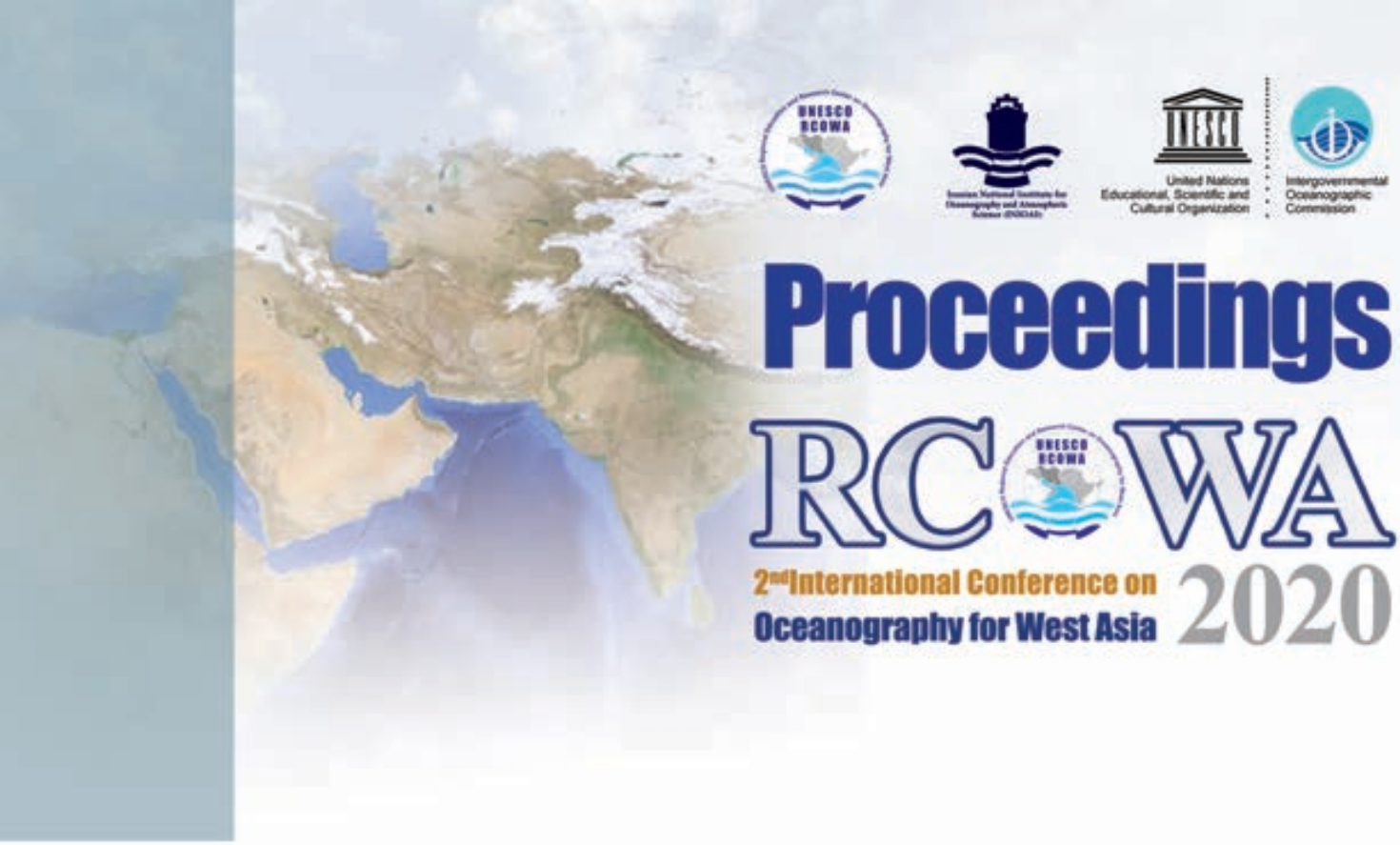

Proceedings

RCOWA 2020

2nd International Conference on Oceanography for West Asia

Scientific Committees

Second International Conference on Oceanography for West Asia

Marine Meteorology, Physical and Satellite Oceanography, Climate Change

Tarbiat Modarres University	Dr. Akbar Rashidi Ebrahim Hesari
IR. of Iran Meteorological Organization	Dr. Behzad Layeghi
Iranian National Intstitute for Oceanography and Atmospheric Science	Dr. Parvin Ghafarian
University of Shahrekord	Dr. Hassan Khaleghi Zavareh
University of Tehran	Dr. Seyed Peyman Badiei
Iran University of Science and Technology (IUST)	Dr. Seyed Mostafa Siadat Mousavi
University of Tehran	Dr. Abbasali Aliakbari Bidokhti
Iranian National Institute for Oceanography and Atmospheric Science	Dr. Keivan Kabiri
IR. of Iran Meteorological Organization	Dr. Majid Azadi
University of Hormozgan	Dr. Mohammad Mehdizadeh
IR. of Iran Meteorological Organization	Dr. Mohammadtaghi Zamanian
University of Tehran	Dr. Masoud Sadrinasab
Iranian National Institute for Oceanography and Atmospheric Science	Dr. Masoud Moradi
University of Guilan	Dr. Mirahmad Lasht Neshaei
Iranian National Institute for Oceanography and Atmospheric Science	Dr. Siamak Jamshidi
Iranian National Institute for Oceanography and Atmospheric Science	Dr. Nafiseh Pegahfar
Iranian National Institute for Oceanography and Atmospheric Science	Dr. Samad Hamzei
Iranian National Institute for Oceanography and Atmospheric Science	Dr. Hossein Farjami
Iranian National Institute for Oceanography and Atmospheric Science	Dr. Jafar Azizpour
Khajeh Nasir Toosi University	Dr. Mohammadreza Mobasheri
Iranian National Institute for Oceanography and Atmospheric Science	Dr. Gholamreza Mohammadpour
HormozganUniversity	Dr. Mohamad Mahdizadeh

Proceedings

RCOWA

2nd International Conference on Oceanography for West Asia 2020

Scientific Committees

Second International Conference on Oceanography for West Asia

Coastal and offshore engineering, Marine hazards

Sahand University	Dr. Ahmadreza Mostafa Gharebaghi
University of Tehran	Dr. Afshin Danehkar
Iranian National Institute for Oceanography and Atmospheric Science	Dr Mohammad Hossein Kazeminezhad
Sharif University of Technology	Dr. Mohammad Said Seif
Chabahar Maritime and Marine University	Dr. Mahmood Nasiri
Iranian National Institute for Oceanography and Atmospheric Science	Dr. Mahmoodreza Akbarpour Jannat
Amirkabir University of Technology	Dr. Mahdi Iranmanesh
University of Tehran	Dr. Naser Hadjizadeh Zaker
University of Science and Technology	Dr. Naser Shabakhti
Iranian National Institute for Oceanography and Atmospheric Science	Dr. Vahid Chegini
Iran University of Science and Technology	Dr. Abbas Bakhtiyari Yeganeh
University of Tehran	Dr. Masoud Montazeri Namin
Iranian National Institute for Oceanography and Atmospheric Science	Dr. Ali Khoshkholgh
Aalborg University, Denmark	Dr. Babak Bani Jamali
Iranian National Institute for Oceanography and Atmospheric Science	Dr. Masoud Mahmoodof

Proceedings

RCOWA 2020

2nd International Conference on Oceanography for West Asia

Scientific Committees

Second International Conference on Oceanography for West Asia

Marine Biology and Fisheries

Khorramshahr University of Marine Science and Technology	Dr. Ahmad Savari
University of Tehran	Dr. Arash Javanshir Khoei
Iranian National Institute for Oceanography and Atmospheric Science	Dr. Behrooz Abtahi
Caspian Sea Ecology Research Center	Dr. Hassan Nasrolladzadeh Saravi
Agricultural Research, Education and Extension Organization	Dr. Seyed Aminollah Taghavai Motlagh
Tarbiat Modarres University	Dr. Seyed Jafar Seifabadi Mokhtari
Kharazmi University	Dr. Shahrbanoo Oryan
Iranian National Institute for Oceanography and Atmospheric Science	Dr. Abdolvahab Maghsoudlou
University of Tehran	Dr. Ali Naderloo
Shahid Beheshti University	Dr. Ali Nasrollahi
University of Tehran	Dr. Alireza Sari
Shahid Beheshti University	Dr. Mohammadreza Shokri
Iranian Fisheries Science Research Institute	Dr. Mahmood Bahmani
University of Hormozgan	Dr. Morteza Yousefzadi
Urmia University	Dr. Nasser Agh
Iranian National Institute for Oceanography and Atmospheric Science	Dr. Hoda Khaledi
Iranian National Institute for Oceanography and Atmospheric Science	Dr. Farzaneh Momtazi
Iranian National Institute for Oceanography and Atmospheric Science	Dr. Ahmad Manbouhi

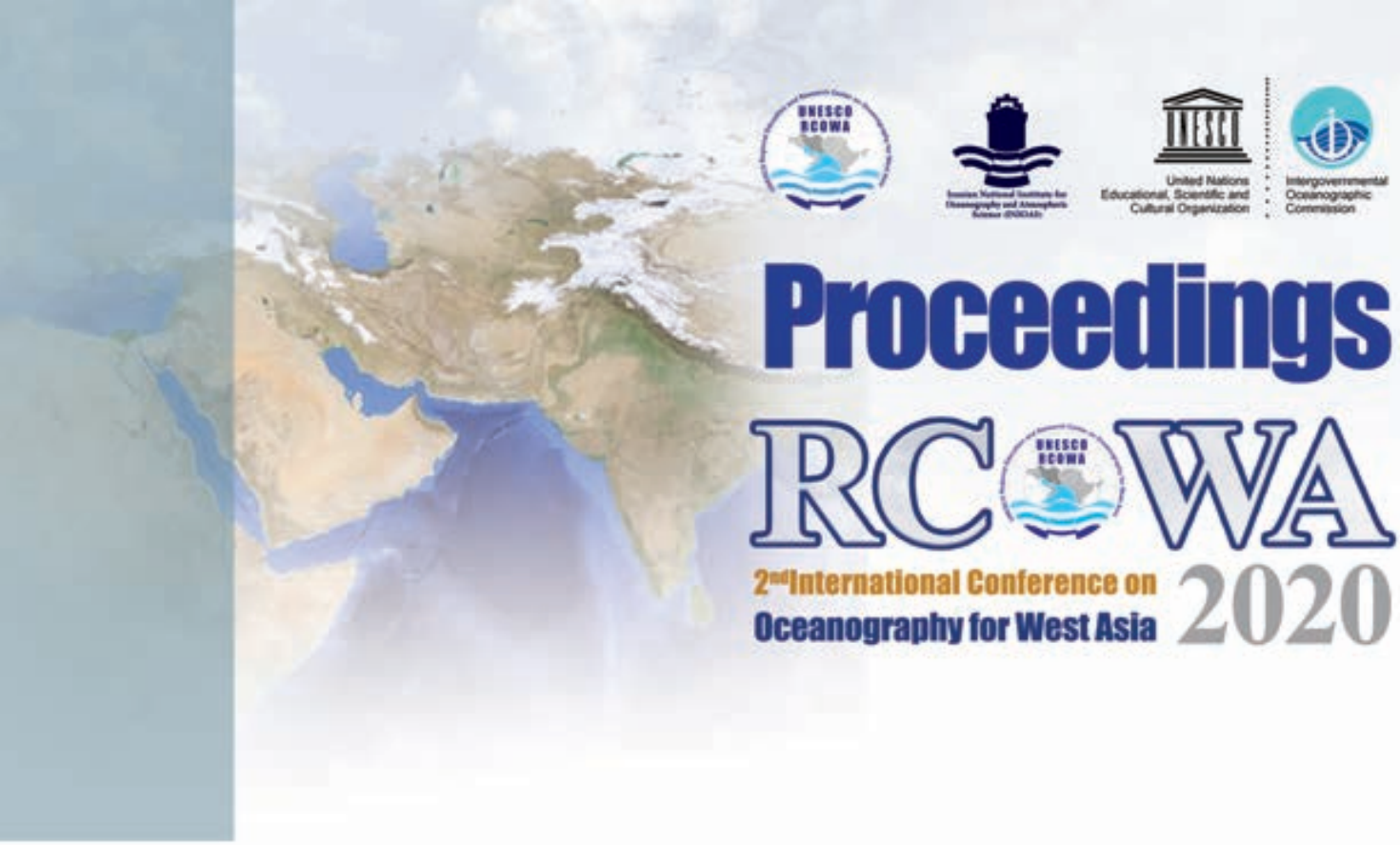

Scientific Committees

Second International Conference on Oceanography for West Asia

Chemical and Biogeochemical Oceanography, Marine Pollutions

Iranian National Institute for Oceanography and Atmospheric Science	Dr. Abolfazl Saleh
Institute of Geophysics, University of Tehran	Dr. Omid Alizadeh Chubari
Tarbiat Modarres University	Dr. Hassan Zareh Mayvan
Iranian National Institute for Oceanography and Atmospheric Science	Dr. Hamid Alizadeh K. Lahijani
Iranian National Institute for Oceanography and Atmospheric Science	Dr. Ali Mehdinia
Tarbiat Modarres University	Dr. Alireza Riyahi Bakhtiyari
Iranian National Institute for Oceanography and Atmospheric Science	Dr. Homeira Agah
Iranian National Institute for Oceanography and Atmospheric Science	Dr. Maryam Ghaemi
Iranian Fisheries Science Research Institute ,	Dr. Nima Poorang
Geological Survey and Mineral Exploration of Iran	Dr. Raziyeh Lak
Iranian National Institute for Oceanography and Atmospheric Science	Dr. Hamid Ershadifar
Iranian National Institute for Oceanography and Atmospheric Science	Dr. Abdolmajid Naderi
Iranian National Institute for Oceanography and Atmospheric Science	Dr. Hadi Gerivani
Iranian National Institute for Oceanography and Atmospheric Science	Dr. Mehri Seyeh Hashroudi

Proceedings

RCOWA 2020

2nd International Conference on Oceanography for West Asia

Scientific Committees

Second International Conference on Oceanography for West Asia

Ocean Policy, Ocean Literacy

University of Tehran	Dr. Ahmad Momeni Rad
Persian Gulf University	Dr. Parviz Bavarsad
Iranian National Institute for Oceanography and Atmospheric Science	Dr. Hamid Alizadeh K. Lahijani
University of Tehran	Dr. Mehdi Soltani

Proceedings

RCOWA

2nd International Conference on Oceanography for West Asia 2020

Scientific Committees

Second International Conference on Oceanography for West Asia

Ocean-Atmosphere Metadata

Shahid Beheshti University

Iranian National Institute for Oceanography and Atmospheric Science

Dr. Seyed Mohammad Sadegh Movahed

Dr. Parvin Ghafarian

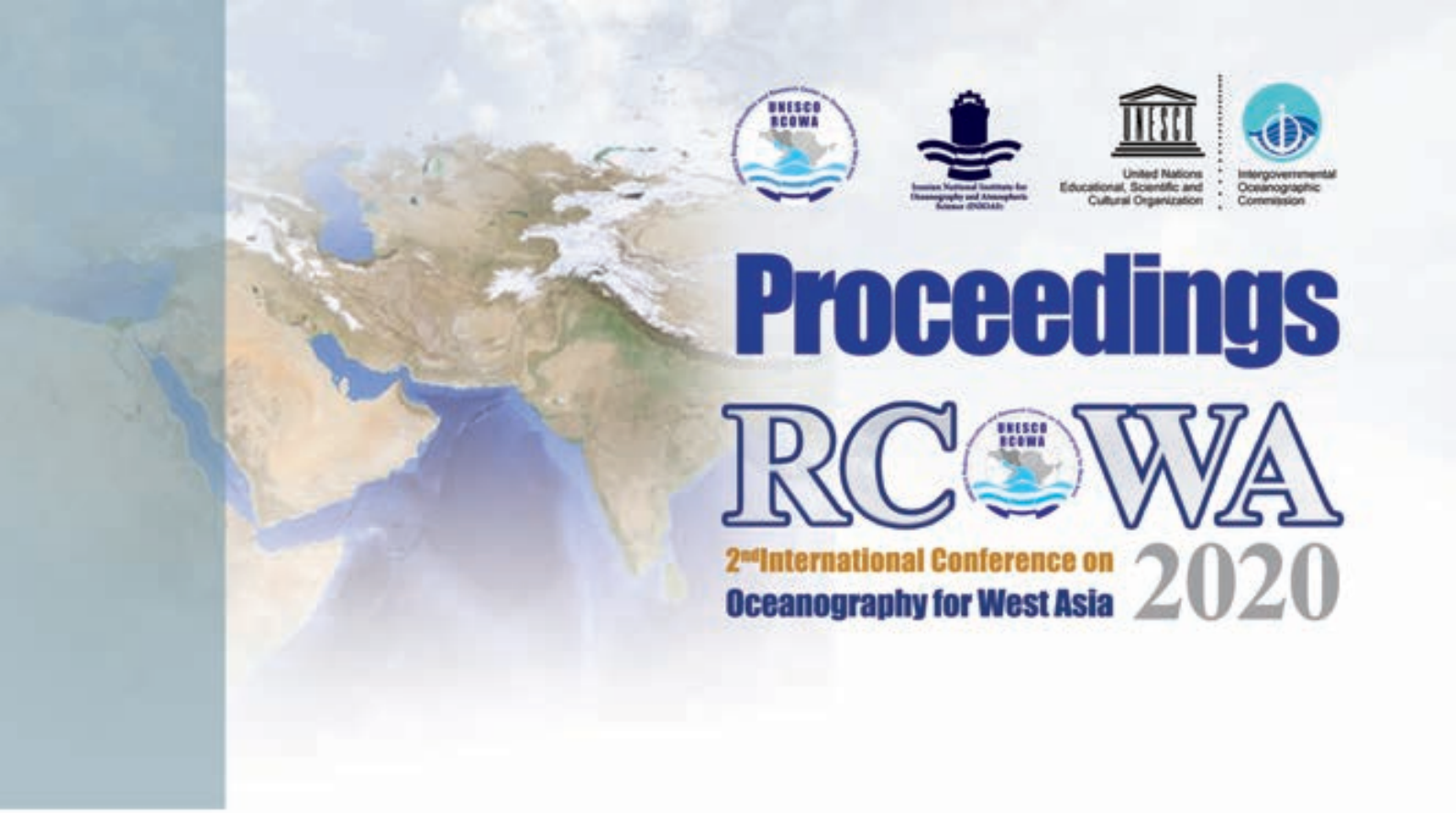

International Scientific Committee

Second International Conference on Oceanography for West Asia

Executive Secretary of the Intergovernmental Oceanographic Commission and Assistant Director General of UNESCO	Dr. Vladimir Ryabinin
Director of Indian National Centre for Ocean Information Services, India	Dr Srinivasa Kumar Tummala
Officer in Charge UNESCO IOC Perth Office	Dr. Nick D Adamo
Environment and Life Sciences Research Center, Kuwaite Institute for Scientific Research, Kuwait	Dr. Saif Uddin
Liege University and co-chair of the IOC Expert Group on Deoxygenation GO2NE	Dr. Marilaure Gregroire
Postdoctoral Research Fellow University of Toronto	Dr Marjan Barzandeh

Proceedings

RCOWA 2020

2nd International Conference on Oceanography for West Asia

International Scientific Committee

Second International Conference on Oceanography for West Asia

Director General of Meteorology	Dr. Juma Al-Maskari
IOC Regional Liaison Officer	Mr Justin Ahanhanzo
Head - Perth Programme Office of the Intergovernmental Oceanographic Commission of UNESCO (IOC PPO)	Dr. Nick D'Adamo
Former IOC Deputy Executive Secretary	Dr. Iouri Oliouninet
Centre National de la Recherche Scientifique / French National Centre for Scientific Research	Nick Mariney
Aix-Marseille University	Christophe Morhange
Maison Mediterranenne des Sciences de l'Homme, Lampea	Suzanne Leroy
Quaternary Ecosystems, Aix-en-Provence, France	
Shirshov Institute of Oceanology	Andrey G. Kostianoy
Shiloshav Institute Oceanology	Andrei Ivanov
Moscow Stat unit	Tama Yanina
Executive Director of INOC	Mustafa Ergun
Dokuz Eylul University	Gunay Cifci
University of Koln	Martin Kchl
Natural History Musoum Berlin Curtor of Crustaceama	Oliver Coleman

Proceedings

RCOWA

2nd International Conference on Oceanography for West Asia 2020

Second International Conference on Oceanography for West Asia

Coordinator & public relations	Dr. Babak Moradi
Member of Organizing Committee	Manoochehr Mohamadi
Coordinator of Information Technology	Farhad Heydari
Member of Organizing Committee	Farrokh Alavian Ghavanini
Member of Organizing Committee	Hamid Zarehe
Member of Organizing Committee	Leila Nasrollahi
Member of Organizing Committee	Valiollah Omrani
Coordinator of Webinars	Zahra Nejadfallah
Coordinator of Website and advertisement, designer	Mohamad Mahdipourvahid
Coordinator of International Relations, Moderator of Opening Ceremony	Fahimeh Foroughi
Coordinator of the Secretariat	Faramarz Ebadi
Coordinator of the Conference hall	Seyed Mostafa Shadab
Member of Organizing Committee	Ahmad Asadollahi

United Nations Educational, Scientific and Cultural Organization

Intergovernmental Oceanographic Commission

Proceedings

RC WA

2nd International Conference on Oceanography for West Asia 2020

Workshop-Webinars

Second International Conference on Oceanography for West Asia

Conference Organizing Committee

Trends of Coral Reefs of the Persian Gulf and the Gulf of Oman

Dr. Hamid Rezaei
Dr. Amir Ghazilou
Mr. Jahangir Vajedsamiei
Miss. Mahshid Oladi

Microplastics Pollution in Marine Environment

Prof. Saif Ud din
Dr. Sajad Abbasi
Dr. Kamalodin Kor
Dr. Ali Mehdinia
Dr. Zahra Taghizadeh

Marine Biogeochemical Processes in the Perspective of Climate Change

Dr. Omid Alizadeh
Dr. Behzad Layeghi
Mr. Maziar Gholami
Dr. Gholamreza Mohamadpour
Dr. Mélanie Gaillard

Tsunami Early Warning System

Dr. Srinivasa K Tummala |
Mr. Harald Spahn
Mr. Ardito M Kodijat

United Nations Educational, Scientific and Cultural Organization

Intergovernmental Oceanographic Commission

Proceedings

RCOWA

2nd International Conference on Oceanography for West Asia 2020

Graphic and Layout Designer

Second International Conference on Oceanography for West Asia

Graphic and Layout and Designer

Mohammad Mehdipourvahid

2nd International Conference on Oceanography for West Asia

16 , 17 Sept. 2020 Iran. Tehran

Contents

2nd International Conference on Oceanography for West Asia

16 , 17 Sept. 2020 Iran. Tehran

Normal alkanes and parent PAHs in sediments from the Eastern Persian Gulf: spatial structure and implications for autochthonous, allochthonous and petroleum-originated contaminants

Aghadadashi, Vahid [1]*; Mehdinia, Ali [2]; Riyahi Bakhtiari, Alireza [3]; Molaei, Saeideh [4]

1. PhD graduate, Iranian National Institute for Oceanography and Atmospheric Science, Tehran, Iran, nature11.ngo@gmail.com

2. Associate Professor, Iranian National Institute for Oceanography and Atmospheric Science, Tehran, Iran, mehdinia@inio.ac.ir

3. Full Professor, Tarbiat Modares University (TMU), Noor, Mazandaran, Iran, riahi@modares.ac.ir

4. PhD graduate, Kharazmi University, Tehran, Iran, smolaei@gmail.com

Keywords: *GIS; geo-statistics; n-alkanes and PAHs, Persian Gulf; Sediment; Source identification*

1. Introduction

The Persian Gulf is a strategic region and contains huge reservoirs of gas and petroleum. It supports nearly one-fourth of the world's energy demands (Sheppard et al., 2010). The extensive oil and gas related activities have turned the Persian Gulf to a well-known oil receiving area. The oil and oil related activities introduce a vast variety of eco-pollutants to the Persian Gulf. The oil pollution in the Persian Gulf is about 3% of the global total or nearly 50 times the average of a similar-sized marine environment (Khan and Al-Ajmi, 1998). Mixtures of parent and substituted oil related eco-pollutants mainly Polycyclic Aromatic Hydrocarbons (PAHs) and n-alkanes are of particular importance (de Mora et al., 2010). PAHs are widespread and bio-resistant chemicals. They can produce and release into the marine environments by natural and anthropogenic activities (Neşer et al., 2012). The seas are assumed to be the final receptors of PAHs and the other eco-pollutants. The hydrophobic nature of PAHs connects PAHs to the particulate matters. It facilitates gravimetrical deposition of PAHs in sedimentary substrates. The bottom sediments, which are below the aerobic surface layer, can store the PAHs relatively unchanged long after their initial release. Postponed toxic effects subsequently can take place and influence the structure of benthic communities (Charles et al., 2012).

2. Materials and methods

The sampling region is located between Northern latitude 27°54'57.76"–27°24'50.52"N and Eastern longitude 51°23'49.97"–52°40'13.02"E which nearly covers 815.31 square nautical miles (~2800 km2). In a systematic sampling methodology, the region was divided to 24 transects which were separated by nearly 2.7 nautical miles distances. The

first sampling stations of all transects were selected as nearshore stations (~0.27–0.8 nautical miles off the shoreline) and the successive stations were sampled at distances including 1.62, 3.24, 5.4, 8.1, and 10.8 nautical miles off the shore in average. In summary, a matrix was formed by sampling from 6 horizontal legs in about 24 vertical transects. However, the plan was not practical for both national Parks, and the Parks were sampled separately. Therefore, the surface sediments (0–5 cm) from 134 stations were gathered using a Van Veen sampler.

Taking the granulometric dilution effect into account, bulk sediments were sieved (mesh number 60) in laboratory and < 250 µm. The dried and size normalized sediments were homogenized prior to extraction. Then, the sediment samples (4 g) were spiked with 100 ng g−1 surrogate standards of naphthalene-*d8*, antherancene-*d10*, chrysene-*d12* and perylene-*d12*. The sediments were extracted by a microwave sample extraction system (Ethos 1, Milestone, Italy). Microwave extraction was established at 150 °C for 20 min, using 30 mL of solvent mixture of *n*-hexane-acetone (1:1, v/v). After the extraction, the supernatant organic extract was carefully decanted from the extraction vessels and the samples were re-extracted by 10 mL of dichloromethane (DCM) for 7 min at 100 °C. Then, two extracts of each sample were combined together and the activated copper wires were added to remove the sulfur content from the extracts overnight. After these steps, all following procedures were carried out according to guidelines of MOOPAM (2000), recommended for the analysis of marine sediments. The analysis was performed with a Gas chromatography-mass spectrometry (GC–MS) model 6890N GC system equipped with a 5973 mass detector.

3. Results and discussion

Surface sediments (n =121) were gathered from nearly 1% of the Persian Gulf's basin to evaluate spatial pattern and source apportionment of $\sum_{24}n$-alkanes and $\sum_{16}$parent-PAHs. Levels of $\sum_{24}n$-alkanes and $\sum_{16}$parent-PAHs were in the range of 1.98-814 ng g^{-1} dw (mean= 174.31) and 2.29 to 206.59 µg g^{-1} dw (mean= 11.22), respectively. Therefore, the region was low to moderate polluted in general. To reveal spatial patterns of the deposited eco-pollutants, a combined GIS, geo-statistics and autocorrelation analyses were employed. In the case of PAHs, Global Moran's *I* index outlined the presence of significant $\sum_{16}$PAHs clusters in the region (Moran's *I* index =0.62, Z-score =25.6). Anselin Moran's *I* index specified locations of the significant low or high spatial clusters where offshore of the Pars South Special Economic Energy Zone (PSEEZ) recognized as a High-High clustered area. The levels of random and structural variance of $\sum_{16}$PAHs were about 0.083 and 0.154 ng, respectively. Nugget to sill ratio confirmed that $\sum_{16}$PAHs have got a moderate level of spatial structure. Prediction and standard error maps of $\sum_{16}$PAHs, produced by ordinary kriging, suggested that more samples should be taken from the high clustered region for upcoming studies. Fuzzy logic functions (OR and AND) were used to develop eco-risk maps. It made obvious that the potential hazards of PAHs were considerable at the vicinity of petrochemical facilities, i.e, the Nayband Marine National Park.

Moran's *I* indices suggested that $\sum_{24}n$-alkanes were randomly distributed in sampling space in general. One noticeable exception was a significant spatial High-High cluster (Z-score =8.6). Profile of *n*-alkanes observed for this cluster maximized at n-C_{20}, n-C_{18}, n-C_{16} and n-C_{22}. Detection of very low Carbon Preference Indices and strong even Carbon-numbered predominance suggested that bacterial inputs were the process making this cluster. The data relevant to the

diagnostic ratios of deposited *n*-alkanes were used to make GIS-based layers. With combination of the mentioned layers in GIS environment, Source Apportionment Maps were produced for individual sources, including; Petrogenic Source Apportionment Map, Allochthonous Source Apportionment Map and, Autochthonous Source Apportionment Map. With reference to the maps, *in-situ* production of organic materials was widespread in the studied space and allochthonous and petroleum-based inputs were not traceable for 73.8% and 24.7% of the area, respectively. In addition, Petrogenic Source Apportionment Map proposed that petroleum-originated contaminants were probably limited to 6.32 km^2 of the sampling matrix. The biogenic inputs (autochthonous and allochthonous inputs) and not the petroleum contaminants were the main source of *n*-alkanes deposited in the studied zones.

References:

1. Sheppard, C.R.C., Al-Husiani, M., Al-Jamali, F., Al-Yamani, F., Baldwin, R., Bishop, J,. et al., 2010. Persian Gulf: a young sea in decline. A review. Mar. Pollut. Bull. 60, 13–38.

2. Khan, N.Y., Al-Ajmi, D., 1998. Post-war imperatives for the sustainable management of Persian Gulf ecosystem. Environ. Int. 24 (1–2), 239–248.

3. de Mora, S., Tolosa, I., Fowler, S.W., Villeneuve, J.-P., Cassi, R., Cattini, C., 2010. Distribution of petroleum hydrocarbons and organochlorinated contaminants in marine biota and coastal sediments from the ROPME Sea Area during 2005. Mar. Pollut. Bull. 60 (12), 2323–2349.

4. Neşer, G., Kontas, A., Ünsalan, D., et al., 2012. Polycyclic aromatic and aliphatic hydrocarbons pollution at the coast of Aliag ˘a (Turkey) ship recycling zone. Mar. Pollut. Bull. 64, 1055–1059.

5. Charles, F., Nozais, C., Pruski, A.M., Bourgeois, S., Méjanelle, L., Vétion, G., et al., 2012. Ecodynamics of PAHs at a peri-urban site of the French Mediterranean Sea. Environ. Pollut. 171, 256–264.

2nd International Conference on Oceanography for West Asia

16 , 17 Sept. 2020 Iran. Tehran

Sperm motility in marine fishes – a review

Alavi, Sayyed Mohammad Hadi *

School of Biology, College of Science, University of Tehran, P. O. Box: 14155-6455, Tehran, Iran.
e-mail: hadi.alavi@ut.ac.ir or smhalavi1@gmail.com

Keywords: *ATP; Axoneme; Ions; Osmolality; Seminal plasma*

1. Introduction

Fish and fishery products are important sources of protein and essential micronutrients for balanced nutrition and good health. In per capita terms, fishery product consumption has grown from 9.0 kg in 1961 to 20.3 kg in 2016. Global production of fish, crustaceans, mollusks and other aquatic animals increased from 39.2 million tons in 1961 to 170.9 million tons in 2016. Of these totals, capture production has increased from 37.1 million tons in 1961 to 90.9 million tons in 2016. Aquaculture production has increased from 1.5 million tons in 1961 to 13.1 and 80 million tons in 1990 and 2016 respectively (FAO, 2018).

The fishery organization has been growing in many countries to manage and control capture production and aquaculture of high-value aquatic animals. In aquaculture, scientific research dealing with commercially important species is essential to establish broodstock population and to develop methods for artificial reproduction and rearing in captivity with critical consideration to environmental sustainability, economy sustainability, and social sustainability (Alavi et al., 2008). In male broodstock management, *studying endocrine regulation of spermatogenesis, hormonal stimulation of sperm maturation, and sperm biology are critical to develop the methods for artificial reproduction by optimizing insemination protocol, to develop aquaculture by generating polyploid populations, and to preserve endangered species from extinction by cryopreservation of sperm (Alavi et al., 2008; Mylonas et al., 2010).*

The present study is a comprehensive review on our current understanding and a state-of-the-art in sperm motility signaling in *marine fishes.* Followed by a brief introduction to motility apparatus of sperm and kinetics of sperm motility, sperm motility signaling is discussed with emphasis on physiological roles of plasma membrane of spermatozoa, water and ion channels, and intracellular messengers.

2. Sperm morphology and the motility apparatus in marine fishes

A spermatozoon in marine fish is differentiated into a head, a midpiece and a flagellum (Figure 1) (Jamieson 1991). The head does not have the acrosome and contains nucleus which transferring haploid set of the chromosome into the next generation. Mitochondria, proximal centriole and distal centriole are located in the midpiece. Mitochondria supply energy for the flagellar beating. Both proximal and distal centrioles consist of nine peripheral triplets of microtubules. The distal centriole organizes formation of the flagellum. *Sperm motility is generated by a typical scaffold of "9+2" microtubules called the "axoneme".*

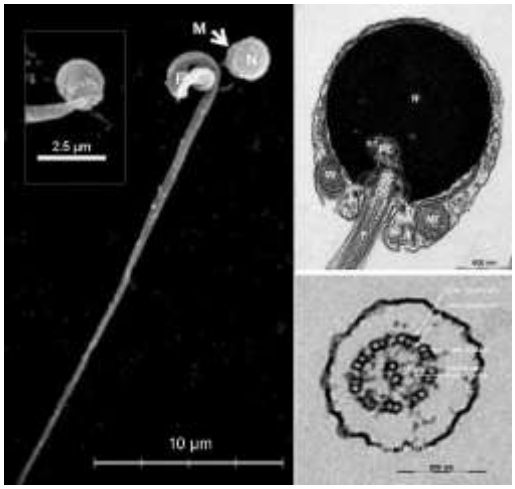

Figure 1. Spermatozoa of Atlantic halibut (*Hippoglossus hippoglossus*). (Left) Scanning electron microscopy shows head, midpiece and flagellum of sperm. (Left, insert) Symmetrical pattern position of sperm. (Right, Top) Longitudinal section of head region, midpiece and flagellum. (Right, Bottom) A cross section of the flagellum showing the axonome with 9+2 microtubule structure. Head (N), midpiece (M), flagellum (F), nuclear notch (nn), distal centriole (DC), proximal centriole (PC), and mitochondria (Mt). Reference: Alavi et al., 2010

3. Kinetics of sperm motility in marine fishes

Sperm is immotile in the seminal plasma or the sperm duct, and their motility is triggered right after discharge into the aquatic environment. Duration of spermatozoa motility highly varies among fishes, however it is generally limited to a short period (Alavi et al., 2019). The physiological reason(s) for inter-species variations of sperm motility duration is not fully understood. It has been hypothesized that there is a correlation between initial adenosine triphosphate (ATP) content and duration of spermatozoa motility (Cosson 2010). After initiation of motility, percentage of motile spermatozoa, spermatozoa velocity, beating frequency of the flagellum, flagellar wave length and amplitude decrease, while both the number of waves and their degree of curvatures increase. Decreases in percentage of spermatozoa motility and spermatozoa velocity are mainly due to depletion of intracellular ATP stores required for axonemal beating (Alavi et al., 2019).

4. Sperm motility in marine fishes

Sperm is quiescent and motile in electrolyte and nonelectrolyte solutions iso-osmotic and hyper-osmotic to the seminal plasma, respectively (Figure 2). Changing extracellular osmolality from hyper-osmotic to hypo-osmotic electrolyte or nonelectrolyte solutions reversibly suppresses sperm motility, indicating that a hyper-osmolality

signal triggers initiation of sperm motility in marine fishes. A hyper-osmotic signal triggers sperm motility in marine fishes (*Figure 3)*. In a hyper-osmotic medium, increases in $[K^+]_i$ and $[Ca^{2+}]_i$ concentrations occur due to decrease in the volume of spermatozoon. Various types of water channels (aquaporins) are involved in the regulation of the sperm volume as well as stretch-activated channels. Aquaporins are involved in the regulation of $[Ca^{2+}]_i$. $[Ca^{2+}]_i$ rise is mainly supplied by $[Ca^{2+}]_i$ stores rather than Ca^{2+} influx. Moreover, $[Ca^{2+}]_i$ is regulated by NCX. Increase in $[Ca^{2+}]_i$ regulate Ca^{2+}/CaM-dependent protein kinase that are involved in the initiation of axonemal beating in pufferfish and sea bream. Phosphorylation of these proteins is cAMP-dependent, and thus inhibited by inhibition of PKA. In some marine fishes including the Atlantic croaker, the spotted seatrout, red drum, and southern flounder sperm, 20β-S stimulates hypermotility via mPRα expressed in the midpiece or the flagellum. The 20β-S-induced sperm hypermotility is associated with an increase in $[Ca^{2+}]_i$, which in turn activates adenylyl cyclase to produce cAMP (Morisawa 2008; Alavi et al., 2019)

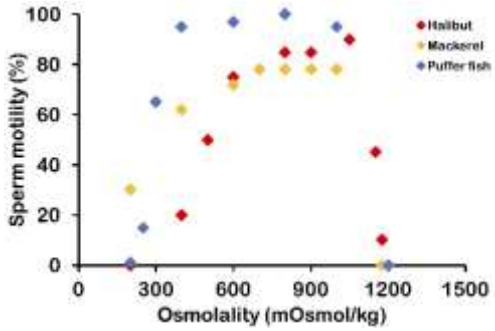

Figure 2. *The effects of osmolality on initial percentage of motile spermatozoa in marine fishes. Species:* Atlantic halibut (*Hippoglossus hippoglossus*) (Billard et al., 1993), mackerel (Trachurus mediterraneus), pufferfish (*Takifugu niphobles*) (Oda and Morisawa 1993).

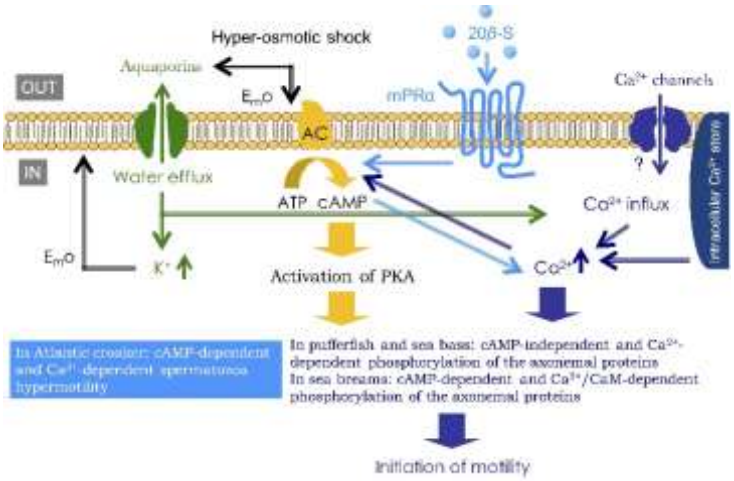

Figure 3. *Sperm motility signaling in marine fishes. Reference: Alavi et al., 2019*

References

1. Alavi SMH, Cosson J, Bondarenko O, Linhart O. Sperm motility in fishes: (III) diversity of regulatory signals from membrane to the axoneme. Theriogenology 2019;136:143-165.

2. Alavi SMH, Butts IAE, Hatef A, Mommens M, Trippel EA, et al. Sperm morphology, ATP content and analysis of motility in Atlantic halibut (*Hippoglossus hippoglossus* L.). Can J Zool 2011;89:219-228.

3. Alavi SMH, Cosson JJ, Coward K, Rafiee G. Fish Spermatology. Alpha Science Ltd; 2008.

4. *Billard R, Cosson J, Crim LW. Motility of fresh and aged halibut sperm. Aquat Living Resour 1993;6:67-75.*

5. Cosson J. Frenetic activation of fish spermatozoa flagella entails short-term motility, portending their precocious decadence. J Fish Biol 2010;76:240-279.

6. FAO. Fishery and Aquaculture Statistics 2016. Rome: FAO publication; 2018.

7. Jamieson BGM. Fish evolution and systematic: Evidence from spermatozoa. Cambridge University Press; 1991.

8. Lahnsteiner F, Patzner R. Sperm motility in the marine teleosts *Boops boops*, *Diplodus sargus*, *Mullus barbutus* and *Trachurus mediterraneus*. J Fish Biol 1998;52:726-742.

9. *Morisawa M. Adaptation and strategy for fertilization in the sperm of teleost fishes. J Appl Ichthyol 2008;24:362-370.*

10. Mylonas CC, Fostier A, Zanuy S. Broodstock management and hormonal manipulations of fish reproduction. Gen Comp Endocrinol 2010;165:516-534.

11. *Oda A, Morisawa M. Rises of intracellular Ca^{2+} and pH mediate the initiation of sperm motility by hyperosmolality in marine teleosts. Cell Motil Cytoskeleton 1993;25:171-178.*

2nd International Conference on Oceanography for West Asia

16 , 17 Sept. 2020 Iran. Tehran

Trace and Rare earth elements geochemistry as indicators of source-area composition and paleoredox conditions in Makran zone (Chabahar area), South Iran

Amjadi, S.[1,2]; Mahmudy Gharaie, M.H.[1]*; Lahijani H.A.K.[2]; Mosavi harami, R.[1]; Mahbobi, A.; Naderi M.[2]

1. Department of Geology, Faculty of Science, Ferdowsi University of Mashhad, Mashhad, Iran
2. Marine Geology Department, Iranian National Institute for Oceanography and Atmospheric Sciences (INIOAS), Tehran, Iran

Keywords *Sedimentary geochemistry, core sediment, paleoredox, oxygenation condition, Makran*

1. Introduction

The importance of sediment geochemistry is well known in understanding clastic sedimentary basin evolutions and identification of the sediment sources (McLennan et al., 1983). As well as, geochemistry studies has great potential to the regional tectonic setting in each sedimentary facies cycles (Bhatia, 1983; Bhatia and Crook, 1986; Roser and Korseh, 1986). Therefore, rare earth elements (REE) and trace elements because of their chemical resistance in the natural environments are the good indicators to identification of source rock geochemistry, sedimentary processes and probably low grade metamorphism (Taylor and McLennan, 1985).

Geochemical parameters, also, have used in many studies in order to defining palaeobasin oxidation and reduction conditions (Cullers, 2002; Armstrong-Altrin et al., 2003; Dobrzinski et al., 2004). Meanwhile, Cerium (Ce3+) and Europium (Eu2+) because of their different behaviors in oxidation and reduction environments are broadly used for palaeo-environmental analysis (Wilde et al, 1996).

The Makran accretionary prism was formed due to the subduction of the Arabian plate under the Eurasian plate since Cenozoic (Harms et al., 1984). The sediments within the accretionary complex are largely recycled from the material eroded from the Iran, Pakistan and India collision belt (Fruehn et al., 1997). , The aim of this study is identify the source rock characteristics and reconstruct paleo-oxygen conditions by using trace, and rare earth elements.

2. Materials and methods

Oman Sea monitoring cruise was undertaken by Iranian national institute of oceanography and atmospheric science (INIO-AS). During this cruise five gravity cores were obtained from the Oman sea continental shelf. The location of the studies cores depicted in figure 1. The granulometric parameters were analyzed in INIO-AS laboratory. Fifteen sub-samples were taken from five core sediments and have been treated for elemental analysis using inductively coupled plasma-mass spectrometry (ICP-MS) in ALS Chemex Laboratory. REE elements are normalized by chondrite values (Taylor and McLennan, 1985).

3. Results

The result of this study reveals that PAAS normalized patterns of trace elements are represented a moderate depletion of Co, Ni, V,Ba, Sr, Rb, Zr, U, whereas, Nb contents are enriched with respect to those of PAAS.

The results of elements ration such as La/Th and Th/Sc and Th/Co vs. La/Sc plot is suggested a felsic source rock for the imported sediment. In the case of Eu/Eu* vs (Gd/Yb)N, all samples were felt below the Eu/Eu*=0.85 line it suggested the probably source of the sediments are from post-Archean and near to Granitoids hinterland rocks. The HREE depletion [(Gd/Yb)N<2] is common in the Archean rocks and is essentially absent in the Post-Archean rocks (Taylor and McLennan, 1985). The positive anomaly of Ce/Ce* is ranged between 1.01 to 1.08 that is addressed an oxidizing conditional in environment

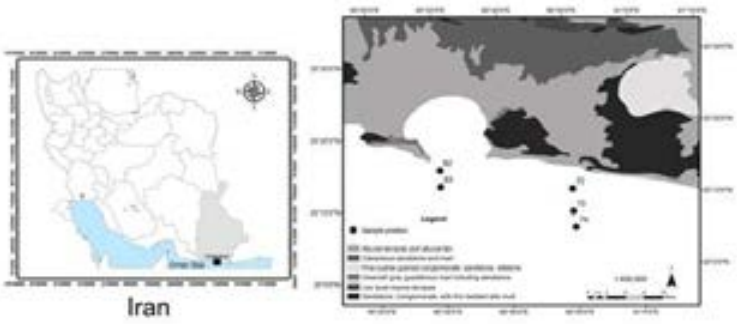

Figure 1) the location of the study area and coring site

4. Discussion and conclusion

The REE patterns and La/Sc, Th/Sc, Th/Co, Cr/Th ratios of cores sediment samples were comparable with those of sediments derived from felsic and basic rocks, upper continental crust (UCC) and post-Archean Australian average shale (PAAS) ratios, which reveal that these ratios are within the range of felsic rocks composition. The La/Sc vs. Th/Co plot also suggests the felsic nature of the source rocks. In terms of the (Gd/Yb)n and Eu/Eu*, most of the studied core sediment samples are comparable with the Post-Archean craton complexes, some of which resemble the average composition of the (PAAS) pattern along with (La/Yb)n ratio suggest enrichment of the light REE (LREE) relative to heavy REE (HREE) with the weak negative Eu/Eu* anomaly implying that the dominant source may have been from felsic and intermediate rocks. The geochemical parameters such as U, U/Th,

V/Cr, and Cu/Zn ratios and positive anomaly of Ce/Ce* indicate that the study core sediments were deposited in an oxic environment.

References

1. Armstrong-Altrin, J.S., Verma, S.P., Madhavaraju, J., Lee, Y.I., Ramasamy, S., 2003. Geochemistry of Late Miocene Kudankulam Limestones, South India: International Geology Review. 45(1): 16-26.
2. Bhatia, M. R., 1983. Plate tectonics and geochemical composition of sandstones: Journal of Geology. 91: 611-627.
3. Bhatia, M.R. and Crook, K.A.W., 1986. Trace element characteristics of greywackes and tectonic setting discrimination of sedimentary basins, Contrib. Mineral. Petrol., Vol 92: 181-193.
4. Cullers, R.L., 2002. Implications of elemental concentrations for prov- enance, redox conditions, and metamorphic studies of shales and limestones near Pueblo, CO, USA: Chemical Geology. 191(4): 305-327.
5. Dobrzinski, N., Bahlburg, H., Strauss, H., Zhang, Q.R., 2004. Geochemical climate proxies applied to the Neoproterozoic glacial succession on the Yangtze Platform, South China, in Jenkins, G. et al. (eds.), The extreme Proterozoic: Geology, Geochemistry and Climate: American Geophysical Union Monograph Series, 146, 13-32.
6. Fruehn, J., White, R.S., Minshull, T.A., 1997. Internal deformation and compaction of the Makran accretionary wedge. Terra Nova. 9: 101–104.
7. Mclennan, S.M., Taylor, S.R., Eriksson, K.A, 1983. Geochemistry of Archaean shales from the the Pilbara Supergroup, Western Austalia: Geochimica et Cosmochimica Acta. 47(7): 1211-1222.
8. Roser, B.P. and Korsch, R.J, 1986. Determination of tectonic setting of sandstone-mudstone suites using SiO2 content and KO ratio: Journal of Geology, 94(5): 635-650.
9. Taylor, S.R., McLennan, S., 1985. The Continental Crust: Its Composition and Evolution: Blackwell, Oxford, 312 p.
10. Wilde, P., Quinby-Hunt, M.S., Erdtmann, B.D., 1996. The whole-rock cerium anomaly: a potential indicator of eustatic sea-level changes in shales of the anoxic facies. Geol. 101: 43-53.

2nd International Conference on Oceanography for West Asia

16 , 17 Sept. 2020 Iran. Tehran

Study of the Effect of Gonu Tropical Cyclone on the Oman Coastlines Inland Flooding (Case Study: The Coastline of Sur)

Banan Dalalian, Masoud [1*]; Shokatian Beiragh, Mehrdad [2]; Golshani, Aliasghar [3]; Mojtahedi, Alireza [4]; Lotfollahi Yaghin, Mohammad Ali[5]

1. Department of Civil Engineering, University of Tabriz
2. Department of Civil Engineering, University of Tabriz
3. Department of Civil Engineering, Central Branch of Tehran Azad University
4. Department of Civil Engineering, University of Tabriz
5. Department of Civil Engineering, University of Tabriz

*masoud.banan92@ms.tabrizu.ac.ir

Keywords: *Flood Hazard, Risk, Tropical Cyclone Gonu, Sur.*

1.Introduction

Due to increasing the earth's temperature, the conditions and the frequency of tropical cyclones in the oceans have been increased [1]. Based on the statistics, there are over 80 tropical cyclones worldwide annually [2]. The tropical cyclones in the Atlantic and Eastern Pacific Oceans are known as Hurricane, the Western Pacific Ocean as Typhoon and the Indian Ocean and the Arabian Sea as Cyclone [3]. After forming the cyclones in the Arabian Sea, they mostly move towards the south and southeast Oman, west India and south Pakistan and rarely enter the Oman Sea [4]. However, these cyclones can move different paths, affecting the coasts of countries such as Iran and even the United Arab Emirates. The Gonu cyclone has been the strongest cyclone ever formed in the Arabian Sea, influencing the Arabian Peninsula and parts of southern Iran from the 2007/06/02 to 2007/06/07 (Figure 1-a). It killed 49 people of the coast of Oman and 23 people on the southern coast of Iran. In addition, the financial damage by this storm estimated as $ 4 billion in Oman and about $ 215 million in Iran [5]. Therefore, investigating the consequences of cyclones and their modeling to determine the most hazardous zone on the coasts for future management and planning is an issue. In addition, evaluating the impact of the storms occurred in neighboring countries of Iran greatly helps manage the future storm crisis due to the random nature of the storm tracks and the lack of measured data. Regarding the vulnerability of sandy beaches against flooding, overwash and erosion, the present study aims to evaluate the impact of inland flooding by Gonu cyclone on the coastline of Sur.

The previous studies and modeling were concentrated more on evaluation and predicting the effects of offshore storms, however increasing the wave height may affect coasts and land areas as well as offshore areas. The Gonu cyclone caused some flooding by the storm surge in some parts of Oman coast including the port of Muscat, Qirat, Sur, and Ras al-Hadd. The flood damage in Sur Port was significant in which approximately 4294 residential homes were damaged during the storm [6]. The flooding hazard assessment for Sur port and understanding how Gonu cyclone occurred such a destructive event is the purpose of this study. This information could be useful for disaster risk reduction. In this study, the flood caused by Gonu cyclone in the coastal part of Sur Port was modeled by MIKE 21 modeling software. Further, the results of a bigger model related to the Monitoring and modeling of Makran Coastline project [7] were used to define the boundary conditions of the present smaller model. The considered area is shown in Figure 1-b and the dominant direction of the waves in this area during the cyclone is from the East and South-West, and the wave height in the offshore could reach up to 9 meters.

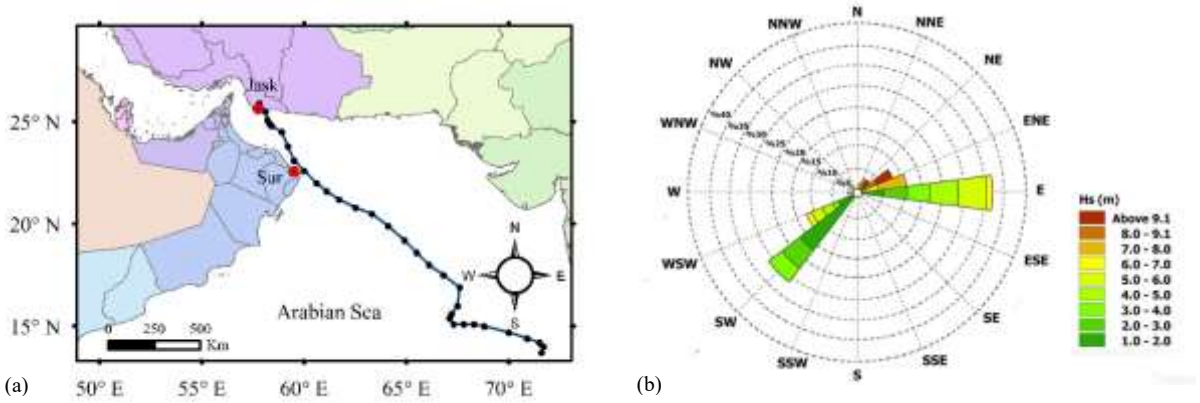

Figure 1) a. Gonu cyclone track, b. Wave rose for Sur port during the Gonu cyclone extracted from Makran model [7].

2.Materials and methods

In this study, the MIKE 21 Cyclone Wind Generation tool was utilized to generate the wind and pressure field of the cyclone. The Young and Sobey [8], Holland [9], and Rankine [10] vortex models were used to generate the wind and pressure ifelds during the . assage of the Gonu cyclone. Cyclone position, central pressure, maximum sustained wind speed, and radius to the maximum wind (R_{Vmax}) are the model's requirement input data [11]. International BT Archive for Climate Stewardship (IBTrACS) global tropical cyclone database has been used to obtain these data. The results were compared with observed wind and pressure data obtained from 3 hourly Jask meteorology synoptic station and the European Centre for Medium-Range Weather Forecasts (ECMWF) reanalysis ERA5 data. ERA5 has a special resolution of 0.25 and temporal resolution of an hour. Due to the proximity of the Gonu cyclone track to the Jask station (about 16 km), the ECMWF ERA5 could not capture the cyclone wind and pressure fields, however, ERA5 is accurate enough in non-cyclonic weather conditions. The analytical vortex models well captured the wind and pressure field during cyclone passage from the study area (Figure 2).

The topographic data (bathymetry and hypsometry), has been generated by merging two different datasets. The Digital Elevation Model (DEM), which could be interpolated onto the model, was created for the shore zone as hypsometry data. The bathymetry dataset was complemented by the General Bathymetric Chart of the Ocean (GEBCO). However, due to the importance of sea depth data near the shore, the shore profile of the study area was modified according to McLachlan et al [12].

The Gonu tropical cyclone has formed from 2007/06/02 to 2007/06/07. The coupled MIKE 21 HD/SW (hydrodynamic/spectral wave) model was used to simulate the inundation depth and the flow velocity. The MIKE 21 simulation was performed for a period of approximately seven days from 2007/05/31 to 2007/07/07 on the coast of Sur and a time interval of 300 seconds. The model extends 14 km offshore from the case study site, over an area of 110 km^2. The unstructured mesh includes 34515 elements with 17606 nodes (Figure 3-a). The largest elements have a resolution of 0.5 km, but the grid resolution becomes finer towards the coast with the smallest resolutions in the Sur coastal zone of approximately 15 m.

In this study, the surface elevation was applied at the northern open boundary, while the current speed was applied at eastern and western open boundaries. The boundary conditions were extracted from Makran MIKE 21/3 coupled model [7] which covered the Arabian sea and Persian Gulf. Young and Sobey vortex model were used to generate the wind and pressure ifeld. in Makran model. ECMWF ERA-Interim wave dataset with resolution of 0.75 degree were used as wave parametric boundary condition at the open boundary located on 10° N latitude in Makran model.

HYCOM GOFS 3.1 database with spatial resolution of 0.08° and temporal resolution of 3-hour were used to compare with the simulated surface elevation at the point with coordinates of 22°38'24.00" N 59°36'0.00" E. The calibration parameters of the MIKE 21 model were chosen based on the minimization of the error in the water level simulation. Figure 3-b shows a comparison between the HYCOM GOFS 3.1 data and the simulated water level. It can be seen that the numerical result reasonably matches the HYCOM GOFS 3.1 data. Note that the HYCOM GOFS 3.1 water level data does not exist between the 2007/06/04 12:00 AM and 2007/06/06 12:00 PM.

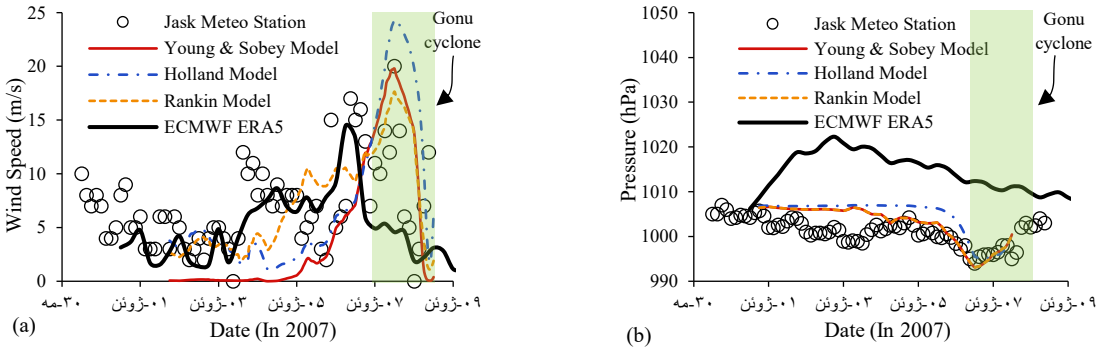

Figure 2) Comparison of the (a) wind and (b) pressure data from the analytical vortex models and ECMWF ERA5 at Jask synoptic station during Gonu cyclone.

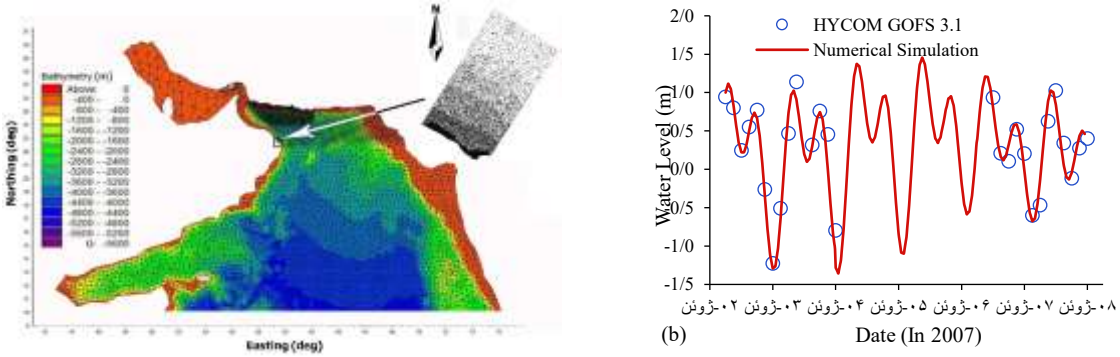

Figure 3) a. Computational domain and mesh used in this study, b. Comparison between the HYCOM GOFS 3.1 data and the simulated water level during the Gonu cyclone

3.Results and Discussion

Gonu cyclone generated storm surge which was destructive at Sur port. Figure 4 shows the Storm Surge in the Sur port during the Gonu cyclone event. As shown in Figure 4, when the cyclone passed by the considering area, storm surge near the Sur shore achieved its peak value. Meanwhile, it seems that, there are no significant differences among the results of storm surge from different analytical vortex models.

Figure 5 shows the spatial map of flood characteristic for inundation depth and flow velocity. Maximum inundation depth occurs along the shoreline over the central part of the study area (Figure 5-a) with the values ~1.3 m. Furthermore, for most of the western part of the model, inundation depth increases up to ~1.1 m, while maximum inundation depth in the eastern part of the model is approximately less than 1 m. The flow velocity pattern for the storm event is presented in Figure 5-b. The maximum flow velocity is varying all over the study area with its maximum magnitude more than 0.9 m/s.

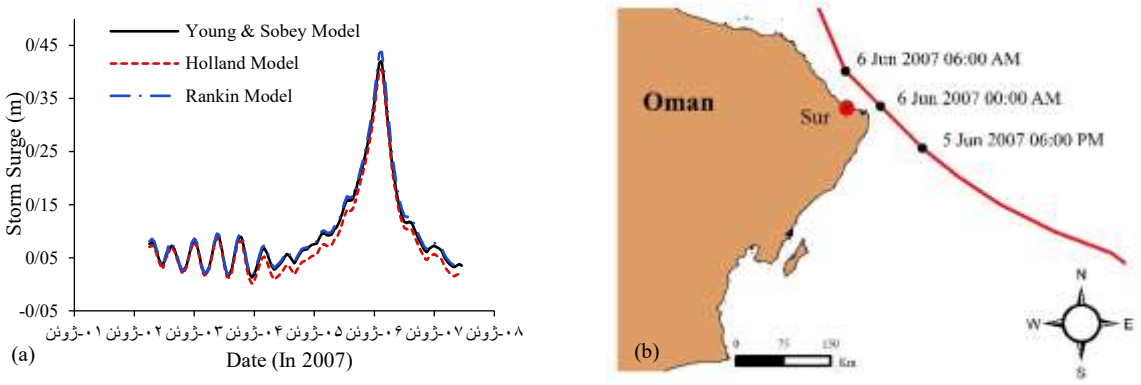

Figure 4) a. Comparison of Storm surge generated by the Young and Sobey, Holland, and Rankine vortex models near the Sur shore during Gonu cyclone, b. Gonu cyclone track passing by the coastline of Sur port

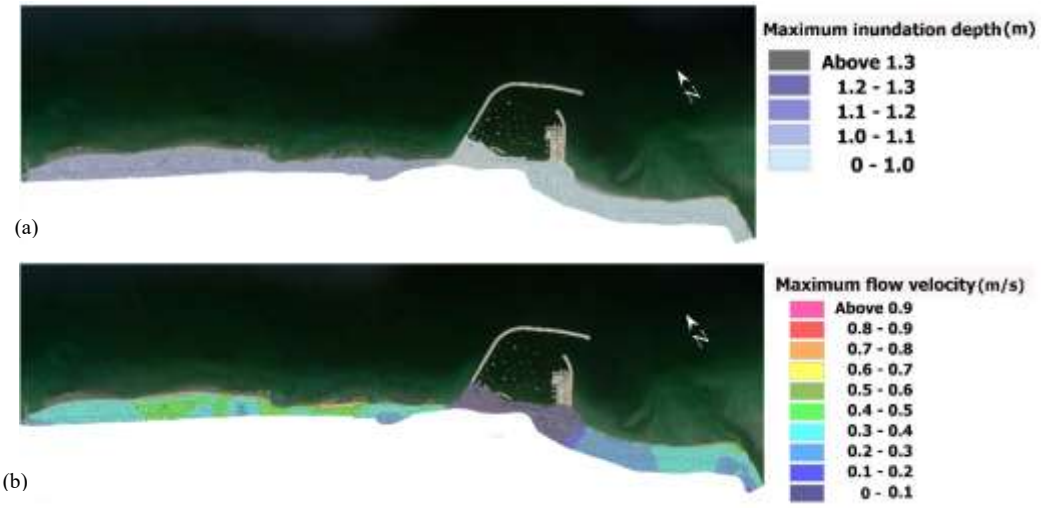

Figure 5) a. maximum inundation depth b. maximum flow velocity in the study area. Values represent the maximum value recorded over the duration of the simulation

In this study, the flood hazard is calculated through a matrix (Table 1), which is based on the inundation depth, flow velocity and the vulnerability of the area. Vulnerability or in the other hand nature of area is based on the type of buildings, the construction methods and land-use at three levels: Low (Multi-story apartments), Medium (Typical residential area (2-storey); commercial and industrial properties), and High (Bungalows, mobile homes, busy roads, parks, single story schools, campsites, etc.) vulnerabilities [13].

Table 1) Flood hazard matrix thresholds as a function of inundation depth and flow velocity and nature of area

Inundation depth × Flow velocity (m^2/s)	Nature of Area		
	Low Vulnerability	Medium Vulnerability	High Vulnerability
<0.25	Low Risk	Low Risk	Low Risk
0.25-0.50	Low Risk	Medium Risk	Medium Risk
0.50-1.10	Medium Risk	Medium Risk	High Risk
1.10-7.00	Medium Risk	High Risk	Extreme Risk
>7.00	Extreme Risk	Extreme Risk	Extreme Risk

The flood hazard map based on the literature discussed above and according to the Table 1, are reported in Figure 6. As shown in Figure 6, approximately 5% of the coast is assigned to the High risk class, 49% is of Medium, and 46% of Low risk. The area with a low risk to life is located mostly in the central and eastern parts of the model in

which the breakwater located. While the area with high risk to life shown in the western part of Sur coast. The medium risk to life zone exists in both the east and western parts of the coast.

Figure 6) Flood hazard map in the study area

4.Conclusion

this study, the Gonu cyclone inland flood hazard was investigated using numerical simulation. A coupled MIKE 21 HD/SW (hydrodynamic/spectral wave) model was utilized for this purpose. Furthermore, the Young and Sobey, Holland, and Rankine analytical vortex models were used to generate the wind and pressure ifelds during the passage of Gonu cyclone The results indicate that:

- ✓ The analytical vortex models well captured the wind and pressure field during the storm event, however, the ECMWF ERA5 data did not capture wind and pressure field accurately, due to the proximity of the Gonu cyclone track to study area. However, the ECMWF ERA5 data is accurate enough in non-cyclonic weather conditions.
- ✓ The numerical results of water level reasonably matches the reanalysis HYCOM GOFS 3.1 data.
- ✓ The storm surge near the Sur shore achieved its peak value of 0.44 meter (by the Rankine vortex model). Meanwhile, it seems that, there are no significant differences among the results of storm surge from different analytical vortex models.
- ✓ Maximum inundation depth occurs along the shoreline over the central part of the study area with the values ~1.3 m. For the most of the western part of the model, inundation depth increases up to ~1.1 m, while maximum inundation depth in the eastern part of the model is approximately less than 1 m. Meanwhile, the maximum flow velocity is varying all over the study area with its maximum magnitude more than 0.9 m/s.
- ✓ The flood hazard map shows that 5% of the coast is at High risk, 49% is at Medium risk, and 46% is at Low risk class.

References

1. Emanuel, K. 2005. Increasing destructiveness of tropical cyclones over the past 30 years. Nature, 436(7051), 686.

2. Henderson-Sellers, A., Zhang, H., Berz, G., Emanuel, K., Gray, W., Landsea, C., ... and McGuffie, K. 1998. Tropical cyclones and global climate change: A post-IPCC assessment. Bulletin of the American Meteorological Society, 79(1), 19-38.

3. Golshani, A., & Taebi, S. 2008. Numerical modeling and warning procedure for Gonu super cyclone along Iranian Coastlines. In Solutions to Coastal Disasters 2008 (pp. 268-275).

4. Dibajnia, M., Soltanpour, M., Nairn, R., and Allahyar, M. 2010. Cyclone Gonu: the most intense tropical cyclone on record in the Arabian Sea. In Indian Ocean Tropical Cyclones and Climate Change. Springer, Dordrecht. 149-157.

5. Fritz, H.M., Blount, C.D., Albusaidi, F.B., and Al-Harthy, A.H.M. 2010. Cyclone Gonu storm surge in Oman. Estuarine, Coastal and Shelf Science, 86(1), 102-106.

6. Al-Awadhi, T. 2010. The Use of RS and GIS to Evaluate the Effects of Tropical Cyclones: a Case Study from A'Seeb, Muscat after GONU Cyclone. In 1st WMO International Conference on Indian Ocean Tropical Cyclones and Climate Change, Muscat, Sultanate of Oman, 8-11 March 2009 (p. 95).

7. Study reports of Monitoring and Modelling Studies of Markan Coastlines, 2017, Ports and Maritime Organization (PMO).

8. Young, I. R., and Sobey, R. J. 1981. The numerical prediction of tropical cyclone wind-waves. Department of Civil & Systems Engineering, James Cook University of North Queensland.

9. Holland, G. J. 1980. An Analytic Model of the Wind and Pressure Profiles in Hurricanes. Monthly Weather Review, 108, 1212-1218.

10. Rankine, W. J. M. 1872. A manual of applied mechanics, Charles Griffin and Company.

11. DHI, 2014. Mike 21 Cyclone wind Generation Tool Scientific Documentation.

12. McLachlan, A., Fisher, M., Al-Habsi, H. N., Al-Shukairi, S. S., Al-Habsi, A. M. 1998. Ecology of sandy beaches in Oman. Journal of Coastal Conservation, 4(2), 181-190.

13. Priest, S.J., Wilson, T., Tapsell, S.M., Penning-Rowsell, E.C., Viavattene, C., Fernandez Bilbao, A. 2007. Building a Model to Estimate Risk to Life for European Flood Events. Project Report.

2nd International Conference on Oceanography for West Asia

16 , 17 Sept. 2020 Iran. Tehran

Geochemical and Environmental Survey of Elements in the Superficial deposits of Caspian Sea sediments: Application of Geoaccumulation Index, Enrichment, and Contamination Factors for Assessing Elemental Contaminations

Besharati, Pouya [1]; Parsinezhad, Shahrzad [2]; Zamani Pedram, Masoud [3]; Sajjad Azizi, Amir [4]

1. Msc. In Geochemistry, Faculty of Earthscience, Kharazmi University, Tehran
2. Msc. In Economical Geology, Faculty of Earthscience, Azad University, Lahijan
3. Phd. In Sedimentology ,Wurzburg, Germany
4. Msc. In Organic Chemistry, Payam e Nour University, Tehran

1. Introduction

The studied area is located in southern part of Caspian Sea, at Langaroud geological map (scale: 1: 100000) of Guilan province. The geographic coordinates are 50°, 00′, 00″ - 50°, 30′, 00″ E and 37°, 00′, 00″ - 37°, 30′, 00″ N. Elements specially heavy metals are toxic and causes serious problems to environmens as they are long persistent and not easily oxidized, degraded, removed, or converted to less harmful components through biological or chemical processes (Sharifuzzaman and et al., 2016). Sediments served as excellent indicator of metal pollution in coastal environments as larg inputs (>90 %) of heavy metals ultimately find their way to the estuarine zone and on the continental shelf (Yeasts and Wewers, 1983; Satpathy and et al., 2012).Twenty one samples of superficial deposits were collected from the 3- 47 meter depths during the summer of 2019 using a grab sampler. The samples were oven- dried at 80 (°c) for 1 day and sieved through a 2-mm sieve to remove large materials and stored in closed plastic bags and send to lab. All samples were analysed via ICP- MS and XRF in laboratory of the Geological Survey of Iran. All statistical methods were applied to process the analytical data in terms of its distribution and correlation among the studied parameters. To calculate the statistical parameters and identify the relationship among elements in sediments and assessment of the their possible sources, Pearson's correlation coefficient analysis and dendrogram of cluster analysis for elements were perfomed via SPSS and Excell software in present study.

The assessment of elements contamination is usually done by calculating Enrichment Factor (EF), Contamination Factor (CF), and Geo- accumulation Index (Igeo). Iron (Fe) is commonly selected as normalizing element because it is a Quasi- Conservative Tracer of the natural metal- bearing phases in fluvial and coastal sediments (Schiff and Weisberg 1999; Turner and Millward, 2000). The average crustal abundance data used to background elements

values because regional values havn′t been suggested.The results of comparisons between bulk element's concentrations and their mean elemental abundences of Earth's crust indicate the elements arranged according to their abundences in superficial deposits of Caspian Sea as follows : Al> Ca> Fe> Mg> Ti> Na> K> S> Mn. Calculations of the Enrichment Factor (EF) according to the degree of Taylor (1964) classification, shows most of elements studied have minor enrichments, Ca, Cd, Mo, and S have moderate enrichments, and S has moderately severe enrichment just in one sampling station. In the present investigation, the degree of sediment's contamination was evaluated using a Contamination Factor (CF), according to the degree of Hakanson (1980) and Pazi(2011) classifications. The values of CF identify most of elements studied have low and moderate contaminations. Also Pb, Cr, Cd, As, Zn, Ti, Ca, Fe, S, and Mo are considerable, and Ca, Cd, As, and S have high contamination in several sampling stations. Müller (1979), as well as others have used the concentration of elements in shale and the average crustal abundences data as a substitute for select background elemental values, while regional background haven't been suggested (Christophoridis, 2009; Rubio, 2000; Hu, 2013). The Geo-accumulation Index (Igeo) indicates all elements studied are unpolluted and unpolluted to moderately polluted for 1 and 2 classes according to the Müller (1979) classification. Bivariate correlation (Pearson, two- tailed) matrices between the studied elements were conducted to investigate potential sources of them and are shown in. Various degree of correlations were found some significant correlations, both positive and negative in study area showed. According to correlation coefficients indicate and interpretation of relationship intensity of Pearson correlation (adapted of Morton and et al., 1996; Zou and et al., 2003):

A: Al- K, Rb- K, and Rb- Al show strongly positive correlation and identify same sources for them.

B: Mn- K show strongly negative correlation and its indicate different sources for them.

C: there are moderately positive correlation between Ca- Na, Pb- Fe, Ni- Al, Ni- Mg, Mn- Fe, Cu-Ni, Co- Cu, Cd-Fe, Cd-Cu, Cd-Co, Ba- Na, and As- S. therefore we can propose same sources for them. According to the dendrogram of elements, they contents in two major clusters, "A" and "B" Ca and Al were clustered in "A" . Na, K, and Mg formed clustered and Fe joins to them as "B1". Finally, As, Mo, Cd, Co, Pb, Cu, Ni, Rb, Zn, Ba, Mn, S, and Ti formed "B2" that grouped to "B1" and make major cluster "B".

Pay attention to geochemical affinity, behavior of each clusters and geological setting specially distribution of suitable lithogeochemical media for their elements, we propose several sources for clusters. Its clear that both types of geogenic and anthropogenic origins exist, but what is very important in transporting elements to continental shelf and superficial deposits of Capian Sea, seems to be the specific role of streams and rivers. They will obviously transmit elements from humanity, industrial, and agricultural activities. Howevere strongly seems to be a hybrid geogenic sources as elemental origin in studied area, or there are probably both acidic and basic rocks. Gabbroes and basalts as the sources of the Cu, Cr, Ni, Fe, Mg, Co, and rhyolites, ignembrites, acidic tuffs also metamorphosed sediments (slates and phyllites) as the origins of the As, Cd, Mo, Pb. It should be considered

that the function of streams causes dissolution and leaching the elements due to weathering of rocks, specially hidden ophiolites units, metal- bearing clay minerals, organic matter containing metals, sulfide compounds of elements that left over from lagoons dried and oxidize in oxidative conditions.

References:

1. A.Aghanabati,2004, Geology of iran , pp:586
2. Al- Edresy M., O Wasel S., Al- Hagibi A., echological risk assessment of heavy metals in coastal sediments between Al- haymah and Al- mokha, south red sea, yemen, 2019, international journal of hydrology.
3. Hakanson L., ecological risk index for aquatic pollution control, a sedimentological approach, 1980, water Res 14: 975- 1001
4. Müller, G., the heavy metal pollution of the sediments of Neckars and its tributary: a stocktaking, 1981, scientific Research.
5. Sharifuzzaman S.M., Rahman H., Ashekuzzaman S.M., Islam M., Chowdhury R., Hossain M., heavy metals accumulation in coastal sediments, 2016, Springer Japan.
6. Zou, correlation and simple linear regression 1, 2003, department of Radilogy, Harvard medical School.

2nd International Conference on Oceanography for West Asia

16 , 17 Sept. 2020 Iran. Tehran

Geochemical and Environmental Survey of Elements in the Superficial deposits of Caspian Sea sediments: Application of Geoaccumulation Index, Enrichment, and Contamination Factors for Assessing Elemental Contaminations

Besharati, Pouya [1]; Parsinezhad, Shahrzad [2]; Zamani Pedram, Masoud [3]; Sajjad Azizi, Amir [4]

1. Msc. In Geochemistry, Faculty of Earthscience, Kharazmi University, Tehran
2. Msc. In Economical Geology, Faculty of Earthscience, Azad University, Lahijan
3. Phd. In Sedimentology ,Wurzburg, Germany
4. Msc. In Organic Chemistry, Payam e Nour University, Tehran

Abstract:

The studied area is located in southern part of Caspian Sea, at Langaroud geological map (scale: 1: 100000) of Guilan province. 21 samples of superficial deposits were analysed via ICP- MS and XRF in laboratory of the Geological Survey of Iran. Element's concentrations arranged according to their abundences as follows : Al> Ca> Fe> Mg> Ti> Na> K> S> Mn. Most of elements studied have minor enrichments, Ca, Cd, Mo, and S have moderate, and S has moderately severe enrichment. Most of elements studied have low and moderate contaminations. Also Pb, Cr, Cd, As, Zn, Ti, Ca, Fe, S, and Mo are considerable, and Ca, Cd, As, and S have high contamination in several sampling stations. The Geo-accumulation Index (Igeo) indicates all elements studied are unpolluted and unpolluted to moderately polluted for 1 and 2 classes according to the Müller (1979) classification. Pay attention to geochemical affinity, behavior of each clusters and geological setting specially distribution of suitable lithogeochemical media for their elements, we propose both types of geogenic and anthropogenic origins for them.

Keywords: *Geochemistry, Enrichment factor, Contamination factor, Geo- accumulation index, Caspian Sea*

1.Introduction

The studied area is located in southern part of Caspian Sea, at Langaroud geological map (scale: 1: 100000) of Guilan province. The geographic coordinates are 50°, 00′, 00″ - 50°, 30′, 00″ E and 37°, 00′, 00″ - 37°, 30′, 00″ N (fig. 1). Elements specially heavy metals are toxic and causes serious problems to environmens as they are long persistent and not easily oxidized, degraded, removed, or converted to less harmful components through biological or chemical processes (Sharifuzzaman and et al., 2016). Sediments served as excellent indicator of metal pollution in coastal environments as larg inputs (>90 %) of heavy metals ultimately find their way to the estuarine zone and on the continental shelf (Yeasts and Wewers, 1983; Satpathy and et al., 2012).

2. Materials and Methods

Twenty one samples of superficial deposits were collected from the 3- 47 meter depths during the summer of 2019 using a grab sampler. The samples were oven- dried at 80 (°c) for 1 day and sieved through a 2-mm sieve to remove large materials and stored in closed plastic bags and send to lab. All samples were analysed via ICP- MS and XRF in laboratory of the Geological Survey of Iran. All statistical methods were applied to process the analytical data in terms of its distribution and correlation among the studied parameters. To calculate the statistical parameters and identify the relationship among elements in sediments and assessment of the their possible sources, Pearson's correlation coefficient analysis and dendrogram of cluster analysis for elements were perfomed via SPSS and Excell software in present study.The assessment of elements contamination is usually done by calculating Enrichment Factor (EF), Contamination Factor (CF), and Geo- accumulation Index (Igeo). Iron (Fe) is commonly selected as normalizing element because it is a Quasi- Conservative Tracer of the natural metal- bearing phases in fluvial and coastal sediments (Schiff and Weisberg 1999; Turner and Millward, 2000). The average crustal abundance data used to background elements values because regional values havn't been suggested.

3.Results

The results of comparisons between bulk element's concentrations and their mean elemental abundences of Earth's crust indicate the elements arranged according to their abundences in superficial deposits of Caspian Sea as follows : Al> Ca> Fe> Mg> Ti> Na> K> S> Mn. Calculations of the Enrichment Factor (EF) according to the degree of Taylor (1964) classification, shows most of elements studied have minor enrichments, Ca, Cd, Mo, and S have moderate enrichments, and S has moderately severe enrichment just in one sampling station. In the present investigation, the degree of sediment's contamination was evaluated using a Contamination Factor (CF), according to the degree of Hakanson (1980) and Pazi(2011) classifications. The values of CF identify most of elements studied have low and moderate contaminations. Also Pb, Cr, Cd, As, Zn, Ti, Ca, Fe, S, and Mo are considerable, and Ca, Cd, As, and S have high contamination in several sampling stations. Müller (1979), as well as others have used the concentration of elements in shale and the average crustal abundences data as a substitute for select background elemental values, while regional background haven't been suggested (Christophoridis, 2009; Rubio, 2000; Hu, 2013). The Geo-accumulation Index (Igeo) indicates all elements studied are unpolluted and unpolluted to moderately polluted for 1 and 2 classes according to the Müller (1979) classification.

Bivariate correlation (Pearson, two- tailed) matrices between the studied elements were conducted to investigate potential sources of them and are shown in figure 2. Various degree of correlations were found some significant correlations, both positive and negative in study area showed. According to correlation coefficients indicate and interpretation of relationship intensity of Pearson correlation (adapted of Morton and et al., 1996; Zou and et al., 2003):

A: Al- K, Rb- K, and Rb- Al show strongly positive correlation and identify same sources for them.

B: Mn- K show strongly negative correlation and its indicate different sources for them.

C: there are moderately positive correlation between Ca- Na, Pb- Fe, Ni- Al, Ni- Mg, Mn- Fe, Cu-Ni, Co- Cu, Cd-Fe, Cd-Cu, Cd-Co, Ba- Na, and As- S. therefore we can propose same sources for them. According to the dendrogram of elements, they contents in two major clusters, “A” and “B” (Fig 3). Ca and Al were clustered in “A” . Na, K, and Mg formed clustered and Fe joins to them as “B1”. Finally, As, Mo, Cd, Co, Pb, Cu, Ni, Rb, Zn, Ba, Mn, S, and Ti formed “B2” that grouped to “B1” and make major cluster “B”.

Pay attention to geochemical affinity, behavior of each clusters and geological setting specially distribution of suitable lithogeochemical media for their elements, we propose several sources for clusters. Its clear that both types of geogenic and anthropogenic origins exist, but what is very important in transporting elements to continental shelf and superficial deposits of Capian Sea, seems to be the specific role of streams and rivers. They will obviously transmit elements from humanity, industrial, and agricultural activities. Howevere strongly seems to be a hybrid geogenic sources as elemental origin in studied area, or there are probably both acidic and basic rocks. Gabbroes and basalts as the sources of the Cu, Cr, Ni, Fe, Mg, Co, and rhyolites, ignembrites, acidic tuffs also metamorphosed sediments (slates and phyllites) as the origins of the As, Cd, Mo, Pb. It should be considered that the function of streams causes dissolution and leaching the elements due to weathering of rocks, specially hidden ophiolites units, metal- bearing clay minerals, organic matter containing metals, sulfide compounds of elements that left over from lagoons dried and oxidize in oxidative conditions.

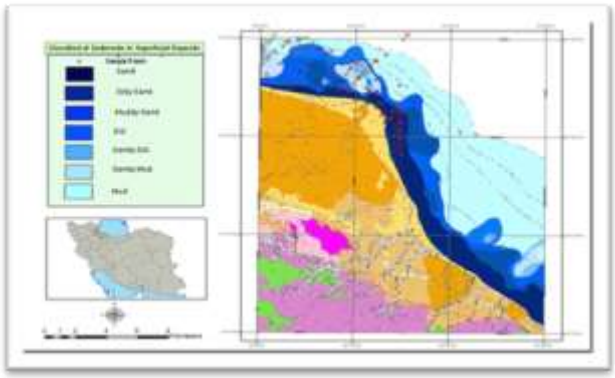

Fig 1. Modified map of the study area showing sampling sites on the type of sediments distributions map in superficial deposits of Caspian Sea (Karimkhani and et al., 2016)

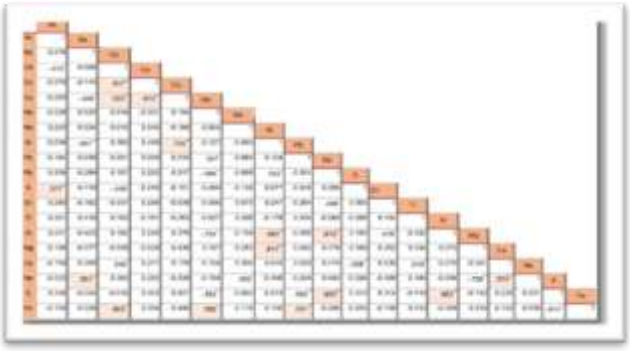

Fig 2. Correlation coefficients between the elements of superficial deposits in Caspian Sea sediments

*correlation is significant at the 0.05 level (p=0.05)(2-tailed)

**correlation is significant at the 0.01 level (p=0.01)(2-tailed)

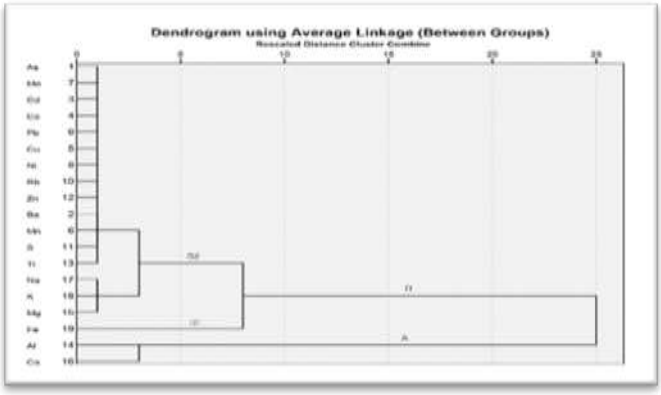

Fig 3. Denrogram of cluster analysis for elements of superficial deposits in Caspian Sea sediments

Refrence :

1. Al- Edresy M., O Wasel S., Al- Hagibi A., echological risk assessment of heavy metals in coastal sediments between Al- haymah and Al- mokha, south red sea, yemen, 2019, international journal of hydrology.

2. Hakanson L., ecological risk index for aquatic pollution control, a sedimentological approach, 1980, water Res 14: 975- 1001

3. Müller, G., the heavy metal pollution of the sediments of Neckars and its tributary: a stocktaking, 1981, scientific Research.

4. Sharifuzzaman S.M., Rahman H., Ashekuzzaman S.M., Islam M., Chowdhury R., Hossain M., heavy metals accumulation in coastal sediments, 2016, Springer Japan.

5. Zou, correlation and simple linear regression 1, 2003, department of Radilogy, Harvard medical School.

2nd International Conference on Oceanography for West Asia

16 , 17 Sept. 2020 Iran. Tehran

First records of two Naididae (Annelida: Oligochaeta) species from Cheshmehkileh and Sardabrood estuaries in the South Caspian Sea, Iran

Erfani, Meysam

Coldwater Fishes Research Center, Iranian Fisheries Science Research Institute, Agricultural Research, Education and Extension Organization, Tonekabon, Iran.

meysamtavoli@yahoo.com

***Keywords**: First record, Nais elinguis, Nais variabilis, Estuaries, South Caspian Sea.*

1. Introduction

Aquatic oligochaetes is one of the main groups of macroinvertebrates and include about 1100 species of 13 families (Martin *et al*., 2008) and have a worldwide distribution. They commonly inhabit sediments of rivers, streams, lakes, marshes, ponds, springs and ground-waters (Collado and Schmelz, 2001) showing that this species has been adapted to a very wide variety of habitats and environments, such as freshwater, brackish or sea water. Naididae is a large group of freshwater oligochaete (Smutna *et al*., 2008), while 238 Naididae species are known worldwide (Martin *et al*., 2008) of which approximately 26 species belong to the genus *Nais*.

Among studies which have been done on aquatic macroinvertebrates fauna in Iran, oligochaetes have been identified at the family level, and a few studies have been carried out at the species level. Besides, some work has been done regarding the Oligochaeta in Iran such as Stephenson (1920), Egglishaw (1980), Pourang (1996), Aliyev and Ahmadi (2010), Ahmadi *et al.* (2011, 2012), Ardalan *et al.* (2011), Basim *et al.* (2012), Jablonska and Pesic, (2014) and Nazarhaghighi *et al.* (2014). Upon these findings, 23 species of aquatic oligochaetes have been reported from inland waters of Iran so far, 11 species from Naididae and only 2 species from genus *Nais*: *N. Communis* (Stephenson, 1920) and *N. Pardalis* (Nazarhaghighi *et al*., 2014).

The aim of this study is to introduce *Nais elinguis* and *N. variabilis* from Iran for the first time and their distribution pattern along Cheshmehkileh and Sardabrood estuaries in South Caspian Sea basin.

2. Materials and methods

The Cheshmehkileh is a mountainous and permanent water river in North of Iran (Mazandaran province), originates in the Alamot region (Northen of Central Alborz mountains) with total length approximately 80 km,

average annual discharge 55 million m^3, average slop 6.5 % and basin area 1200 km^2 grafts to Caspian Sea on Tonekabon city. The Sardabrood is another mountainous and permanent water river in North of Iran (Mazandaran province), originates in the Kelardasht region (Northen of Central Alborz mountains) with total length approximately 67 km, average annual discharge 100 million m^3, average slop 6.4 % and basin area 450 km^2 grafts to Caspian Sea on Chalus city.

This study was carried out between November 2014 and September 2015 and random sampling was done at six stations with three replicates for each sampling along each river bimonthly (Fig. 1 and Table 1). Sampling was done using 0.03 m^2 Van Veen grab for soft sediments at estuary area and 0.1 m^2, 0.2 mm-mesh size Surber for inner parts of the river with pebbles.

In total, 72 sediment samples were collected. The Samples were fixed *in situ* using a 5% formalin solution. In the laboratory, sediments were sieved through mesh sizes of 1, 0.5 and 0.25 mm and specimens were preserved in 70% ethanol and then sorted and counted under a stereomicroscope (Nikon SMZ800, Japan) and eventually wet weight of worms were measured by digital balance (0.0001 gr, Mettler Toledo, AB204-N). For identification at species level, worm specimens were mounted on slide glasses in Amman's lactophenol clearing agent (Smith, 2001) and covered by a coverslip and left for several hours to a day or two, and then for observation of setae and other details using microscope (Nikon E200 & Nikon DIGTAL SIGHT DS Camera, Japan). The main identification keys used were Pinder (2010), Krieger and Stearns (2010), Smith (2001), Pinder and Brinkhurst (1994), Brinkhurst and Wetzel (1984), Brinkhurst (1986, 1971a,b). The statistical analysis was performed by SPSS 22. Previous to the analysis, data were tested for the normality using Kolmogorov-Smirnov test. In case if the data were normal, one - way analysis of variance (ANOVA) test was used to determine the relationship between the biological variables among the stations and months of sampling.

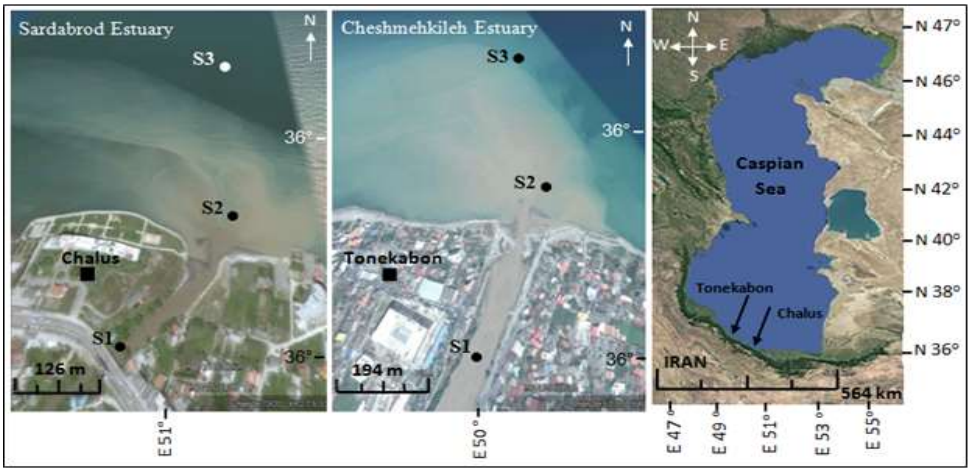

Figure 1) Study areas and location of sampling stations in Cheshmehkileh and Sardabrood estuaries.

Table 1) Sampling stations characteristics

Station	Latitude	Longitude	Sampling location	Water type	Substratum nature
S1	N 36° 49' 6.3"	E 50° 52' 52.3"	Cheshmehkileh river	Freshwater	Gravel, Sand, Silt, Clay, Vegetation
S2	N 36° 49' ۲۰/۰"	E 50° 53' 9.3"	Cheshmehkileh river mouth	Semibrackish	Gravel, Sand, Silt
S3	N 36° 49' ۳۵/۹"	E 50° 53' 24.6"	Cheshmehkileh estuary	Brackish	Sand, Silt, Clay
S1	N 36° 41' ۱۱/۹"	E 51° 23' 55.4"	Sardabrood river	Freshwater	Gravel, Sand, Silt, Clay, Vegetation
S2	N 36° 41' ۲۲/۲"	E 51° 24' 8.7"	Sardabrood river mouth	Semibrackish	Gravel, Sand, Silt
S3	N 36° 41' ۳۹/۹"	E 51° 24' 26.3"	Sardabrood estuary	Brackish	Sand, Silt, Clay

3. Results

The systematic account and description for the described species is as follows:

Kingdom: Animalia **Phylum:** Annelida Linnaeus, 1758 **Class:** Clitellata Linnaeus, 1740 **Subclass:** Oligochaeta **Order:** Haplotaxida Grube, 1850 **Family:** Naididae Ehrenberg, 1828 **Subfamily:** Naidinae Ehrenberg, 1828 **Genus:** *Nais* Müller, 1773 **1- Species:** *Nais elinguis* Müller, 1773 **2- Species:** *Nais variabilis* Piguet, 1906

Morphological descriptions:

- *Nais elinguis* Müller, 1773

Prostomium is without proboscis and most specimens have no eyes. Worms are olive gray or dark yellow with brown spots (Fig. 2A). Worms body were 1.4 to 2.9 mm in length, 0.1 to 0.3 mm in diameter and number of segments 12–28. Dorsal chaetae beginning in segment VI (Fig. 2B), hairs 1–3 per dorsal bundle (most worms have 2-3 hairs per bundle), 140–290 µm long, needles 1–3 per dorsal bundle (most worms have 2-3 needles per bundle) (Fig. 2E, F). The needles with two long parallel teeth, distal (upper) tooth slightly longer than proximal (lower) tooth, 35-70 µm long, with a distal nodulus (Fig. 2G). Ventral chaetae 2-5 per bundle, bifid crotchets, 40–105 µm long, with a median or slightly distal nodulus, those of II-V 4–5 per bundle and slightly longer, straighter and thinner than the rest, with upper tooth 1.5–2 longer and thinner than lower (Fig. 2D), Posterior Ventral chaetae 2-3 per bundle (Fig. 2C). No sexual individuals were detected during study period.

- *Nais variabilis* Piguet, 1906

Prostomium is without proboscis and most specimens have no eyes. Worms are olive gray or dark yellow with brown spots (Fig. 3A). Worms body were 0.9 to 2.6 mm in length, 0.1 to 0.3 mm in diameter and number of segments 10–35. Dorsal chaetae beginning in segment VI (Fig. 3B), hairs 1–2 per dorsal bundle (most worms have 1 hairs per bundle), 110–250 µm long, needles 1–2 per dorsal bundle (most worms have 1 needles per bundle) (Fig. 3E, F and G). The needles with two short parallel teeth, 32-70 µm long, with a distal nodulus (Fig. 3G). Ventral chaetae 2-5 per bundle, bifid crotchets, 40–95 µm long, with a median or slightly distal nodulus, upper

tooth 1.5–2 longer and thinner than lower (Fig. 3C and D), Posterior Ventral chaetae 2-3 per bundle (Fig. 3D). No sexual individuals were detected during study period.

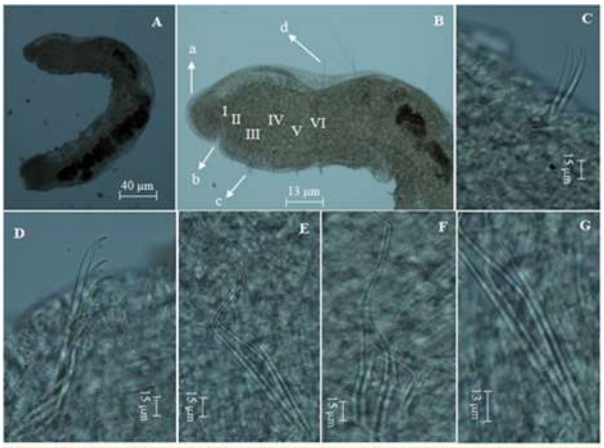

Figure 2) *Nais elinguis* A, General body form; B, Anterior end of the body (a: Prostomium; b: Mouth; c: Ventral bundle; d: Dorsal hair chaetae beginning in segment VI); C, Ventral chaeta bundle in posterior part of body; D, Ventral chaeta bundle in anterior part of body; E, Dorsal chaeta bundle (2 hairs and 2 needles); F, Dorsal chaeta bundle (3 hairs and 3 needles); G, 2 dorsal needles chaeta.

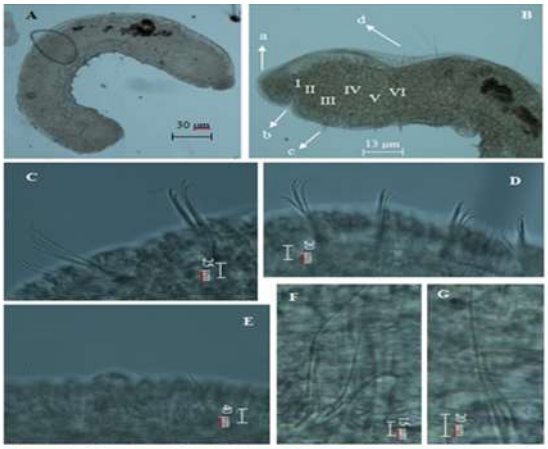

Figure 3: *Nais variabilis*. A, General body form; B, Anterior end of the body (a: Prostomium; b: Mouth; c: Ventral bundle; d: Dorsal hair chaetae beginning in segment VI); C, Ventral chaeta bundle in posterior part of body; D, Ventral chaeta bundle in anterior part of body; E, Dorsal chaeta bundle (1 hair and 1 needle); F, Dorsal chaeta bundle (2 hairs and 2 needles); G, 1 dorsal hair and needle chaeta.

4. Discussion and conclusion

During one year sampling in Cheshmehkileh and Sardabrood estuary, 526 individuals of *Nais elinguis* and 396 individuals of *Nais variabilis* were examined. These species were recorded for the first time from Iran. This paper updated a short checklist of Iranian aquatic oligochaetes to 25 species (for Naididae to 13 species and for *Nais* genus to 4 species). In Table 2, the identified species of Naididae from Iran until now are listed and these species (*N. elinguis* and *N. variabilis*) were not in the list. In this study, *N. elinguis* and *N. variabilis* were permanent inhabitant during all period of sampling.

Table 2) List of identified Naididae species from Iran

	Species	Reference
1	*Aulophorus furcatus* Oken, 1815	Ahmadi *et al.*, 2012
2	*Chaetogaster diastrophus* Gruithuisen,1828	Stephenson, 1920
3	*Chaetogaster limnaei* Baer,1827	Stephenson, 1920; Jablonska and Pesic, 2014
4	*Dero dorsalis* Ferroniere, 1899	Jablonska and Pesic, 2014
5	*Dero digitata* Müller, 1773	Nazarhaghighi *et al.,* 2014
6	*Nais communis* Piguet, 1906	Stephenson, 1920
7	*Nais pardalis* Piguet, 1906	Nazarhaghighi *et al*., 2014
8	*Ophidonais serpentina* Müller, 1774	Ardalan *et al*., 2011; Nazarhaghighi *et al*., 2014
9	*Pristina breviseta* Bourne, 1891	Jablonska and Pesic, 2014
10	*Stylaria lacustris* Linnaeus, 1767	Stephenson, 1920; Aliyev and Ahmadi, 2010; Ahmadi *et al*., 2012; Nazarhaghighi *et al*., 2014
11	*Slavina appendiculata* dUdekem, 1855	Nazarhaghighi *et al*., 2014
12	*Nais elinguis* Müller, 1773	Present study
13	*Nais variabilis* Piguet, 1906	Present study

According to the results of this study, *N. elinguis* and *N. variabilis* strongly peaked at the initial cold period (from November to May) and falls at the time of summer solstice. The peak (higher mean numbers) appeared to link to the rather instable river flow regime (the first spate sampled) and the time of strong discharge fluctuations.

The naid oligochaete *N. elinguis* and *N. variabilis* were only observed in station 1 and 2, higher in fresh water than brackish ecosystems, in both Cheshmehkileh and Sardabrood estuaries, while commonly found around the world in freshwater, tidal freshwater, and sometimes in brackish environments, it is rarely observed in higher salinity like marine coastal waters (Verdonschot, 1999). Density of these species in Cheshmehkileh estuary were higher than Sardabrood.

References

1. Ahmadi, R., Mohebbi, F., Hagigi, P., Esmailly, L. and Salmanzadeh, R., 2011. Macro-invertebrates in the Wetlands of the Zarrineh estuary at the south of Urmia Lake (Iran). *International Journal of Environmental Resources*, 5(4), 1047-1052.

2. Ahmadi, R., Aliyev, A., Seidgar, M., Bayramov, A. and Ganji, S., 2012. Macroinvertebrate communities differences on riverine parts and reservoirs of Zarrineh river. *American Journal of Agricultural and Biological Sciences*, 7(1), 71-75.

3. Aliyev, A. and Ahmadi, R., 2010. Biodiversity of benthic invertebrates in Aras river. *Iranian Scientific Fisheries Journal*, 19: 131-142.

4. Ardalan, A.A., Mooraki, N. and Sadeghi, M.S. 2011. Occurrence of *Ophidonais serpentina* in Potamon persicum from Jajrood river, Iran. *Iranian Journal of Fisheries Sciences*, 10 (1): 177-180.

5. Basim, Y., Farzadkia, M., Jaafarzadeh, N. and Hendrickx, T., 2012. Sludge reduction by *Lumbriculus variegatus* in Ahvaz wastewater treatment plant. *Iranian Journal of Environmental Health Science & Engineering*, 9, 4, 5p.

6. Brinkhurst, R.O., 1971a. The aquatic Oligochaeta known from Australia, New Zealand, Tasmania, and the Adjacent Islands. University of Queensland Papers, Department of Zoology, III(8), 34.

7. Brinkhurst, R.O., 1971b. A guide for the identification of British aquatic Oligochaeta. Freshwater biological association, Scientific publication, Titus Wilson & Sons LTD. Kendal, 22, 55.

8. Brinkhurst, R.O. and Wetzel, M.J., 1984. Aquatic Oligochaeta of the world: supplement a catalogue of new freshwater species, descriptions and revisions. *Canadian Technical Report of Hydrography and Ocean Sciences*, 44, 101.

9. Brinkhurst, R.O., 1986. Guide to the freshwater aquatic Microdrile oligochaetes of North America. *Canadian Special Publication of Fisheries and Aquatic Sciences*, 84, 259.

10. Collado, R. and Schmelz, R.M., 2001. Oligochaete distribution patterns in two German hardwater lakes of different trophic state. *Limnologica*, 31(4):317-328.

11. Egglishaw, H.J., 1980. Benthic invertebrates of streams on the Alburz Mountain Range near Tehran, Iran. *Hydrobiologia*, 69 (1-2): 49-55.

12. Jablonska, A. and Pesic, V., 2014. Five species of aquatic oligochaetes new to Iran with an updated checklist. Oceanological and Hydrobiological Studies, *International Journal of Oceanography and Hydrobiology*, 43(1), 100-105. Doi: 10.2478/s13545-014-0121-3.

13. Krieger, K. A. and Stearns, A. M., 2010. Atlas of the aquatic oligochaete worms. Recorded at the Old Woman Creek, Heidelberg University, Ohio, USA, 32 P.

14. Martin, P., Martinez-Ansemil, E., Pinder, A., Timm, T. and Wetzel, M.J., 2008. Global diversity of oligochaetous clitellates ("Oligochaeta"; Clitellata) in freshwater. *Hydrobiologia*, 595:117-127.

15. Nazarhaghighi, F., Timm, T., Mousavi Nadoushan, R., Shabanipour, N., Fatemi, M.R. and Mashinchian Moradi, A., 2014. Oligochaetes (Annelida, Clitellata) in the Anzali International Wetland, north-western Iran. *Estonian Journal of Ecology*, 63(3), 130-144. Doi: 10.3176/eco.2014.3.02.

16. Pinder, A.M. and Brinkhurst, R.O., 1994. A preliminary guide to the identification of the microdrile Oligochaeta of Australian inland waters. Cooperative research center for freshwater ecology, Albury, 1, 144.

17. Pinder, A., 2010. Tools for identifying selected Australian aquatic oligochaetes (Clitellata: Annelida). Museum Victoria Science Reports, 13, 1-26.

18. Pourang, N., 1996. Heavy metal concentrations in surficial sediments and benthic macroinvertebrates from Anzali wetland, Iran. *Hydrobiologia*, 331: 53-61.

19. Smith, D.G., 2001. Pennak's freshwater invertebrates of the United States, Porifera to Crustacea. Fourth edition, Johns Wiley & Sons, 664 P.

20. Smutna, M., Hilscherova, K., Paskova, V. and Marsalek, B., 2008. Biochemical parameters in *Tubifex tubifex* as an integral part of complex sediment toxicity assessment. *J. Soil. Sediment*, 8:154-164.

21. Stephenson, J., 1920. On a collection of Oligochaeta from the lesser known parts of India and from eastern Persia. Memoirs of the Indian Museum, 7 (3): 191-261.

22. Verdonschot, P.F.M., 1999. Micro-distribution of oligochaetes in a soft-bottomed lowland stream (Elsbeek; The Netherlands). *Hydrobiologia*, 406:149-163.

2nd International Conference on Oceanography for West Asia

16 , 17 Sept. 2020 Iran. Tehran

Harmful Algal Bloom (HABs) Problems for Marine Cage Culture (with Emphasis on West Asian Waters)

Ghanaatian, H. [1,2,4]; Hoveizavi, Sh. [1*]; Chenari, F. [3]; Jamali, H. [4]

1. Marine Biology Department, Marine Science and Oceanography Faculty, Khorramshahr University of Marine Science and Technology (KMSU), Khorramshahr, Khuzestan, Iran

2. Marine Fish Hatchery Department, Niksa Co., Tehran, Iran

3. Mariculture Department, Mahiran, Protein Gostar Sina Co., Tehran, Iran

4. Iranian Fisheries Organization (IFO), Bushehr, Iran

[*]shafa2004@gmail.com

Abstract:

Harmful algal blooms (HABs) are a natural phenomenon caused by some planktonic species, especially dinoflagellates. Despite the naturalness of this phenomenon, in addition to natural stresses, anthropogenic pollutions and the entry of municipal and industrial effluents and sewage into aquatic ecosystems cause the stability and intensification of this phenomenon. Increasing the rate of this natural phenomenon in aquatic environments leads to economic reduction of fishery, aquaculture. It may effect on human health and will cause some environmental impacts. In recent years, marine cage culture has flourished in West Asia include Persian Gulf and Oman Sea. A potential hazard to this industry is HAB. Anticipating ways to deal with this potential phenomenon will help manage cage farms in times of crisis. Three effective ways to control this phenomenon are mechanical controls, including the use of clay or ultrasonic waves, biological controls, and finally chemical controls. In this study, the risk of available methods is investigated and the method that has the least risk to the environment and farmed fish is proposed.

Keywords: *Cage culture, Red tide, Persian Gulf, Oman Sea*

2nd International Conference on Oceanography for West Asia

16 , 17 Sept. 2020 Iran. Tehran

Effect of Carbonate Content on Geotechnical properties of subseafloor Sediments in the Northern Persian Gulf

Fattahi Bandpey, Maryam [1]; Hafezi Moghaddas, Naser [2]; Ghafoori, Mohammad [3]; Moussavi Harami, Reza [4]; Kazem Shiroodi, Sadjad[5]

1. Geology Department, Ferdowsi University of Mashhad, Mashhad, Iran, m.fattahibandpey@mail.um.ac.ir
2. Geology Department, Ferdowsi University of Mashhad, Mashhad, Iran, nhafezi@um.ac.ir
3. Geology Department, Ferdowsi University of Mashhad, Mashhad, Iran, Ghafoori@um.ac.ir
4. Geology Department, Ferdowsi University of Mashhad, Mashhad, Iran, Harami@um.ac.ir

Iranian offshore oil company IOOC, Tehran, Iran, sshiroodi@iooc.co.ir

Keywords: *Persian Gulf, Marine sediments, Shear strength, Carbonate content, Atterberg limits,*

1. Introduction

In this paper, the effect of carbonate content on geotechnical properties of subseafloor sediments of northern Persian Gulf, were studied. The Persian Gulf is surrounded by Arabian platform in the south and Zagros mountain range in the north and is structurally a part of the Zagros simply folded belt. This basin is a marginal, epicontinental sea with a length of about 1000 and width of 200 to 300 km, covering an area of approximately 226,000 km2. The average water depth is about 35 m. The northern part of the Persian Gulf is deeper than the southern part of this basin. Iranian coastline, northern part, consists of the steeply dipping anticlines trending NW-SE. In the southern part, the Arabian marine shelf is wider and gentler, with less water depth than the Iranian shelf. This basin can be separated into two major sedimentary basins: a northern, Iranian part, which is strongly influenced by fluviatile sedimentation, and a southern, Arabian part, carbonate domain of mainly autochthonous, pure carbonates with aeolian-derived siliciclastic admixture.

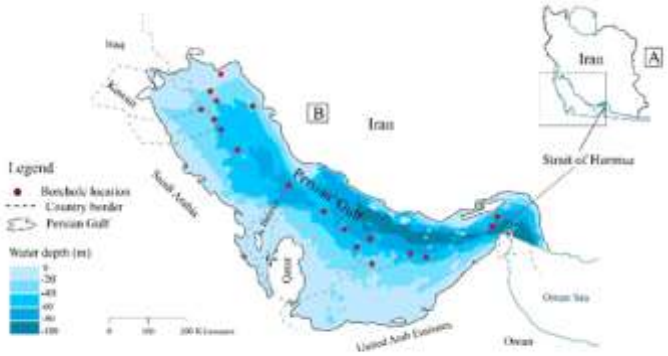

Figure 1) Study area: Iranian (northern) part of Persian Gulf and locations of boreholes.

2. Materials and methods

Due to the lack of geotechnical databases of study area, the first and most important part of this research was thus to gather data and information as much as possible to develop a geotechnical database. Many site investigations have been carried out within the Iranian oil and gas fields of Persian Gulf over the years for numerous projects. The majority of these information is unpublished and resides in the archives of offices of the many oil companies and geotechnical labs in Iran. The authors have tried to gather as much as possible of this unpublished data to develop a geotechnical database to investigate the geological engineering condition of the study are. In the next step, scatterplots of geotechnical parameters versus carbonate content and depth were drawn to compare the relationship between geotechnical parameters to different values of carbonate content.

3. Results

Plots of shear strength versus depth for two group of sediments (carbonate content >40% and carbonate content <40%) illustrated different trends (Fig. 2). Shear strength in sediments with carbonate content <40% shows lower values with average about 9 KPa. The shear strength in the sediments with carbonate content >40% is variable and show higher values with an average about 45 KPa (Table. 1). Also results showed that by increasing the carbonate content, Atterberg limits were decreased.

Table 1) Average values of shear strength in two group of carbonate sediments

Carbonate content of sediment	Shear Strength (Su)		
	Min	Max	Average
Carbonate content <40%	1	40	9
Carbonate content>40%	1	200	45

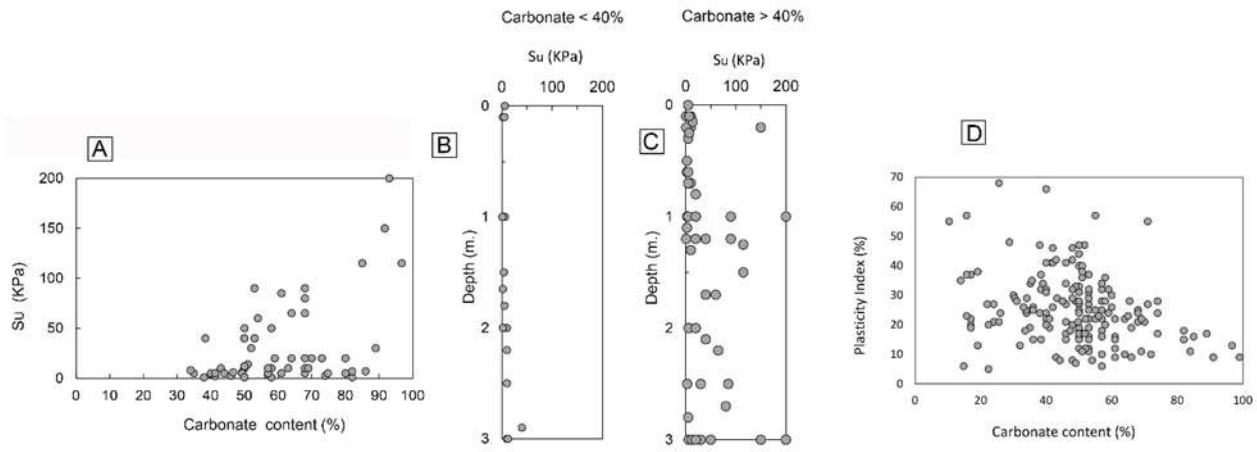

Figure 2) a. Variation of shear strength (Su) with carbonate content. b and c. Scatterplots of shear strength versus depth for two group of sediments (1. carbonate content >40% and 2.carbonate content <40%). d. Variation of plasticity index with carbonate content.

3. Discussion and conclusion

The effect of carbonate content on geotechnical properties of subseafloor sediments of northern Persian Gulf, was studied. Geotechnical data and information related marine structure in Iranian oil and gas fields were gathered and a geotechnical database was prepared. Scatterplots of some geotechnical parameters (Atterberg limits, shear strength) versus carbonate content were drawn to study the relationship between these parameters and variable amount of carbonate content. The most values of shear strength were related to sediments with higher percent of carbonate content. Also results showed that by increasing the carbonate content, Atterberg limits were decreased.

References

1. 1. Alavi, M., (2007). Structures of the Zagros fold-thrust belt in Iran. Am. J. Sci. 307 (9), 1064-1095

2. 2. Diester-Haas, L., (1973). Holocene climate in the Persian Gulf as deduced from grain-size andpteropod distribution. Mar Geol 14, 207–223.

3. 3. Purser, BH., Seibold, E., (1973). The principle environmental factors influencing Holocene sedimentation and diagenesis in the Persian Gulf. In: Purser BH (ed) The Persian Gulf: Holocene carbonate sedimentation and diagenesis in a shallow epicontinental sea. Springer, New York, pp 1–10

4. 4. Kassler, P., 1973. The structural and geomorphic evolution of the Persian Gulf. In: Purser BH (ed) The Persian Gulf: Holocene carbonate sedimentation and diagenesis in a shallow epicontinental sea. Springer, New York, pp 11–32.

5. 5. Kenter, J.A.M. and Schlager, W., 1989. A comparison of shear strength in calcareous and siliciclastic marine sediments. Mar. Geol., 88:145 152

6. 6. Demars, K.R. (1975). Strength and stress-strain behavior of deep-ocean carbonate soils. Ph.D. issertation, Department of Ocean Engineering, University of Rhode Island.

2nd International Conference on Oceanography for West Asia

16 , 17 Sept. 2020 Iran. Tehran

Estimation of the recent sedimentation rate in the eastern side of the southern Caspian Sea

Gerivani, Hadi[1*]; Putans, Victoria [2]; A.Lahijani, Hamid [1]

1. Iranian National Institute for Oceanography and Atmospheric Sciences, Tehran, Iran.
2. Shirshov Institute of Oceanology, Russian Academy of Sciences, Moscow, Russia.

Keywords *Sedimentation Rate; Southern Caspian Sea; Marine Geology; Holocene.*

1. Introduction

Sediment history of large lakes shows chronological records in sediments and also can provide valuable information about environmental changes [1-4]. Sedimentation rate has been taken into consideration as one of the important parameters to assess the history of sedimentation process in a basin.

In the southern Caspian Sea (CS), the western side of the basin is characterized by high sedimentation rate and some studies presented estimation of sedimentation rate for this area [5]. The rate of deposition has been estimated for deep area of the southern CS to be around 0.1–0.15 mm/yr [6-7]. According to the literature, there is not any estimation of sedimentation rate for the eastern side of the basin however due to low sediment supply by rivers; very low sedimentation rate is expected for this area.

The eastern coast of the southern CS is characterized by relatively gentle slope in sea and land [8]. From south to north, water depth increases from a few meters close to southern coastline to 1025 m in the center of southern Caspian basin [9-10]. The source of clastic sediments in the area comes from Kope-Dagh and Alborz mountains by several inflowing rivers including Tajan, Babolrud, Haraz, Neka and Talar [11]. According to Lahijani et al., 2019 [12], the area is fed by the calcareous formations that bring carbonates into the sea. Moreover, due to arid climate and the gentle slope shelf, conditions are favorable for chemical and biological activities that lead to carbonate enriched sediments. Siliciclastic sediments dominate in the west parts of the area.

The aim of the present study is estimating sedimentation rate in the eastern side of the southern CS analyzing four collected sediment cores.

2. Materials and methods

The four cores considered in this study (fig. 1) are located along a profile that starts from the depth of about 400 m close to the southern coastline (BS400) and continues NW, down to the depth of about 700 m (TS02). From the morphological

point of view, the study area includes a shelf area with the width of around 50 km in the south, then a relatively steep slope between the water depth of 100 m and 550 m where the cores BS400 and BS500 are located, and at the end, a wide area with gentle slope in water depth below 550 m where the cores BS600 and TS02 are situated. Using a MS2C Bartington Magnetic Susceptibility Meter, magnetic susceptibility (MS) of the intact sediment cores were measured at the INIOAS laboratory with 1 cm increment. Then the cores were split using a hand-made core splitter. XRF scanning were implemented on the two half cores that had already been analyzed for MS, to determine any geochemical changes along the cores BS400 and BS600, using an ITRAX core scanner at CEREGE laboratory, Aix-Marseille University. Mo tube with 30 kv, 45mA, 15s were used for scanning. Before scanning, the cores were radiographed for overall density and structure by 40 kv, 45mA, 400ms. Other half of the cores BS400, BS500 and BS600 were subsampled systematically. Totally, 201 sediment sub-samples were tested to measure Grain size, calcium carbonate, and organic matter (OM) contents for sedimentological analysis at the INIOAS laboratory. Prior to the sample treatments, all the samples were oven dried at 60°C. For each sample, dry sediments (4g) were burnt at 550°C for 4h to calculate O.M. contents and then the samples were burnt at 950°C for a further 2h to calculate carbonate contents. All samples were granulometrically characterized by a Horiba Laser Scattering Particle Size Analyzer la-950. It should be noted that the core ST02 had been analyzed by Lahijani et al., 2019 [12] with the same methods (except granulometrical analyses).

Using geochemical and sedimentary parameters, different beds were detected and correlated in the cores. Then, the ages of two main sedimentary events were determined, correlating with previous studies, which were used to estimate the rate of sedimentation.

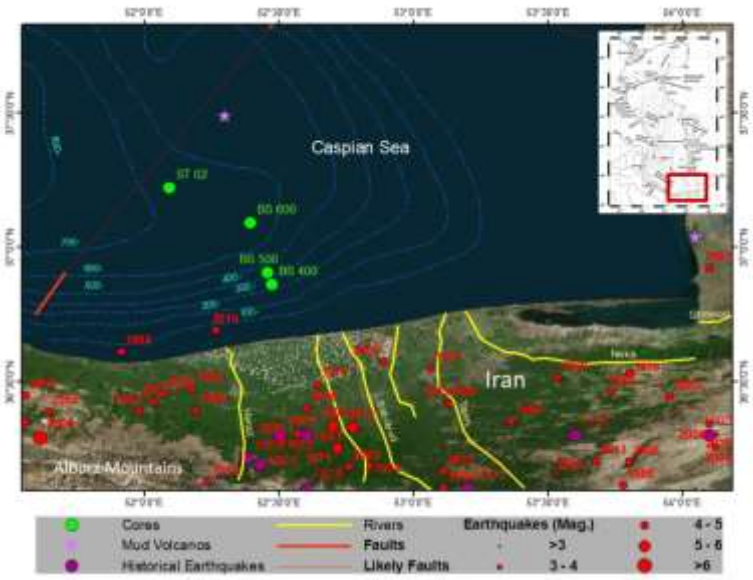

Figure 1) The map of the study area in the southern CS and the location of cores used in this study.

3. Results

Based on XRF scan analysis, different patterns of wiggling of the concentration of measured elements were observed for every core and also for different groups of elements. In the core of BS400, the concentration of most of the elements is decreasing from the core top down to 40 cm, increasing between 40 to 80 cm and thereafter stable down to the core bottom. In the core of BS600, lithogenic elements (Si, Zr, Ti, Mn, Rb, and Fe) show low variation along the core. The concentration of Ca and Sr (biogenic elements) are increasing from top to bottom of the core and are highly correlated

each other. In the core of ST02, the MS value shows two main peaks in the depth of 20-30 cm and 60-70 cm. Based on granulometrical analyses, all sediments in the BS400 fall within the range of medium to fine silts. Sand particles were detected just in a horizon at top of the core (4-6 cm). Coarse silts are observed in some horizons with maximum content less than 3% in horizon 4-6 cm from the top of the core. Clay and silt content behave in opposite trends. The MS varies through the core and seems to be in direct relationship with grain size. Generally, the MS value in the deeper part of the core is higher in compare to the upper part. The sediments of core BS500 generally are in the range of silt without any sand. The average and maximum amount of clay in the core are less than 18% and 25%, respectively. More than 70% of the sediments are composed of fine and very fine silts and coarse silt is evident just in three horizons in the upper and middle parts of the core. The calcium carbonate content oscillates with a trend opposite to that of O.M. content. Unfortunately, for this core, data of XRF scan has not been available and the photo was not taken with satisfy quality. Fine and very fine silts are the major sediment contributors of the core BS600. No sand particle was reported. Coarse silt is observed just in a horizon in depth 34 to 36 cm with content less than 1% and the average amount of medium silt in the core is less than 2%. The ratio of coarse and medium silts to very fine silt plus clay shows higher values for some horizons which seems to be in direct correlation with MS.

4. Discussion and conclusion

According to the different geochemical and sedimentological parameters, core loges were correlated as shown in figure 2 and then referring to previous studies, two main events in the area were detected and their ages were estimated. For proper correlating, step by step from the top to the base of the cores, we detected in both cores the same horizons according to the variation of different parameters (especially MS, Ca and Ti/Ca). The boundary between Holocene and Pleistocene in core ST02 was determined refereeing to previous studies and chemical characteristics of the sediments by Lahijani et al. (2019)[12]. The considerable change in core ST02 was observed at the depth of ~68 cm highlighted by a decrease of Ti and an increase of Ca which indicates the Holocene/ Pleistocene transition in the southern and central basins of the CS [6, 13, 14]. In addition, the sharp increase in MS values observed in ST02 waslinked to Amudarya River avulsion into the CS by Lahijani et al., (2019)[12] that brought detrital material into the basin and occurred around 5000 BP [15].

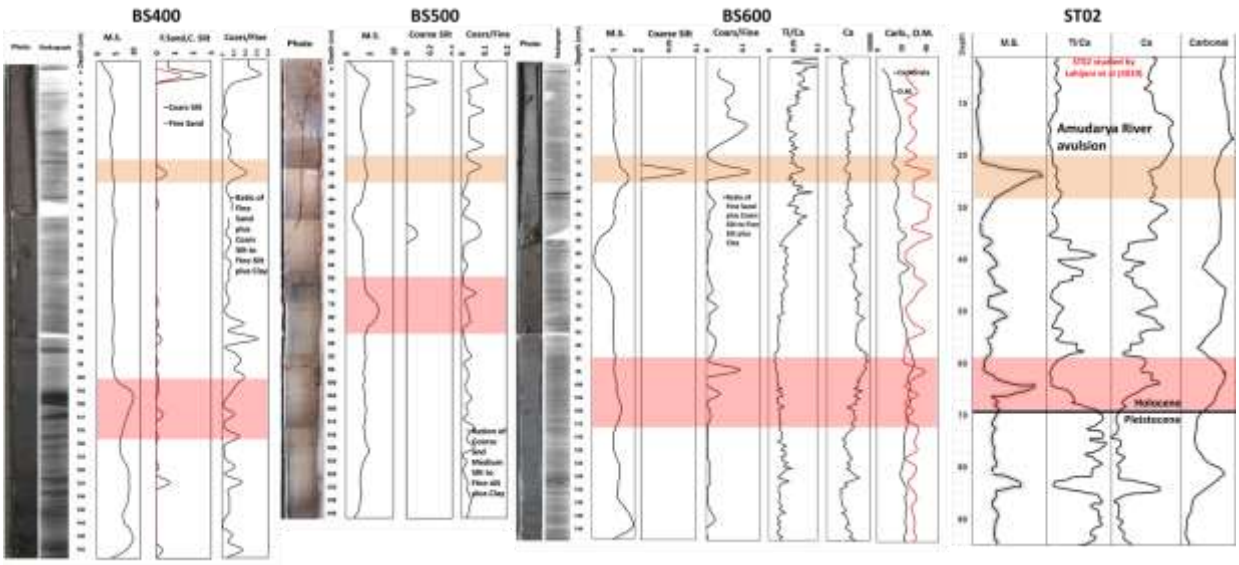

Figure 2) Correlation of the core logs.

Considering to the conditions discussed previously, relatively low sedimentation rate is expected for the eastern side of the southern CS; equal to or lower than 0.1–0.15mm/yr estimated for deep basin of CS in Holocene by Chalié et al. (1997) [6] and Pierret et al. (2012)[7]. Here, supposing the 5000 BP for the date of Amudarya River avulsion, the sedimentation rates are estimated between 0.07 and 0.04 mm/yr for the historical time of the southern CS as shown in figure 3. Supposing 11650 years for Holocene, average sedimentation rates for whole Holocene and the time between beginning of Holocene and 5000 BP are estimated 0.1-0.06 mm/yr and 0.12-0.07 mm/yr, respectively. Sedimentation rates for Holocene show a general declining trend like the rates for historical time but the rate for BS500 is lower than that is expected considering to the trend. Decreasing trend of the rates respect to distance from shoreline seems reasonable because for areas farther from the shoreline, energy of rivers and currents and consequently the size and volume of detrital sediments drop further. Lower sedimentation rate for BS500 probably happened as a result of mass movements in sea bottom during the time between beginning of Holocene and 5000 years BP.

The rate of sedimentation in the period before 5000 years ago is about twice that rate in the period after this time. Water level of the Caspian Sea increased very fast, around 18 m, during the beginning of Holocene and 7000 BP [16]. The higher rate of sedimentation in the period before 5000 BP occurred due to the fast rise in sea level which had been associated with enhanced rainfall intensity and increased terrestrial sediment delivery.

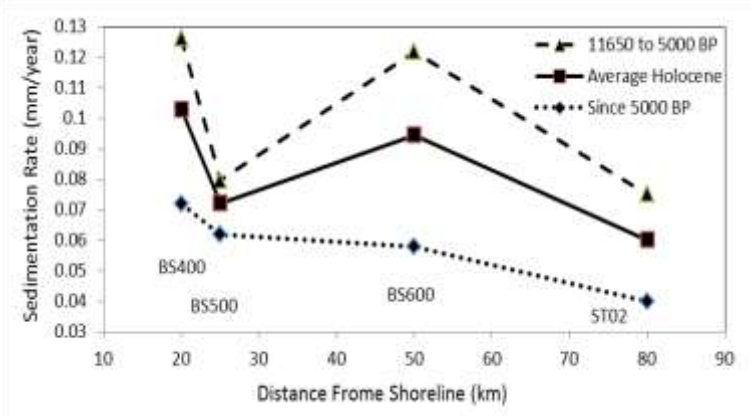

Figure 3) Estimated sedimentation rates for the cores during historical time and Holocene which show decreasing trends from shoreline to deep basin.

Acknowledgments:

Authors would like to thank the Iranian National Institute for Oceanography and Atmospheric Science for providing financial and laboratorial support. Also, authors would like to thank CEREGE laboratory of Aix-Marseille University for XRF Scan tests.

References

1. Colman SM, Baucom PC, Bratton JF, Cronin TM, McGeehin JP, Willard D, Zimmerman AR, Vogt PR (2002) Radiocarbon dating, chronologic framework, and changes in accumulation rates of Holocene estuarine sediments from Chesapeake Bay. Quat Res 57(1):58‑70.

2. Tylmann W, Bonk A, Goslar T, Wulf S, Grosjean M (2016) Calibrating ^{210}Pb dating results with varve chronology and independent chronostratigraphic markers: problems and implications. Quat Geochronol 32:1‑10.

3. Corcoran M, Sherif MI, Smalley C, Li A, Rockne KJ, Giesy JP, Sturchio NC (2018) Accumulation rates, focusing factors, and chronologies from depth profiles of ^{210}Pb and ^{137}Cs in sediments of the Laurentian Great Lakes. J Great Lakes Res 44(4):693‑704.

4. Abbasi, A. (2019) 210Pb and 137Cs based techniques for the estimation of sediment chronologies and sediment rates in the Anzali Lagoon, Caspian Sea. J Radioanal Nucl Chem 322, 319–330. https://doi.org/10.1007/s10967-019-06739-8.

5. Lahijani, H., Tavakoli, V., Amini, A., 2008. River mouth configuration in south Caspian coast, Iran. Environ. Sci. 5, 65–86.

6. Chalié, F., Escudié, A.-S., Badaut-Trauth, D., Blanc, G., Blans-Valleron, M.-M., Brigault, S., Desprairies, A., Ferronsky, V.I., Giannesini, P.-J., Gibert, E., Guichard, F., Jelinowska, A., Massault, M., Mélières, F., Tribovillard, N., Tucholka, P., Gasse, F., 1997. The glacial-post glacial transition in the southern Caspian sea. C. R. Acad. Sci. Paris, sér. IIa, t 324, 309–316.

7. Pierret, M.C., Chabaux, F., Leroy, S.A.G., Causse, C., 2012. A record of Late Quaternary continental weathering in the sediment of the Caspian Sea: evidence from U-Th, Sr isotopes, trace element and palynological data. Quat. Sci. Rev. 51, 40–55.

8. Lahijani, H.A.K., Rahimpour-Bonab, H., Tavakoli, V., Hosseindoost, M., 2009. Evidence for late Holocene highstands in central guilan–east mazanderan, South Caspian coast, Iran. Quat. Int. 197 (1), 55–71.

9. Leontiev, O.K., Maev, N.G., Richagov, G.I., 1977. Geomorphology of the Caspian Coast and Sea, Moscow State University, Moscow ([In Russian]).

10. Voropaev, G.V., 1986. The Caspian Sea: Hydrology and Hydrochemistry, Nauka, Moscow ([In Russian]).

11. Lahijani, H.A.K., Abbasian, H., Naderi Beni, A., Leroy, S.A., Haghani, S., Habibi, P., Hosseindust, M., Shahkarami, S., Yeganeh, S., Zandinasab, Z. and Tavakoli, V., 2018. Sediment distribution pattern of the South Caspian Sea: possible hydroclimatic implications. Canadian Journal of Earth Sciences, (999), pp.1-17.

12. Lahijani, H.A., Beni, A.N., Tudryn, A., Hosseindoust, M., Habibi, P. and Pourkerman, M., 2019. Unraveling extreme events from deep water cores of the south Caspian Sea. Quaternary International.

13. Jelinowska, A., Tucholka, P., Badau-Trauth, D., 1999. Magnetic mineral variations of South Caspian sea sediments at laminae scale. Phys. Chem. Earth 24 (9), 823–828.

14. Jelinowska, A., Tucholka, P., Guichard, F., Lefèvre, I., Badaut-Trauth, D., Chalié, F., Gasse, F., Tribovillard, N., Desprairies, A., 1998. Mineral magnetic study of late quaternary south Caspian sea sediments: palaeoenvironmental implications. Geophys. J. Int. 133 499–509.

15. Leroy, S., Marret, F., Gibert, E., Chalié, F., Reyss, J.-L., Arpe, K., 2007. River inflow and salinity changes in the Caspian Sea during the last 5500 years. Quat. Sci. Rev. 26 (25–28), 3359–3383.

16. Rychagov, G.I., 1997. Holocene oscillations of the Caspian Sea, and forecasts based on palaeogeographical reconstructions. Quat. Int. 41– 42, 167–172.

2nd International Conference on Oceanography for West Asia

16 , 17 Sept. 2020 Iran. Tehran

Adelie Penguin Habitats Affected by Climate Change

Ghanaatian, Hamed [1]; Safahieh, Alireza [1*]; Kabiri, Keivan [2]; Savari, Ahmad [1]

1. Marine Biology Department, Faculty of Marine Science & Oceanography, Khorramshahr University of Marine Science and Technology (KMSU), Khorramshahr, Khuzestan, Iran

2. Department of Marine Remote Sensing, Iranian National Institute for Oceanography and Atmospheric Science (INIOAS), Tehran, Iran

[*]safahieh@hotmail.com

Abstract:

Since the state of ice masses is known as one of the most sensitive indicators of climate change, studies on the Polar Regions are of particular importance. Antarctica is the southernmost continent on Earth in the southern hemisphere, surrounded by oceanic waters. Despite international administration and a relatively low human presence, Antarctica has been affected by human activities and various pollutions, including post-industrial greenhouse gases, have affected the region. Due to its small population (about 1,000 people in research centers) and its vast expanse of ocean, it is known as a pristine area that has made global climate change traceable. Adelie Penguins are one of the only five species of penguins living in the Antarctica. Changes in ice masses under the influence of climate change have had a direct impact on the quality of Adelie penguin's habitats and life. Remotely sensed sea surface temperature data and primary production in surrounded waters combined with sea ice concentration information for last two decades in models, indicate changes in habitat suitability of Adelie penguins. Regional migration and decrease on individuals and habitats for Adelie penguins forecasted based on data analyses and models.

Keywords: *Pygoscelis adeliae, Antarctica, Global warming, Southern Ocean*

1. Introduction

The Antarctica is the only continent to be governed by the surrounding waters under an international treaty (ATS). Despite international administration and a relatively low human presence, Antarctica has been affected by human activities and various pollutions, including post-industrial greenhouse gases, have affected the region. Due to its small population (about 1,000 people in research centers) and its vast expanse of ocean, it is known as a unique area that has made global climate change traceable. A small number of vertebrates live in the Antarctica, most of which are confined to the subcontinental area and Islands. Antarctic marine animals include penguins, blue whales, killer whales, colossal squids, and fur seals. Among the few animals living in the Antarctic, penguins, which are considered seabirds, are prominent species.

Adelie penguins (*Pygoscelis adeliae*) are among five species of penguins living in the Antarctic (Adelie, Emperor, Gentoo, Chinstrap and Macaroni Penguins). Adelie penguins lay their eggs all over the Antarctic coasts and surrounding

islands wherever they are exposed to rocks. Among the 17 species of penguins, the most scientific studies have been done on Adelie species (Ainley and Pennycook, 2015). These penguins make their nests from pebbles found on land in the spring. They choose a sloping surface so that water can pass through the nest when the snow melts. Feeding is a problem in early spring; when the ice packs are not yet broken. They may have to walk more than 50 kilometers on ice to reach the sea before feeding. Penguins always return to the same nest and mate if they do not have a problem (Ainley, 2002).

Climate change means any specific change in patterns expected for the average climate situation, which occurs over a long period of time in a specific region or for the global climate as a whole. Climate change is due to fluctuations in the Earth, natural processes around it and the impact of human activity on it. External factors that can shape the climate are often called climatic forces and include processes such as fluctuations in solar radiation, the rotation of the Earth, and the amount of greenhouse gases.

Change in ice masses is known as one of the most sensitive indicators of climate change, which increases mainly during the cooling period (such as the short glacial period) and begins to decline during the warming period on average time scales (Ainley, 2002). Changes in ice masses have a direct impact on the quality of life of dependent animal species. Among these animals are penguins. Studies have shown that the presence or absence of Adelie penguins is directly related to the amount of ice masses in the surrounding waters. Adelie penguins are dependent on sea ice (icebergs, glaciers, ice sheets and ice shelves are all dry). When the ice cover of the ocean reaches 70%, the work becomes difficult for the penguins. 20% coverage is ideal. If the sea ice is completely gone, the penguins will disappear, but more subtle changes will be important before that (Ainley and Pennycook, 2015).

Penguins, can be included in the list of endangered and endangered species (in the annual observations of BirdLife International in 2011, the Adelie penguin was declared an endangered species, but in the past and future years it was considered the least concern and this indicates the borderline of this species (BirdLife International., 2011 & 2018)). In the present study, the habitats of Adelie penguins as a creature that is a pioneer to this variability (Ainley, 2002), using remote sensing technology, have been investigated. Finally, the future situation will be predicted using the habitat models.

2. Material and methods

Due to extended studied area size, environmental data was collected using satellite imagery and remote sensing techniques. These data include physical data such as surface water temperature (SST) and sea ice concentration (SIC), as well as bioavailability data such as chlorophyll a (CHL-*a*) changes. Due to the short food chain, high chlorophyll indicates the availability of penguin food sources. The SeaWiFS sensor on the SeaStar satellite with 8 bands in the optical range (VNIR) is primarily designed and used to measure chlorophyll (Zheng *et al*., 2017). MODIS sensor data (bands 8 to 16) are also used in chlorophyll studies in waters around the Antarctica (Zeng *et al*., 2016).

On the other hand, MODIS data is used to obtain water surface temperature; Landsat thermal bands (bands 10 and 11) are used for higher spatial resolution (Cahyono *et al*., 2017). In examining the extent of sea ice concentration, most

research focuses on the use of microwave (both passive and active (radar)) images, although thermal and optical have also been used.

3. Conclusion

Recent two decade data analyses showed that global warming has caused increase in sea surface temperatures and decrease in the ice surface of the Southern Ocean and surrounding seas especially in the Antarctic Western Cape and more northerly latitudes. Favorite habitats for Adelie penguin breeding colonies, towards the Ross Sea have increased and some restriction happened to north west areas like Antarctic peninsula and higher latitude Islands. Results indicate that continuation of the current trend of global warming, threatens the desirability of the current habitats of Adelie penguins.

Climate change affects the habitat suitability of organisms in different ways. Global warming seems to have affected Adelie penguins, their food resources and their environmental conditions, and it is likely that in the future years these valuable species will continue to drift from northern offerings to colder southern regions. Results for this study indicate that sea ice concentration (SIC), sea surface temperature (SST) and primary production that explained as available hunting rate in other studies and directly is related to CHL were among the most important environmental factors (Emmerson and Southwell, 2011; Ainley and Pennycook, 2015). Survey on sensitive environments and species known as bellwether of climate change will have significant benefits and existence of models that can predict the future will be of great help to international decision-makers.

References:

1. Ainley D. G., (2002) The Ade´lie Penguin: Bellwether of Climate Change. Columbia University Press, New York.
2. Ainley, D. and Pennycook, J., (2015). Adelie Penguin Response to Climate Change at the Individual, Colony and Metapopulation Levels., Penguin Science in hopes of attracting future scientists to the field project. Los Gatos , California.
3. BirdLife International., (2011). Pygoscelis adeliae. The IUCN Red List of Threatened Species 2011.
4. BirdLife International., (2018). Pygoscelis adeliae. The IUCN Red List of Threatened Species 2018.
5. Cahyono, A. B., Saptarini, D., Pribadi, C. B. and Armono, H. D., (2017). Estimation of Sea Surface Temperature (SST) Using Split Window Methods for Monitoring Industrial Activity in Coastal Area, Applied Mechanics and Materials, 862: 90-95.
6. Emmerson, L., Southwell, C., (2011). Ade´lie penguin survival: age structure, temporal variability and environmental influences. Oecologia, 167: 1–15.
7. Zeng, C., Xu, H. and Fischer, A. M., (2016). Chlorophyll-a Estimation Around the Antarctica Peninsula Using Satellite Algorithms: Hints from Field Water Leaving Reflectance. Sensors, 16(12): 2075.

8. Zheng, G. and DiGiacomo, P. M., (2017). Remote sensing of chlorophyll-a in coastal waters based on the light absorption coefficient of phytoplankton. Remote Sensing of Environment, 201: 331-341.

2nd International Conference on Oceanography for West Asia

16 , 17 Sept. 2020 Iran. Tehran

Cost Analysis in Rubble Mound Breakwater Design in Fishing Port (Case Study Multipurpose Breakwaters in Persian Gulf and Oman Sea)

Ghasemi, Ali [1*]; Rezaee Mazyak, Ahmad [1]; Hoseini, Seyed Mehdi [2]

1*. Pars Geometry Consultants, ghasemi.ali89@gmail.com

1. Tarbiat Modares University, ahmadrezaee2010@gmail.com

2. Qom University, hosseinimehdi1373@gmail.com

Keywords*: Rubble Mound breakwater, Fishing ports, Cost Analysis*

1. Introduction

A breakwater is a structure constructed to form a harbor with a basin so protected from the effect of waves to provide safe berthing for fishing vessels and other types of ships. Constructing breakwaters is the major part of the harbor cost construction. In some codes, the following steps are considered for breakwaters design: determine project requirement, technical and design consideration, cost aspect, environmental consideration, and social face[1].

In project definition and initial design, cost analysis played a vital role in selecting the type of breakwater. In this study, cost analysis and volume material examination for fishing port have done.

Multipurpose Breakwaters

In the present study, some ports on the Iranian coasts of Persian Gulf and Oman Sea like Mollou, Berkeh Soflein, Suza, Surgalm, Jod, Goordim, and Guater have examined. The location and layout of these harbors respectively display in Figure 1 and Figure 2. Also, port characteristics, hydraulic situations, and transport distance for different ports exhibited in table 1.

Figure1) Location of ports in coast line

Table 1) Breakwaters characteristics

B.W name	B.W Length (m)	Depth of entrance (m C.D)	Max. design wave height (m)	Transport distance (km)
Berkeh Soflein	1025	-3.6	1.71	12
Mollou	1110	-3.6	3.01	15
Suza	1124	-5.0	2.84	8
Surgalm	1687	-2.5	2.96	30
Jod	1705	-3.5	3.1	15
Goordim	1100	-3.5	3.28	3
Guater	860	-3.6	3.35	25

Figure2) Layout of Harbours

Guater, Goordim, Jod, and Surgalm are ports which on the northern coast of Oman Sea. So, they are facing waves coming from oceans. On the other hand, Berkeh Soflein, Mollou, and Suza are on the Persian Gulf.

2. Results

In the following, the materials used for each layer and cost of different layers compared for mentioned harbors. For example result for Guatr harbor demonstrated in figure 2-A ,and figure 2-B. By checking these diagrams for all mentioned harbors, it turns out that while the most considerable part of the material volume ratio belongs to the core layer, the amour layer plays a vital role in coast ratio.

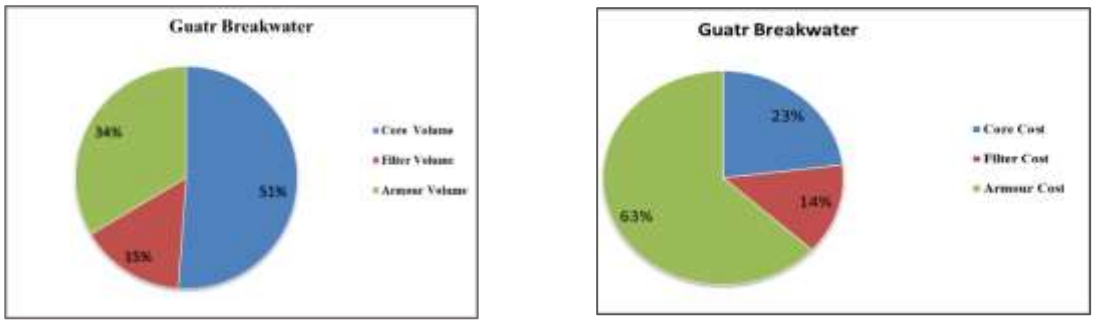

A **B**

Figure3) A: Material volume ratio for each layer B: Cost ratio for each layer

Evaluation of the results of the present study shows that the average consumption of filter and armor layers were 8% and 10% more than Rock Manual results, respectively. This difference is due to the project implementation conditions and quality of materials in our country.

A comparison of used materials shows the material volume is proportional to $(\text{Depth})^2$ in armor core layer. According to this study, the results of comparing the volume of used materials for different layers with the entrance depth and the wave height are presented in Table 2[2].

Table 2) Material volume proportion and calibration to parameters

Layer	Volume proportion According to Rock Manual (%)	Volume proportion According to this study (%)	Proportionality to Depth	Proportionality to Wave Height
Core	40-70	45-55	$\propto \text{Depth}^2$	–
Filter	5 – 20	15-25	$\propto \text{Depth}$	–
Armor	10 - 30	25-35	$\propto \text{Depth}$	$\propto H_s^{3.73}$

In consideration of the study area, the material volume per meter, and the cost per meter for each breakwater are displayed in Table 3. In this cost analysis, the effect of transport distance is considered.

Table 3. Used material and cost per meter

Breakwater	Used material Volume (per meter)	Cost per meter (million rial)
Berkeh Soflein	119	75
Mollou	188	170
Suza	259	324
Surgalm	173	305
Jod	278.9	484
Goordim	247	278
Guatr	281	478

3. Conclusion

In this study, cost analysis and material volume study analysis have done by using collected data from different projects on the southern coast of the Persian Gulf and Oman Sea. By consideration of the location of the project, this study can help engineers to estimate the cost and volume of material for different layers of the breakwater.

References

1. U. S. A. C. O. Engineers, Coastal engineering manual, vol. 1110. 2002.
2. C. I. Research, I. Association, C. C. U. R. en R. (Netherlands), and C. d'études maritimes et fluviales (France), The rock manual: the use of rock in hydraulic engineering, vol. 683. Ciria, 2007.

2nd International Conference on Oceanography for West Asia

16 , 17 Sept. 2020 Iran. Tehran

Characterization of a growth anomaly in *Acropora valida* corals of the Gulf of Oman

Ghazilou, Amir [1*]; Ershadifar, Hamid [1]; Kor, Kamalodin [1]

1. Iranian National Institute for Oceanography and Atmospheric Science

Keywords: *epitheliomas; hard coral; skeleton; aragonite*

1. Introduction

Corals have become increasingly afflicted with diseases caused by both external factors and internal malfunctions (Rosenberg and Loya, 2013). The common signs of a coral disease include bleaching, tissue loss, abnormal growth, and/or mortality. Growth anomalies (GAs) are more prevalent in Indo-pacific corals than Caribbean or Atlantic communities (Aeby et al., 2011). Hypertrophy, hyperplasia, and/or neoplasia may cause GAs (Kathryn et al., 2004). Hyperplastic masses are associated with the proliferation of all types of cells (with some levels of atrophy) and with the retention of pigmentation (Loya et al., 1984). In contrast, calicoblastic epitheliomas (CEs) are easily identified by their bleached appearance, indicating the loss of zooxanthellae from gastrodermal cells (Peters et al., 1986). The soft tissue of the CEs consists of proliferated gastrovascular canals and associated calicoblastic epidermis (with no mucosal cells), leading to degenerated polyp structure (Peters et al., 1986). CEs have been reported from *Acropora* populations in the southern Gulf of Oman (Coles and Seapy, 1998). The tumors appeared as dense masses 2 mm to 5 cm in diameter on *Acropora valenciennesi* corals. The severity of CEs can be high, with up to 43 tumors per colony in 1993. The growth rates of single masses were >10 mm/y.

A CE outbreak was observed during winter 2020 on *Acropora* corals in Chabahar Bay in the northern Gulf of Oman. The aim of this study was to determine the prevalence of CEs in *Acropora valida* populations in Chabahar Bay and to characterize the texture and main chemical composition of the skeletons in the CEs.

2. Materials and methods

Study area

Coral reefs in Chabahar Bay are mainly within its eastern border (25.319160°N, 60.614798°E). The hard-coral fauna of the bay consists of 17 species in seven families distributed as both natural and transplanted patches

(Ajdari et al., 2013; Aminrad and Azini, 2013). A. valida and Pocillopora damicornis corals are abundant in the area (Ghazilou et al., 2019).

Sampling and analytical procedure

A primary field survey of CE prevalence and virulence was performed along a 100-m transect in January 2020. A 100-m tape measure was laid parallel to the shoreline at a depth of ~5 m, and all hard-coral colonies were photographed along four intermittent segments 20 m in length and 5 m in width (Hill and Loder, 2013). The results of our survey indicated that only Acropora corals were afflicted. Approximately 10 A. valida colonies with tumors were sampled and transferred to the laboratory. Each sample consisted of a region of tumor and adjacent normal branches. The samples were sonicated for 30 min in distilled water, and the tumor areas and a 1-m fragment of normal branches (approximately 0.5 cm below the branch tips) were carefully cut using stainless-steel scissors. A total of five sample sets were used for determining the organic-matter (OM) content using the loss-on-ignition method (Hoogsteen et al., 2018) and the total carbonate content using a Bernard calcimeter. The other sample sets were used for studying skeletal structure and composition. The soft tissues of these samples were removed by immersion in a commercial hypochlorite (~2.5% active chlorine) solution for 24 h (Altvater et al., 2017). The treated samples were cleaned in distilled water and used for further analyses .

The crystalline structures of powdered tissue samples were analyzed using a Philips PW1730 X-ray diffractometer (Cu-Ka beam, λ=1.540498 Å, 40 kV, 30 mA, step size=0.05 deg, 2Θ range=10-80), and the carbonate properties of both the normal branches and the tumors were investigated by Raman spectroscopy (Teksan®, Iran), with the laser line operating at 532 nm. The microstructure and texture of gold-coated samples were examined using scanning electron microscopy (SEM FEI Quanta 200) at 2 kV.

Selected elemental compositions of both types of tissue were analyzed by ICP-MS. (Loya et al., 1984) reported that CE formation in Acropora was induced by increased water temperature and the resultant exposure to ultraviolet

radiation. Only concentrations of temperature-tracer elements (Ca, Li, Sr, and Mg) were thus measured by ICP-MS (Hathorne et al., 2013). Half a gram of each sample (N=4 for normal tissue and N=4 for tumors, powdered) was dissolved in 25 ml of 0.3M HNO3 and diluted to 2% of the original concentration (modified from (Hathorne et al., 2013)).

Statistical analysis

An independent t-test was used to compare total OM and carbonate contents and elemental ratios between normal tissue and tumors. The data were assessed for assumptions of normality and homoscedasticity using Shapiro-Wilk and Levene's tests, respectively.

3. Results

The tumors were assigned to type-A growth anomalies (nodular masses with a few large polyps fused together (Fig. 1a) and exhibiting a lower degenerative status compared to type-B growth anomalies (Burns et al., 2011)) based on gross morphology. Tumor prevalence was 7.7± 0.6% (mean± SD) at the study site, and mean severity (expressed as the percentage of the total planar area affected per colony) was 17.5 ±2.5%. The number of masses per colony varied from 1 to 6 (2.5±1.69 masses per colony).

OM and carbonate contents were ~50% lower in the tumors (Table 1). X-ray diffraction indicated that both tumors and tumor-tissue skeletons contained single-phase aragonite (Fig. 1b). The Raman spectra confirmed the aragonite nature of the skeletons (peaks at positions ~150, 203, 705, and 1085 cm−1). A weak peak was also detected in the tumor spectra at the 270 cm−1 position (Fig 1c).

The Sr/Ca and Na/Ca ratios were the lowest and highest element/Ca ratios in the tumor skeletons, respectively, and Mg/Ca was the highest ratio in normal tissue. Comparisons between tissues indicated higher Na/Ca and Mg/Ca ratios in the tumor-tissue skeletons (Table 1).

Shingles (i.e. skeletal fibers) were present on the skeletal surfaces of both normal tissues and tumors (Fig. 1d, e). Shingles were present throughout the tumor area, but no shingle-like structures were detected in some parts of the coenosteal spinulae of normal tissue (Fig. 1d). The growing fronts of the shingles were more extended, and the inter-shingle distances were smaller, in the tumors (Fig. 1e).

4. Discussion and conclusion

Only a few studies have reported neoplasms (tumors) in hard corals, but they may be common. Neoplasms have been recorded from 10 genera of hard corals, with Acropora the most susceptible genus (Longin, 2006). We only observed CEs on Acropora. Acropora corals are generally very susceptible to bleaching, and successive bleaching events may hinder the resistance of these corals to disease (Muller et al., 2018; Pratchett et al., 2013).

The results of our XRD and Raman analyses agreed well with those of previous studies, which concluded that neoplastic skeletons of hard coral were composed of aragonite (Akiva et al., 2018; Bak, 1983). Not all of the aragonite content of tumor skeletons, however, may be crystalline, supported by the detection of some peaks at the 270 cm−1 position of the tumor Raman spectra (Akiva et al., 2018) and by the relatively higher Mg/Ca ratios in these tissues (Meibom et al., 2008). These findings may indicate the presence of highly active and uncompartmentalized zones of growth in the tumor tissues (Von Euw et al., 2017). Skeletal formation in corals is a two-step process, the initial establishment of centers of calcification (COCs) and the subsequent replacement of the COCs by aragonite fibers (AFs) (Meibom et al., 2008). The architecture of the skeleton is structured by the pattern of COC distribution, and the AFs strengthen the tissue. COCs and AFs are produced by various cell types in the calicoblastic epidermis (Meibom et al., 2008). The malfunction of COC-producing cells may thus lead to

the formation of globular masses in the CEs. The exact cause of CEs is not fully understood, (Coles and Seapy, 1998) proposed that these neoplasms may be caused by ultraviolet damage.

Tumors may currently be less prevalent and severe in our study area, but the progression of disease may be highly energetically exhausting and lethal to smaller colonies (Bak, 1983). Further research is thus needed to monitor the rate of growth of tumors.

References

1. Aeby, G.S., Williams, G.J., Franklin, E.C., Haapkyla, J., Harvell, C.D., Neale, S., Page, C.A., Raymundo, L., Vargas-Ángel, B., Willis, B.L., Work, T.M., Davy, S.K., 2011. Growth Anomalies on the Coral Genera Acropora and Porites Are Strongly Associated with Host Density and Human Population Size across the Indo-Pacific. PLOS ONE 6, e16887.

2. Ajdari, D., Motallebi, A.A., Sharifrohani, M., Sanjani, S., Ajdari, Z., Hajirezaee, S., Zaiton Ibrahim, Z., 2013. Coral relocation in Chabahar Bay, the North-east of Oman Sea. Iranian Journal of Fisheries Sciences 12, 241-247.

3. Akiva, A., Neder, M., Kahil, K., Gavriel, R., Pinkas, I., Goobes, G., Mass, T., 2018. Minerals in the pre-settled coral Stylophora pistillata crystallize via protein and ion changes. Nat Commun 9, 1880.

4. Altvater, L., de Messano, L.V.R., Andrade, M., Apolinário, M., Coutinho, R., 2017. Use of sodium hypochlorite as a control method for the non-indigenous coral species *Tubastraea coccinea* Lesson, 1829. Management of Biological Invasions 8, 197.

5. Aminrad, T., Azini, M.R., 2013. New and Previous Records of Scleractinian Corals from Chabahar Bay, Sistan & Baluchistan, Iran. Ecopersia 1, 407-418.

6. Bak, R.P.M., 1983. Neoplasia, regeneration and growth in the reef-building coral Acropora palmata. Marine Biology 77, 221-227.

7. Burns, J.H.R., Rozet, N.K., Takabayashi, M., 2011. Morphology, severity, and distribution of growth anomalies in the coral, Montipora capitata, at Wai‘ōpae, Hawai‘i. Coral Reefs 30, 819-826.

8. Coles, S.L., Seapy, D.G., 1998. Ultra-violet absorbing compounds and tumorous growths on acroporid corals from Bandar Khayran, Gulf of Oman, Indian Ocean. Coral Reefs 17, 195-198.

9. Ghazilou, A., Koochaknejad, E., Ershadifar, H., Negarestan, H., Kor, K., Baskaleh, G., 2019. Infestation biology of Phallusia nigra (Tunicata, Phlebobranchia) on hard corals in a subtropical bay. Marine Ecology Progress Series 626, 135-143.

10. Hathorne, E.C., Felis, T., Suzuki, A., Kawahata, H., Cabioch, G., 2013. Lithium in the aragonite skeletons of massive Porites corals: A new tool to reconstruct tropical sea surface temperatures. Paleoceanography 28, 143-152.

11. Hill, J., Loder, J., 2013. Reef Check Australia Survey Methods. Reef Check Foundation Ltd.

12. Hoogsteen, M.J.J., Lantinga, E.A., Bakker, E.J., Tittonell, P.A., 2018. An Evaluation of the Loss-on-Ignition Method for Determining the Soil Organic Matter Content of Calcareous Soils. Communications in Soil Science and Plant Analysis 49, 1541-1552.

13. Kathryn, P.S., James, W.P., Cecilia, T., 2004. Disease and immunity in Caribbean and Indo-Pacific zooxanthellate corals. Marine Ecology Progress Series 266, 273-302.

14. Longin, T.K., 2006. Coral disease dynamics in the central Philippines. Diseases of Aquatic Organisms 69, 9-21.

15. Loya, Y., Bull, G., Pichon, M., 1984. Tumor formations in scleractinian corals. Helgoländer Meeresuntersuchungen 37, 99-112.

16. Meibom, A., Cuif, J.P., Houlbreque, F., Mostefaoui, S., Dauphin, Y., Meibom, K.L., Dunbar, R., 2008. Compositional variations at ultra-structure length scales in coral skeleton. Geochimica et Cosmochimica Acta 72, 1555-1569.

17. Muller, E.M., Bartels, E., Baums, I.B., 2018. Bleaching causes loss of disease resistance within the threatened coral species Acropora cervicornis. Elife 7, e35066.

18. Peters, E.C., Halas, J.C., McCarty, H.B., 1986. Calicoblastic Neoplasms in Acropora palmata, With a Review of Reports on Anomalies of Growth and Form in Corals2. JNCI: Journal of the National Cancer Institute 76, 895-912.

19. Pratchett, M.S., McCowan, D., Maynard, J.A., Heron, S.F., 2013. Changes in bleaching susceptibility among corals subject to ocean warming and recurrent bleaching in Moorea, French Polynesia. PloS one 8, e70443-e70443.

20. Rosenberg, E., Loya, Y., 2013. Coral health and disease. Springer Science & Business Media.

21. Von Euw, S., Zhang, Q., Manichev, V., Murali, N., Gross, J., Feldman, L.C., Gustafsson, T., Flach, C., Mendelsohn, R., Falkowski, P.G., 2017. Biological control of aragonite formation in stony corals. Science 356, 933-938.

Table 1. Organic matter (OM), carbonate contents and skeletal elemental ratios of normal *Acropora Valida* and the tumorous tissue. Dissimilar superscript letter indicate significant difference at $p< 0.05$ level.

	Normal	Tumor
OM (%)	37.86 ± 6.46^{b}	15.89 ± 1.94^{a}
Carbonate content (%)	13.125 ± 0.250^{a}	30.25 ± 2.33^{b}
Sr/Ca (mmol mol_{-1})	0.8817 ± 0.0239^{a}	0.8775 ± 0.0438^{a}
Mg/Ca (mmol mol_{-1})	4.2348±0.0667a	4.4152±0.0271b
Li/Ca (mmol mol_{-1})	0.0720 ± 0.0311^{a}	0.1737 ± 0.0627^{a}
Na/Ca (mmol mol_{-1})	3.084 ± 0.113^{a}	5.046 ± 0.951^{a}
Mg/Li (mmol mol_{-1})	6.81 ± 2.35^{a}	2.72 ± 1.19^{a}
Li/Mg (mmol mol_{-1})	1.631 ± 0.704^{b}	4.09 ± 1.43^{a}

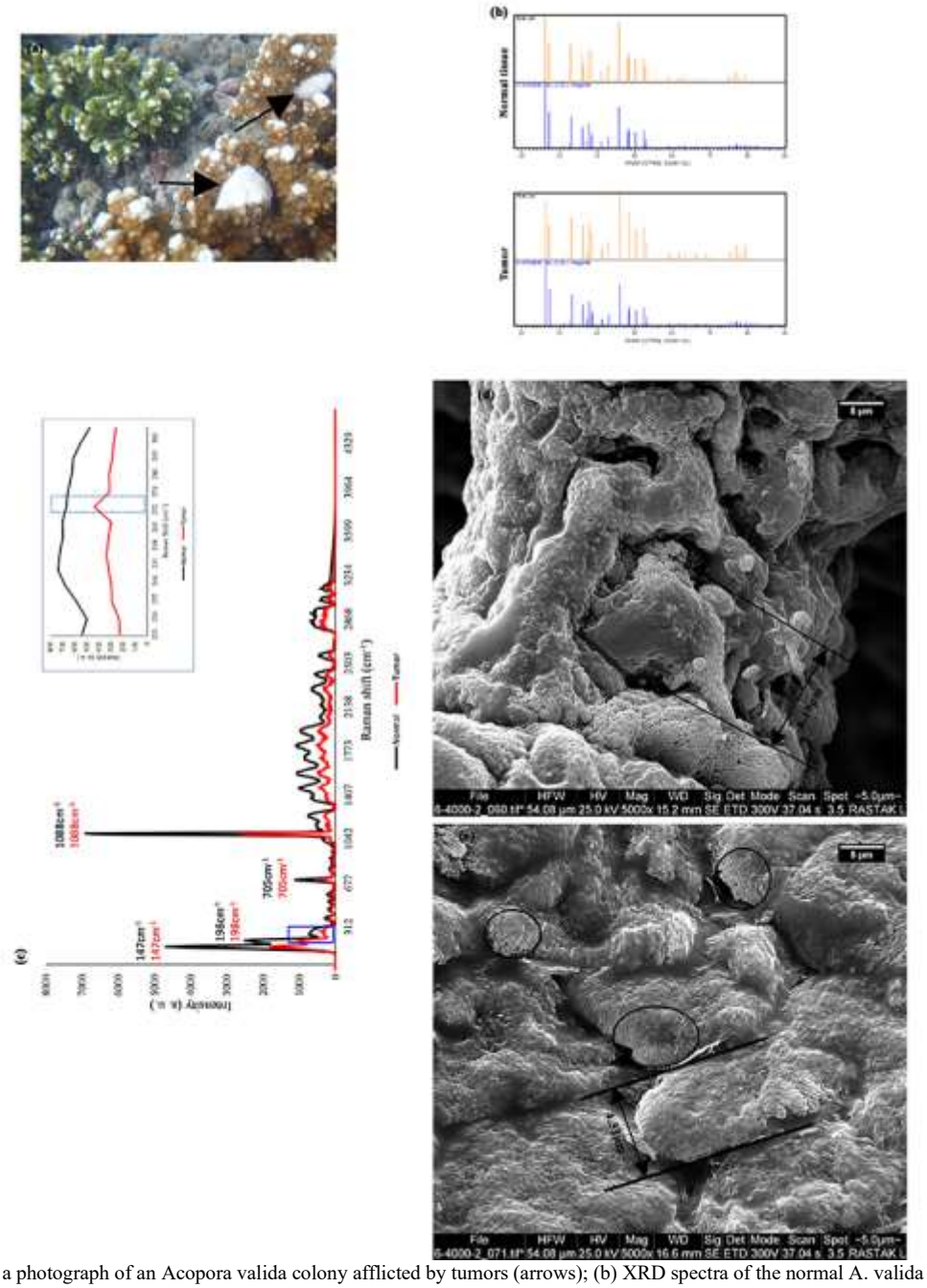

Fig 1. (a) a photograph of an Acopora valida colony afflicted by tumors (arrows); (b) XRD spectra of the normal A. valida skeleton (orange), the tumorous tissue (orange) and the reference spectrum of aragonite, R080142 (blue); (c) Raman spectra of the normal (black) and the tumorous (red) skeleton of A. valida; (d) SEM photograph of the skeleton in A. valida; (e) SEM photograph of skeletal surface of tumorous tissue. Circles indicate aragonite fibers.

2nd International Conference on Oceanography for West Asia

16 , 17 Sept. 2020 Iran. Tehran

Impacts of marine debris on ocean health: A review

Gheshlaghi, Pegah [1*]; Daliri, Moslem [2]

1. PhD student of Fisheries Department, Faculty of Marine Sciences and Technology, University of Hormozgan, Iran

2. Fisheries Department, Faculty of Marine Sciences and Technology, University of Hormozgan, Iran

Abstract

Marine debris is a globally known environmental problem of increasing concern among experts in this field. Marine ecosystems worldwide are influenced by human-made waste. marine debris produces a large-scale kind of unfavorable ocean health, safety, environmental, economic, and cultural impacts. Most marine litter has a meager decomposition rate, leading to a continuous, but significant increase in the coastal and marine environment. marine debris is a vital source of chemical contaminants to the marine environment. The present review addresses the environmental and biological impacts on coastal and ocean biodiversity and provides practical solutions to tackle the marine debris to decreasing destructive effects on ocean health.

Keywords*: Ocean health, marine debris, marine pollution, marine litter.*

1. Introduction

Marine debris is one of the significant challenges for humankind and one of the greatest menaces to the sustainability of marine ecosystems. The main reasons for increasing marine debris are a loss of adequate regular waste management and inadequate wastewater processing, ineffectual corporate social responsibility, natural hazards, illegal dumping, and littering (The important role of marine debris networks to prevent and reduce ocean plastic pollution, 2019). Studies show that within 4.8 and 12.7 million metric tons of plastic enter the oceans every year (Plastic waste inputs from land into the ocean, 2015). The National Oceanic and Atmospheric Administration (NOAA) defines marine debris as “any persistent solid material that is manufactured or processed and directly or indirectly, intentionally or unintentionally disposed of or abandoned into the marine environment…” (http://marinedebris.noaa.gov/) (Plastic marine debris: Sources, distribution and impacts on coastal and ocean biodiversity, 2016), (The Ecotoxicology of Plastic Marine Debris, 2011). Marine debris includes consumer things such as metal, cans, fiberglass, rubber, cigarettes, glass or plastic bottles, balloons, bags, and other manufactured and produced substances that end up in the ocean and along the shore. It additionally includes fishing gear such as line, ropes, hooks, buoys, and other materials lost on or near shore, or deliberately or accidentally discarded at ocean or sea. Marine debris in oceans is an aesthetic problem; it provokes considerable costs and can severely

impact marine organisms and habitats. (Plastic marine debris: Sources, distribution and impacts on coastal and ocean biodiversity, 2016). The most significant percentage of the part of marine debris consists of small sachets, paste tube, the cap, plastic bits, spoon, syringe, straw, pen assorted, bead, hair clips, the plastic and sponge (Influence of river discharge on deposition of marine litter, 2013).

2. Discussion

Worldwide, marine debris, specifically plastic debris, acts the potential to display an increasing menace to the ocean and human health, aquatic and wildlife, economies, and a variety of saltwater and freshwater ecosystems (The important role of marine debris networks to prevent and reduce ocean plastic pollution, 2019). Amongst the first 20 ocean polluters are Sri Lanka, Philippines, Indonesia and countries with long coastlines, such as China and Vietnam (Plastic waste inputs from land into the ocean, 2015). In the following, we refer to the environmental and biological impacts of marine debris on the health of the oceans:

A. Environmental impacts of marine debris

Numerous marine organisms and animals have been killed or injured by marine debris mainly because they become entangled in it or mistake marine debris for food and ingest it. Marine debris originates from both sea-based sources and land and can travel infinite distances. It also injures and kills wildlife, has the potential to transport chemical contaminants, and may pose a menace to the ocean and human health (Plastic marine debris: Sources, distribution and impacts on coastal and ocean biodiversity, 2016). In following, a summary of the impacts of marine debris on benthic ecology and in mangrove and coral reef ecosystems is provided:

Impacts of marine debris on benthic ecology

Usually, good human population density leads to an increase in the amount of debris entering the estuaries that begin to dump waste in the open areas and directly into the estuaries. In some open areas, the basement becomes dead zones and has layers of marine debris, and there was no benthic fauna. The plastics, when got trapped in the benthic ecosystem, develop a micro-community on them. Several studies have indicated that microplastics are mostly from the fishery. Fishing related activities have been found to increase the quantity of plastic in the marine substrate (Impacts of marine litter on coastal and marine benthic ecosystems, 2019).

Impacts of marine debris in mangrove and coral reef ecosystems

The impact of marine debris on mangrove physiology has not been studied intensively, but obviously, we know that Mangroves have been found to act as traps for marine debris. Nowadays, direct dumping of domestic waste obstructs the mangrove's tidal flow and decreases the healthy environment and habitat of several juvenile fishes and shrimps. The result of marine debris on coral reefs has been observed in many areas (Impacts of marine litter on coastal and marine benthic ecosystems, 2019). In some Islands, most of the debris was recognized, ultimately leading to the mortality of corals (A quantification of the standing stock of macro-debris in Majuro, 2019);

furthermore, marine debris prevented the penetration of light in some areas (Effect of marine litter on Palk bay corals in India, 2018), (Marine debris impedes coral reef endurance- a situational remark from the Rameswaram Island, 2018).

B. Biological impacts of marine debris

Globally, at least 86 % of sea turtle species, 36 % of seabird species, and 23% of marine mammal species are known to be influenced by marine debris, especially from plastic (Morbidity in a juvenile green sea turtle (Chelonia mydas) due to ocean-borne plastic, 2009). Ingested marine debris has been found to decrease stomach capacity, limit growth, lead to internal distress, Moreover, create an intestinal blockage; further, it can occur in strangulation, reduction of feeding capability, and in some cases drowning (Plastic Debris in a Nesting Leatherback Turtle in French Guiana, 2010), (Entanglement of grey seals Halichoerus grypus at a haul out site in Cornwall, UK, 2012). A significant concern about the toxic aggregates associated with plastics is that they can interrupt hormone management in the cells of organisms, it can change reproductive capacity and mating habits, and negatively influence offspring (Definition, classification and mechanism of action of endocrine disrupting chemicals. , 2010). Over 80% of recorded events between organisms and marine debris were associated with plastic, while 11% of all reported encounters are with microplastics (Secretariat of the Convention on Biological Diversity and Scientific and Technical Advisory Panel GEF, Impacts of Marine Debris on Biodiversity: , (2012a).). In following, a summary of the impacts of marine debris in the food chain and on human health is provided:

Impacts of marine debris in the food chain

Marine debris such as Microplastics has been seen even in the Arctic and Sub-Arctic Sea with a potential transfer in the benthic trophic food chain (Impacts of marine litter on coastal and marine benthic ecosystems, 2019). in coastal China, microplastics were observed in the muscle, gut, and gills, meaning the warning to human beings via the food chain (The occurrence of microplastic in specific organs in commercially caught fishes from coast and estuary, 2019). Throughout feeding experiments using crabs and mussels, it has been shown that microspheres are carried through the food chain and that these small particles enter the stomach, ovary, and gills of crabs (Trophic level transfer of microplastic: Mytilus edulis (L.) to Carcinus maenas, 2013). These investigations indicate that ocean health, benthic ecosystems, and fauna, which depend on this, face a severe problem.

Impacts of marine debris on human health

Degradation of the ecosystem and habitats services is one of the significant consequences of marine debris on human health, fishing by lost nets and pots can remove invertebrates and fish targeted by regional commercial fisheries. marine debris decreases the aesthetic and recreational values of shores and marine resources and leads

to reduce tourism. Further, fishing gear that is lost or discarded at sea may have the most significant result on humans due to impediments to commercial fishing. After that, marine debris can block ship propellers or steering systems and direct damage to vessels and Interfere with navigation. Furthermore, medical wastes, such as punctures syringes, glass and other sharp, dangerous items that are washed up on beaches, transfer of infections and disease, result in direct risks to beachgoers and may present a health risk, on the other hand, while human swimming may be injured by sharp debris accumulating on beaches. On the other hand, fish and crustaceans meant for human consumption may include (micro) plastics and act as a human health risk, and also, marine litter poses a safety risk for crews of sea vessels (Plastic marine debris: Sources, distribution and impacts on coastal and ocean biodiversity, 2016).

3. Conclusions

Based on our findings, Marine debris is a problem along oceans, coastal waters, estuaries, and shorelines everywhere in the world. It is any human-made, solid material that gains entrance into waterways either directly or indirectly and transboundary, as they were found in the marine environment and moved by currents to different direction; thus, we suggest more comprehensive future study about the result of marine debris on ecosystem especially on organisms in the water or ecological alteration in distribution pattern, human health, and economic loss (Plastic marine debris: Sources, distribution and impacts on coastal and ocean biodiversity, 2016). (Marine debris in Indonesia: A review of research and status, 2019). Studies show that marine debris in the benthic habitat affects the biota and decreases the primary productivity of the ecosystem micro-algal biomass reduced drastically, clearly indicating the impact on benthic ecosystems. It has been observed that an essential need to have a mass coastal benthic cleansing program is followed by proper solid waste collection and segregation mechanisms all over the world. Also, there are still many information gaps correlating to sources, transport patterns, distribution marine debris impacts (The important role of marine debris networks to prevent and reduce ocean plastic pollution, 2019). Furthermore, the numbers of marine animals affected by negative interactions with marine debris, definitely show, that actual amounts of marine debris necessitate being decreased (Harm caused by marine litter, 2016). Recycling is the prevalent solution to the overuse of any marine debris, such as plastics. Thermal degradation may

be the latest solution to repurposing and recycling plastics without creating further environmental degradation. marine debris is one of the significant problems identified by fishermen, and they have demanded a solution for this. It is recommended that there be a National marine debris management Strategy with particular aims for the prevention and control of debris accumulating, spreading, and coastal and marine ecosystems affecting the fish production to increasing menace to resource sustainability. A mixture of law and the improvement of ecological awareness through training are expected to be the best way to solve such environmental problems, As a consequence, fines for those who litter in the oceans or coasts and incentives for prevention and waste reduction

(Marine debris occurrence and treatment: A review, 2016). It is vital to increase consciousness among people about the significance of this issue and remind them what is thrown into the sea does not disappear. However, notwithstanding global efforts, remind them that those abandoned items do not deteriorate and are very harmful to marine environments. The final solution to marine debris prevention is to perform a reliable marine debris strategy, namely the idea of "Zero debris."

Practical solutions to tackle marine debris

- ✓ The most practical method to overcome and decrease the damaging consequences of marine debris in the ocean is to prevent it from entering the marine ecosystem in the first place. This process needs to organize an improved understanding of debris at the regional, local, and national levels; improved waste control efforts; education; anti-dumping campaigns; development of technology solutions; decreasing disadvantages of fishing gear at sea; and incentives to decrease debris .
- ✓ Education is additionally essential in order to promote the actual condition of health in the oceans and could effectively change the manners of people, particularly starting during childhood, and schools should organize activities every year to clean nearby shores (Marine debris occurrence and treatment: A review, 2016).
- ✓ The conversion of marine debris to adhesive is a cost-effective, eco-friendly, practical, and economical method.
- ✓ An essential part of marine debris is connected to the fishing industry. It has been recommended that fishers follow some guidelines for waste disposal at ports, use bait boxes and complete programs for fishing nets recycling (Marine debris occurrence and treatment: A review, 2016).
- ✓ Plastic is now an essential part of the everyday activity of human life, and one cannot control out the problems of plastic, but its disadvantages can be decreased to some extent; accordingly, it has to be controlled by human administration.
- ✓ Recycling is one of the most recognized methods possible to decrease the result of waste in landfills and the ecosystem through the reuse of materials.

References

1. (GEF), G. E. ((2012a).). Secretariat of the Convention on Biological Diversity and Scientific and Technical Advisory Panel GEF, Impacts of Marine Debris on Biodiversity: . Current Status and Potential Solutions, 67: 9. Montreal .
2. Allen, R. J. (2012). Entanglement of grey seals Halichoerus grypus at a haul out site in Cornwall, UK. Mar. Pollut. Bull 64(12):, 2815-2819.
3. Brander, S. M. (2011). The Ecotoxicology of Plastic Marine Debris. Am. Biol. Teach., 73(8): , 474-478.

4. Iñiguez, M., Conesa, J., & Fullana, A. M. (2016). Marine debris occurrence and treatment: A review. Renewable and Sustainable Energy Reviews 64, 394-402.

5. Jambeck, J. R. (2015). Plastic waste inputs from land into the ocean. Science 347, 6223, 768-771.

6. K, F. P. (2013). Trophic level transfer of microplastic: Mytilus edulis (L.) to Carcinus maenas. Environmental Pollution. 177 , p1-3.

7. Kandziora, J. H. (2019). The important role of marine debris networks to prevent and reduce ocean plastic pollution. Marine pollution bulletin, 141, 657-662.

8. Kripa, V. (2019). Impacts of marine litter on coastal and marine benthic ecosystems. Fishery Environment Management Division1, 85-90.

9. Plot, V. a. (2010). Plastic Debris in a Nesting Leatherback Turtle in French Guiana. Chelonian Conserv. Biol., 9(2): , 267–270.

10. Prabhakar R. Pawar, S. S. (2016). Plastic marine debris: Sources, distribution and impacts on coastal and ocean biodiversity. PENCIL Publication of Biological Sciences Vol. 3(1):, 40-54.

11. Purba, N. H. (2019). Marine debris in Indonesia: A review of research and status. Marine Pollution Bulletin, 146, 134-144.

12. Ranith, R. V. (2018). Marine debris impedes coral reef endurance- a situational remark from the Rameswaram Island. Indian Ocean. Ibid, (p. p.38).

13. Richards, Z. T. (2019). A quantification of the standing stock of macro-debris in Majuro. Marine Pollution. Bull 62, 1963-1701.

14. Senthilnathan. L, R. R. (2018). Effect of marine litter on Palk bay corals in India. National Conference on Marine Debris (COMAD 2018), (p. p.86). Kochi, p.86.

15. Stamper, M. A. (2009). Morbidity in a juvenile green sea turtle (Chelonia mydas) due to ocean-borne plastic. J. Zoo Wildl. Med., 40(1): , 196-198.

16. Su L, H. D. (2019). The occurrence of microplastic in specific organs in commercially caught fishes from coast and estuary. Hazardous Materials. 365 , p716-724.

17. Sulochanan, B. L. (2013). Influence of river discharge on deposition of marine litter. Marine Fisheries Information Service T&E Ser.,, No. 216.

18. Werner, S. A. (2016). Harm caused by marine litter. (MSFD GES TG Marine Litter - Thematic Report; No. EUR 28317). European Union.

19. Wuttke, W. J.-W. (2010). Definition, classification and mechanism of action of endocrine disrupting chemicals. . Hormones, 9: , 9-15.

2nd International Conference on Oceanography for West Asia

16 , 17 Sept. 2020 Iran. Tehran

A Green-Resilient Assessment of Industrial Developments in Persian Gulf (Case Study: Natural Gas Production)

Hemmati Tahoune, Mohamad Hasan [1]; Jamali, Gholamreza [2*]

1. Ph.D. Student in industrial Management, Faculty of Business and Economics Sciences, Persian Gulf University, Bushehr, Iran

2. Assistant Prof, Faculty of Business and Economics, Persian Gulf University, Bushehr, Iran

***Keywords**: Persian Gulf, Green Production, Resiliency, Natural Gas Supply Chain, Fuzzy MCDM*

1. Introduction

High economic value of hydrocarbon reservoirs result in recent worldwide industrialization of the sallow and deep seas. Growing global demand for energy result in increasing offshore oil and gas projects which made environmental management challenging. There is also growing concern about the impact that offshore activities through the supply chain have on the environment, and efforts are underway to develop appropriate policies that would reduce adverse environmental impacts (Salem Y. Lakhal, 2007). Along the exploration and production of oil and gas, different environmental impacts may occur including indirect & direct physical disturbances. indirect disturbances like sound and traffic and direct disturbances like disposal of drilling cutting & drilling mud into sea, toxic material emission to sea water and air and harm impact on sea bed due to pipeline installation and decommissioning. Therefore, the green supply chain management in fossil energy development sector was one of the main issues in supply chain management. (ErikE.Corde, 2016)

Beside the environmental issues, due to heavy investment on marine oil and gas projects, risk assessment is an inherent part of supply chain management. To mitigate the risk and overcome successfully with disturbances the term of "resiliency" has recently attracted much attention among supply chain researchers. In the field of supply chain management, resiliency may be explicated as the ability of supply chains to return to normal conditions after a disruption. Therefore, a resilient supply chain can react to a disturbance, regardless if this is emerged due to a natural disaster or a terror attack (Urciuoli *et al*., 2014).

In recent years by development of south pars gas field in Persian gulf of IRAN , a vast network of gas pipeline distributed over the country for gas transmission for both residential and commercial subscribers. The focus of this study is to enhance the level of greenness and resiliency of natural gas supply chain in IRAN. For this purpose, a fuzzy MCDM

method is used to indicate the level of resiliency and greenness of each entity in natural gas supply chain and finally the facilities with higher GRI (Green-Resilient Index) is proposed to remain in chain.

In this study, through vast literature review and field observations, reduction in direct sea contamination and reduction in indirect sea contamination regarded as greenness elements and robustness, agility, leanness and flexibility considered as resiliency pillars. The concept of these elements in present study are defined as follow:

Reduction in direct sea contamination including all efforts to:

- ✓ increase the level of waste management (reduce sea contamination by managing disposals in different stage of natural gas exploration production)
- ✓ minimize the emissions of toxic gas (by-product of burning gas) to the air in refineries
- ✓ minimize disposal of different toxic materials like sulfur to seawater
- ✓ minimize the sea bed damages in exploration and drilling phase

Reduction in indirect sea contamination represents the activities to minimize indirect impacts like sound pollution and traffic

Robustness indicate the ability to resist disturbance along the supply network through existence of alternative suppliers or rapidly incorporate to new suppliers.

Agility investigate the level of adaption of supply chain to changes in competitive environment or customer preference through establish a good communications with partners to capture and adsorb unpredicted demand.

Leanness represent the efficiency of supply chain to minimize the excess / waste and operate in an efficient manner and quick delivery products to end customers.

Flexibility assess how fast is supply chain network to react easily to changes, whilst controlling of costs and lead-times.

2. Materials and methods

In natural gas supply chain, natural gas is transmitted to reifneries from.platform (gas wells) through sea lines. After processing the natural gas in refineries, it transported to compressor stations. In these stations, gas pressure increase by reducing its volume. Pressurized gas is then transmitted to the city gates through pipeline for delivery to commercial and residential subscribers as the end consumer of this chain. As our focus in this study is the offshore part of natural gas supply chain, the supply chain of case study involves three sets of facilities: platforms, refineries and compressor stations.

The method represented in this study helps decision makers to enhance a green-resilient supply chain performance. A fuzzy MCDM method is used to obtain the green-resilient index for each facility. First, fuzzy AHP is used to obtain importance weights for each resiliency and greenness element individually and in each set of supply chain facilities. Then, weight of each facilities, calculated with respect to each element. At the final step, the result of fuzzy AHP and the fuzzy method are combined to indicate each facility green-resilient index.

To conduct fuzzy method pairwise comparison between elements should be done. To this purpose, five point scale linguistic terms and the corresponding triangular fuzzy numbers are used to evaluate green-resilient elements. A group of experts among managers of natural gas supply chain scores each element using the given linguistic term. Linguistic term also used for investigation of each facility regarding each green-resilient element. In next step, fuzzy technique is conducted to calculate the final green-resilient index (Mohammed *et al.,* 2018).

3. Results

In this section, a real case study of a natural gas supply chain, which consist of 3 platforms (contain more than 50 gas wells), 5 refineries and 6 compressor stations are tested to evaluate the ability of the proposed fuzzy multi criteria decision making technique. Five experts were asked to evaluate and compare green-resilient elements and base of these results the importance weight for each element obtained using fuzzy AHP.

Table1) Weight for each green-resilient elements

	resilient elements weight				Green elements weight	
	Robustness	Agility	Leanness	Flexibility	Sea contamination	Toxic material
Expert1	0.327	0.286	0.144	0.243	0.663	0.337
Experts 2&3	0.237	0.251	0.243	0.269	0.49	0.51
Experts 4&5	0.231	0.258	0.261	0.250	0.39	0.61

In next step, the developed fuzzy technique used to combine importance weights and each facility evaluation regarding the green-resilient elements, to obtain final GRI (Green-Resilient Index) for each facility in supply chain. As table 2 shows, platform1 has the highest GRI and platform3 has the weakest condition. For refineries, the second & sixth facility has the maximum resiliency index, refinery3 has the minimum value, and for compressor stations, compressor stations 4 has the maximum value while compressor stations 3 has the lowest GRI.

Table 2) Weight of facilities regarding each resiliency elements and final green-resilient index

	Facility weight regarding resilient elements				Facility weight regarding green elements		Green-Resilient Index		
Facility	Robustness	Agility	Leanness	Flexibility	Di-Contamination	Indi-Contamination	RI	GI	GRI
Platform1	0.401	0.352	0.400	0.519	0.361	0.425	0.416	0.383	0.80
Platform2	0.293	0.273	0.201	0.364	0.329	0.373	0.291	0.344	0.63
Platform3	0.376	0.374	0.400	0.117	0.311	0.202	0.316	0.274	0.59
Refinery 1	0.187	0.185	0.172	0.183	0.200	0.211	0.182	0.206	0.39
Refinery 2	0.221	0.205	0.219	0.216	0.223	0.165	0.215	0.193	0.41
Refinery 3	0.201	0.205	0.195	0.216	0.178	0.198	0.205	0.188	0.39
Refinery 4	0.189	0.201	0.219	0.179	0.192	0.231	0.197	0.212	0.41
Refinery 5	0.203	0.203	0.195	0.205	0.207	0.195	0.202	0.201	0.40
C-Station 1	0.166	0.163	0.146	0.153	0.143	0.175	0.157	0.163	0.32
C-Station 2	0.152	0.186	0.178	0.186	0.187	0.134	0.176	0.155	0.33
C-Station 3	0.168	0.132	0.156	0.126	0.150	0.165	0.145	0.159	0.30
C-Station 4	0.173	0.173	0.178	0.164	0.183	0.185	0.172	0.184	0.36
C-Station 5	0.169	0.161	0.165	0.186	0.175	0.165	0.170	0.169	0.34
C-Station 6	0.172	0.186	0.178	0.186	0.162	0.176	0.181	0.171	0.35

4. Discussion and conclusion

IRAN is a country with a huge offshore gas reservoir in PERSIAN GULF. Heavy investment made to develop this huge gas reservoir in recent years. PERSIAN GULF environmental considerations is the biggest challenges in development of this reservoir. At the same time, because of especial political and strategically situation, it is important to build a resilience supply chain which have enough strength to survive from different incident and return to its original or better condition. In addition, growing demand for energy and high dependence on export again highlighted the necessity of resiliency in energy supply chain.

The focus of this research is on accurate evaluation and enhancement of green-resilient level of natural gas supply chain. To this aim, a local natural gas supply chain, which encompasses 3 gas well platforms, 5 refineries and 6 compressor stations is considered. This study proposed an approach for the organizations to find their status of greenness & resilience by calculating an index through determining and ranking the green-resilient elements. The results show that the proposed technique can be used as a tool for organizations to evaluate a supply chain network structure regarding the greenness & resilience aspects.

References

1. A. Mohammed, I., Harris, A., Soroka, R. & Nujoom. (2018). A hybrid MCDM-fuzzy multi-objective programming approach for a G-Resilient supply chain network design. *Computers & Industrial Engineering*
2. ErikE.Corde. (2016). Environmental Impacts of the Deep-Water Oil and Gas Industry: A Review to Guide Management Strategies. *FrontiersinEnvironmentalScience*.
3. Luca Urciuoli, Sangeeta Mohanty & ElseGerine Boekesteijn. (2014). The resilience of energy supply chains: a multiple case study approach on oil and gas supply chains to Europe. *Supply Chain Management: An International Journal*, 64-63.
4. R.Rajesh. (2019). A fuzzy approach to analyzing the level of resilience in manufacturing supply chains. *Sustainable Production and Consumption, 18*, 224–236.
5. Salem Y. Lakhal, S. H. (2007). Green supply chain parameters for a Canadian petroleum refinery company. *Int. J. Environmental Technology and Management, 7*, 56-67.

2nd International Conference on Oceanography for West Asia

16 , 17 Sept. 2020 Iran. Tehran

Climate Change Impacts on Coastlines in Eastern Coast of India: A Systematic Approach for Monitoring and Management of Coastal Region

K. K. Basheer Ahammed [1*]; Arvind Chandra Pandey [1]

Department of Geo Informatics, Central University of Jharkhand, Ranchi, Jharkhand India. 835 205

Abstract

Climate change is one of the major threatens that coastal areas facing, and these coastal areas already stressed by human activity and large populations. East coast experiencing rapid urbanization in recent decades, there are two megacities viz; Calcutta and Chennai are frequently affected by cyclonic surges. Due to regional climate change, the rate of sea-level rise is gradually increasing. These changes in the coastal regions will result in permanent inundation in the low laying areas. Coastlines are sensitive to sea-level rise, increasing trend of cyclones and associated storms, increases in precipitation, and changes in the ocean temperatures, thus the impact will be much higher in the coastal regions. Conflict of large scale anthropogenic activities and bio rich marine ecosystem are already a concern in the eastern coast. Addressing the additional stress of climate change may require new approaches to managing land, water, waste, and ecosystems. Therefore, the study conducted on the eastern coast and identified the locations under vulnerability using a digital elevation model with extreme surge height, sea level rise rate, historical cyclone events, and intensity. The study conducted on the east coast of India, consisting of four states and one union territory. Hence, the study observed that West Bengal, Odisha, and Andhra Pradesh are the most vulnerable states, whereas Tamil Nadu and Puducherry least sensitive regions on the eastern coast. Around 8000Km^2 areas observed under susceptible to storm surges. This study revealed that the use of the geospatial application is the most reliable and coast effective approach for disaster preparedness and management. The result obtained from the present study may serve the baseline information for disaster management planning in the area.

Keywords Climate Change; Tropical Cyclone; Storm Surge; SLR; GIS

1.Introductions

The coastal environment is dynamic; this dynamism the result of 'constantly changing types of interactions among the ocean, atmosphere, land, and people'(Elnabwy et al., 2020; A. A. Kumar & Kunte, 2012). Coastlines are not static entities but fluctuate at a short-term seasonal level as well as a longer-term climatic-change level (T. S. Kumar et al., 2010). However, much development in the littoral zone occurs with the intention of 'stabilizing the shoreline,' creating a conflict between human use and the coastline's natural processes (Ford et al., 2019). The dynamic systems found on the coast are under increasing pressure by anthropogenic development (Nicholls, 1995; United Nations Environment Programme, (UNEP), 2007). Developmental pressures within the coastal zone are set to increase as its population rises. It is estimating that by 2050, 91% of the world's coast will be impacted by development (Chandrasekar, 2013; Kannan

et al., 2016; Pickard & Emery, 2016; United Nations Environment Programme, (UNEP), 2007). The pressure is not only exerted from within the coastal zone but increasingly on a broader, more global scale (Ranasinghe, 2016).

Ultimately, with population and development growing at a rapid rate, the world's coastal environments are under increasing stress. This pressure is exuberated by the growing threat of climate change and the significant impact the consequences of such a climatic shift will have on the world's coastal regions. Relative sea-levels are predicted to rise, increasing the risk of erosion and inundation, coupled with an increased likelihood of extreme weather events and storm surges (Carter, 1988; Kilibarda et al., 2014; Micallef et al., 2018). In this context, the need for effective coastal management is paramount and therefore, it is not surprising that ideas such as Integrated Coastal Zone Management have risen in prominence over the last few decades (Carter & Woodroffe, 1997). One tool used to help facilitate coastal management has been coastal vulnerability assessments; such assessments involve mapping certain areas of coastline that are particularly vulnerable to the impacts of erosion, sea-level rise, flooding, and extreme weather events(Bird, 2011; Pavlopoulos et al., 2009; Ramesh et al., 2017). Using a selection of parameters that indicate vulnerability (such as beach width and coastal slope), such assessments are useful in offering a quick and cost-effective means for those involved with coastal zone management, providing a general overview of where current or future areas of risk might lay(Carter & Woodroffe, 1997; Khamis et al., 2017). The exact methodology of these coastal vulnerability assessments varies greatly worldwide. Some make use of dozens of parameters and others only a handful, with some parameters being conceived as more critical in one study, less so in another (Camilleri et al., 2017).

2.Materials and methods

In this section, discussing various data and methods adopted for vulnerability studies. There are varieties of tools and techniques are available to study climate vulnerability (Cutter et al., 2003). The study carried out along the eastern coast of India using geospatial tools and techniques (Figure 1). The study addressed the significant climate change impact on the coastlines. Extreme surge height, Historical cyclone tracks, and sea-level rise are used as primary parameters to estimate the climate change vulnerability.

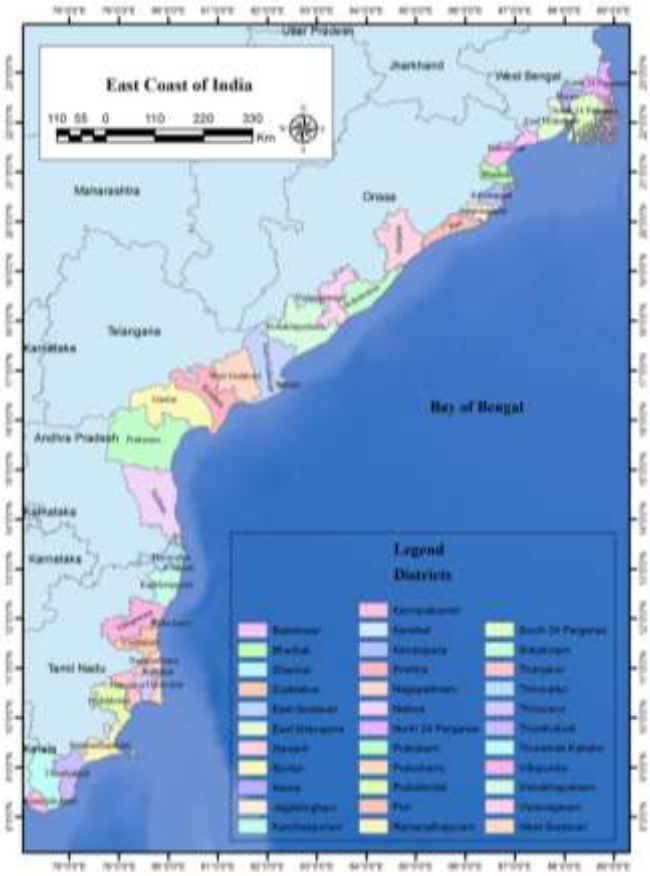

Figure 1) Study Area

The present study utilised tide gauge data and satellite altimetry data to estimate the sea level trend of the study area. Tide gauge data for sea level trend analysis was acquired from Global Sea-level Observing System (GLOSS) for the stations Chennai, Vishakhapatnam, Paradip, Gandra, Diamond Harbour, Haldia, and Port Blair, whereas, satellite altimetry data acquired from AVISO^{+} for the Bay of Bengal. Sea level data available from 1916 to 2008 and altimetry data collected for the period 1993-2018 was used to estimate the sea level change rate.

The winds drive large waves and storm surge onshore, and heavy rains raise rivers. Coastal inundation may get by various climatic variations and extreme weather conditions like wave setup, high tide, and storm surge, inland flood, and sea-level rise, etc. Earlier studies evidence that maximum relative water level rise of five meters or more are found along the east coast of India (Mohapatra, 2015; Rao et al., 2007). To identify the potential surge affected area, the study area further analyzed with 5-meter contour lines along the eastern coastlines and calculated area within the elevation and identified flood-prone areas. Cyclone intensity for the study area observed using historical cyclone events occurred in the past decades. Historical cyclone data were collected from the Global Risk Data Platform (GRDP) and IMD Cyclone atlas for the period 1975 to 2014. Further, these data used to locate cyclone-prone areas. Further various spatial analysis and Geostatistical tools are used to analyze and map preparation. Population growth and density are calculated using the Census of India population database. Data were collected from the year 2001 and 2011 year report, and the data further classified into five different risk classes based on vulnerability.

The present study analyzed the exposure index and sensitivity index to calculate the integrated coastal vulnerability index. Exposure index calculated by using the three variables viz, Cyclone, Storm surge, and sea level, and the sensitivity is calculated using the population growth and density. Further, the integrated coastal vulnerability is calculated using the equation given below (Equation 1).

$$ICVI = e_i + s_i/2 \quad \text{(Equation 1)}$$

Where

ICVI represents the Integrated Coastal Vulnerability Index

e_i stand for the Exposure index

s_i stands for the Sensitivity index

ei/si can be calculated using the equation given below

$$e_i/s_i = (a_x+b_x+c_x+d_x)/n \quad \text{(Equation 2)}$$

Where,

a, b, c, represents the variables (i.e. Cyclone intensity, extreme surge height, sea level rise), ***x*** represent the ranking value of the particular variable (value between 1and 5) the ***n*** represents the number of the variables.

Further, the values are analyzed and mapped using the geospatial application

3.Results

Relative Sea level rise

Sea level rise is the most coastal hazard that exacerbates the problems posed by storm surges, tsunami, shoreline changes, and saltwater intrusion (Mimura, 2013). It is crucial to study the coastal regional elevation to identifying and estimate the vulnerability of coastal regions to these impacts. During the last decades, there are many studies carried out on sea-level rise vulnerability assessment focused mainly on identifying areas located low elevation. One meter sea level rise in the coast may shift shoreline position around 2.5 Km (Figure 2) (Shetye et al., 1990). Both tide gauge and satellite altimetry data depict that the rate of sea level in the northern Bay of Bengal experiencing a higher rate but the lesser rate in the southern. High and low sea level rise observed in the station Haldia and Chennai, respectively. Based on the satellite altimetry, the rate of sea level is perceived as 3.94 mm/year between 1993 and 2018, whereas, from 2004 to 2014, the rate of sea-level rise was 4.45 mm/year. This report shows that the sea level rise is gradually increasing, and the rate of sea-level growth may be higher in the coming decades. The study observed that the West Bengal is the most vulnerable region and Tamil Nadu is the least vulnerable state to sea-level rise.

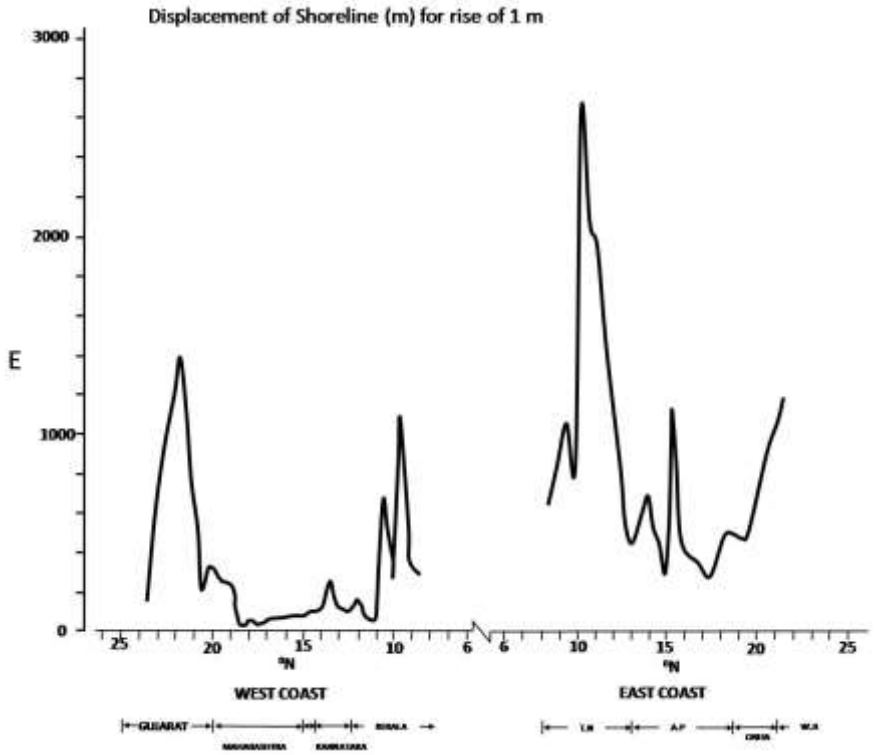

Figure 2) Estimate of distance by which coastline will recode if sea level rises by 1 m, shown as a function of latitude of the east and the west coastline

Tropical Cyclone and Storm Surges

The Indian subcontinent is one of the worst affected regions in the world and is exposed to nearly ten %of the world's tropical cyclones. The majorities of them have their initial genesis over the Bay of Bengal and strike the east coast of India(Das, 2009).In recent years, there has been considerable concern regarding the vulnerability of coasts due to cyclones and associated surges because of projected global warming and sea-level rise (Dube et al., 2009). The frequency of the hurricane was 2/yr from 1970 to 1989, whereas between 1990 and 2010, it increased to 3/yr in each state, and it is also estimated that the frequency will increase up to 6/yr in the coming decade. The present study observed that the Odisha state is the most cyclone-affected the state in India. However, 24 Paragana and Midnapur districts in the West Bengal are the most vulnerable districts in the country, which are affected around 35 cyclones since 1891. According to the historical track record, the entire eastern coast except for the southern tip of Tamil Nadu is vulnerable to cyclone (Figure 3). West Bengal experienced around 69 cyclones since 1891, whereas Andhra Pradesh experienced 79 Cyclones, and Tamil Nadu experienced 54 cyclones since 1981. Puducherry is the least affected area on the eastern coast; only eight cyclones are affected since 1981. Increasing the intensity and frequency of the cyclone dismantled the coastline as well as economic stability.

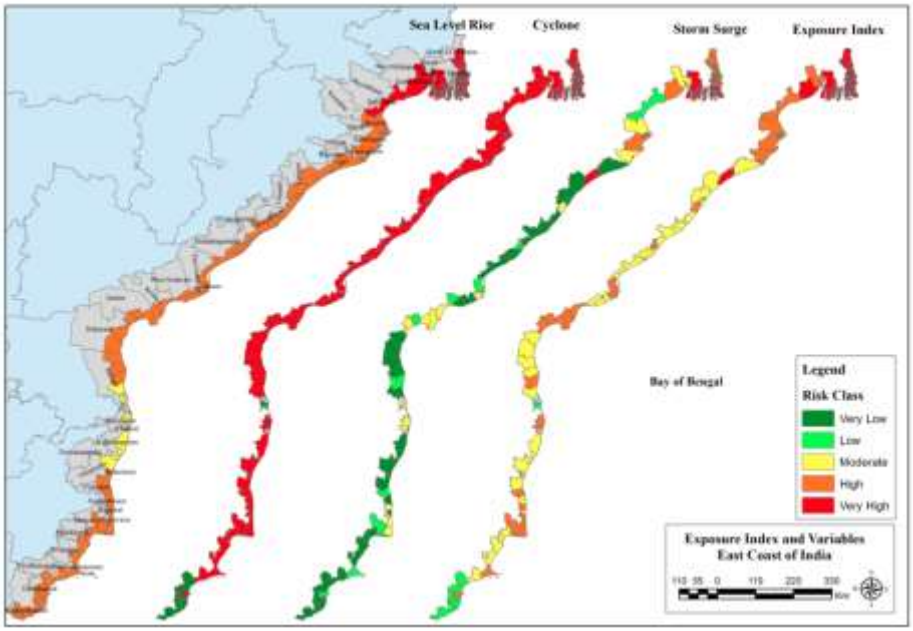

Figure 3) Exposure Index and variables used for the exposure index analysis

Based on the historical storm surge events, surge height observed 5 meters as an average, and the study found around 22176 Km^2 areas under vulnerability to storm surges on the eastern coast of India. It shares about 30% of the total coastal taluk. Based on 5-meter surge height, the West Bengal coast will be the most affected state. About 75% (8113 Km^2) (Figure 4, 5) of the total coastal taluk will be inundated due to the storm surge. Following Odisha shares the second position with 35 % (5995 Km^2) and Andhra Pradesh shares 18% (4511 Km^2), Tamilnadu 16% (3350 Km^2), and Puducherry 1% (4Km^2). In the state of West Bengal, five out of the six coastal taluks are under very high vulnerability (Figure 3, 4), I.e., above 70% of the area coming beneath 5 meters. However, two out of eight coastal taluks are under high vulnerability in the Odisha state. There no taluks are coming under the very high vulnerability in the state of Andhra Pradesh, Puducherry, and Tamil Nadu. However, the coastal villages lying below 5 meters will be inundated.

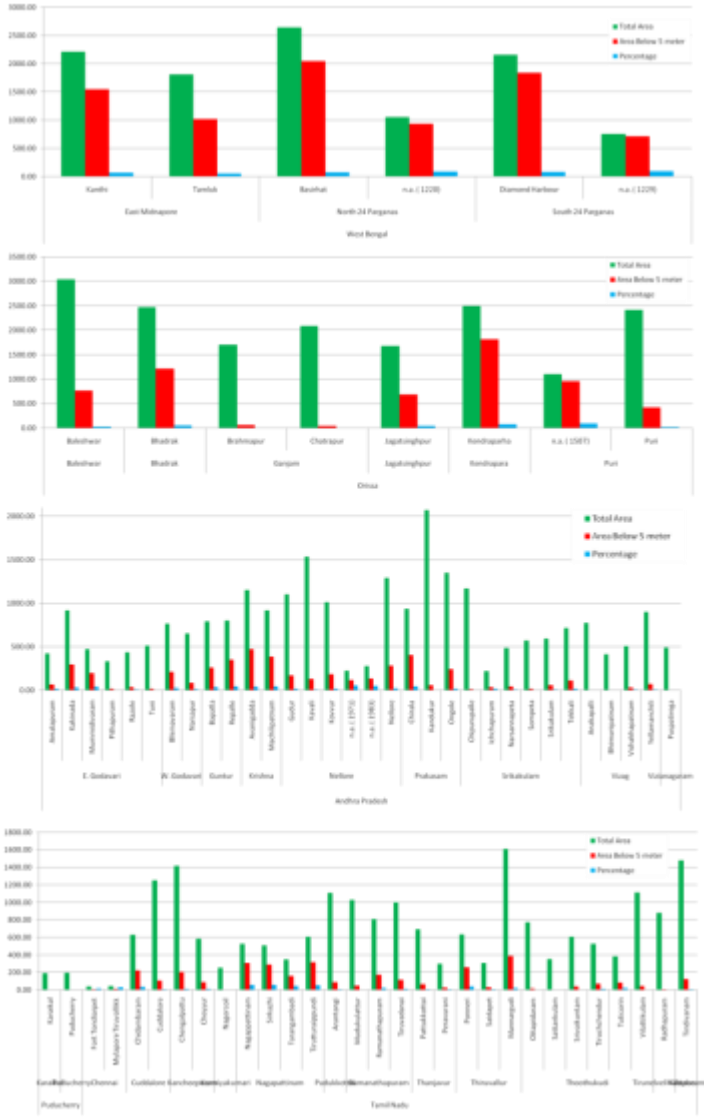

Figure 4) Potential storm surge impact area for east coast India

Vulnerability of the coastal population

Coastal zones are exposed to a range of coastal hazards, including sea-level rise with their associated impacts. At the same time, they are more densely populated than the inland (Nicholls et al., 2014). On the eastern coast of India, ten among the 34 coastal districts are had a very high population density. Among them, five out of five areas laying in the West Bengal namely, Nadia, North 24 Parganas, South 24 Parganas, Houra and Purba Medinipur. The remaining five districts are shares by three districts in Tamil Nadu and two districts in Puducherry viz, Thiruvallur, Chennai, Kanyakumari, Puducherry and Karaikal (Figure 5, 6). Population growth is considerably higher in the coastal regions than in inland areas, and there is an ongoing trend of coastal migration, which is associated with global demographic changes (McGranahan et al., 2007; Small et al., 2000; Small & Nicholls, 2003). Coastal population growth and urbanization rates are outstripping the demographic development of the hinterland, driven by rapid economic growth and coastward migration (Neumann et al., 2015). However, on the eastern coast is observed in a different scenario.

Thiruvallur, Kanchipuram, and Puducherry districts were found very high population growth. Among them, two of them contributed by Tamil Nadu and remaining districts shares by Puduchery (Figure 5, 6).

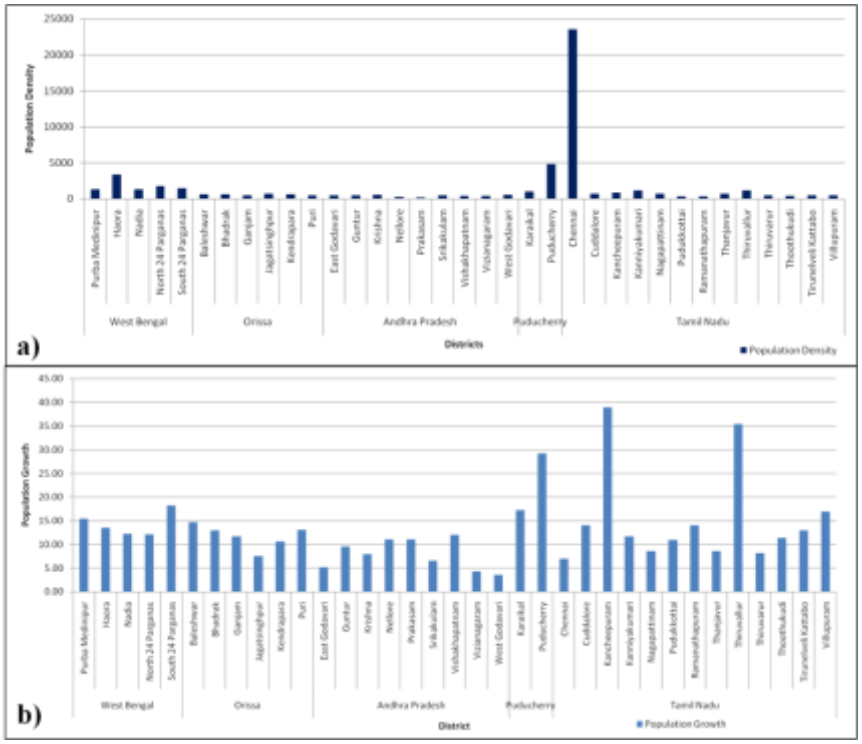

Figure 6) Population distribution along the east coast of India a) District wise Population density b) District wise population growth

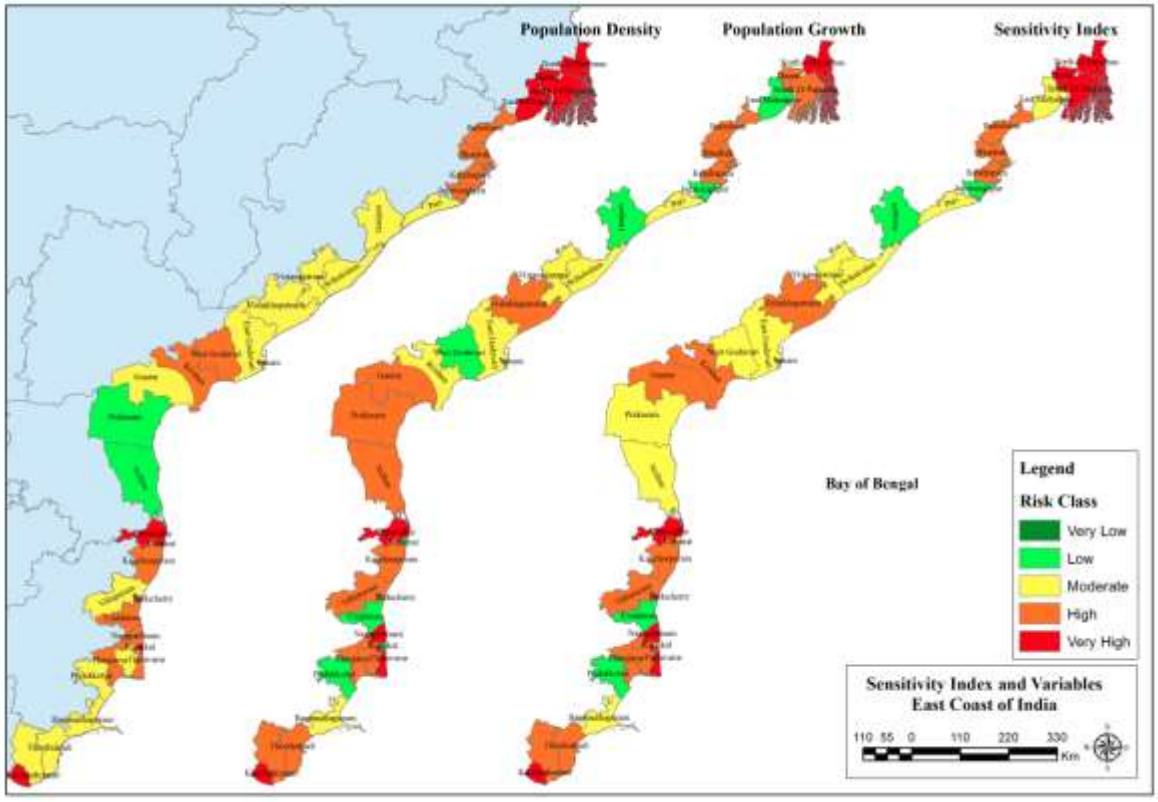

Figure 7) Sensitivity Index and variables used for the sensitivity index analysis

Exposure Index

The present study examined the exposure index and revealed that the most of the districts observed high exposure index. Around 71 % (22 Districts) of the districts are observed in the high exposure zone (Table.). However, nine percentages (3 districts) of the districts was recorded very high exposure index. Among them two districts are contributed by the W. Bengal and one by Odisha. Moderate and low exposure observed with 13% (4 distrcits) and 6 % (2 districts) districts respectively (Figure 3). Whereas, there is no districts found under very low exposure. The highest exposure index value is recorded in the district of South 24 Paragnas (WB) with the value 4.9, whereas, the lowest value is observed in the district of Thirunelveli and Kanyakumari (TN) with the value 2. Low and moderate exposed districts are recorded in the Tamilnadu state, whereas the highest values are mainly observed in the northern states such as Andhra Pradesh, Odisha and West Bengal.

Sensitivity Index

The present study revealed that the east coast of India is very high sensitivity to coastal hazards. Sensitivity index calculated using the variables population growth and density and observed around 20% (7 districts) of the districts very high sensitivity, following that, 35% (12 districts) of the districts observed with high sensitivity. However, around 32% (11 districts) of the districts observed with moderate sensitivity. Four districts (11%) also observed in low sensitivity. Whereas, no districts observed with very low sensitivity. Districts such as Thiruvallur, North 24 Parganas, Kanniyakumari are recorded highest sensitivity index with the value 5, whereas, the lowest value is observed in Ganjam and Pudukkottai district with the value 1.5. based on the sensitivity index, highest values mainly contributed by Tamil Nadu and West Bengal, Whereas, the same time, lowest value also contributed by Tamil Nadu shared with Odisha state (Figure 7).

Integrated Coastal Vulnerability Analysis

Vulnerability analysis has been calculated using the exposure and sensitivity variables. The results depict that the half (19 districts) of the districts exhibit high vulnerable, whereas 18% (6 districts) of the districts exhibit very high vulnerable. However, 27% (9 Districts) of the district observed moderate vulnerability (Figure 8). The study also investigated the state distribution of vulnerable districts and very high vulnerability is more exhibits in West Bengal state, 3 out of 6 districts is shared by west Bengal, Tamil Nadu shares two districts, and Odisha contributed one districts. Eight out of the nine districts of the Andhra Pradesh are observed high vulnerability, whereas the southern district Nellore is found the moderate vulnerability. Following that, Tamil Nadu and Odisha contributed six and three districts in high vulnerability, respectively, whereas, only one district is found in the West Bengal. Moderate vulnerability is mainly dominated in the Tamil Nadu coastline. The Tamil Nadu state contributes five out of the nine districts. However, Odisha added two districts, and the Puducherry added one district in moderate vulnerability. There are no districts found in the low and very low vulnerability class. Most of the high vulnerable districts are observed in the west Bengal and Tamil Nadu states, however, the lowest value also observed in the Tamil Nadu state with Odisha and West Bengal. The

present study is an emphasis on the requirement of the adaptation and disaster management policy to minimize the impact of the climate change impact.

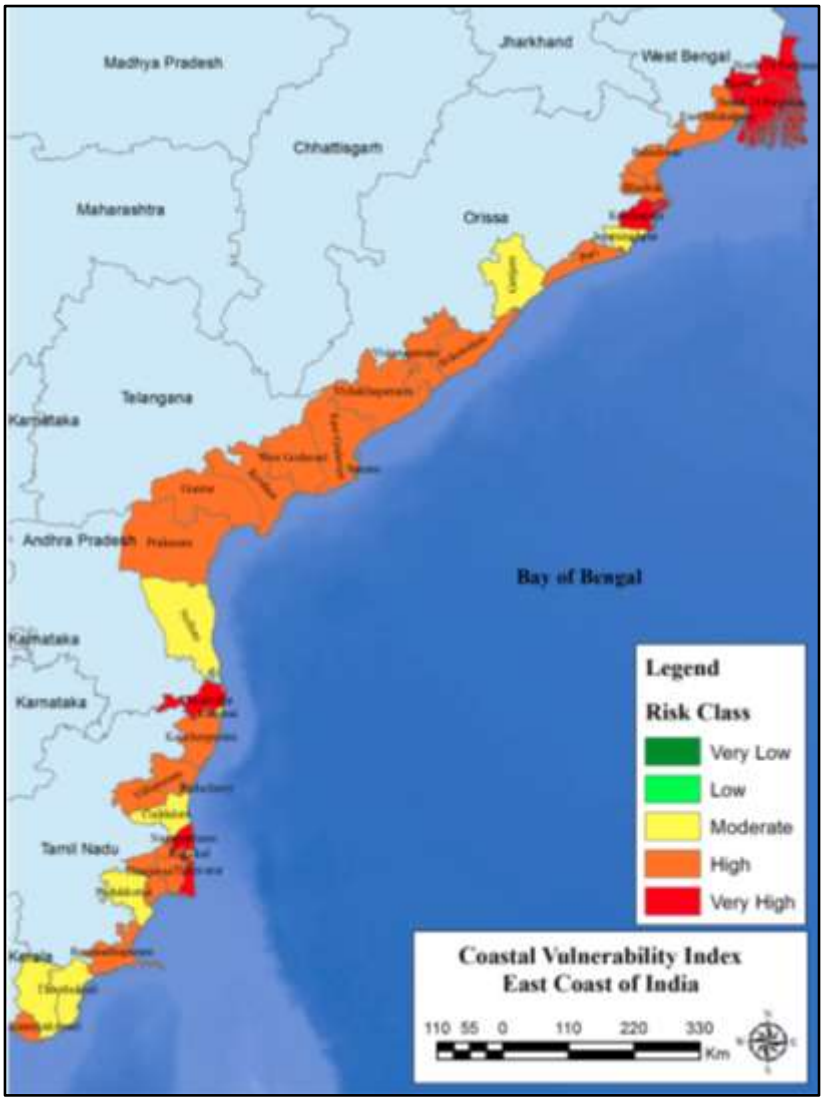

Figure) Spatial distribution of the integrated coastal vulnerability index

4. Discussion and conclusion

The global coastline around the world is facing crucial climate change and associated extreme events, which unbalancing the global economy as well as resources. The present study envisages the horrible impact which will undergo along the east coast of India. Tropical cyclone and storm surges are the major threat on the east coast. The present study observed the two-third of the east coast is laying the high vulnerability zone. Mohanty et al., 2015 analyzed the historical storm surge, and he reported in his paper that Balasore, Medinipur, and 24 North Paragana are recorded the highest surge level with a 30-meter height. The present study also justified his analysis based on historical surge events; West Bengal is one of the most affected states on the east coast of India. Additionally, west Bengal is the most densely populated state in the republic of India; also, one of the oldest and biggest metropolitan city in the world is situated in the West Bengal state. The highest rate of sea-level rise is also observed in the Haldia station which is also located on the West Bengal coast. Hence, the study is signifying the importance of the monitoring and management of the coastal resource and habitant.

Similarly, Odisha and Andhra Pradesh are also vulnerable to climate change impact. Recently cyclone Fani is dismantled the Odisha coastline, and which resulted in the state economy and livelihood (Abhilash, 2019; Pattnaik, 2019). This proves the failure of the existing disaster management policy and mitigation strategies. In this contest, a systematic approach is to be developed and implemented in the vulnerability coast. Increasing the adaptive capacity measures and essential infrastructure development such as coastal roadways, cyclone shelter houses, and primary health facilities will reduce the human causalities and post disaster impact. In the Andra Pradesh coast, Krishna Godavari deltaic plain is the most vulnerable region, low elevated, and the deltaic nature of the topography is increasing the impact. Krishna and Godavari deltaic plain also have large areas of mangroves, which will reduce the effect of extreme events. However, anthropogenic activities in the region resulted in the degradation of the mangroves.

In the last four decades, tremendous wetlands transformed into aquaculture activities(Basheer Ahammed & Pandey, 2019), whereas the Tamilnadu coast is the least vulnerable to extreme events in comparison to the other states. In the 2004 tsunami, in among the other region, Chidambaram City has survived the tsunami impact by the Pichavaram mangrove forest, which is largest artificial mangrove in the country (T. S. Kumar et al., 2012). Therefore, this is reminding the importance of coastal resources and natural barriers. The present study canvassed the vulnerability of the coast and the potential impact of climate change, and the effect will be much higher in the coming decades. Climate Central reported that the Significant part of the West Bengal, Odisha and Andhra Pradesh will be inundated by 2050(Kulp & Strauss, 2019). The study also reported that half of the Calcutta city will be flooded by the sea level rise (Reference). Therefore, a meaningful consideration is required for the monitoring and management of coastal resources and habitats.

The impacts of climate change are likely to worsen problems that coastal areas already face. The existing challenges that affect coastal ecosystems, such as shoreline erosion, coastal flooding, and water pollution, are already a concern in many areas. Addressing the additional stress of climate change may require new approaches to managing land, water, waste, and ecosystems. In this contest, understanding the vulnerability and risk to the coastal population is needed to be analyzed. The variabilities used in the present study are not exhaustive, but the result of the present study will give a piece of baseline information for the comprehensive analysis and decision making. The coastal land is gradually sinking where the rate of relative sea-level rise is larger than the global rate. Some of the fastest rates of relative sea-level rise in India are occurring in areas where the land is sinking, including parts of the Sundarbans deltas. Global warming and unexpected climate changes expand the ocean and make storm patterns more energetic and dangerous.

Consequently it will affect most of the world's coastlines through inundation and increased erosion. On the eastern coast, it is observed that the intensity and the frequency of cyclonic surges are raised in the last decades. Understanding of coastal morphological response to climate change and sea-level rise is quite underdeveloped. Therefore, this study gives a regional level study to understand the climate change impacts on the coastlines. This study revealed that the use of the geospatial applications is the most reliable and coast effective approach for disaster preparedness and

management. The result obtained from the present study may serve the baseline information for disaster management planning in the area.

References

1. Abhilash, P. C. (2019). *Flood to Fani: Climate-Related Disasters Taking a Toll on Sustainable Development*.
2. Basheer Ahammed, K. K., & Pandey, A. C. (2019). Geoinformatics based assessment of coastal multi-hazard vulnerability along the East Coast of India. *Spatial Information Research*, *27*(3), 295–307. https://doi.org/10.1007_s41324-018-00236-y
3. Bird, E. (2011). *Coastal Geomorphology An Introduction Second Edition*. John Wiley & Sons Ltd, The Atrium, Southern Gate, Chichester,.
4. Camilleri, S., De Giglio, M., Stecchi, F., & Pérez-Hurtado, A. (2017). Land use and land cover change analysis in predominantly man-made coastal wetlands: Towards a methodological framework. *Wetlands Ecology and Management*, *25*(1), 23–43. https://doi.org/10.1007/s11273-016-9500-4
5. Carter, R. W. G. (1988). *Coastal environments: An introduction to the physical, ecological and cultual systems of coastlines.* Academic Press.
6. Carter, R. W. G., & Woodroffe, C. D. (1997). Coastal evolution. *Coastal Evolution, Edited by RWG Carter and CD Woodroffe and Foreword by Orson van de Plassche, Pp. 539. ISBN 0521598907. Cambridge, UK: Cambridge University Press, April 1997.*, 539.
7. Chandrasekar, N. (2013). Coastal Vulnerability and Shoreline Changes for Southern Tip of India-Remote Sensing and GIS Approach. *Journal of Earth Science & Climatic Change*, *04*(04). https://doi.org/10.4172/2157-7617.1000144
8. Cutter, S. L., Boruff, B. J., & Shirley, W. L. (2003). Social vulnerability to environmental hazards. *Social Science Quarterly*, *84*(2), 242–261.
9. Das, S. (2009). *Can mangroves minimize property loss during big storms? An analysis of house damage due to the super cyclone in Orissa*. SANDEE.
10. Dube, S. K., Jain, I., Rao, A. D., & Murty, T. S. (2009). Storm surge modelling for the Bay of Bengal and Arabian Sea. *Natural Hazards*, *51*(1), 3–27.
11. Elnabwy, M. T., Elbeltagi, E., El Banna, M. M., Elshikh, M. M., Motawa, I., & Kaloop, M. R. (2020). An Approach Based on Landsat Images for Shoreline Monitoring to Support Integrated Coastal Management—A Case Study, Ezbet Elborg, Nile Delta, Egypt. *ISPRS International Journal of Geo-Information*, *9*(4), 199.
12. Ford, A., Barr, S., Dawson, R., Virgo, J., Batty, M., & Hall, J. (2019). A multi-scale urban integrated assessment framework for climate change studies: A flooding application. *Computers, Environment and Urban Systems*, *75*, 229–243.
13. Kannan, R., Ramanamurthy, M. V., & Kanungo, A. (2016). Shoreline Change Monitoring in Nellore Coast at East Coast Andhra Pradesh District Using Remote Sensing and GIS. *J Fisheries Livest Prod*, *4*, 161. https://doi.org/10.4172/2332-2608.1000161

14. Khamis, Z. A., Kalliola, R., & Käyhkö, N. (2017). Geographical characterization of the Zanzibar coastal zone and its management perspectives. *Ocean & Coastal Management*, *149*, 116–134. https://doi.org/10.1016/j.ocecoaman.2017.10.003

15. Kilibarda, Z., Graves, N., Dorton, M., & Dorton, R. (2014). Changes in beach gravel lithology caused by anthropogenic activities along the southern coast of Lake Michigan, USA. *Environmental Earth Sciences*, *71*(3), 1249–1266. https://doi.org/10.1007/s12665-013-2529-2

16. Kulp, S. A., & Strauss, B. H. (2019). New elevation data triple estimates of global vulnerability to sea-level rise and coastal flooding. *Nature Communications*, *10*(1), 1–12.

17. Kumar, A. A., & Kunte, P. D. (2012). Coastal vulnerability assessment for Chennai, east coast of India using geospatial techniques. *Natural Hazards*, *64*(1), 853–872.

18. Kumar, T. S., Mahendra, R. S., Nayak, S., Radhakrishnan, K., & Sahu, K. C. (2010). Coastal vulnerability assessment for Orissa State, east coast of India. *Journal of Coastal Research*, 523–534.

19. Kumar, T. S., Mahendra, R. S., Nayak, S., Radhakrishnan, K., & Sahu, K. C. (2012). Identification of hot spots and well managed areas of Pichavaram mangrove using Landsat TM and Resourcesat—1 LISS IV: An example of coastal resource conservation along Tamil Nadu Coast, India. *Journal of Coastal Conservation*, *16*(1), 1–12.

20. McGranahan, G., Balk, D., & Anderson, B. (2007). The rising tide: Assessing the risks of climate change and human settlements in low elevation coastal zones. *Environment and Urbanization*, *19*(1), 17–37.

21. Micallef, S., Micallef, A., & Galdies, C. (2018). Application of the Coastal Hazard Wheel to assess erosion on the Maltese coast. *Ocean & Coastal Management*, *156*, 209–222. https://doi.org/10.1016/j.ocecoaman.2017.06.005

22. Mimura, N. (2013). Sea-level rise caused by climate change and its implications for society. *Proceedings of the Japan Academy, Series B*, *89*(7), 281–301.

23. Mohanty, U. C., Osuri, K. K., Tallapragada, V., Marks, F. D., Pattanayak, S., Mohapatra, M., Rathore, L. S., Gopalakrishnan, S. G., & Niyogi, D. (2015). A great escape from the Bay of Bengal "Super Sapphire–Phailin" Tropical cyclone: A case of improved weather forecast and societal response for disaster mitigation. *Earth Interactions*, *19*(17), 1–11.

24. Mohapatra, M. (2015). Cyclone hazard proneness of districts of India. *Journal of Earth System Science*, *124*(3), 515–526.

25. Neumann, B., Vafeidis, A. T., Zimmermann, J., & Nicholls, R. J. (2015). Future coastal population growth and exposure to sea-level rise and coastal flooding-a global assessment. *PloS One*, *10*(3), e0118571.

26. Nicholls, R. J. (1995). Coastal megacities and climate change. *GeoJournal*, *37*(3), 369–379. https://doi.org/10.1007/BF00814018

27. Nicholls, R. J., Hanson, S. E., Lowe, J. A., Warrick, R. A., Lu, X., & Long, A. J. (2014). Sea-level scenarios for evaluating coastal impacts. *Wiley Interdisciplinary Reviews: Climate Change*, *5*(1), 129–150.

28. Pattnaik, S. (2019). Multipurpose Cyclone Shelters and Caste Discrimination. *Economic & Political Weekly*, *54*(21), 13.

29. Pavlopoulos, K., Evelpidou, N., & Vassilopoulos, A. (2009). Methodology-Techniques. In *Mapping Geomorphological Environments* (pp. 5–47). Springer. https://doi.org/10.1007/978-3-642-01950-0_1

30. Pickard, G. L., & Emery, W. J. (2016). *Descriptive physical oceanography: An introduction*. Elsevier. https://doi.org/10.1016/b978-0-08-026279-6.50006-2

31. Ramesh, R., Purvaja, R., Krishnan, P., Lakshmi, A., Abhilash, K. R., & Kingsley, P. W. (2017). Conservation of Coastal Wetlands: An Appraisal of the Policy and Legal Framework in South Asian Nations. In *Wetland Science* (pp. 515–544). Springer. https://doi.org/10.1007/978-81-322-3715-0_27

32. Ranasinghe, R. (2016). Assessing climate change impacts on open sandy coasts: A review. *Earth-Science Reviews*, *160*, 320–332. https://doi.org/10.1016/j.earscirev.2016.07.011

33. Rao, A. D., Chittibabu, P., Murty, T. S., Dube, S. K., & Mohanty, U. C. (2007). Vulnerability from storm surges and cyclone wind fields on the coast of Andhra Pradesh, India. *Natural Hazards*, *41*(3), 515–529. https://doi.org/10.1007/s11069-006-9047-4

34. Shetye, S. R., Gouveia, A. D., & Pathak, M. C. (1990). Vulnerability of the Indian coastal region to damage from sea level rise. *Curr Sci*, *59*(3), 152–156.

35. Small, C., Gornitz, V., & Cohen, J. E. (2000). Coastal hazards and the global distribution of human population. *Environmental Geosciences*, *7*(1), 3–12.

36. Small, C., & Nicholls, R. J. (2003). A global analysis of human settlement in coastal zones. *Journal of Coastal Research*, 584–599.

37. United Nations Environment Programme, (UNEP). (2007). *Physical Alteration and Destruction of Habitats.* http://www.gpa.unep.org/content.html

2nd International Conference on Oceanography for West Asia

16 , 17 Sept. 2020 Iran. Tehran

Abundance of Zooplankton in Surface Waters of the South Caspian Sea

Rahnama, Reza [1]*; Hamzehpour, Ali [1]

1. Iranian National Institute for Oceanography and Atmospheric Science (INIOAS).

* Corresponding author, Email: reza.rah@inio.ac.ir

Abstract:

In this study diversity and abundance of zooplankton in south Caspian Sea offshore waters were investigated. During the first season of oceanographic cruise in winter 2014 at southern part of Caspian Sea, 8 stations at offshore waters of south Caspian Sea were selected. Totally, 4 Holopelankton and 6 meroplankton were identified. Among the identified zooplanktonic groups, Copepods were the main zooplanktonic group that constituted about 53% of total abundance and 65% of total biomass.They were dominant in all stations. Predominant species of copepods was *Acartia tonsa*. Its abundance was between (106±42 ind.m^{-3}) and (1545±181 ind.m^{-3}). After *A. tonsa*, lamellibranch larvae had the highest abundance in all stations (18%) and fish larvae was at second place in terms of biomass (27%). Results showed after invasion of *M. leidyi*, composition and abundance of zooplankton in south Caspian Sea waters greatly changed.

***Keywords**: Plankton, Cladocera, Copepod, Diversity, Abundance*

1. Introduction

The southern Caspian is the deepest with oceanic depths of over 1000 m and accounts 66% of the total water volume. Environmental conditions in the Caspian Sea significantly changed under the impact of human activities. Caspian Sea has significantly altered during the past 30 years, apart from natural changes attributable largely to sea level variability (Rodionov, 1994). Anthropogenic pollution is a significant threat on the biodiversity of the Caspian Sea (Salmanov, 1999; Aladin and Plotnikov, 2004). Impacts on the ecosystem notably are from domestic pollutants including various detergents, industrial pollutants, especially heavy metals and agricultural pollutants, in particular nutrients owing to over fertilization and pesticides. The faunal composition of Caspian Sea has changed totally during last decades (since 1970) because of its water level fluctuations, human manipulation and the entrance of an alien invasive species of a Ctenophore jellyfish. During 80s *Mnemiopsis leidyi* (originated from the north Atlantic waters) transferred to the Black Sea, Azof, Marmara and east Mediterranean Seas and then to Caspian Sea (Shiganova, 1993; Dumont, 1995; Shiganova et al., 2001; Fuentes et al., 2010). Zooplanktons are recognized among the best indicators to be particularly useful to investigate and document environmental changes (Sipkay et al., 2009). Major zooplankton taxa have short life cycle and the community structure is able to reflect real-time scenario as it is less enforced by the stability of individuals from previous years (Richardson, 2008). Through the direct ingestion of phytoplankton, zooplankton influence population

and species dynamics; through excretion and secretion, they contribute to the decomposition and circulation of organic matter in aquatic ecosystems and stimulate algae growth. Zooplanktons are the prey for fish and other aquatic animals; they play an important role in aquatic ecosystems (Guangjun, 2013). There are no documents on diversity and abundance of zooplanktons in south Caspian Sea's offshore waters. Most of the studies focus on investigating the composition and abundance of zooplankton in near shore waters. Most of the studies on zooplankton in south Caspian Sea water were carried out by Iranian Fisheries Research Organization (IFRO). Several studies have been undertaken regarding the zooplankton communities and their structures alongside Iranian coasts in the southern parts of the Caspian Sea in recent years such as: (Rowshantabari, 2000; Laloei et al., 2004; Hashemian et al., 2006; Hosseini et al., 2011 and *etc…*).No study has been done on the community of zooplankton in the offshore water of south Caspian Sea. Furthermore, regarding to the effects of alien species invasion (*M. leidyi*) in Caspian Sea, studying the structure and biomass of zooplankton in the offshore water of south Caspian Sea has high importance.

2. Material and Methods

One transect with 8 stations were selected (Table 1). The distance among sampling stations was 30 km. sampling was conducted in winter season (April 2014

Samples were collected by zooplankton net (100 µm mesh with a 0.36 m mouth diameter) by vertical hauling from10m depth. After collecting, specimens were preserved in a 4% formaldehyde seawater solution. In the laboratory samples were studied in a Bogarov tray contained 0.5 ml of each sample (Postel et al., 2000). Biomass of zooplankton was estimated from the shape of each species (Petipa, 1957) and an invert microscope was used for identifying them. Zooplankton taxonomic classification was performed based on (Birshtein et al., 1968; Kusmorskaya, 1964; Kuticova, 1970). Biomass and abundance data were calculated as per cubic meter.

3. Results

Physico-chemical parameters of sea water are shown in (Fig2). The range of salinity was from (12.52 $g.Kg^{-1}$) at station 1 to (12.87 $g.Kg^{-1}$) at station 3. Maximum temperature was (13.80^0C) at station 4 and minimum was (11.70^0C) at station 3. Station 7 had the highest value of pH (8.67) and the lowest was found at station 4 (8.60). DO values were found maximum and minimum (10.54 and 9.97 $mg.L^{-1}$) at stations 7 and 4 respectively. Figure 3 shows nutrients concentration in all stations. Nitrite concentration only measured at station 1 (2.13 $\mu g.L^{-1}$) and it was not detectable in the other stations. The highest concentration of nitrate was found at station 3 (42.05 $\mu g.L^{-1}$) and the lowest was at station 1 (4.28 $\mu g.L^{-1}$). Also the range of silicate concentration was between (12 $\mu g.L^{-1}$) at station 1 and (156 $\mu g.L^{-1}$) at station 4. In all stations concentration of Phosphate was not detectable. Based on the cluster analysis, all stations were divided in two main groups; group A contained the station with the lowest concentrations of all abiotic parameters measured. On the other hand, group B contained two subgroups: B_1contained three stations with high concentration of silicate. B_2 contained four stations with medium concentration of silicate (Fig 4). Both axes from the Principal Components Analysis (PCA) explained 66% of the total variance. In component 1, most positive correlation was found among salinity, silicate and nitrate, being negatively correlated to the nitrite. In component 2, most positive correlation was

found between DO and pH (Fig 5), having negative correlation with temperature. Dispersal of stations may be explained by nitrate and silicate concentrations. In this study a total number 4 Holopelankton and 6 meroplankton were identified, including: (*Acartia tonsa* and Nauplius of *A. tonsa*; Copepoda – *Asplanchna priodonta*; Rotifera – *Podon polyphemoides*; Cladocera - Larvae of *Nereis diversicolor*; Nereididae - Cypris, nauplius and cirrus stages of *Balanus improvises*; Cirripedia - Lamellibranch larvae;bivalvia and Fish larvae).

Table 2 shows the average abundance of the identified zooplanktons in each of the 8 stations. As shown, *Acartia tonsa* has the highest abundance at station 5 (1545±181 ind.m^{-3}) followed by Nauplis of *A. tonsa* (1168±232 ind.m-3) at the same station. The lowest abundance belongs to Cypris of *Balanus improvisus* (64±22 ind.m^{-3}) at station 4. Among all stations, $S_{5/N}$ has the highest abundance of total zooplanktons (426±524 ind.m^{-3}) and S_8 has the lowest abundance of total zooplanktons (43±48 ind.m^{-3}).

Also there was significant correlation between abundance of some of the zooplanktons and environmental parameters. Nauplius of *B. improvisus* had significant correlation with temperature ($P<0.01$). Cirrus stage of *B. improvisus* showed significant correlation with DO ($P<0.05$). Significant correlation was also found between *A. priodonta* and Silicate ($P<0.05$). *Nereis diversicolor* had significant correlation with silicate, nitrate ($P<0.05$) and nitrite, salinity ($P<0.01$). *P. polyphemoides* significantly correlated to DO ($P<0.01$) and salinity ($P<0.05$). Fish larvae and Lamellibranch larvae showed significant correlation with DO ($P<0.05$ and $P<0.01$ respectively) (Table 3).

Acartia tonsa has the highest total abundance (509±472 ind.m^{-3}) of all zooplanktons, followed by Nauplius of *A. tonsa* (389±362 ind.m^{-3}) and Lamellibranch larvae (294±200 ind.m^{-3}). Fish larvae have the lowest total abundance (13±37 ind.m^{-3}). Abundance percentages of zooplanktonic groupd are shown in Figure 6. So, Copepoda has the highest percentage of abundance (53%) followed by Lamellibranch larvae and Cirripedia (18 and 15% respectively). The lowest percentages belong to Polychaeta (Nereididae) and Fish larvae (1%). Distribution types of zooplanktons are shown in (Table 4). Half of zooplanktons had uniform and other had spotty distribution in stations.

Acartia tonsa has the highest amount of biomass (80 mg.m^{-3}) followed by Fish larvae (37 mg.m^{-3}). The lowest amount of biomass belong to Nauplius of *B. improvises* and *N. diversicolor* (0.41 and 0.44 mg.m^{-3} respectively). The highest percentage of biomass among all zooplanktonic groups belongs to Copepoda (63%) and followed by Fish larvae (27%). Also, Polychaeta (*N. diversicolor*) has the lowest percentage of biomass among all groups (0.3%) (Fig 7).

References:

1. Aladin, N.V.,& Plotnikov, I.S. (2004). The Caspian Sea. Lake Basin management initiative. Thematic Paper. Moscow, Russia.

2. APHA, (1985). Standard Methods for the Examination of Water and Wastewater. (16th ed). Washington, USA.

2nd International Conference on Oceanography for West Asia

16 , 17 Sept. 2020 Iran. Tehran

Lead Bioaccumulation and Its Effect on Condition Indices in Zebra Mussel (*Dreissena polymorpha*) From Anzali Wetland – Caspian Sea: Laboratory Experiment

Rahnama, Reza [1]*; Javanshir, Arash [2] ; Hamzehpour, Ali [1]; Darvish Bastami, Kazem [1]

1. Iranian National Institute for Oceanography and Atmospheric Science (INIOAS).

2.University of Tehran, Department of Fisheries and Environment, Faculty of Natural Resources, Iran

* Corresponding author, email: reza.rah@inio.ac.ir

Abstract

In this study the bioaccumulation of lead by zebra mussel and its effect on mussel's condition indices in the laboratory condition were investigated. The mussels were exposed to the four lead concentrations (2, 48, 93 and 455 $\mu g.L^{-1}$), that they were relevant with natural lead levels in four sites of the Anzali wetland. The lead concentration was only observed in the soft tissue of the zebra mussels when compared to its valves. Our results suggest that the accumulation of lead in the soft tissue of the mussels was affected by two factors: (1) exposure time (2) lead concentration in the ambient water. In this study all mussels in all treatments had equal exposure time, so the significant differences in lead concentrations in the soft tissue of mussels are due to the differences in lead concentrations between treatments. In the treatment with highest concentration of lead (455 $\mu g.L^{-1}$), the most accumulation of lead in the soft tissue of mussels was observed while in the treatment with lowest concentration of lead (2 $\mu g.L^{-1}$), the lowest accumulation of lead in the soft tissue of mussels was observed. Despite differences in metal accumulation, no significant differences ($p>0.005$) in condition indices TCI (tissue dry wt. / shell weight) and SCI (tissue dry wt.*100/shell length) were observed among the mussels in control and lead treatments. Besides the metal pollution, other environmental factors, such as food availability, could affect the mussel's condition. But in our experiment we removed the effect of food by not feeding; therefore lead is the main effective factor on mussel's condition.

Keywords: *Condition index, Dreissena polymorpha, Bivalve Bioaccumulation, Lead contamination, heavy metals*

1. Introduction

Dreissena polymorpha is a sessile suspension-feeder, attached with byssal threads to firm substrate near to the water surface (Gundacker et al. 1998). D .polymorpha plays an important role in eutrophication control by grazing phytoplankton, bacteria and other inert detritic materials from water body (Noordhuis et al., 1992; Reeders et al. 1992). Filtration activity leads to high retention of water, particles and pollutants. Zebra mussel accumulates high amounts of potentially toxic heavy metals and is therefore widely considered as a bio-monitoring organism (Neumann et al. 1992; Secor et al. 1993; Camusso et al. 1994). Zebra mussels remove metals from the water column, incorporate metals in their tissues, and deposit metals on the bottom of the sediments in the form of pseudofeces (Klerks et al. 1997). In

aquatic ecosystem metals are present in physicochemical forms ranging from simple ions to colloids to metals sorbed on or incorporated in suspended particles. Dissolved metals are generally an important source of metals to suspension-feeding bivalves (Klerks et al., 1997). Lead is one of the important heavy metals in aquatic ecosystems which can be accumulated by zebra mussel in high amounts. *D. polymorpha* cannot regulate the concentration of Lead in its body (Amiard et al., 1987). Environmental Lead contamination arises from various sources including mining, smelting, refining, manufacturing processes (battery plants), paints and pigments, also atmospheric emissions from motor vehicles, combustion of coal, recycling of batteries, incineration of municipal solid wastes and hazardous wastes (FDA, 1993). Lead particles emitted during the past use of leaded gasoline are also in the soil, especially near major highways (FDA, 1998). In this study we wanted to elucidate the potential of lead bioaccumulation in the laboratory condition.

2. Materials and Methods

Zebra mussels were taken from relatively unpolluted area in Anzali wetland. They were picked up from the stems of aquatic plant (*Fragmites* sp). After collecting, mussels were carried to the laboratory staying the adaptation period being in a plastic aquarium, containing 10 liters of fresh filtered water (0.45 µm) from the sampling site. During this period (15 days), mussels fed with the *chlorella* spp that cultivated used of Guillard cultivation environment (Guillard et al., 1962) and the water was continuously aerated. After adaptation period, mussels were selected by length range (12-25 mm), and exposed to four Lead treatments (2, 48, 93 and 455 $\mu g.L^{-1}$) that made up using stock solution 1000 $mg.L^{-1}Pb(NO_3)_2$ (Bleeker et al., 1992). Each Lead treatment consisted of 15 individuals. During the experiment period mussels were not fed and the experimental temperature was kept constant at 25°C.

Metal analysis

Five mussels collected from each treatment every five days, and analyzed for their lead content in soft tissue. Soft tissues of the mussels were removed from the shell, byssus threads were also removed. Soft tissue dry weight was determined with oven at 60°C for 24 h (Klerks et al., 1997, Pessatti et al., 2002). The soft tissues were digested in 5 mL concentrated HNO_3 with 2 mL distilled water added. After refluxing for 4 h at 120°C, 2 mL of H_2O_2 (30%, Fisher certified grade) was added and heating was continued for an additional 2 h. after cooling, the tissue digest was filtered using glass-fiber filters and brought up to volume (25 mL) using 0.4 M HNO_3. The samples were analyzed for lead by FAAS (furnace atomic adsorption spectrometer, Perkin Elmer 5100PC). Quality control of metal analysis was performed, using destruction blanks and reference materials (IAEA shrimp MA-A-3/TM and NIST water SRM 1643c). The measured values were in good agreement with the certified values (< 10% deviation).

Condition indices

Two different indices were used to assess the effect of stress on the physiological integrity of the mussels. 15 mussels were placed in aquarium containing 10 L water without lead for 15 days. These mussels played control role for experiment. For accurate comparison of condition indices, during this period mussels not fed. Mussels were dissected and the shell length (up to 0.1 mm) and wet soft tissue weight (ww) (up to 0.01 mg) were measured. After drying at 60 °C for 24 hours, dry soft tissue weight (dw) and dry shell weight (sw) were determined on a Mettler H54 balance to the

nearest 0.1 mg. The same measurements were taken on the mussels from the lead treatments. These measurements were used to calculate two condition indices: Tissue Condition Index (TCI = tissue dry wt. /shell wt.) (Mersch et al., 1996; Soto et al., 2000) and the Shell Condition Index (SCI = tissue dry wt.*100/shell length) (Payne et al., 1999).

3. Results

Results suggest that parts of dissolved concentration in the water are able to be accumulated in the soft tissue of mussels. This concentration as shown in Figure 1 is related to initial concentration of Lead components in the water body. Regressions in all 4 treatments indicate also more metal found in the water, more is accumulated in soft tissue. With consideration of results of 4 treatments as differences in initial concentration one can note that the reduction rates remained constant during 15 days of experiments. But the ability of reduction of metal by animal decreased during the period of experiments or with exposure time *ad libitum* (Figure 2). But it is clear that at the beginning of exposure maximum rate of reduction was observed while after 15 days of exposure only a few part of lead was taken up from the water body. This suggests that mussels have a limit in their absorption activity.

When the averages of accumulation by zebra mussels soft tissue is considered (Figure 3), it is suggested that, despite of the same compartment of absorption in four treatments, the absorption at minimum concentration of 2 $\mu g.L^{-1}$ remains the lowest value obtained in our experiments. The average concentrations in soft tissue in two treatments of 48 and 93 $\mu g.L^{-1}$ showed no significant differences (Table 1) and suggest that the absorption in certain ranges to be independent of ambient concentration of heavy metal. But it is possible that this limit can break when the ambient concentration increased. In the case of high concentration of 455 $\mu g.L^{-1}$ the concentration in soft tissue arrived to its high value compared to other treatments and differences were significant ($P<0.05$) (Table 1).

Net accumulation rates of lead by mussels also varied between treatments. As it is showed in table 2, the least accumulation rate (0.0019 $\mu gPb.gDW^{-1}.day^{-1}$) of lead was measured at the lowest concentration of 2 $\mu g.L^{-1}$ while, the highest accumulation rate was observed in 455 $\mu g.L^{-1}$ (0.593 $\mu gPb.gDW^{-1}.day^{-1}$). These results still suggest that the lead specific accumulation (i.e. divided to its weight) to be dependent to ambient water concentration. It is possible that lead or another heavy metal accumulation to be a non selective activity only related to respiration activity not measured in this study.

The lead concentrations in the soft tissue of the exposed mussels to lead treatments increased with the exposure time. Linear regression analysis revealed net accumulation rates for lead between 0.0019 and 0.593 $\mu g.gDW^{-1}.day^{-1}$ (table 2). For lead the highest accumulation rate was found for the treatment that had highest lead concentration (455 $\mu g.L^{-1}$), followed by 93, 48 and 2 $\mu g.L^{-1}$. The lead concentration in each of the treatments had substantial effects on the lead accumulation rate. The mean value of tissue condition index (TCI) of zebra mussels at the control and lead treatments are showed in figure 4. No significant differences for this index were found among the treatments (table 3). Likewise, when only the pollution gradient was considered no significant differences were found among the treatments and the TCI did not follow the pollution gradient. Within the individual treatment however, the TCI changed in function of time with the lowest condition at the longest period of exposure (figure 5). The mean value of shell condition index (SCI) of

zebra mussels at the control and lead treatments are showed in (figure 6). No significant differences for this index were found among the treatments (table 4). Within the individual treatment the SCI changed in function of time with the lowest condition at the longest period of exposure (figure

References

1. Amiard, J.C., C. Amiard-Triquet, B. Berthet and C. Metayer, 1987. Comparative study of the patterns of bioaccumulation of essential (Cu, Zn) and non-essential (Cd, Lead) trace metals in various estuarine and coastal organisms. J. Exp. Mar. Biol. Ecol., 106:73-89.

2. Bleeker, E.A.J., M.H.S. Kraak and C.Davids, 1992. Ecotoxicity of Lead to the zebra mussel *Dreissena polymorpha*, Pallas. Hydrobiol. Bull. 25: 233-236.

3. Borgmann, U., W.P. Norwood and C. Clarke, 1993. Accumulation, regulation and toxicity of copper, zinc, Lead and mercury in *Hyalella azteca*. Hydrobiologia 225, 79-89.

4. Camusso, M., R. Balestrini, F. Muriano and M. Mariani, 1994. Use of freshwater mussel *Dreissena polymorpha* to assess Trace Metal Pollution in the Lower River Po (Italy), Chemosphere 29 (4), 729-745.

5. FDA (1993), Guidance document for Lead in shellfish, States Food and Drug Administration. Washington, D.C.

6. FDA (1998), Dangers of Lead still linger, ed. Farley, D. United States Food and Drug Administration. FDA Consumer. Washington, D.C.

7. Guillard, R.R.L., Rhyter, J.H., 1962. Studies of marine planktonic diatoms. I. cyclotella nana Hustedt&Detonula confervacea (cleve). Can. J. Micrbiol., 8: 229-239.

8. Gundacker, C., 1998. Tissue-specific heavy metal (Cd, Lead, Cu, Zn) Deposition in natural population of the zebra mussel (*Dreissena polymorpha*). Chemosphere, Vol. 38, No. 14, pp. 3339-3356.

9. Kilgour, B.W., Mackie, G.L., Baker, M.A., Keppel, R., 1994. Effects of salinity on the Condition and survival of zebra mussels (Dreissena polymorpha). Estuaries 17, 385-393.

10. Klerks, Paul L., Peter C. Fraleigh, and Jay E. Lawniczak, 1997. Effects of the exotic zebra mussel *(Dreissena polymorpha*) on metal cycling in Lake Erie. Can. J. Fish. Aquat. Sci. 54: 1630-1638.

11. Kraak, M.H.S., D. Lavy, W.H.M. Peeters and C. Davids, 1992. Chronic ecotoxicity of copper and cadmium to the zebra mussel *Dreissena polymorpha*. Arch. Environ. Contan. Toxicol. 23: 363-369.

2nd International Conference on Oceanography for West Asia

16 , 17 Sept. 2020 Iran. Tehran

Numerical modeling of the Phet Tropical Cyclone Wavefield

Rezaee Mazyak, Ahmad [1]; Shafieefar, Mehdi [2*]

1. Ph.D student of marine structures, Tarbiat ModaresUniversity
2*. Professor of marine structures, Tarbiat ModaresUniversity, shafiee@modares.ac.ir

Keywords *Phet, Tropical Cyclone, Reanalysis wind field, Parametric wind*

1. Introduction

Due to the climate changes and global warming, the occurrence rate of tropical cyclones has been increased. The southeastern and southern coasts of Iran have also been affected by such climatic and environmental hazards. Gonu (2007), Phet (2010) and Kyarr (2019) tropical cyclones are samples of tropical cyclones that have affected the northern coasts of the Oman Sea. Many studies have been conducted on the modeling of the tropical cyclones effects. Some researches have reviewed the wind field characteristics of tropical cyclones [1-3]. In some other researches, the wave characteristics and related issues to the tropical cyclones oceanography have been investigated [4-7].

A review of previous studies shows that the wind field is of high importance for investigating the tropical cyclones' wave field. Therefore, the effect of wind field accuracy on the wave field intensity and pattern during the tropical cyclone Phet has been investigated in the present study. For this purpose, the wind fields obtained via the Holland parametric model and reanalysis data (CFSR and ERA-Interim) have been examined during the tropical cyclone Phet.

2. Material and Methods

Phet is one of the most severe tropical cyclone occurred in the Arabian Sea in June 2010. Figure 1 shows the position of the center, track, and severity and weakness of the tropical cyclone Phet.

(a)

Phet		
Date/Time	Type	Maximum Wind Speed (knot)
2010/06/01 06h	Tropical Storm	55
2010/06/01 18h	Hurricane Category 1	75
2010/06/02 00h	Hurricane Category 2	90
2010/06/02 06h	Hurricane Category 4	115
2010/06/02 12h	Hurricane Category 4	125
2010/06/03 06h	Hurricane Category 4	115
2010/06/03 12h	Hurricane Category 3	110
2010/06/04 00h	Hurricane Category 2	90
2010/06/04 06h	Hurricane Category 1	75
2010/06/04 18h	Tropical Storm	55

(b)

Figure 1) The track of cyclone Gonu and its development process

The data used in the present study include measurement, Best Track (BT), and reanalysis data. In order to evaluate the wave field, the measurement data of the Chabahar Buoy have been used. Wave characteristics such as Significant wave height, peak period and mean wave direction were compared with the measurement data. Figure 1 shows the the Chabahar buoy positions relative to the cyclone track. Also, the best track data of joint typhoon warning center (JTWC), ECMWF (ERA-Interim) and Climate Forecast System Reanalysis (CFSR) wind field and wave data of the Wavewatch III data for open boundary is used. In addition, based on the findings of the literature, the Holland parametric model has been used to hindcast the wind field [8].

Numerous third-generation wave propagation models can be used in order to model the waves from deep water to the coastlines. SWAN, Wavewatch III, MIKE21-SW, and TOMAWAC are examples of these models. Due to the capabilities of the MIKE21-SW model and its successful usage in previous studies, this model has been chosen for the present simulation.

3. Results and discussion

Figure 2 compare the time history and scatter plot diagrams of the significant wave height, peak period, and mean wave direction of waves due to different wind fields at the Chabahar buoy. Investigation of the results according to different wind field illustrated that the Holland parametric model is suitable for estimating the wave characteristics. The results of the pattern of changes and maximum value of significant wave height, peak wave period due to seas and swell and mean wave direction from Holland wind field have the highest correlation with measurement data.

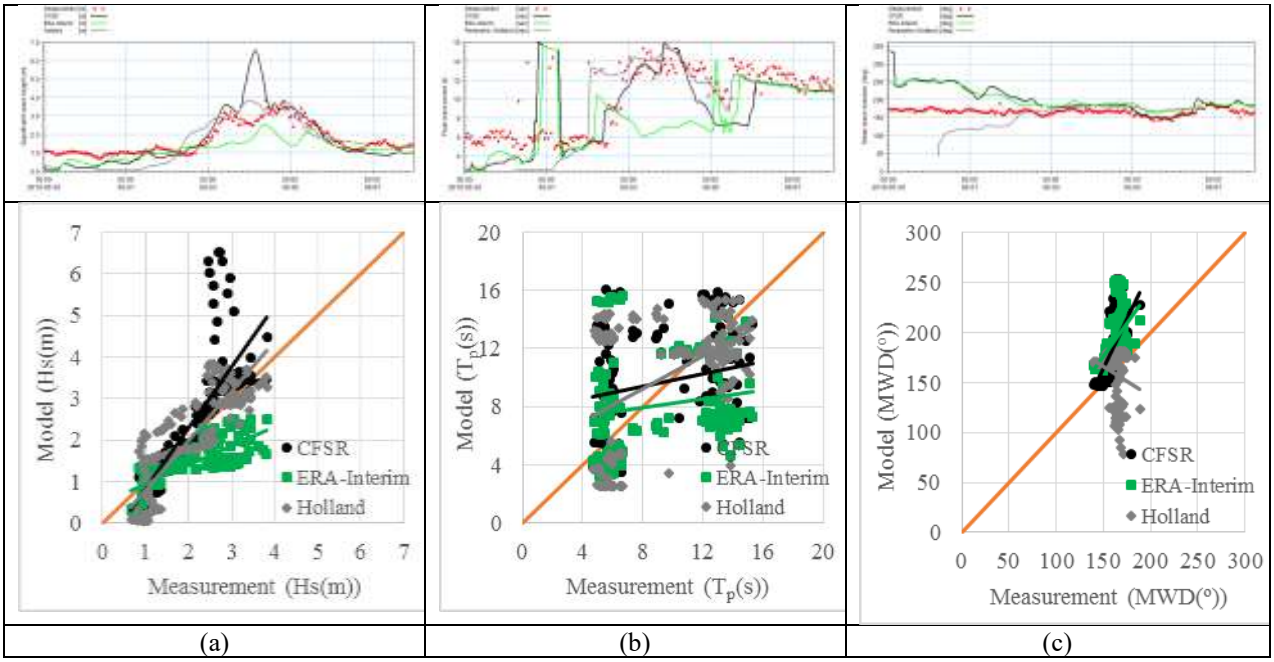

Figure 2) Time history of the (a) significant wave height, (b) peak period and (c) mean wave direction according to different wind fields

Due to distant of measurement station from the track of cyclone Phet, a general examination of the wave field may provid suitable information. Hence, in the present study, the wave field has been investigated as a whole from the maximum wave height point of view. This approach can further demonstrate the overall accuracy of the employed wind

field. The maximum wave height values for different wind fields are exhibited in Figures 3. Figure 8 shows the maximum significant wave height which are estimated as about 15 and 13 m based on the Holland parametric model and CFSR wind fields, respectively. Also, the maximum wave height obtained from the ERA-Interim model is about 6 m.

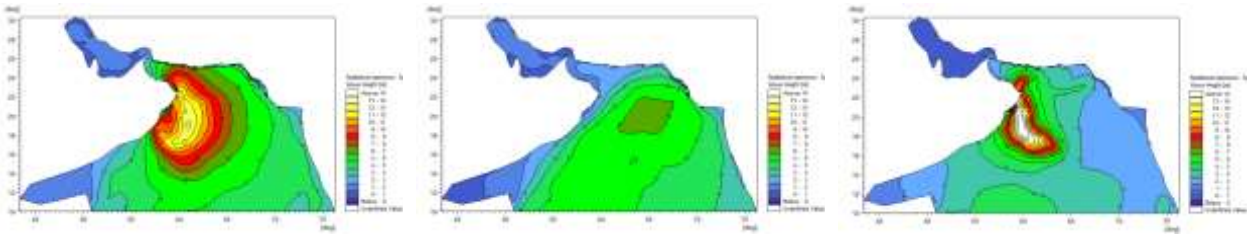

(a) (b) (c)

Figure 3) Maximum wave height based on the wind fields of (a) CFSR, (b) ERA-Interim and (c) Holland parametric model

4. Conclusion

In the present study, the wave field results obtained via three different wind fields during the tropical cyclone Phet have been investigated. The results of the investigations are summarized as below:

- ✓ Comparison of the wave field results obtained from the wind fields of ERA-Interim and CFSR reanalysis data with the measurements indicated an appropriate agreement. Examination of the significant wave height shows that the results based on the ERA-Interim and CFSR are underestimate and overestimate, respectively. However, the investigation of the maximum wave height values in the computational domains shows that the maximum observed values based on the ERA-Interim do not adapt well to the track and development direction of the cyclone.

- ✓ Investigation of the wave field resulting from the Holland parametric model illustrated the sufficient accuracy of this model in estimating the wave height. The result obtained via the Holland parametric model estimated the maximum wave height caused by cyclone Phet in deep water to be about 15 m.

References

1. Alimohammadi, M., & Malakooti, H. (2018). Sensitivity of simulated cyclone Gonu intensity and track to variety of parameterizations: Advanced hurricane WRF model application. Journal of Earth System Science, 127(3). doi: 10.1007/s12040-018-0941-4.

2. Yaghoobi Kalourazi, Mehdi, Siadatmousavi, Seyed Mostafa, Yeganeh-Bakhtiary, Abbas, & Jose, Felix. (2019). Simulating tropical storms in the Gulf of Mexico using analytical models. Oceanologia. doi: 10.1016/j.oceano.2019.11.001

3. Liu, Fei, & Sasaki, Jun. (2019). Hybrid methods combining atmospheric reanalysis data and a parametric typhoon model to hindcast storm surges in Tokyo Bay. Scientific Reports, 9(1). doi: 10.1038/s41598-019-48728-7

4. Allahdadi, Mohammad Nabi, Chaichitehrani, Nazanin, Jose, Felix, Nasrollahi, Ali, Afshar, Amin, & Allahyar, Mohammadreza. (2018). Cyclone-generated Storm Surge in the Northern Gulf of Oman: A Field Data Analysis during Cyclone Gonu. American Journal of Fluid Dynamics, 8(1), 10-18.

5. Allahdadi, Mohammad Nabi, Chaichitehrani, Nazanin, Allahyar, Mohammadreza, & McGee, Laura. (2017). Wave Spectral Patterns during a Historical Cyclone: A Numerical Model for Cyclone Gonu in the Northern Oman Sea. Open Journal of Fluid Dynamics, 7(02), 131.

6. Ghader, Sarmad, Yazgi, Daniel, Haghshenas, S Abbas, Arab, Azadeh Razavi, Attari, Morteza Jedari, Bakhtiari, Arash, & Zinsazboroujerdi, Hamid. (2016). Hindcasting tropical storm events in the Oman sea. Journal of Coastal Research, 75(sp1), 1087-1091.

7. Mashhadi, Leila, Zaker, Nasser Hadjizadeh, Soltanpour, Mohsen, & Moghimi, Saeed. (2015). Study of the Gonu Tropical Cyclone in the Arabian Sea. Journal of Coastal Research, 31(3), 616-623.

8. Rezaee Mazyak, A., Shafieefar, M., Sanayei, M., Shafieefar, A., (2015). Evaluation of Parametric wind field for modeling tropical cyclone in Makran coast (Case study: Gonu and Phet). 17th Conference on Marine Industries.

2nd International Conference on Oceanography for West Asia

16 , 17 Sept. 2020 Iran. Tehran

The Optimization of Outfall Systems in ro Desalination Plants (Case Study: Bandar Abbas Desalination System)

Rezaei Mazyak, Ahmad [1*]; Ghasemi, Ali [2]; Mashhadi, Mansoure [2]

1. Civil & Environmental Engineering Faculty, Tarbiat Modares University
2. Marine Structures and Port Engineering, Pars Geometry Consulting Engineers

***Keywords**: Outfall systems, seawater desalination, dilution*

1. Introduction

The outfall system is a medium to discharge the liquid waste generated by desalination plants, refineries and power plants to the marine environment. Optimal design and operation of an outfall system reduces the concentration of pollutants returned to the marine environment. To design an efficient brine discharge system, some major issues must be thoroughly investigated including near-field considerations, marine environment, far-field considerations, water recirculation and desired dilution.

Numerous researches have been carried out to study the different elements of outfall systems and related design basics. Comparing experimental data and results of Cormix software, Bleninger and Jirka (2008) determined the optimal angle of discharge ports on the basis of sea bottom slope to achieve the maximum dilution [1]. Jiang et al. (2012) measured the minimum surface dilution for various water depths [2]. Roberts and Abbessi (2014) investigated the effects of multiport configurations, i.e. port distance, angle of ports and environmental conditions such as current speed and direction on obtained dilution [3].

In this paper, the outfall system of Bandar Abbas desalination plant is designed and optimized in accordance with an optimization algorithm. For this purpose, the requirements and design criteria of outfall systems are presented and the hydraulic design and salinity distribution are discussed, using CorHyd and VISJET models.

2. Materials and methods

An outfall system consists of three key components, which are weir box, outfall pipeline and diffuser, from onshore to offshore, respectively (Figure 1-a). Any mistake in design of these components would lead to decrease in dilution and arising economic and environmental issues.

The weir box provides the sufficient head for brine discharge and maintain the pressure at a constant level. The height of weir box is related to tidal levels and head loss in pipeline and diffuser and is obtained by the sum of total head loss

with the highest astronomical tide level (HAT). In order to prevent air entrainment, it is recommended that the top of outfall pipeline in the point where it leaves the weir box be in the range 0.5-1.5 m below LLW [5].

The seawater discharge pipeline is also considered as one of the most significant constituent of outfall system. The amount of linear head loss depends on the pipeline material. According to Michael Peleg research, GRP pipelines are exposed to biofouling and marine growth about 10 times more than HDPE pipes [6]. Therefore, HDPE pipe can be a more careful choice. The roughness of HDPE pipes varies between 0.05 mm and 2 mm for new pipe [5].

To design diffuser and ports, there are four major factors to consider including 1- dilution requirements, 2- configuration of ports and risers, 3- the angle and direction of diffuser and 4- hydraulics requirements. Since the discharged brine obtains a denser fluid in comparison with sea water, a negatively buoyant jet is formed. In order to ensure the sufficient dilution and prevent air inclusion in diffuser, densimetric Froude number (Fr) of the jet must be greater than 1 [7]. Studies on Fr show if Fr is greater than 10, the dilution is independent of it [7] and for sufficient dilution, Fr is assumed between 20 and 25 [1].

Generally, the design of outfall systems depends on several interacting parameters. Figure 1-b shows the design flowchart, which leads to an optimized outfall system.

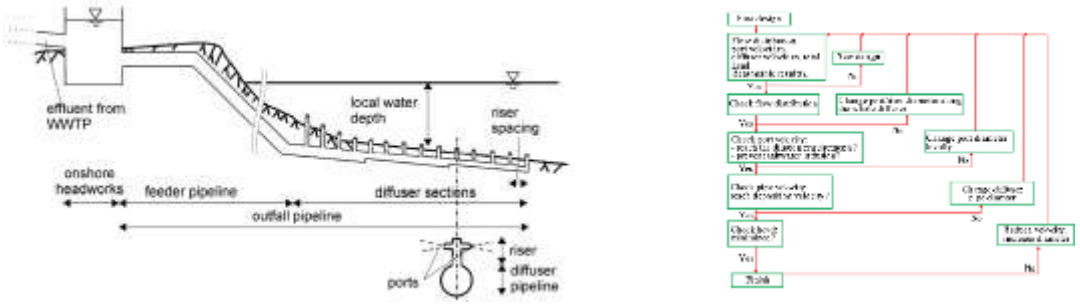

Figure 1) a. Components of outfall system [4], b. Schematization of general diffuser design algorithm [4]

Study area

Bandar Abbas desalination system is located in the northern coasts of Persian Gulf in Hormozgan province This plant has a capacity of 1,000,000 m^3 desalinated water per day, with a RO recovery rate varying from 33% to 41% (Table 1). The length of discharge pipeline is about 1200 m, which is considered from weir box to diffuser. The local depth in diffuser position is 10 m. Two seawater HDPE pipelines with an inner diameter of 2500 mm transit the brine to the sea. The increase of roughness due to long term operation of the pipe is considered in design procedure. To enhance the dilution rate, 7 ports are located on each pipeline with inner diameter of 0.6m, angle of 30 degrees (relative to the horizontal axis) and 5.25 m distance between ports.

Table 1) Minimum and maximum flow rate of Bandar Abbas desalination plant

	Qmin (m^3/day) (Recovery rate = 33%)	Qm (Recov
Intake	3030303	
Outfall	2030303	

3. Results and discussion

Figure 2) Location of study area

CorHyd is applied to assess the densimetric Froud number and flow distribution in the diffuser section and the ports. According to Figure 2-a, the Fr is greater than 10 in all ports with an average value of 16.5, which ensures the desirable dilution. Figure 2-b also shows the flow distribution in ports. The discharge flow difference in all ports is less than 10%, which means the flow distributes uniformly among the ports, and the dilution requirements are met in diffuser section.

VISJET model is applied to check the efficiency of diffusers [8]. The experimental results of Bashitialshaaer et al are used to validate the model [9] (Figure 3). Comparing the results of model and experimental data shows the model results are reliable. The effluent discharge pattern for the three diffusers is shown in (Figure 4) with and without presence of marine currents. In Addition, no plumes interference is observed in model results, which admits the adequate distance between ports. The maximum trajectory of the jet is about 8 meter, meaning the jets do not interact with water surface. Moreover, at the distance of 15 m from discharge point, the brine concentration reduces about 90%, which admits the sufficient dilution.

4. Conclusion

In this paper, the hydraulic design criteria and requirements for design of outfall systems are discussed. Determining the height of the weir box depends on the amount of head drop in the offshore pipeline and diffuser. Therefore, as a general rule the head loss should be minimized. The comparing HDPE and GRP pipe material shows that efficiency of the system is improved when HDPE material is installed, due to the less rate of biofouling. Diffuser system is designed considering four aspects: the dilution requirements, the geometry and arrangement of the risers and ports, the direction of the diffuser and the hydraulic considerations.

The results of numerical modeling of salinity distribution with CorHyd and VISJET models in Bandar Abbas desalination plant show that the brine concentration reduces about 90% at the distance of 15 m from discharge point. Also, there is no interference between the plums, which indicates the proper functioning of the system.

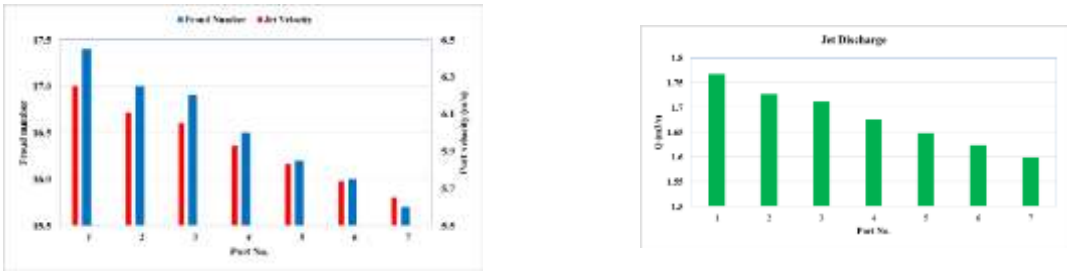

a. b.

Figure 2) CorHyd results: a. Comparison of densimetric Froude number and velocity in each port for recovery rate of 33%, b. Flow distribution in diffuser section

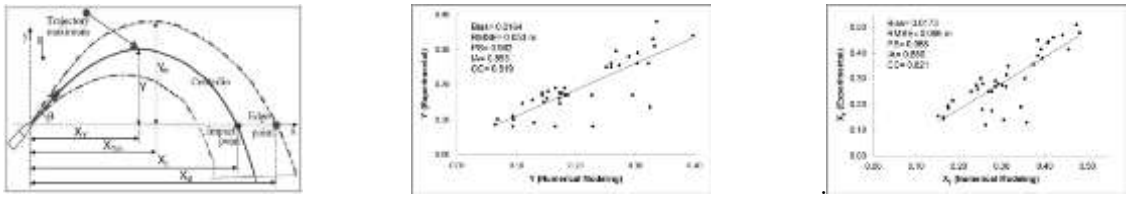

a. b. c.

Figure 3) Comparison of VISJET results with experimental data: a. The parameters of experimental model, b. Comparison of vertical trajectory, c. Comparison of impact point)

a. b.

Figure 4) The results of VISJET model for Bandar Abbas desalination plant (a. VISJET results in the absence of marine currents, b. VISJET results with presence of marine currents)

References

1. Bleninger, T., & Jirka, G. H. (2008). Modelling and environmentally sound management of brine discharges from desalination plants. Desalination, 221(1-3), 585-597.
2. Jiang, B. L.-K.-W. (2012). Mixing of 45° inclined dense jets in shallow coastal waters: surface impact dilution. Third International Symposium on Shallow Flows.
3. Roberts, P. J., & Abessi, O. (2014). Optimization of desalination diffusers using three-dimensional laser-induced fluorescence. Agreement Number R11 AC81, 535.
4. Bleninger, T., & Jirka, G. H. (2005). User's Manual for CORHYD: An Internal Diffuser Hydraulics Model. Institute for Hydromechanics, University Karlsruhe, Germany.
5. Pipe Life, Technical Catalogue for Submarine Installations of Polyethylene Pipe.
6. Michael Peleg (Miki), Intake Pipes _ Internal Sediments and Marine Growths
7. Zhang, H., & Baddour, R. E. (1998). Maximum penetration of vertical round dense jets at small and large Froude numbers. Journal of Hydraulic Engineering, 124(5), 550-553.

8. Lee, J. H., Cheung, V., Wang, W. P., & Cheung, S. K. (2000, July). Lagrangian modeling and visualization of rosette outfall plumes. In Proc. Hydroinformatics (Vol. 8). Iowa: University of Iowa.

9. Bashitialshaaer, R., Larson, M., and Persson, K. M. (2012). "An Experimental Investigation on Inclined Negatively Buoyant Jets." Water, 4(4), 720-738.

2nd International Conference on Oceanography for West Asia

16 , 17 Sept. 2020 Iran. Tehran

Environmental Impact Assessment of Subsea Power Cables between Kish Island and Gorzeh, Persian Gulf

Rezai, H.; Kabiri, K.; Samimi; K. & Amini, N.

Iranian National Institute for Oceanography and Atmospheric Sciences, Dept. of Marine Biology, Tehran-IRAN

e-mail: rezaihamid1@hotmail.com

Abstract

The environmental impact of 17 km long subsea cables between Kish Island and Gorzeh in the northern Persian Gulf before the construction phase on benthos and in particular coral reefs was studied. Underwater photography and video inspection of the bottom, observations of the bottom habitats by scuba-divers, sampling and laboratory analysis of macrozoobenthos were conducted. In zoobenthos group composition and abundance which could have been clearly related to cable installation were analyzed. The construction will not have any serious effect on benthos, however corals in the vicinity of Kish Island will be damaged slightly. Most organisms have their own ability to recover and resettle after the construction.

***Keywords**: Marine environment, subsea cables, zoobenthos, Baltic Sea, Persian Gulf*

1. Introduction

In addition to pressure from traditional activities such as fishery, shipping and oil pollution, the Persian Gulf ecosystem is being subjected to Increasing pressure from various technical constructions. These installations include fixed links, barrages, oil and gas terminals, oil rigs, pipelines, telec-communication cables and high voltage installations for electrical energy transfer. Energy transfer via underwater power cables is done to improve the exploitation of the various power systems in countries located on the Persian Gulf (PreussenElectra, 1994; So¨derberg and Johnson, 1997). In contrast to land grid systems, which generally use alternating current, this type of installation uses high voltage direct current.

The transmission of electrical energy through underwater high voltage direct current (XPLE) lines has been the subject of public concern due to the possible ecological effects of cable installation and operation. These include

mechanical damage to marine life on the bottom, the chemical effects related to the release of toxic chlorine from anodes and the influence of physical fields on macrofauna and migrating fish.

Almost no studies on the interaction between various Persian Gulf cables can be found in the open literature. However, some information regarding the assessment of anticipated environmental effects is available in Rezai *et al.* (2010, 2011). The information included in these reports comes from the results of field studies.

The objectives of the present study were: *i*) to monitor the environmental impact before the cable operations, and *ii*) to determine the impact of the Kish-Gorzeh subsea power cables before the cable operations on benthos. Due to a lack of bottom macrophytes along the cable route, macrozoobenthos was an obvious indicator of physical disturbances on the bottom. Macrozoobenthos communities are relatively stable and they are dominated by long-lived, sedentary species with limited seasonal variability (Bonsdorff, 1983; Sousa, 1984; Bonsdorff et al., 1995).

2. Materials and methods

Field measurements along the selected route (Fig. 2) included visual observations by divers, documentation by divers using a video camera

(Sony T-100) and macrozoobenthos sampling (ven veen Grab). Seventeen stations were designated based on different sediment types and at different depths along the cable route (Fig. 3). Of these, 16 stations were located along the cable route (cable stations) and another 1 station (reference station) was located approximately 1 nautical mile west of the planned cable route. Samples were collected during fair weather, and location of the sampling sites was determined to within a few meters using a GPS positioning system.

The environmental impact monitoring aimed to track the change of water quality and biological resources before the subsea cable construction. Parameters included temperature, salinity, DO, turbidity and suspended solids.

The data of biological resources which have been divided into 2 groups included coral reefs and macrobenthos. Benthos samples were taken in triplicate at every sampling location using a van veen grab with a 250 cm^2 catching surface and a maximum penetration depth of 25 cm. Every benthos sample was sieved separately through a 1 mm sieve, which selects the benthos fraction defined as macrozoobenthos. The sieved samples were then preserved with 4% buffered formaldehyde. In the laboratory, macrozoobenthos were identified to groups.

3. Results

- A total of 18 taxa of macrozoobenthos were identified—15 species and 3 undetermined taxa (Oligochaeta, Hydrobiidae and Gammaridae). Crustacea
- was the most diverse group, followed by Polychaeta and Bivalvia. (Andrulewicz *et al*., 1999, 2000). The comparisons of species abundance and biomass between 1999 and 2000 are presented in Figs. 5 and 6. The lowest mean values among the stations along the cable route were observed in 2000 in study area 1, while in study areas 2, 3 and 4 the mean values were very similar in 1999 and 2000. The data were subjected to variance analysis
- (ANOVA test) to determine the significance of differences of various parameters between cable and reference stations. It was noted that the differences in the mean values of abundance and biomass in study area

- 1 (Figs. 5 and 6) were relatively high; simultaneously variability was also high. Therefore, it is impossible to determine whether these differences are related to cable installation. The impact of the construction phase on the macrozoobenthos is apparent at the deepest station, study area 4, where the mean size of individuals changed as abundance increased and biomass decreased. This may indicate that, following bottom disturbances, the macrozoobenthos recovered and resettled the impacted area around the cable.

4. Conclusion

The studies conducted prior to cable installation (2011).The cable itself was buried in the hard and soft bottom, and only on the hard stone and boulder bottom in the north eastern part of the Island did the cable appear in some places on the surface of the bottom. Studies of macrozoobenthos indicated that there were no obvious changes in macrozoobenthos abundance which could be related to bottom disturbance caused by cable construction. In study area 4, which is the deepest station with a significantly less dynamic bottom than those of other study areas, some indications that the construction phase could have had an impact were noted in that the mean size of individuals was smaller one year after cable installation. The construction of subsea power cables from Kish Island to mainland Gorzeh improves the living quality of residents and reduce fossil fuel.

2nd International Conference on Oceanography for West Asia

16 , 17 Sept. 2020 Iran. Tehran

Makran coastal plain deposits (SE Iran), a potential source of aeolian sediments; insights from sedimentology and geochemistry

Kaveh, Firouz Amaneh [1,4*]; Mohammadi, Ali [2, 4]; Lak, Razyeh [3, 4]

1. Iranian National Institute for Oceanography and Atmospheric Science (INIOAS), Tehran, Iran
2. Eurasia Institute of Earth Sciences, Istanbul Technical University, Istanbul, Turkey
3. Research Institute for Earth Sciences, Geological Survey of Iran, Tehran, Iran
4. Marine Geology Department, Geological Survey of Iran, Tehran, Iran

Abstract:

The coastal plain of the Hormoz Strait and Oman Sea in southeastern Iran have huge watershed, dry climate and annual precipitation of less than 98 mm/yr. To study sedimentology and sediment geochemistry of the Oman Sea, 46 samples of surficial sediments were collected from Minab, near the Hormoz Strait, to the Guater Gulf near the Pakistan border. Granulometry, calcimetry, elemental analysis (ICP), mineralogy and clay determination by XRD were carried out at the Geological Survey of Iran.The analyses show that sediments are mostly very poorly to moderately sorted sandy mud, mud, muddy sand and sand. They statistically classify as coarse-skewed, fine-skewed, and near symmetrical with very leptokurtic to leptokurtic, platykurtic to very platykurtic and mesokurtic distributions. Calcite, quartz and feldspar are the three dominant minerals in variable proportions. Halite is the fourth important constituent. Chlorite, illite, kaolinite and poligorskite are frequent clay minerals. Montmorillonite is found in the eastern part of the Oman coastal plain, from Chabahar to the Pakistan border. Conversely, poligorskite is found only in the coastal plain of the Hormoz Strait. Cluster and factor analyses of elements reveal lead and cadmium of likely anthropogenic origin, yet at concentrations lower than authorized levels in sediments. Accordingly, they present no risk to the local population. Geochemical and mineralogical evidence shows that parts of sodium, calcium, strontium, barium, and phosphorus are chemically and biochemically produced in the region, as supported by their inverse relationship to the earth elements. Shell fragments and corals contribute Ca and Sr. Other elements (Al, Fe, Cr, Co, Zn, Zr, Mn, Ti, Mg, U, Ti, Th) have also a clastic origin, denoting erosion of ophiolite, mélange zones and turbidites of Makran. They entered the basin as clastic carbonates and aeolian sediments. Poligorskite, in particular, reached the Makran coast through the winds coming from the western part of the Persian Gulf.

This work shows that the clastic, chemical-biochemical and anthropogenic processes influence the elements distribution of Makran coastal sediments. The local rivers and winds are the important processes controlling present-day sedimentation there.

Keywords *(Makran coastal plain, Aeolian dust, Sedimentology, Sediment Geochemistry)*

1. Introduction

Low topography, strong wind systems and availability of fine and loose grains made coastal plains as an important sources for aeolian sediment studies (Das et al., 2008). The Makran coast of Iran and Pakistan is one of the plains with few dry playas, which produces 12 percent of dust storm of the world (Prins et al., 2000). The coastal plain of the Hormoz Strait and Oman Sea in southeastern Iran have huge watershed, dry climate and annual precipitation of less than 98 mm/yr. The mentioned characteristics of Makran coast provide opportunity to study aeolian sediments. Accordingly, the main aim of this research is to find out the main controlling processes for sediment deposition and element distribution in the Makran coast.

2. Material and methods

To study sedimentology and sedimentary geochemistry of the Oman Sea, 64 samples of surficial sediments were taken from Minab near the Hormoz Strait as far as the Guater Gulf near Pakistan border. Sediment samples prepared from a mixture of samples as a regular graded. In fact, each sample is mixed with 64 samples of surface sediment (Fig. 1), which covers 1600 m^2. Granulometry, calcimetry, elemental analysis (ICP), mineralogy and clay determination by XRD were carried out at the Geological Survey of Iran.

3. Results and discussion

- Sedimentology

Based on granulometric study sediments are classified (according to Folk, 1974) into four main type: Mud, Sandy Mud, Muddy Sand and Sand. The analyses show that sediments are mostly very poorly to moderately sorted. Statistically they are classified as coarse-skewed, fine-skewed, and near symmetrical with very leptokurtic to leptokurtic, platykurtic to very platykurtic and mesokurtic distributions.

Calcite, quartz and feldspar are the three dominant minerals in variable proportions. Halite is the fourth important constituent. Chlorite, illite, kaolinite and poligorskite are frequent clay minerals. Montmorillonite is found in the eastern part of the Oman coastal plain, from Chabahar to the Pakistan border. Conversely, poligorskite is found only in the coastal plain of the Hormoz Strait.

One of importance source of the Gulf of Oman recent sediment is aeolian sediments, which mostly transport from north (Makran coast and some dray Playa in Iran and Pakistan) and west (Arabia Desert). A part of fine grain sediments (30%) of Gulf of Oman have aeolian source.

- Sediment Geochemistry

Cluster and factor analyses of elements reveal lead and cadmium of likely anthropogenic origin, yet at concentrations lower than authorized levels in sediments. Accordingly, they present no risk to the local population. Geochemical and mineralogical evidence shows that parts of sodium, calcium, strontium, barium, and phosphorus

are chemically and biochemically produced in the region, as supported by their inverse relationship to the earth elements. Shell fragments and corals contribute Ca and Sr. Other elements (Al, Fe, Cr, Co, Zn, Zr, Mn, Ti, Mg, U, Ti, Th) have also a clastic origin, denoting erosion of ophiolite, mélange zones and turbidites of Makran. They entered the basin as clastic carbonates and aeolian sediments.

Four main processes (clastic, chemical, biochemical and Anthropogenic) contoroled the element distribution in Makran coast sediment.

Fig. 1) a: Sampling points along the Iranian Makran Coast. b: Satellite image from Dust storm in the Gulf of Oman over the Makran Coast (MODIS June 16, 2004). c: Movement of sand dune on the roads and residential areas..

4. Conclusions

- The major contributors in sediments are mud, sandy mud, muddy sand and sand.

- Mineralogy of sediment contains calcite, quartz, feldspar and halite.

- Major clay minerals are chlorite, illite, kaolinite and poligorskite, respectively.

- Four main processes (clastic, chemical, biochemical and anthropogenic) controlled the element distribution in Makran coast sediment.

- Arsenic and cadmium are anthropogenic elements in Makran coast.

- The main source of heavy element such as Cr, Ni, and Zn is Makran ophiolite mélange.

- Due to morphology, climatology and sedimentological parameters, Makran coast is a great and important source of aeolian sediments and dust storm in SE of Iran and even in south Asia.

References

1. Das, S.S., Maurya, A.S., Pandey, A.C., Bhan, U. and Rai, A.K., 2008. Influence of sediment source and monsoonal variations on the late Quaternary clay mineral assemblages at ODP site 728A, northwestern Arabian Sea. Current Science, pp.1320-1326.
2. Folk, R.L., 1974. Petrology of sedimentary rocks: Hemphill Pub. Co., Austin, Texas, 63.
3. Prins, M.A., Postma, G. and Weltje, G.J., 2000. Controls on terrigenous sediment supply to the Arabian Sea during the late Quaternary: the Makran continental slope. Marine Geology, 169 (3-4), pp.351-371.

2nd International Conference on Oceanography for West Asia

16 , 17 Sept. 2020 Iran. Tehran

Magnetic Signature of the Sediment Cores of the Persian Gulf and Gulf of Oman: Implication for Sea-Level Changes during the Holocene

Lahijani, H. A. K[1].; Naderi, M[1]; Amjadi, S[1].; Pourkerman, M[1]

1-Iranian National Institute for Oceanography and Atmospheric Science(INIOAS), No. 3, Etemadzadeh St., Fatemi Ave, Tehran, Iran

Keywords *Persian Gulf, Oman Sea, Holocene, paleoclimate, magnetic susceptibility*

1. Introduction

The Persian Gulf (PG) as a shallow semi enclosed basin and Gulf of Oman (GO) a deep basin remnant of Neothetis located in arid climate. The bottom morphology of two basins inherited from long geological history of compression processes between Arabian and Eurasian plates as well as paleoclimate events. In the PG, fluvial systems mainly from the northern part supply terrigenous sediment originating from Zagros and Taurus mountains. The southern part with limited drainage is dominated by carbonate and evaporates. Bottom sediment of the PG were investigated to uncover role of marine organisms in carbonate and organic matter content of modern sediments (Houbolt, 1957; Sugden, 1963; Evans, 1966). A comprehensive study about modern and Holocene sedimentation in the PG is introduced by Purser (1973). Distribution pattern shows increasing grain size from north to south with domination of carbonate (Baltzer and Purser, 1990). Proximity of northern part to the Zagros along with other influencing factors including relatively deeper sub basin, more fluvial supply and lesser carbonate sedimentation contributed to the mixed sedimentation.

Magnetic susceptibility widely has been applied for marine sediment cores as an inexpensive and nondestructive method (Hounslow and Maher,1999; Hoogakker et al., 2004; Larrasoaña et al, 2008). Signature of depositional environment and sediment sources are reflected in the MS signals of the marine achieves (Bloemendal and de Menocal, 1989; Hoogakker et al., 2004). Climatic events and their consequences in changing sediment sources could be untraveled as susceptibility values. Dust and terrigenous inputs display higher MS values (Hounslow and Maher, 1999). Post-depositional processes could influence on the MS signals, however using young short cores with taking into account the specification of the environment, MS values could unearth paleoclimate events (Hatfield and Stoner 2013). Using short cores of the northern PG and GO we aim to decipher past drives on the sedimentation in these areas.

2. Materials and methods

30 legs with 120 stations were selected for sampling in the Persian Gulf and Gulf of Oman. 27 cores were obtained via gravity corer during Persian Gulf and Gulf of Oman Oceanographic Studies (PG-GOOS) cruises (Fig 1). The cores were transferred to the Iranian National Institute for Oceanography and Atmospheric Science (INIOAS) coastal affiliations laboratories in order to measuring nondestructive Magnetic Susceptibility (MS) analysis. MS was measured using a Bartington MS2C 100-mm diameter loop sensor with an MS2 meter. Data acquisition performed on 1 cm interval and high variability of data normalized regarding the mean value of each core.

3. Results

The MS results demonstrate that within the interval of 20–60 cm of northwestern PG cores, minimums of MS occur, however the base and top parts have higher values in MS. The cores of south eastern PG display frequent fluctuations in MS. Five cores have much higher MS values compared to the other PG cores. MS signal value in the cores of SH are up to three times higher than those in the PG. The core close to the PG have two picks in base and top while two other cores close to the GO have picks in top and middle parts. In the GO the MS value along the cores display different variations and range between 2.5 x 10-5 to 5.5 x 10-5 SI. Most cores in the PG and SH have thickness up to 140 cm and GO cores up to 160 cm. The overall picture is that in the PG the cores close to the northern mainland demonstrate higher MS value and their MS increase drastically in the SH and again decrease in the GO, however the MS value in the GO cores is higher than of the PG cores.

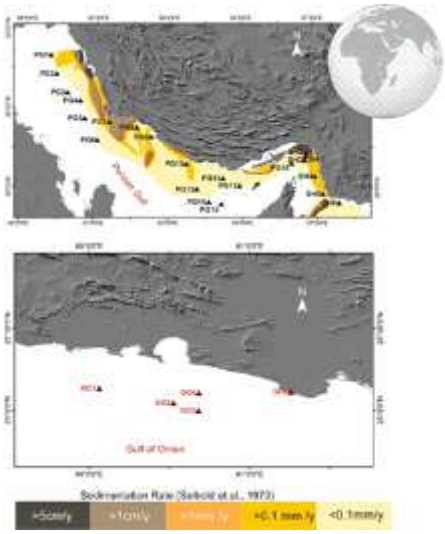

Figure 1) The location of sampling sites and sedimentation rate in the northern site of The Persian Gulf and straite of Hormuz

4. Discussion and conclusion

The magnetic susceptibility in the Holocene sediments of the Persian Gulf, Strait of Hormoz and Gulf of Oman display considerable variations spatially and temporally. The highest value observed in the Strait of Hormoz that reflect this area as accommodation space of terrigenous sediments through the Persian Gulf both during the highstand and lowstand. The Persian Gulf sediment with high biological and chemical carbonate reflect lowest

MS values, however the GO with frequent ephemeral flooding and mass wasting has higher MS value. Higher MS value in the most cores indicates overall wetter climate during the late Holocene, while lower MS could be attributed to the lesser detrital inputs during dry periods.

References

1. Baltzer, F., & Purser, B. H. (1990). Modern alluvial fan and deltaic sedimentation in a foreland tectonic setting: the lower Mesopotamian plain and the Persian Gulf. Sedimentary Geology, 67(3-4), 175-197.
2. Bloemendal, J., deMenocal, P.B.,1989. Evidence for a change in the periodicity of tropical climate cycles at 2.4 Myr from whole-core magnetic susceptibility measurements. Nature 342, 897–900.
3. Evans, G. (1966). A discussion concerning the floor of the northwest Indian Ocean-The recent sedimentary facies of the Persian Gulf region. Philosophical Transactions of the Royal Society of London. Series A, Mathematical and Physical Sciences, 259(1099), 291-298.
4. Hatfield R.G., and Stoner J.S. (2013) Magnetic Proxies and Susceptibility. In: Elias S.A. (ed.) The Encyclopedia of Quaternary Science, vol. 2, pp. 884-898. Amsterdam: Elsevier.
5. Hoogakker, B. A. A., Rothwell, R. G., Rohling, E. J., Paterne, M., Stow, D. A. V., Herrle, J. O., & Clayton, T. (2004). Variations in terrigenous dilution in western Mediterranean Sea pelagic sediments in response to climate change during the last glacial cycle. Marine Geology, 211(1-2), 21-43.
6. Houbolt, J. J. H. C. (1957). Surface sediments of the Persian Gulf near the Qatar Peninsula. Mouton.
7. Hounslow, M.W., Maher, B.A., 1999. Source of the climate signal recorded by magnetic susceptibility variations in Indian Ocean sediments. J. Geophys. Res.104, 5047–5061.
8. Larrasoaña, J. C., Roberts, A. P., & Rohling, E. J. (2008). Magnetic susceptibility of eastern Mediterranean marine sediments as a proxy for Saharan dust supply?. Marine Geology, 254(3-4), 224-229.
9. Purser, B. H., & Evans, G. R. A. H. A. M. (1973). Regional sedimentation along the Trucial coast, SE Persian Gulf. In The Persian Gulf (pp. 211-231). Springer, Berlin, Heidelberg.
10. Sugden, W. (1963). Some aspects of sedimentation in the Persian Gulf. Journal of Sedimentary Research, 33(2), 355-364.

2nd International Conference on Oceanography for West Asia

16 , 17 Sept. 2020 Iran. Tehran

Why living marine Catfish *Plotosus lineatus* in Persian Gulf is unique amongst teleosts?

Malakpour Kolbadinezhad, Salman [1, 2,3]; M. Wilson Jonathan [*1,2,4]

1. Centro Interdisciplinar de Investigação Marinha e Ambiental (CIIMAR/CIMAR), Universidade do Porto, Porto, Portugal.

2. Instituto de Ciências Biomédicas de Abel Salazar (ICBAS), Universidade do Porto, Porto, Portugal.

3. Coldwater Fisheries Research Center (CFRC), Iranian Fisheries Sciences Research Institute (IFSRI), Agricultural Research, Education and Extension Organization, Tonekabon, Iran.

4 .Department of Biology, Wilfrid Laurier University, Waterloo, Canada

*corresponding e-mail: s.malakpoor@gmail.com

Abstract

Unlike other marine teleosts, the Plotosidae catfish reportedly have an extra-branchial salt secreting dendritic organ (DO). Three salinity acclimation for 10 days [brackishwater (BW) 3‰, seawater (SWcontrol) 34‰ and hypersaline water (HSW) 60‰] was used to investigate the osmoregulatory abilities of Plotosus lineatus through measurements of blood chemistry, muscle water content (MWC), Na+/K+-ATPase (NKA) activity and ion transporter expression in gills and DO using immunoblotting (IB), immunohistochemistry. HSW represented a significant osmoregulatory challenge with elevated mortality (36%), plasma osmolality and ions, and hematocrit, and decreased MWC. DO NKA activity and protein were significantly higher than other organs at all salinities. DO mass thus total DO NKA activity was higher, indicating higher overall capacity at HSW although elevated Hsp70 levels indicate a cellular stress and possible pathological condition. BW acclimation resulted in lower NKA activity in both gill and DO. Cl- levels were better regulated and the resulting strong ion ratio in BW suggests a metabolic acidosis. Strong NKA and NKCC1 co-localization was observed in DO parenchymal cells, which was rare in gills ionocytes. NKCC1 expression was only detected (IB) in DO which was highest at HSW. CFTR localize apically to DO NKA-IR cells. Taken together, the demonstration of high NKA activity in DO coexpressed with NKCC1 and apical CFTR indicates the presence of the conserved secondary active Cl- secretion mechanism found in other ion transporting epithelia suggesting a convergent evolution with other vertebrate salt secreting organs.

Keywords*: Plotosus lineatus, osmoregulation, gill, dendritic organ, Na^+/K^+-ATPase*

1. Introduction

Osmoregulatory organs in teleost fishes including the gills, kidney and digestive tract are involved in maintenance of body fluid balance (Marshall and Grosell, 2006; Takei and Hwang, 2016). Gills are the first organ to directly sense external osmotic changes that also facilitate either compensatory active uptake (in freshwater) or excretion (in saltwater) of monovalent ions (Na^+, K^+, and Cl^-) to maintain plasma osmolality within a narrow range depending on the environmental salinity (Evans, 2008; Takei and Hwang, 2016). Marine teleosts are hypoosmotic to their environment, which leads to osmotic water loss. They compensate by drinking seawater and absorbing the ingested water by solute (Na^+ and Cl^-)-linked water transport in the intestine (see review by Grosell, 2010). In contrast, in freshwater fishes the role of the intestine is minor in osmoregulation, which are hyperosmotic to the environment (Takei and Hwang, 2016). However, ion uptake by the intestine can be substantial in feeding fishes (Wood and Bucking, 2011).

In freshwater or seawater, the regulation of the osmolality and ion levels of body fluids of fishes is done actively (Edwards and Marshall, 2012). The plasma osmolalities of euryhaline teleost species of freshwater and marine origin vary, however, in seawater they are maintained at less than 480 mOsm/kg H_2O (Varsamos et al., 2005). The effects of changing salinity on plasma osmolality and circulating electrolytes has been reported in a number of euryhaline teleosts (e.g. Christensen et al., 2012; Sardella et al., 2008; Kang et al., 2008; Tait et al., 2017). The Plotosidae catfish *Plotosus lineatus* is native to Indo-Pacific coastal waters from Japan to the Red Sea and East Africa and have recently invaded the Mediterranean (Lanzing, 1967; Froese and Pauly, 2018) and Persian Gulf (https://www.oceandocs.org/handle/1834/9339). They are amphidromous and are found in marine and brackishwater, and have also been reported in freshwater (Froese and Pauly, 2018).

The DO is a small fleshy external organ situated on the ventral caudal surface of Plotosidae catfishes, in both sexes from early life stages, that is very close to the urogenital papilla (Hirota, 1895; Lanzing, 1967; Laurenson et al., 1993). The parenchymal cells of the DO form glandular acini that are covered by a stratified squamous epithelium (Van Lennep and Lanzing, 1967; Van Lennep, 1968). Descriptive morphological studies in the gills and DO of *Plotosus lineatus* suggested cellular similarity to fish gill ionocytes and elasmobranch rectal gland cells (Pucke and Umminger, 1979; Van Lennep and Lanzing, 1967; and Van Lennep, 1968). The rectal glands from elasmobranchs and specialized salt glands from marine tetrapods (e.g., the nasal salt gland of marine birds, lachrymal gland of marine turtles, and lingual glands in sea snakes, saltwater crocodiles; Shuttleworth and Hildebrandt, 1999; Kirschner 1980) have similar parenchymal cell characteristics and the mechanism of NaCl excretion is also similar to the teleost gill chloride cells (secondary activity Cl^- secretion) (da Silva et al., 1977; Singer et al., 1998; Marshall and Grosell, 2006). The numerous independent origins of these salt glands leads to the hypothesis of a convergent evolution of salt glands across taxa (Babonis and Evans, 2011).

Since the molecular machinery of the osmoregulatory organs (gill and DO) in *P. lineatus* are unknown, for the first time in the present study we addressed their molecular mechanisms using a combination of enzymatic analysis, immunohistochemistry, immunoblotting and PCR together with key osmoregulatory indicators (plasma ion levels and osmolality, and muscle water and ion levels) in fish acclimated to different salinities. Salinities covered the natural range of Plotosidae catfishes and a more challenging hypersaline condition that can be present in hypersaline estuaries (Lanzing, 1967; Young and Potter, 2002) were used. In doing so we also addressed the possibly of a conservation of mechanisms for ion transport in salt secretory cell similar to other vertebrate salt glands with respect to co-option events where the original function of the organ is displaced (e.g. lachrymal glands of marine turtles have tear production co-opted for the secretion of concentrated salt solution).

2. Material and Methods

2.1. Animals

Striped eel catfish *Plotosus lineatus* (~8-13 g; 12.3- 14.0 cm; n=54) were obtained from the Tropical Marine Centre (TMC) Portugal and transported to the Laboratory of Molecular Physiology CIIMAR (Porto). Fish were originally collected from the wild in Australian waters for TMC. All fish were acclimatized to laboratory conditions in a 100 L tank of seawater (SW) 34‰, with mechanical and biological filtration, UV sterilization, aeration, and temperature control (26-28°C) under a natural photoperiod for three weeks prior to the start of the experiment to avoid any confounding effects of handling stress on osmoregulation (Biswas et al., 2006). The water salinity, pH, temperature and dissolved oxygen were monitored daily with a multimetric probe (WTW 340i, WTW Measurement Systems Inc. Weilheim, Germany).

2.2. Salinity acclimation

Three salinity levels were investigated following at least two weeks experimental acclimation to brackishwater (BW) 3‰, seawater (SW-control) 34‰, or hypersaline water (HSW) 60‰ under uniform holding conditions. The salinity extremes were based on preliminary studies. Initially, groups of 5-6 fish were transferred to 30 L tanks, in which salinity was changed in a stepwise fashion, from 34‰ (main tank) to 3‰ or 60‰ (smaller 30L tanks), by 5‰ per day. Instant Ocean® sea salts were used to prepare a stock solution of 100‰ and diluted to the appropriate salinities. Aquaria were provided with mechanical and biological filtration, UV sterilization and weekly 20% water changes. The fish were used according to the Portuguese Animal Welfare Law (Decreto-Lei no.197/96) and animal protocols were approved by CIIMAR/UP.

2.3. Sampling

Individual marine catfish were netted then euthanized in a separate smaller tank (1L) with an overdose of ethyl-m-amino benzoate-MS-222 (1:5000, pH 7.5 adjusted with $NaHCO_3$; Pharmaq UK), weighed (±0.01 g) and total length (mm) measured. Blood was collected using heparinized capillary tubes following caudal transection then

centrifuged at 13000xg for 5min at room temperature (Heraeus Pico 17 Centrifuge, Thermo Scientific). Hematocrit (Hct) was measured. The isolated plasma was then frozen in liquid nitrogen and kept at −80°C. The following organs were collected: gill and dendritic organ (DO) were snap frozen in liquid nitrogen and were then immediately stored at -80°C. The gastrointestinal tract of *P. lineatus* is relatively short and without a stomach. The anterior intestine was heavily pigmented and easily distinguished from the unpigmented posterior intestine. Gill filaments samples from the second arch on the left side, DO, kidney, and intestine were also excised, immersed in 100µl of ice-cold SEI (150 mM sucrose, 10mM EDTA,50mM imidazole, pH 7.3) buffer and frozen at −80°C. An additional piece of deskinned epaxial muscle (~1 g) was collected into a pre-weighed tube for water and ion analysis. In additional sets of six individuals, the body cavities were opened and then immersion fixed in 10% neutral buffered formalin (NBF 10%) for 24 h and then stored in 70% ethanol at 4°C.

2.4. Ion quantification

The ~1 gram of muscle was dried at 60°C to constant mass for the determination of muscle water content (MWC). The dried muscle samples were digested in 65% nitric acid for 3 days at room temperature. The Na^+ and K^+ concentrations were quantified by flame photometry (model PFP7; Jenway, Felsted, UK) and expressed as µmol · g^{-1} wet mass. Plasma samples were also analyzed by flame photometry (PinAAcle 900T Atomic Absorption Spectrophotometer; Perkin Elmer Waltham MA). Chloride concentration was measured in plasma samples colormetrically (Küffer et al., 1975). Plasma osmolality was determined in fresh samples using freezing-point depression osmometry (Micro-Osmometer, Roebling Co. Berlin Germany) and reported as mOsm kg^{-1} (Malakpour Kolbadinezhad et al., 2012).

2.5. Measurement of Na^+/K^+-ATPase activity

The Na^+/K^+-ATPase (NKA) activity was measured according to McCormick (1993) with modifications by Wilson et al. (2007). After thawing samples in 300 µl SEI (250 mM sucrose, 10 mM EDTA, 50 mM imidazole pH 7.3) buffer, sodium deoxycholate was added to a final concentration of 1%. Tissue was homogenized using a Precellys 24 bead homogenizer (Bertin Technologies, Montigny-le-Bretonneux, France) at 5800 RPM for 2x15s and then immediately centrifuged at 15,000 x g for 5 min at 4°C. Ten µl of supernatant were run in two duplicate sets for the ATPase assay at 340nm with a temperature controlled microplate reader (Powerwave 340; Biotek, Winooski, VT) and Gen5™ reader control and data analysis software for 10-20 min at 25°C. One set of wells contained the assay mixture and the other set assay mixture plus ouabain (1 mM, Sigma– Aldrich Chemical Co.;St. Louis MO) to specifically inhibit NKA activity. Total protein was determined in the remaining supernatant using the Bradford (1976) at 600nm and the results are expressed as µmol ADP mg^{-1} protein h^{-1}. In the case of the DO, the NKA activity is also expressed per DO correcting for body mass, since DO mass increase under HSW conditions.

2.6. Immunoblotting

The unused homogenate from the ATPase assay was mixed with an equal volume of 2x Laemmli's buffer (Laemmli, 1970), heated for 10 min at 70°C and then stored at 4°C. Protein concentration was adjusted to 1 µg μl^{-1} using 1x Laemmli's buffer. Immunoblotting was performed as described in Reis-Santos et al. (2008). Ponceau-S staining of membranes was performed to assess transfer and sample loading consistency. Blots were probed with heterologous rabbit polyclonal antibodies against the α-subunit of NKA (1:500; αR1 antibody; Wilson et al., 2007), bovine cytosolic CA (1:2000, Abcam Cambridge UK; Randall et al., 2014), and V-ATPase B subunit (1:200, B2; Wilson et al., 2007) or mouse monoclonal antibodies against NKCC/NCC (1:200, T4 clone; Developmental Studies Hybridoma Bank (DSHB), U.Iowa USA; Tipsmark et al., 2002, Wilson et al., 2007), heat shock protein (Hsp70) (1:10000, BRM-22 clone; Sigma-Aldrich), and α-tubulin (1:500 12G10 clone, DSHB). The later antibody was used as a loading control for samples. The membranes were rinsed with TTBS (0.05% Tween-20 in Tris Buffered Saline) and then incubated for 1 hour with a goat anti-rabbit or anti-mouse IgG secondary antibodies conjugated to horseradish peroxidase (HRP) and the signal were detected by enhanced chemiluminescence (ECL) using Immobilon Western chemiluminescent HRP substrate (Millipore Corporation, Billerica, MA, USA). Images were acquired using a luminescent image analyzer Fujifilm LAS-4000 mini and image reader software LAS-4000 version.2.0. The area intensity of bands were quantified using the image analysis software program Multi Gauge v3.1 (FUJIFILM, Tokyo Japan) and expressed as a ratio with α-tubulin.

2.7 Immunohistochemistry (IHC)

Immunofluorescence localization was performed according to Reis-Santos et al. (2008). In short, paraffin serial sections were cut and dewaxed followed by a series of xylene baths and rehydrated through a descending ethanol series to water. Antigen retrieval was performed on some sections (Shi et al., 2011) by pretreatment with 0.05% citraconic anhydride (pH 7.3) for 30min at 98°C (Namimatsu et al., 2005) and then with 1% sodium dodecyl sulfate (SDS) in PBS for 5 min (Brown et al., 1996). All sections were then blocked with 5% normal goat serum (NGS) and then incubated with primary rabbit or mouse antibodies to the α-subunit of NKA (αR1), NKCC/NCC (T4), CFTR (R&D systems), and V-ATPase B-subunit (B2) overnight at 4°C, rinsed in TPBS (0.05% tween-20 phosphate buffered saline, pH 7.4), followed by incubation with secondary goat anti-mouse Alexa Fluor 568 and/or goat anti-rabbit Alexa Fluor 488-conjugated antibodies for 1h at 37°C. Sections were stained with DAPI (4',6-diamidino-2phenylindole) and viewed on a Leica DM6000B wide field epifluorescence microscope and micrographs taken with a digital camera (DFC340FX, Leica Microsystems, Wetzlar, Germany) using Leica LAS AF acquisition software. Figures were assembled in Photoshop CS3.

2.8 Statistics

Data are presented as means ± standard error of the mean(SEM). Statistical differences of protein, mRNA expression between groups were determined using one-way analysis of variance (ANOVA) followed by the post

hoc Student-Newman-Keuls (SNK) test (SigmaPlot 11.0 Systat Software, Inc.) in juveniles exposed to different salinities. Data were square root or log transformed in the case of a failed normality test. The fiducial limit was set at 0.05.

3.Results

3.1Osmoregulatory indicators

Plasma and muscle osmoregulatory indicators are presented in Table 1. Plasma Na^+ concentrations correlated positively across the range of acclimation salinity while plasma Cl^- and Ca^{2+} concentrations and osmolality were significantly higher in HSW compared with SW and BW acclimated animals. Plasma osmolality was more than 50% higher in HSW acclimated fish. The resulting plasma strong ion ratio (SIR) was significantly lower in BW fish compared to SW and HSW acclimation. Hematocrit showed a positive correlation with salinity where BW values were half of HSW. Acclimation salinity had no effect on plasma K^+ concentration.

Muscle water content was significantly lower in HSW acclimated fish indicating dehydration but was unaffected by BW acclimation. In contrast, fish condition factor showed a negative correlation with salinity from BW to HSW. Muscle K^+ concentration followed the opposite trend being significantly higher in HSW fish. Muscle Na^+ content did not differ with salinity, which is reflected in a lower Na^+: K^+ ratio in HSW fish. There was mortality (36%) only with HSW acclimation but not in other salinity groups.

3.2NKA activity

In SW *P. lineatus*, the specific NKA activity is lowest in the gill and twenty times higher in the DO (Fig. 1A). In response to salinity acclimation, similar patterns of NKA specific activity were detected in the gill and DO with significantly higher activity in SW acclimated fish compare to both BW and HSW salinities (Fig. 1B, F).

The mass of the DO in SW-control salinity acclimated fish expressed as a percentage of fish body mass was significantly lower compared to BW and HSW salinity groups (Table 1). However, in HSW salinity acclimated fish DO mass was greatest at 213% and 243 % of BW and SW fish, respectively. Since DO mass changed with salinity, we also expressed NKA activity on a whole organ basis corrected for fish mass. The expression of the total DO NKA activity relative to fish body mass shows that in HSW fish DO NKA activity was 1.6 and 2.1 fold higher than in SW and BW fishes, respectively (Fig 1G).

3.3 Immunoblotting

We used antibodies crossreactive with NKA α-subunit, NKCC1, cytosolic carbonic anhydrase, V-ATPase B subunit and Hsp70 to determine how salinity affected the abundance of these important transport and stress related proteins in key osmoregulatory organs: gill and DO. A representative tissue distribution immunoblot is shown in Figure S1 of a SW control fish.

NKA α-subunit expression was detected in all organs of interest as a single band of approximately 100kDa. The relative expression of the NKA α-subunit protein was significantly higher with HSW exposure in the gill and kidney (Fig 2A, B) but was not salinity responsive in either the intestine or DO (Fig. 2C-E) . NKCC/NCC expression was detected only in DO with a pair of prominent immunoreactive bands of 140-260 kDa with some additional higher molecular mass bands sometimes present. Higher NKCC/NCC expression in the HSW salinity acclimated fish relative to BW and SW fish in DO was observed (Fig. S1, 3F). The expression intensities of these bands were approximately 2.7 and 2.5 time greater in HSW acclimated individuals compare to the BW and SW-controls, respectively. Immunoreactivity with the CFTR antibody was observed in the predicted molecular mass range as a single band of 160 kDa in DO of a SW fish (Fig. S1); however, blots for the salinity experiment were not clean, and multiple smaller cross-reactive bands were detected, which made semi-quantification problematic. Because of these difficulties in detecting cross-reactive bands, the antibody was not use in other organs or for quantification.

Ca17 was detected as an approximately 30 kDa band in all organs (Fig. S1, 2F-J). No detectable differences were found in the DO. The V-ATPase B subunit was expressed as a ~56 kDa band in the gill and DO (Fig. S1, 2K-N). The relative protein expression in the gill was highest in HSW compared to BW and SW. No detectable differences were found DO with salinity acclimations.

Hsp70 protein was found in all of the organs of interest as a single 70 kDa immunoreactive band (Fig. 3A-E). Hsp70 showed significantly higher levels with HSW in the DO relative the BW with intermediate SW levels. No other differences with salinity were observed in gill.

3.4 IHC

3.4.1 Gill

The gills of *P. lineatus* have a typical teleost gill organization of filaments with lamellae. In the branchial epithelium strong NKA immunoreactivity (IR) was detected with both α5 and αR1 antibodies in large isolated ovoid cells throughout the cytoplasm with the exception of the apical region (Fig. 4A-I). This NKA cellular staining pattern is typical of teleost fish chloride cell or ionocyte tubular system, which is continuous with the basolateral membrane. There were relatively few of these branchial NKA-IR cells which were present in a heterogeneous distribution limited to a few interlamellar regions over the leading edge of the filament and were absent from the lamella. Experimental salinities did not alter the NKA-IR cell distribution pattern. The secretory Na^+:K^+:$2Cl^-$ cotransporter (NKCC1) expression in gill was rarely detected despite the use of antigen retrieval techniques and positive immunoreactivity in other organs (DO, kidney and intestine) indicating that species specific immunoreactivity problems were not an issue. The colocalization of NKCC1 in more weakly NKA-IR cells in BW and SW fish are shown in Fig. 4A, and D, respectively. Ovoid cells deeper within the filament epithelium showing only NKCC1 staining were observed in HSW (Fig. 4G).The apical localization of CFTR was

detected in some NKA-IR cells with no apparent salinity dependent differences (Fig. 4B, E, H). The V-ATPase H^+-pump was localized in a similar cytoplasmic staining pattern as NKA; however, in separate cells from NKA-IR cells under all acclimation conditions (Fig. 4C, F, I).

3.4.2 Dendritic Organ

The DO of *P. lineatus* are external and have branching irregular lobes that are well vascularized. The large parenchynal cells form acini covered by a squamous stratified layer of epithelial cells. The large ovoid to pear-shaped parenchymal cells of the DO generally showed strong NKA and NKCC1 immunoreactivity throughout the cell indicative of basolateral tubular system staining (Fig. 5A, D, G). However, there is a smaller subpopulation of parenchymal cells that are more angular in shape that have noticeably stronger NKA-IR and lack NKCC-IR. Salinity dependent differences in staining were not observed. The apical chloride channel CFTR was only observed in a SW control fish and was generally not detectable despite the use of antigen retrieval techniques and positive immunoreactivity in other organs (gill) indicating that species specific immunoreactivity problems were not an issue (Fig. 5E). V-ATPase-IR showed rather similar cytosolic localization in of parenchymal cells of the DO ionocytes without salinity dependent differences (Fig. 5C, F, I).

4. Discussion

Plotosus lineatus can osmoregulate across a wide range of salinities (3-34‰) although HSW (60‰) conditions presented a significant challenge. The BW-SW represents the more natural salinity range of Plotosidae catfishes while HSW would only be encountered in closed or inverted estuaries (Lanzing, 1967; Young and Potter, 2002). However, HSW acclimation has allowed us to test the osmoregulatory abilities of *P. lineatus* under more challenging conditions (Gonzalez, 2012). The DO of *P. lineatus* has the molecular machinery for active NaCl secretion using the conserved mechanism of secondary activity Cl^- transport with NKA, NKCC1 and likely CFTR at its core. The gill clearly has a secondary role in ion regulation with few ionocytes and low overall NKA expression. The intestine shows typical attributes of marine teleosts.

4.1 Osmo- and iono-regulatory responses to salinity acclimation

The observed plasma ion concentrations were in the range of other teleost fish species (see review by Freire and Prodocimo, 2007; Whittamore et al., 2012). However, in comparison to other studies in Plotosidae, the plasma Na^+, Cl^- and K^+ concentrations of *P. lineatus* in SW control in the present study were less than those of *P. lineatus* studied by Pucke and Umminger (1979), while Na^+ was not very different from *Cnidoglanis macrocephalus* (Kowarsky, 1973). In both of these studies osmolality was also lower. These observed differences might be due to a number of differences between the studies (sampling and analytical methods, acclimation temperatures 26-28°C versus 19-20°C, species differences). Salinity challenges typically alter plasma osmolality and electrolytes levels in euryhaline teleosts with an initial crisis stage followed by a regulatory stage (Madsen and Naamansen,

1989; Jensen et al., 1998; Wang et al., 2009). *Plotosus lineatus* acclimated to HSW had higher plasma osmolality and ions (except K^+), and hematocrit, and decreased muscle water content (MWC) and condition factor. Together, these data indicate a systemic dehydration due to water loss by osmosis, and elevated plasma osmolality representing disturbances from internal fluid shift, which may be problematic resulting in a stress situation and mortality. Thus long-term survival in HSW is likely limited. As a corollary, the Plotosidae catfish *C. macrocephalus* in the closed hypersaline Wellstead Estuary (Australia) was not found in the most hypersaline areas of the estuary (55‰-112‰; Young and Potter, 2002). The increase in plasma osmolality at 60‰ cannot be accounted for by increases in measured inorganic osmolytes (fall 200 mOsmol/kg short of the total osmolality). Although not measured, organic osmolytes such as neutral free amino acids (e.g. taurine and glycine) or small carbohydrates (e.g. myo-inositol) (Fiess et al., 2007) could possibly be an indicator of pathological tissue damage. In contrast to *P. lineatus*, very salinity tolerant species gradual increase plasma ion levels when acclimated to salinities up to about 70-75‰, but thereafter then increase plasma ions in a linear fashion at higher salinities (see review by Gonzalez 2012).

Plotosus lineatus challenged with BW, or hypoosmotic conditions are able to maintain plasma osmolality and Cl^- levels but not Na^+. *Plotosus lineatus* were better able to regulate Cl^- levels than marine Ariid catfish, which do not have a DO and have higher serum Cl^- levels (Sulya et al., 1960; Pucke and Umminger, 1979). The lower plasma Na^+ and hematocrit suggest a hemodilution but muscle water and ions were stable. Reports regarding the effect of lower salinity on MWC from different species vary from showing no effect (Kang et al., 2008; Woo and Chung, 1995) to increased MWC (Jensen et al., 1998; Kelly et al., 1999; Sinha et al., 2015).

Due to the dominance of the strong ions Na^+ and Cl^- in blood, changes in the Na^+/Cl^- ratio (SIR) has been recommended for indicating acid-base imbalances (Jensen et al., 1998; Sinha et al., 2015). In the present study, the direct measurements of plasma acid-base balance were not done due to the small size of the fish; however, calculations of SIR revealed changes in the plasma levels of weak anions (e.g. HCO_3^-) and thus acid-base balance. The BW SIR suggests a metabolic acidosis which has also been observed in European sea bass *D. labrax*, reared in lower salinity (Sinha et al., 2015). However, this contrasts with work by Jensen et al. (1998) who have reported a markedly increased plasma SIR following transfer to FW and slight decrease in HSW in *D. labrax*. In *P. lineatus*, HSW had no effect on SIR suggesting no alteration in acid-base status.

4.2 Evidence for a role of gills in salt secretion?

The gill is typically linked to active ion regulation in teleost fishes (Evans, 2008). This is reflected in high levels of NKA, a central driver of ion transport, with dependency of the gill NKA to environmental salinity that may be altered by life history stage, species and experimental conditions in some cases (Evans, 2008; Varsamos et al., 2001; Malakpour Kolbadinezhad et al., 2012). However, branchial NKA activity of *P. lineatus* was the lowest of the osmoregulatory organs tested, unresponsive to HSW acclimation, and an order of magnitude lower than levels

in the DO irrespective of salinity. A similar pattern has been reported in the sharks *Carcharhinus leucas* (Pillans et al., 2005) and *Chiloscyllium punctatum* (Cramp et al., 2015) and ray *Dasyatis sabina* (Piermarini and Evans, 2000) which possess the extra-branchial salt secreting organ the rectal gland. In elasmobranchs, the gills have a secondary function in ion regulation (Wilson et al., 2002; Evans, 2008). Our results confirm a similarity between gills of *P. lineatus* (Pucke and Umminger, 1979) and elasmobranchs underlining the potential role of DO in salt excretion (Van Lennep, 1968).

The IHC result of few branchial NKA-IR cells was consistent with NKA activity levels and in contrast to observations in most marine teleost fishes (e.g. alewife *Alosa pseudoharengus* Christensen et al., 2012; tilapia *Sarotherodon melanotheron* Ouattara et al., 2009). The few NKA-IR cells were restricted to the filament epithelium, leaving the lamella unimpeded for gas exchange (Evans 2008; Henriksson et al., 2008). Also, it was very rare to find NKA-IR cells that co-expressed NKCC1, although apical CFTR staining was observed in NKA-IR cells. NKCC1 is a key component of the mechanism of secondary active Cl^- secretion and is abundantly expressed in seawater type gill ionocytes in teleost fishes (see review by Hiroi and McCormick, 2012). In elasmobranchs, NKCC1 mRNA expression has been detected in the gills of spiny dogfish *Squalus acanthias* (Xu et al., 1994); however, in the branchial epithelium of *C. punctatum* NKCC1 could not be immunolocalized (Cramp et al., 2015). This contrasts with the freshwater stingray *Himantura signifer* where NKCC1 is co-expressed in gill NKA-IR cells following BW (20‰) acclimation (Ip et al., 2013). However, the rectal gland is absent in this species. The observation of ovoid cells deep within the filament epithelium which show only NKCC1-IR at HSW are unusual and their potential role has not been determined.

Elasmobranch gills also possess a V-ATPase rich cell that is involved in acid base regulation (Wilson et al., 1997; Piermarini and Evans, 2001; Tresguerres et al., 2006). Based on our IHC results, this cell type also appears in *P. lineatus*, and under HSW conditions immunoblotting results indicated a higher expression level. In killifish, basolateral V-ATPase has also been found in ionocytes (Katoh et al., 2003). Thus if the gills of *P. lineatus* have taken on the primary role in acid-base regulation, these cells maybe involved, although their basal localization in the epithelium makes this less certain.

4.3 Evidence for the role of the dentritic organ in salt secretion?

The higher DO NKA specific activity relative to the other ion regulatory organs, notably the gills, strongly indicates a role for this organ in NaCl secretion. This has also been seen in elasmobranchs with higher rectal gland NKA specific activity compared to their gills (*D. sabina,* Piermarini and Evans, 2000; *C. leucas,* Pillans et al., 2005; *C. punctatum,* Cramp et al., 2015). It has been demonstrated in euryhaline elasmobranchs that rectal gland NKA specific activity is higher in SW compared to FW acclimated animals (Piermarini and Evans, 2000; Pillans et al., 2005), although not in response to a moderate HSW acclimation (40‰; Cramp et al., 2015). In *P.lineatus,* DO NKA specific activity was also higher in SW versus BW (3‰) acclimated fish, but unexpectedly was also

lower in HSW compared to SW fish. We predicted a similar if not higher NKA specific activity (Cramp et al., 2015). However, when we took into consideration the DO mass which was higher in HSW so that the total DO NKA activity was also higher suggesting an increase in overall capacity. In contrast, *C. punctatum* acclimated to 40‰ did not alter rectal gland size (Cramp et al. (2015). However, larger rectal glands of *D. sabina* (Piermarini and Evans, 1998), *Pristis perotteti* (Gerzeli et al., 1976) and *C. leucas* (Gerzeli et al., 1969; Oguri, 1976) captured in SW compared to FW have been reported. Moreover, rectal glands of FW stenohaline elasmobranchs are small to vestigial (Thorson et al., 1978).

However, the apparent hypertrophy of the DO may not be adaptive but rather pathological (inflammation or similar) as supported by the dramatic Hsp70 increase. In either case, it is clear that *P. lineatus* are significantly challenged by HSW and that the DO maybe of limited use under such extreme conditions. Observation of a slightly albeit significantly larger DO in BW compared to the SW control fish suggests a high capacity of *P. lineatus* to move easily between different salinities, however, this was not sufficient to increase DO total NKA activity. Since the tissue sampling for the NKA activity measurement had been done after 14 days of acclimation, time course sampling would be necessary to have a comprehensive view of NKA activity in the DO of *P. lineatus*.

Strong basolateral tubular system immunoreactivity of NKA and NKCC1 in parenchymal cells of the DO indicates an ion secretory role in hypo-osmoregulating. The basolateral distribution of NKA and NKCC1 in other vertebrate salt secreting organs has also been demonstrated (Wilson et al., 2002; Lytle et al., 1995; Evans, 2008; Babonis et al., 2009; Babonis and Evans, 2011). Immunoblot results for NKA α subunit and NKCC (T4) were consistent in molecular mass compared to other vertebrates (Blanco and Mercer, 1998; Lytle et al., 1995, respectively). Finding multiple bands of NKCC might be the result of higher NKCC1 expression and immunoreactivity with either NKCC2 or NCC, reported in different species (Hiroi et al., 2008; Inokuchi et al., 2008; Lorin-Nebel et al., 2006; Christensen et al., 2012; Chew et al., 2015). Alternatively, the lipophilic nature of the NKCC migration through SDS-PAGE gels for immunoblotting analysis, or possibly the glycosylated monomer variability and/or different degrees of glycosylation could explain the banding patterns observed (Pelis et al., 2001; Tipsmark et al., 2002; Christensen et al., 2012; Chew et al., 2015). In BW, detection of NKCC suggests that maintaining a proportion of active NKCC for acid-base and/or cell volume regulation is important (Gamba, 2005) or it may be present as an inactive non-phosphorylated pool to be quickly activated for an acute response to higher salinity (Flemmer et al., 2010; Christensen et al., 2012). Regarding the expected increase of salt loading as a result of increased drinking and passive uptake under HSW conditions (see review by Grosell 2011, Gonzalez 2012), we detected significantly higher protein expression of DO NKCC representing an adaptation to increased salt excretion capacity.

IHC results for CFTR may reveal the possibility of a different isoform, which cannot be consistently recognized by the monoclonal antibody which is raised against a specific epitope of CFTR (Li et al., 2014). Pucke and Umminger (1979) detected an accumulation of Cl^- ions in the DO epithelium and proposed it was functional in

salt secretion. The presence of CFTR in salt glands of birds, elasmobranchs and reptiles has been confirmed (Shuttleworth and Hildebrandt, 1999) although the antibody used in the present study does not show crossreactivity with elasmobranch (J.M. Wilson personal observations), sea snake (Babonis and Evans, 2011) salt glands or salmonid (S.D. McCormick personal observations) gill CFTRs. Although *cftr* transcript was detected in the DO, predicted salinity dependent expression differences were not observed. Obviously, identifying the putative apical Cl^- channel in *P. lineatus* DO in future work would firmly establish the presence of the typical ion secretory cell of vertebrate salt glands.

The inconsistent results between NKA activity, α subunit protein levels and *atp1a1*mRNA expression levels may be related to post-transcriptional, or post-translational processing, phosphorylation state or modulation of the NKA kinetic properties by FXYD proteins interactions, stress or failing physiology (Garty and Karlish, 2006; Tipsmark, 2008; Wang et al., 2008; Tipsmark et al., 2010; Reilly et al., 2011; McDonough et al., 1990; Hauck et al., 2009; Christensen et al., 2012). Further investigation would be necessary to determine the effect of different salinities (FW to hypersaline) on various isoforms of NKA, their mRNA abundance and likely change with salinities that would be helpful in interpreting the osmoregulatory function of the DO. The changes in *P. lineatus* PAT1 mRNA (*slc26a6a*) suggest the possible contribution of the DO to acid-base regulation in *P. lineatus*, although there was a lack of changes in V-ATPase and Ca17 protein expression.

4.4 Cellular stress and salinity

The heat shock proteins (Hsps) are expressed in cells and are involved in maintaining a number of vital cellular processes as part of the cellular stress response (Hightower, 1991; Morimoto and Santoro, 1998; Iwama et al., 2006; Basu et al., 2002). Deane and Woo (2004; 2011) have shown that salinity can induce a cellular stress response. In the DO and kidney Hsp70 levels are highest at HSW indicating a cellular stress requiring the activation of stress protein mechanisms to provide protective actions against stress situations [for more details see review by Deane and Woo, (2011)]. Elevated intracellular ion concentrations typically can be correlates with intracellular damage (Burg et al., 2007). However, given the lack of differences Hsp70 levels in the gills, or intestine at salinity extremes suggests less of a stress compare to the DO and kidney or a different threshold of salt tolerance. In juvenile sharks challenged with HSW (41‰), gill Hsp70 did not change in *Mustelus antarcticus* but did in *Galeorhinus galeus* (Tunnah et al., 2016)

4.5 Summary

In summary, the salt secreting function of the DO has been proposed based on physiological (Kowarsky, 1973), ecological (Lanzing, 1967) and ultrastructural (Van Lennep, 1968) evidence. Our molecular observation summarized in Figure 8, show a strikingly high NKA activity, and localization of NKA, NKCC1 and CFTR in the DO is consistent with the hypothesis suggesting a conservation of rather similar mechanism of ion transporting in secretory cell of vertebrate salt secreting organs (Babonis and Evans, 2011). The gills of *P. lineatus* are

unlike those of other marine teleosts and more similar to the gills of elasmobranch fishes in terms of their significances to ion regulation. The *P. lineatus* kidney is particularly responsive to salinity and requires further study. The unique osmoregulatory strategy of the Plotosidae catfishes amongst the teleosts can be linked to their independent invasion of the marine environment by a freshwater siluriform ancestor (Lanzing, 1967; de Pinna, 2005). However, the breakdown of osmoregulatory homeostasis under HSW conditions indicated that this strategy is of limited use under more extreme salinity conditions.

Acknowledgement

We thank Hugo Santos of BOGA CIIMAR.

Author Contributions

J.M.W. and S.M.K designed the experiments. S.M.K performed the experiments, analyzed the data, and wrote the draft of the manuscript. J.C. and J.M.W. were also involved in the analysis of data and writing and editing of the manuscript.

Competing Interests

The authors declare that no competing interests exist.

FUNDING

This study was supported by an NSERC discovery grant and partial support by the Strategic Funding UID/Multi/04423/2013 through national funds provided by FCT – Foundation for Science and Technology and European Regional Development Fund (ERDF), in the framework of the programme PT2020 to JMW.

Refrences

1. Babonis, L. S., and Evans, D. H. (2011). Morphological and biochemical evidence for the evolution of salt glands in snakes. Comp. Biochem. Physiol. 160A, 400-411. DOI: 10.1016/j.cbpa.2011.07.008

2. Babonis, L. S., Hyndman, K. A., Lillywhite, H. B. and Evans, D. H. (2009). Immunolocalization of Na+/K+-ATPase and Na+:K+:2Cl- Cotransporterr in the tubular epithelia of sea snake salt glands. Comp. Biochem. Physiol. 154A, 535-540. DOI: 10.1016/j.cbpa.2009.08.022

3. Basu, N., Todgham, A. E., Ackerman, P. A., Bibeau, M. R., Nakano, K., Schulte, P. M., et al (2002). Heat shock protein genes and their functional significance in fish. Gene. 295 (2), 173-83.

4. Biswas, A. K., Seoka, M., Takii, K., Maita, M. and Kumai, K. (2006). Stress response of red sea bream (Pagrus major) to acute handling and chronic photoperiod manipulation. Aquaculture 252, 566–572. DOI: 10.1016/j.aquaculture.2005.06.043

5. Blanco, G. and Mercer, R. W. (1998). Isozymes of the Na+/K+-ATPase, heterogeneity in structure, diversity in function. Am. J. Physiol. 275, F633-F650.

6. Bradford, M. M. (1976). A rapid and sensitive method for the quantitation of microgram qualities of protein utilizing the principle of protein-dye binding. Anal. Biochem. 72, 248-254.

7. Brown, D., Lydon, J., McLaughlin, M., Stuart-Tilley, A., Tyszkowski, R., and Alper, S. (1996). Antigen retrieval in cryostat tissue sections and cultured cells by treatment with sodium dodecyl sulfate (SDS). Histochem. Cell Biol. 105(4), 261-267.

8. Burg, M. B., Ferraris, J. D., and Dmitrieva, N. I. (2007). Cellular response to hyperosmotic stresses. Physiol. Rev. 87, 1441-1474. DOI: 10.1152/physrev.00056.2006

9. Chew, S. F., Hiong, K. C., Lam, S. P., Chen, X. L., Ching, B. and Ip, Y. K. (2015). Ammonia exposure increases the expression of Na+:K+:2Cl− Cotransporterr 1a in the gills of the giant mudskipper Periophthalmodon schlosseri . J. Comp. Physiol. B. 185, 57-72. DOI: 10.1007/s00360-014-0867-3

10. Christensen, A. K., Hiroi, J., Schultz, E. T. and McCormick, S. D. (2012). Branchial ionocyte organization and ion-transport protein expression in juvenile alewives acclimated to freshwater or seawater. J. Exp. Biol. 215, 642-652. DOI: 10.1242/jeb.063057

11. Corpet, F. (1988). Multiple sequence alignment with hierarchical clustering. Nucl. Acids Res. 16, 10881-10890.

12. Cramp, R. L., Hansen, M. J., and Franklin, C. E. (2015). Osmoregulation by juvenile brown-banded bamboo sharks Chiloscyllium punctatum in hypo and hyper saline waters. Comp. Biochem. Physiol. 85A, 107-114. DOI: 10.1016/j.cbpa.2015.04.001

13. Cutler, C. P., Sanders, I. L., Hazon, N. and Cramb, G. (1995). Primary sequence, tissue specificity and expression of the Na+/K+-ATPase a1 subunit in the European eel Anguilla anguilla. Comp. Biochem. Physiol. 111B, 567-573.

14. Deane, E. E. and Woo, N. Y. S. (2004). Differential gene expression associated with euryhalinity in sea bream Sparus sarba. Am. J. Physiol. 287, R1054-R1063. DOI: 10.1152/ajpregu.00347.2004

15. Deane, E. E. and Woo, N. Y. S. (2011). Advances and perspectives on the regulation and expression of piscine heat shock proteins. Rev. Fish. Biol. Fish. 21,153-185. DOI: 10.1007/s11160-010-9164-8

16. De Pinna, M. C. (2005). “Diversity of tropical fishes”, in Fish Physiology, The Physiology of Tropical Fishes. Vol. 21, ed. A. Val, A. P. Farrell and C. J. Brauner. (London, Academic Press), pp. 47-84.. DOI: 10.1016/S1546-5098(05)21002-6

17. Edwards, S. L. and Marshall, W. S. (2012). “Principles and Patterns of Osmoregulation and Euryhalinity in Fishes”, in Fish Physiology - Euryhaline Fishes, Vol. 32, ed. S. C. McCormick, A. P. Farrell and C. J. Brauner. (London, Academic Press), pp. 1-44.. DOI: 10.1016/B978-0-12-396951-4.00001-3

18. Esbaugh, A., and Cutler, B. (2016). Intestinal Na+:K+:2Cl- Cotransporter 2 plays a crucial role in hyperosmotic transitions of a euryhaline teleost. Physiol. Rep. 4 22, e13028. DOI: 10.14814/phy2.13028

19. Evans, D. H. (2008). Teleost fish osmoregulation, what have we learned since August Krogh, Homer Smith, and Ancel Keys. Am. J. Physiol. 295, R704-R713. DOI: 10.1152/ajpregu.90337.2008

20. Ferreira-Martins, D., Coimbra, J., Antunes, C. and Wilson, J. M. (2016). Effects of salinity on upstream-migrating, spawning sea lamprey, Petromyzon marinus. Conserv. Physiol. 4, cov064. DOI: 10.1093/conphys/cov064

21. Fiess J. C., Kunkel-Patterson A., Mathias L., Riley L. G., Yancey P. H., Hirano T., et al (2007). Effects of environmental salinity and temperature on osmoregulatory ability, organic osmolytes, and plasma hormone profiles in the Mozambique tilapia, Oreochromis mossambicus. Comp. Biochem. Physiol. 146, 252-264. DOI: 10.1016/j.cbpa.2006.10.027

22. Flemmer, A. W, Monette, M. Y, Djurisic, M., Dowd, B., Darman, R., Gimenez, I., et al (2010). Phosphorylation state of the Na+:K+:2Cl− Cotransporter (NKCC1) in the gills of Atlantic killifish Fundulus heteroclitus during acclimation to water of varying salinity. J. Exp. Biol. 213, 1558-1566. DOI: 10.1242/jeb.039644

23. Freire, C. A. and Prodocimo, V. (2007). “Special challenges to teleost fish osmoregulation in environmentally extreme or unstable habitats”, in Fish Osmoregulation, ed. B. Baldisserotto, J. M. Mancera and B. G. Kapoor. (Science Publishers, Enfield), pp. 249-276. DIO: 10.1201/b10994-10

24. Froese, R., and D. Pauly. Editors. (2018). FishBase. World Wide Web electronic publication. www.fishbase.org, (02/2018)

25. Gamba, G. (2005). Molecular physiology and pathophysiology of electroneutral cationchloride cotransporters. Physiol. Rev. 85, 423-493. DOI: 10.1152/physrev.00011.2004

26. Garty, H. and Karlish, S. J. D. (2006). Role of FXYD proteins in ion transport. Annu. Rev. Physiol. 68, 431-459. DOI: 10.1146/annurev.physiol.68.040104.131852

27. Gerzeli, G., DeStefano, G. F., Bolognani, L., Koenig, K. W., Gervaso, M. V. and Omodeo- Sale, M.F. (1969). Therectalglandinrelationtotheosmoregulatorymechanismsof marine and freshwater elasmobranchs. Boll. Zool. 36, 399–400.

28. Gerzeli, G., de Stefano, G. F., Bolognani, L., Koenig, K. W., Gervaso, M. V., and Omodeo-Salé, M. F. (1976). The rectal gland in relation to the osmoregulatory mechanisms of marine and freshwater elasmobranchs. pp. 619-627. In Investigations of the Ichthyofauna of Nicaraguan Lakes (ed. T. B. Thorson), Lincoln, NE, USA: University of Nebraska-Lincoln.

29. Gonzalez, J. (2012). The physiology of hype-salinity tolerance in teleost fish, a review. J. Comp. Physiol. B 182, 321-329. DOI: 10.1007/s00360-011-0624-9

30. Hauck, C., Potter, T., Bartz, M., Wittwer, T., Wahlers, T., Mehlhorn, U., et al (2009). Isoform specificity of cardiac glycosides binding to human Na^+/K^+-ATPase alpha1beta1, alpha2beta1 and alpha3beta1. Eur. J. Pharmacol. 622, 7-14. DOI: 10.1016/j.ejphar.2009.08.039

31. Henriksson, P., Mandic, M. and Richards, J. G. (2008). The osmorespiratory compromise in sculpins, impaired gas exchange is associated with freshwater tolerance. Physiol. Biochem. Zool. 81, 310-319. DOI: 10.1086/587092

32. Hightower, L. E. (1991). Heat shock, stress proteins, chaperones, and proteotoxicity. Cell. 66, 191-197.

33. Hiroi, J. and McCormick, S. D. (2012). New insights into gill ionocyte and ion transporter function in euryhaline and diadromous fish. Respir. Physiol. Neuro. Biol. 184 (3), 257-268. DOI: 10.1016/j.resp.2012.07.019

34. Hiroi, J., Yasumasu, S., McCormick, S. D., Hwang, P. P. and Kaneko, T. (2008). Evidence for an apical Na-Cl cotransporter involved in ion uptake in a teleost fish. J. Exp. Biol. 211, 2584-2599. DOI: 10.1242/jeb.018663

35. Hirota, S. (1895). On the dendritic appendage of the urogeniatal papilla of a siluroid. J. College. Sci. Tokyo, Japan, 1898-1925.

36. Inokuchi, M., Hiroi, J., Watanabe, S., Lee, K. M. and Kaneko T. (2008). Expression and morphological localization of NHE3, NCC and NKCC1a in branchial mitochondria-rich cells of Mozambique tilapia *Oreochomis mossambicus* acclimated to a wide range of salinities. Comp. Biochem. Physiol. A 151,151-158. DOI: 10.1016/j.cbpa.2008.06.012

37. Ip, Y. K., Hiong, K. C., Wong, S. Z. H., Ching, B., Chen, X. L., Soh, M. M. L., et al (2013). Branchial Na^+:K^+:$2Cl^-$ cotransporter 1 and Na^+/K^+-ATPase α-subunit in a brackish water-type ionocyte of the euryhaline freshwater white-rimmed stingray, *Himantura signifer*. Front. Physiol. 10 4,362. DOI: 10.3389/fphys.2013.00362

38. Iwama, G. K., Afonso, L. O. B. and Vijayan, M. M (2006). "Stress in fish", in the physiology of fishes, ed. D. H. Evans and J. B. Clairborne. (Boca Raton, FL, CRC Press), pp. 319-342. DOI: 10.1111/j.1749-6632.1998.tb09005.x

39. Jensen, M. K., Madsen, S. S. and Kristiansen, K. (1998). Osmoregulation and salinity effects on the expression and activity of Na^+/K^+-ATPase in the gills of European sea bass, *Dicentrarchus labrax* (L.). J. Exp. Zool. 282, 290-300.

40. Kalujnaia, S., McWilliam, I. S., Zaguinaiko, V. A., Feilen, A. L., Nicholson, J., Hazon, N., et al (2007). Transcriptomic approach to the study of osmoregulation in the European eel *Anguilla Anguilla*. Physiol. Genomics. 31(3), 385-401. DOI: 10.1152/physiolgenomics.00059.2007

41. Kang, C. K., Tsai, S. C., Lee, T. H. and Hwang, P. P. (2008). Differential expression of branchial Na^+/K^+-ATPase of two medaka species, *Oryzias latipes* and *Oryzias dancena*, with different salinity tolerances acclimated to fresh water, brackish water and seawater. Comp. Biochem. Physiol. 151A, 566-575. DOI: 10.1016/j.cbpa.2008.07.020

42. Katoh, F., Hyodo, S. and Kaneko, T. (2003). Vacuolar-type proton pump in the basolateral plasma membrane energizes ion uptake in branchial mitochondria-rich cells of killifish *Fundulus heteroclitus*, adapted to a low ion environment. J. Exp. Biol. 206,793-803.

43. Kim, Y. K., Ideuchi, H., Watanabe, S., Park, S. I, Huh, M. and Kaneko, T. (2008). Rectal water absorption in seawater-adapted Japanese eel *Anguilla japonica*. Comp. Biochem. Physiol. 151, 533-541. doi: 10.1016/j.cbpa.2008.07.016

44. Kowarsky, J. (1973). Extra-branchial pathways of salt exchange in a teleost fish. Comp. Biochem. Physiol. 46, 477-486.

45. Kirschner, L. B. (1980). Comparison of vertebrate salt-excreting organs. Am. J. Physiol. 238, R219-R223. DOI: 10.1152/ajpregu.1980.238.3.R219

46. Küffer, H., Richterich, R., Kraft, R., Peheim, E. and Colombo, J. P. (1975). The determination of chloride in plasma and serum (mercury(II)-thiocyanate method) with the Greiner Electronic Selective Analyzer GSA II. Z Klin. Chem. Klin. Biochem. 13(5), 203-11.

47. Laemmli, U. K. (1970) Cleavage of Structural proteins during the assembly of the head of bacteriophage T4. Nature. 227, 680-685.

48. Lanzing W.J.R. (1967). The ultrastructure of glandular cells in the external dendritic organ of some marine catfish. J. Ultrastruct. Res. 18, 333-344.

49. Lanzing W.J.R. (1967). A possible relation between the occurrence of a dendritic organ and the distribution of the Plotosidae (Cypriniformes). Pacific. Sci. 21, 498-502.

50. Li, Z., Lui, E. Y, Wilson, J. M., Ip, Y. K., Lin, Q., Lam, T. J. et al (2014). Expression of key ion transporters in the gill and esophageal-gastrointestinal tract of euryhaline Mozambique tilapia *Oreochromis mossambicus* acclimated to fresh water, seawater and hypersaline water. PLoS One 9(1), e87591. DOI: 10.1371/journal.pone.0087591

51. Liu, Z., Liu, S., Yao, J., Bao, L., Zhang, J., Li, Y., et al (2016). The channel catfish genome sequence provides insights into the evolution of scale formation in teleosts. Nature communications, 7. 11757. DOI: 10.1038/ncomms11757

52. Livak, K. J., and Schmittgen T, D. (2001). Analysis of relative gene expression data using real-time quantitative PCR and the 2(-Delta Delta C(T)) Method. Methods. 25 (4), 402-8. DOI: 10.1006/meth.2001.1262

53. Lorin-Nebel, C., Boulot, V., Bodinier, C. and Charmantier, G. (2006). The Na^+:K^+:2Cl^- cotransporter in the sea bass Dicentrarchus labrax ontogeny, involvement in osmoregulation. J. Exp. Biol. 209, 4908-4922. DOI: 10.1242/jeb.02591

54. Laurenson L. J. B., Neira F. J. and Potter I. C. (1993). Reproductive biology and larval morphology of the marine plotosid *Cnidoglanis macrocephalus* (Teleostei) in a seasonally closed Australian estuary. Hydrobiologia. 268,179-192.

55. Lytle, C., Xu, J. C, Biemesderfer, D. and Forbush, III B, (1995). Distribution and diversity of Na^+:K^+:2Cl^- cotransport proteins, a study with monoclonal antibodies. Am. J. Physiol. 269, C1496-C1505. DOI: 10.1152/ajpcell.1995.269.6.C1496

56. Madsen, S.S., and Naamansen, E. T. (1989). Plasma ionic regulation and gill Na^+/K^+-ATPase changes during rapid transfer to seawater to yearling rainbow trout, *Salmo gairdneri*: time course and seasonal variation. J. Fish Biol. 34, 829-840. DOI: 10.1111/j.1095-8649.1989.tb03367.x

57. Malakpour Kolbadinezhad, S., Hajimoradloo, A., Ghorbani, R., Joshaghani, H. and Wilson, J. M. (2012). Effects of gradual salinity increase on osmoregulation in Caspian roach *Rutilus caspicus*. J. Fish. Biol. 81, 125-134. DOI: 10.1111/j.1095-8649.2012.03317.x

58. Marshall, W. S., Howard, J. A., Cozzi, R. R. F. and Lynch, E. M. (2002a). NaCl and fluid secretion by the intestine of the teleost *Fundulus heteroclitus*, involvement of CFTR. J. Exp. Biol. 205, 745-758.

59. Marshall, W. S., Lynch, E. M. and Cozzi, R. R. F. (2002b). Redistribution of immunofluorescence of CFTR anion channel and NKCC cotransporter in chloride cells during adaptation of the killifish *Fundulus heteroclitu*s to sea water. J. Exp. Biol. 205, 1265-1273.

60. Marshall, W. S. and Grosell, M. (2006). "Ion transport, osmoregulation and acid-base balance", in The Physiology of Fishes, eds. D. H. Evans and J. B Claiborne (Boca Raton, CRC Press), pp. 177-230.

61. McCormick, S. D. (1993). Method for non-lethal hill biopsy and measurement of Na^+/K^+-ATPase activity. Can. J. Fish. Aquat. Sci. 50, 656-658.

62. McDonough, A. A., Geering, K. and Farley, R. A. (1990). The sodium pump needs its beta subunit. FASEB. J. 4(6), 1598-1605.

63. Morimoto, R.I., and Santoro, M.G. (1998). Stress-inducible responses and heat shock proteins, new pharmacologic targets for cytoprotection. Nat. Biotechnol. 16, 833838. DOI: 10.1038/nbt0998-833

64. Namimatsu, S., Ghazizadeh, M. and Sugisaki, Y. (2005). Reversing the effects of formalin fixation with citraconic anhydride and heat, a universal antigen retrieval method. J. Histochem. Cytochem. 53(1), 3-11. DOI: 10.1177/002215540505300102

65. Oguri, M. (1976). Rectal glands of marine and freshwater sharks: Comparative histology; in Thorson, T.B. (ed): Investigations of the Ichthyofauna of Nicaraguan Lakes. Lincoln/Nebr, School of Life Sciences, pp 613‑614.

66. Ouattara, N., Bodinier, C., Negre-Sadargues, G., D'Cotta, H., Messad, S., Charmanteir, G., et al (2009). Changes in gill ionocyte morphology and function following transfer from fresh to hypersaline waters in the tilapia *Sarotherodon melanotheron*. Aquauculture 290,155-164. DOI: 10.1016/j.aquaculture.2009.01.025

67. Pelis, R. M, Zydlewski, J. and McCormick, S. D. (2001). Gill Na^+:K^+:2Cl^- cotransporter abundance and location in Atlantic salmon, effects of seawater and smolting. Am. J. Physiol. 280, R1844-R1852. DOI: 10.1152/ajpregu.2001.280.6.R1844

68. Piermarini, P.M. and Evans, D.H. (1998). Osmoregulation of the Atlantic stingray (*Dasyatis sabina*) from the freshwater Lake Jesup of the St. Johns River, Florida. Physiol. Zool. 71, 553-560.

69. Piermarini, P.M. and Evans, D.H. (2000). Effects of environmental salinity on Na^+/K^+-ATPase in the gills and rectal gland of a euryhaline elasmobranch (*Dasyatis sabina*). J. Exp. Biol. 203, 2957-2966.

70. Piermarini, P. M. and Evans, D. H. (2001). Immunochemical analysis of the vacuolar proton-ATPase B-subunit in the gills of a euryhaline stingray *Dasyatis sabina*, effects of salinity and relation to Na^+/K^+-ATPase. J. Exp. Biol. 204, 3251-3259.

71. Pillans, R. D., Good, J. P, Anderson, W. G., Hazon, N. and Franklin, C. E. (2005). Freshwater to seawater acclimation of juvenile bull sharks *Carcharhinus leucas*, plasma osmolytes and Na^+/K^+-ATPase activity in gill, rectal gland, kidney and intestine. J. Comp. Physiol. B Biochem. Physiol. 175, 37-44. DOI: 10.1007/s00360-004-0460-2

72. Pillans, R. D., Good, J. P, Anderson, W. G., Hazon, N. and Franklin, C. E. (2008). Rectal gland morphology of freshwater and seawater acclimated bull sharks *Carcharhinus leucas*. J. Fish. Biol. 72, 1559–1571. DOI: 10.1111/j.1095-8649.2008.01765.x

73. Pucke, J. and Umminger, B. L. (1979). Histophysiology of the Gills and Dendritic Organ of the Marine Catfish *Plotosus lineatus* in Relation to Osmoregulation. Copeia (2). 357360.

74. Raldúa, D., Otero, D., Fabra, M. and Cerdà, J. (2008). Differential localization and regulation of two aquaporin-1 homologs in the intestinal epithelia of the marine teleost *Sparus aurata*. Am. J. Physiol. Regul. Integr. Comp. Physiol. (294), R993-R1003. DOI: 10.1152/ajpregu.00695.2007

75. Reilly, B. D., Cramp, R. L., Wilson, J. M., Campbell, H. A. and Franklin, C. E. (2011). Branchial osmoregulation in the euryhaline bull shark, *Carcharhinus leucas*, a molecular analysis of ion transporters. J. Exp. Biol. 214, 2883-2895. DOI: 10.1242/jeb.058156

76. Reis-Santos, P., McCormick, S. D. and Wilson, J. M. (2008). Ionoregulatory changes during metamorphosis and salinity exposure of juvenile sea lamprey*, Petromyzon marinus* L. J. Exp. Biol. 211, 978-988. DOI: 10.1242/jeb.014423

77. Rozen, S. and Skaletsky, H. (2000). "Primer3 on the WWW for general users and for biologist programmers", in Bioinformatics Methods and Protocols, Eds. Misener S, Krawetz SA. Humana Press, Totowa New Jersey, 365-386.

78. Santos, C. R. A., Power, D. M., Kille, P., Llewellyn, L., Ramsurn, V., Wigham, T., et al (1997). Cloning and sequencing of a full-length sea bream (*Sparus aurata*) b-actin cDNA. Comp. Biochem. Physiol. 117B, 185-189.

79. Sardella, B.A., Kültz, D., Cech, Jr J. J. and Brauner, C. J. (2008). Salinity-dependent changes in Na^+/K^+-ATPase content of mitochondria-rich cells contribute to differences in thermal tolerance of Mozambique tilapia. J. Comp. Physiol. B 178, 249-256. DOI: 10.1007/s00360-007-0211-2

80. Shih, T. H., Horng, J.L., Hwang, P. P. and Lin, L. Y. (2008). Ammonia excretion by the skin of zebrafish *Danio rerio* larvae. Am. J. Physiol. Cell. Physiol. 295, 1625-1632. DOI: 10.1152/ajpcell.00255.2008.

81. Shuttleworth, T. J. and Hildebrandt, J. P. (1999). Vertebrate salt glands, short- and long-term regulation of function. J. Exp. Zool. 283 (7), 689-701.

82. Sinha AK, Dasan AF, Rasoloniriana R, Pipralia N, Blust R, De Boeck G. 2015. Hypo-osmotic stress-induced physiological and ion-osmoregulatory responses in European sea bass *Dicentrarchus labrax* are modulated differentially by nutritional status. Comp. Biochem. Physiol. 181A: 87-99. DOI:10.1016/j.cbpa.2014.11.024.

83. Silva, P., J. Stoff, M. Field, L. Fine, J.N. Forrest, and Epstein F.H. (1977) Mechanism of active chloride secretion by shark rectal gland: role of Na-K-ATPase in chloride transport. Am. J. Physiol. 233, F298-306.

84. Singer, T. D., Tucker, S. J., Marshall, W. S. and Higgins, C. F. (1998). A divergent CFTR homologue, highly regulated salt transport in the euryhaline teleost *Fundulus heteroclitus*. Am. J. Physiol. Cell. Physiol. 274, C715-C723.

85. Sulya, L. L., Box, B. E. and Gunter, G. (1960). Distribution of some blood constituents in fish from the Gulf of Mexico. Am. J. Physiol. 199, R1177-R1180.

86. Tait, J. C., Mercer E. W., Gerber, L., Robertson, G. N. and Marshall, W. S. (2017). Osmotic versus adrenergic control of ion transport by ionocytes of *Fundulus heteroclitus* in the cold. Comp. Biochem. Physiol. A 203,255-261. DOI: 10.1016/j.cbpa.2016.10.003

87. Takei, Y. and Hwang, P. P. (2016). Homeostatic Responses to Osmotic Stress. In Fish Physiology-Biology of stress in fish. Vol 35 In, Schreck CB, Tort L, Farrell AP, Brauner CJ. Academic Press Inc San Diego, United States Elsevier. pp 208-237. DOI: 10.1016/B978-0-12-802728-8.00006-0

88. Thorson, T.B., Wotton, R. M. and Georgi, T. A. (1978). Rectal gland of freshwater stingrays, Potamotrygon spp. (Chondrichthyes:Potamotrygonidae). Biol. Bull. 154, 508–516.

89. Tipsmark, C. K. (2008). Identification of FXYD protein genes in a teleost, tissue-specific expression and response to salinity change. Am. J. Physiol. Physiol. 294, R1367-R1378. DOI: 10.1152/ajpregu.00454.2007

90. Tipsmark, C. K., Madsen, S. S., Seidelin, M., Christensen, A. S., Cutler, C. P. and Cramb, G. (2002). Dynamics of Na^+:K^+:2Cl^- cotransporter and Na^+/K^+-ATPase expression in the branchial epithelium of brown trout *Salmo trutta* and Atlantic salmon *Salmo salar*. J. Exp. Zool. 293,106-118. DOI: 10.1002/jez.10118

91. Tipsmark, C. K., Mahmmoud, Y. A., Borski, R. J. and Madsen, S. S. (2010). FXYD-11 associates with Na^+/K^+-ATPase in the gill of Atlantic salmon, regulation and localization in relation to changed ion-regulatory status. Am. J. Physiol. Physiol. 299, R1212-R1223. DOI: 10.1152/ajpregu.00015.2010

92. Tresguerres, M., Parks, S. K., Katoh, F. and Goss, G. G. (2006). Microtubule-dependent relocation of branchial V-H^+-ATPase to the basolateral membrane in the Pacific spiny dogfish *Squalus acanthias*, a role in base secretion. J. Exp. Biol. 209,599-609. DOI: 10.1242/jeb.02059

93. Tunnah, L., MacKellar, S. R., Barnett, D. A., MacCormack, T. J., Stehfest, K. M., Morash, A. J., Semmens, J. M. and Currie, S., (2016). Physiological responses to hypersalinity correspond to nursery ground usage in two inshore shark species (*Mustelus antarcticus* and *Galeorhinus galeus*). J. Exp. Biol. 219, 2028-2038.

94. Van Lennep, E. W. (1968). Electron microscopic histochemical studies on salt-excreting glands in elasmobranchs and marine catfish. J. Ultrastruct. Res. 25, 94-108.

95. Van Lennep, E. W. and Lanzing, W. J. R. (1967). The ultrastructure of glandular cells in the external dendritic organ of some marine catfish. J. Ultrastruct. Res. 18, 333-344.

96. Varsamos, S., Connes, R., Diaz, J. P., Barnabé G. and Charmantier, G. (2001). Ontogeny of osmoregulation in the European sea bass *Dicentrarchus labrax* L. Mar. Biol, 138 (5), 909-915.

97. Varsamos, S., Nebel, C. & Charmantier, G. (2005). Ontogeny of osmoregulation in postembryonic fish: a review. Comp. Biochem. Physiol. A 141, 401-429. DOI: 10.1016/j.cbpb.2005.01.013

98. Verdugo, P. (1984). Hydration kinetics of exocytosed mucins in cultured secretory cells of the rabbit trachea, a new model. Ciba. Found. Symp. 109,212-225.

99. Wang, P. J., Lin, C. H., Hwang, H. H. and Lee, T. H. (2008). Branchial FXYD protein expression in response to salinity change and its interaction with Na^+/K^+-ATPase of the euryhaline teleost *Tetraodon nigroviridis*. J. Exp. Biol. 211, 3750-3758. DOI: 10.1242/jeb.018440

100. Watson, C. J., Nordi, W. M. and Esbaugh, A. J. (2014). Osmoregulation and branchial plasticity after acute freshwater transfer in red drum, *Sciaenops ocellatus*. Comp. Biochem. Physiol. 178A, 82-89. DOI: 10.1016/j.cbpa.2014.08.008

101. Wilson, J. M. and Castro, L. F. (2010). "Morphological Diversity of the Gastrointestinal Tract in Fishes," in The Multifuctional Gut of Fish, eds. Grosell, M.; Farrell, A. P, Brauner, C. J. London, Academic Press. pp. 2-44. DIO: 10.1016/S1546-5098(10)03001-3

102. Wilson, J. M., Leitão, A., Gonçalves, A. F., Ferreira, C., Reis-Santos, P., et al (2007). Modulation of branchial ion transporter protein expression by salinity in glass eels *Anguilla anguilla* L. Mar. Biol. 151, 1633-1645.

103. Wilson, J. M., Morgan, J. D., Vogl, A.W. and Randall, D. J. (2002). Branchial mitochondriarich cells in the dogfish *Squalus acanthias*. Comp. Biochem. Physiol 132A, 365-374.

104. Wilson, J. M., Randall, D. J., Donowitz, M., Vogl, A. W. and Ip, Y. K. (2000). Immunolocalization of ion-transport proteins to branchial epithelium mitochondriarich cells in the mudskipper *Periophthalmodon schlosseri*. J. Exp. Biol. 203, 22972310.

105. Wilson, J. M., Randall, D. J., Vogl, W. A., and Iwama, G. K. (1997). Immunolocalization of V-type ATPase in the gills of the shark, *Squalus acanthias*. J. Exp. Zool. 278, 78-86. DOI: 10.1002/(SICI)1097-010X

106. Woo, N. Y. S. and Chung, K. C. (1995). Tolerance of *Pomacanthus imperator* to hypoosmotic salinity, changes in body composition and hepatic enzyme activities. J. Fish. Biol. 47, 70-81. DOI: 10.1111/j.1095-8649.1995.tb01874.x

107. Wood, C.M., Bucking, C. (2011). "The role of feeding in salt and water balance," in Fish Physiology: The Multifunctional Gut of Fishes. Vol 30. Eds. Grosell, M., Farrell, A.P., Brauner, C.J. Academic Press, San Diego, USA, pp. 165-212. DOI: 10.1016/S1546-5098(10)03005-0

108. Xu, J.C., Lytle, C., Zhu, T.T., Payne, J.A., Benz, E. et al. (1994). Molecular cloning and functional expression of the bumetanide-sensitive Na^+:K^+:2Cl^- cotransporter. Proc. Natl. Acad. Sci. USA. 91, 2201-2205.

109. Zadunaisky, J. A. (1984). "The chloride cell, the active transport of chloride and the paracellular pathways," in, Fish Physiology, Vol. 10B. ed. Randall WSH and DJ. Academic Press, Orlando, pp 130-176.

110. Zuchelkowski, E. M., Lantz, R. C. and Hinton, D. E. (1986) Skin mucous cell response to acid stress in male and female brown bullhead catfish, *Ictalurus nebulosus* (Lesueur). Aquat. Toxicol. 8,139-148. DOI: 10.1016/0166-445X(86)90060-3

Table 1. Fish morphometrics: condition factor (K) and DO mass (mg DO per g body mass); plasma Na^+, Cl^-, K^+, and Ca^{2+} concentrations and osmolality, hematocrit, strong ion ratio (SIR; Na^+:Cl^-) and muscle water content (MWC%), Na^+ and K^+ concentrations, and Na^+/K^+ ratio of *P. lineatus* acclimated to [brackish water (BW) 3‰, seawater (SW control) 34‰, and hypersaline water (HSW) 60‰]. Data are means ± SEM. (n=7-9). Salinity difference within a given parameter that do not share the same letter(s) are significantly different from one another.

Morphometrics			
Condition Factor (K)	5.75 ± 0.1 [a]	4.60 ± 0.1 [b]	4.17 ± 0.1 [c]
mg DO /g body mass	1.25 ± 0.06 [a]	0.90 ± 0.04 [b]	2.65 ± 0.10 [c]
Plasma	BW (3‰)	SW Control (34‰)	HSW (60‰)
Na^+(mmol l^{-1})	119.8 ± 5.4[a]	152.6 ± 5.6 [b]	186.2 ± 16.7 [c]
Cl^- (mmol l-1)	125.5 ±4.2 [a]	127.8 ± 3.9 [a]	148.7 ± 8.0 [b]
K^+(mmol l^{-1})	4.6 ± 0.5	5.1 ± 0.4	5.1 ± 0.3
Ca^{2+} (mmol l^{-1})	2.6 ± 0.2 [a]	3.0 ± 0.2 [a]	3.8 ± 0.5 [b]
Osmolality(mOsm)	391.2 ± 25.1 [a]	374.4 ± 26.0 [a]	588.0 ± 48.7 [b]
Hematocrit (%)	15.3 ± 1.2 [a]	23.3 ± 2.8 [b]	29.2 ± 1.7 [c]
SIR (Na^+:Cl^- ratio)	0.96 ± 0.04 [a]	1.20 ± 0.06 [b]	1.24 ± 0.0 [b]
Muscle			
MWC (%)	86.6 ± 1.7 [a]	87.5 ± 1.6 [a]	77.4± 0.3 [b]
Na^+(mmol kg^{-1})	66.9 ± 8.9	64.2 ± 4.2	67.4± 5.0
K^+(mmol kg^{-1})	138.5 ± 9.6 [a]	138.6 ± 2.4 [a]	204.0 ± 8.0[b]
Na^+:K^+ ratio	0.48 ± 0.92 [a]	0.46 ± 1.73 [a]	0.33 ± 0.63 [b]

List of figures

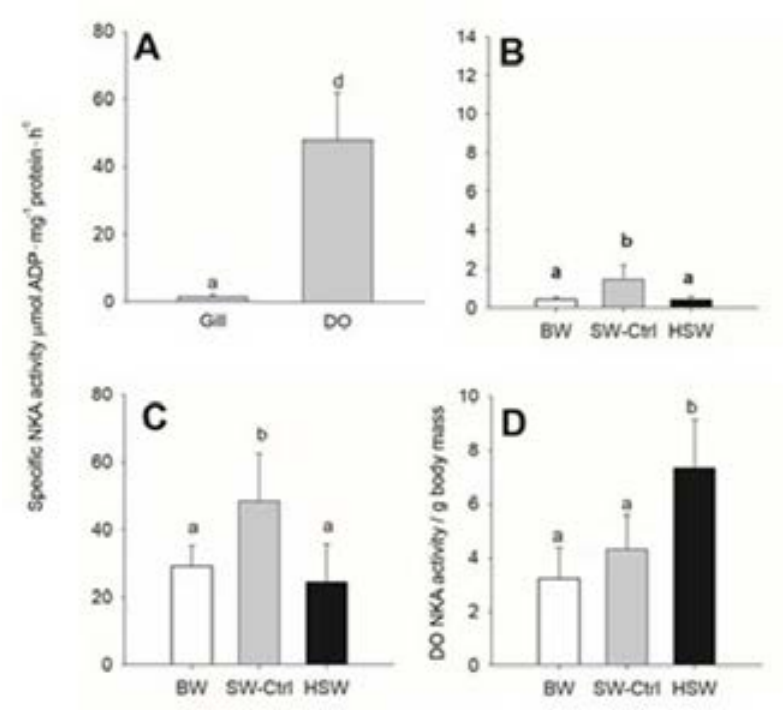

Figure 1. Na^+/K^+-ATP (NKA) activity in different osmoregulatory organs of SW acclimated *P.lineatus* (A). Organ specific NKA activity [gill (B) and dendritic organ (C) in *P. lineatus* acclimated to brackishwater (BW) 3‰, seawater (SW control) 34‰, and hypersaline water (HSW) 60‰. Total DO NKA activity per g body mass (D). Values are means ± SEM. (n=5-6). Different lower case letters indicate a significant difference between organs (A) and with salinity within each tissue (A-D) ($P < 0.05$).

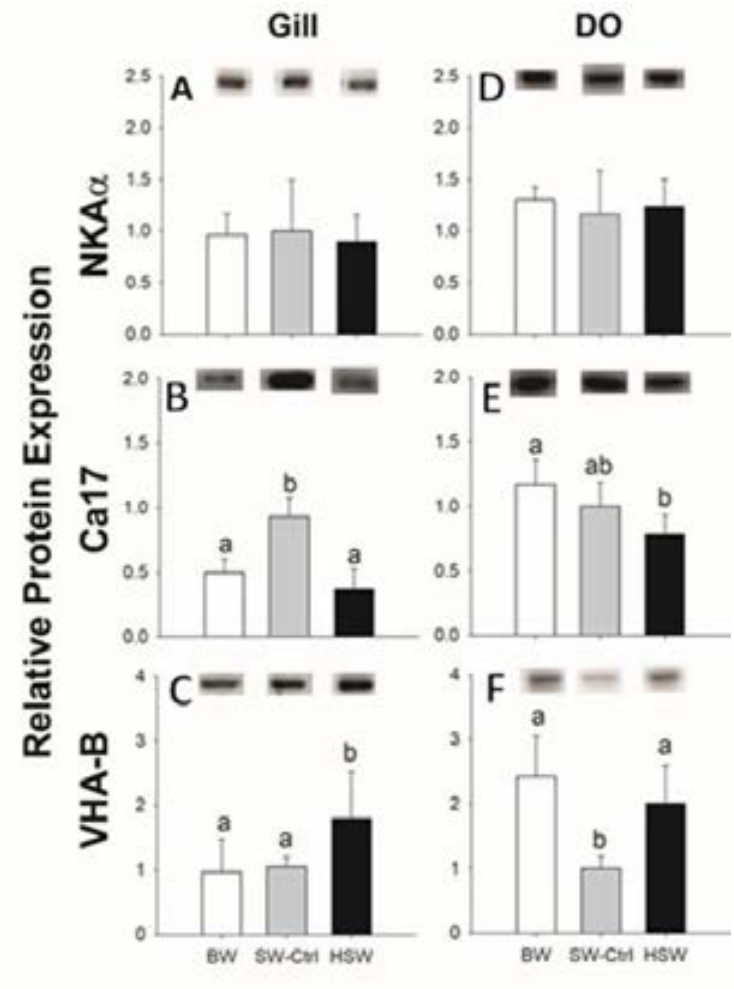

Figure 2. Immunoblotting relative expression of NKA α-subunit (αR1 antibody; A-E), cytosolic carbonic anhydrase (Ca17; F-J) and V-ATPase B subunit (B2 antibody; K-N) in the gill (A) and DO (B) *P. lineatus* were acclimated to [brackishwater (BW) 3‰, seawater (SW control) 34‰, and hypersaline water (HSW) 60‰]. α tubulin (12G10 antibody) was used as a loading control. Values are presented as means ± SEM of protein abundance (n=5-6). Different letters indicate a significant difference between salinities, one-way analysis of variance (ANOVA) and SNK ($P < 0.05$).

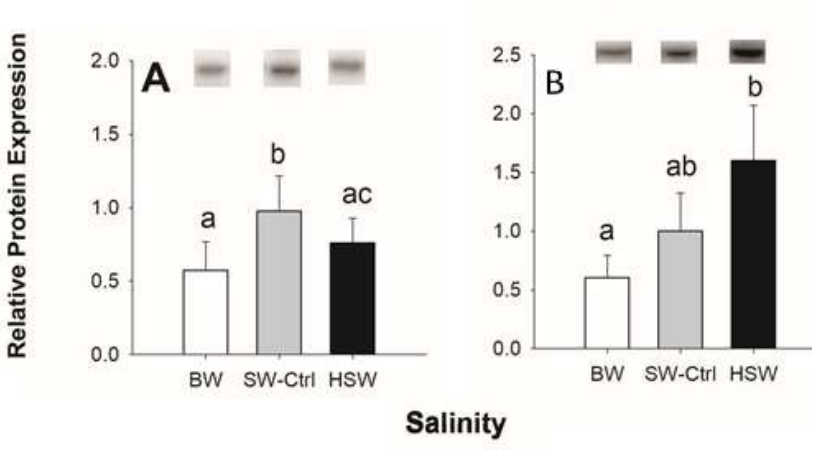

Figure 3. Immunoblotting relative expression of heat shock protein 70 (Hsp70) in the gill (A), DO (B) and NKCC in dendritic organ (F) of *P. lineatus* acclimated to [brackishwater (BW) 3‰, seawater (SW control) 34‰, hypersaline water (HSW) 60‰]. α tubulin (12G10 antibody) was used as a loading control. Values are means ± SEM of protein abundance (n=5-6). Different letter indicates a significant difference between salinities, one-way ANOVA and SNK ($P < 0.05$).

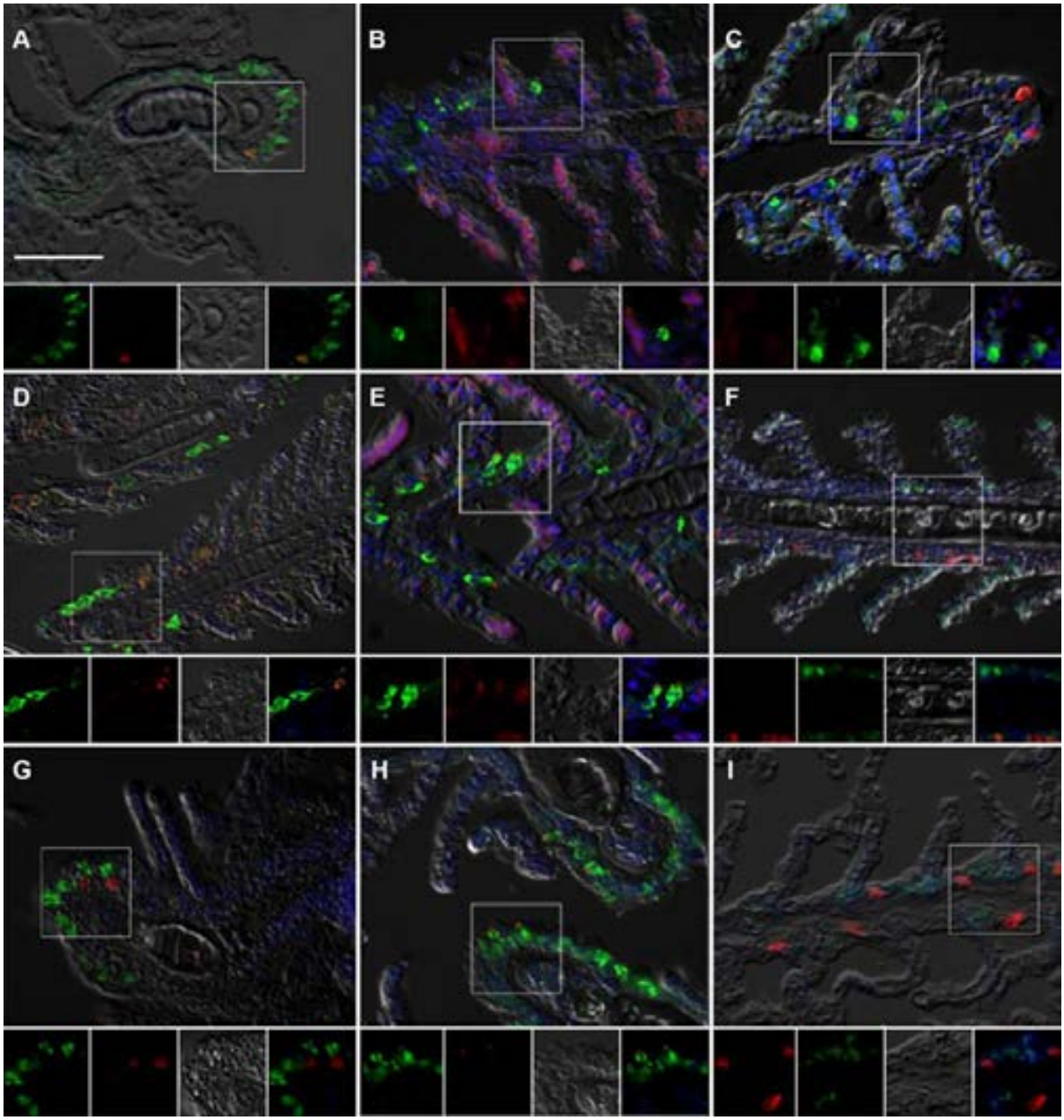

Figure 4. Immunofluorescence localization of Na^+/K^+-ATPase (αR1, green A,B,D,E,G,H) with NKCC1 (T4, red A,D,G) and CFTR (red, B,E,H) or Na^+/K^+-ATPase (α5, red C,F,I) with V-ATPase (B2, green C,F,I) in the gills of *P. lineatus*. Acclimation was performed in brackish water (BW) 3‰ (A-C), seawater (SW control) 34‰ (D-F) and hypersaline water (HSW) 60‰ (G-I). Sections were counter stained with DAPI nuclear staining (blue) and overlaid with the differential interference contrast (DIC) images. Insets show the separate channels of the framed area in the respective panels (A-I). In A,D,G arrowheads indicate NKCC1 IR cells and arrows NKA-IR cells. In B,E,H, arrows indicate CFTR+NKA IR cells, astrerisks red blood cell non-specific fluorescence. In C,F,I, arrows indicate V-ATPase IR cells and arrows NKA IR cells. Scale bar 100 µm.

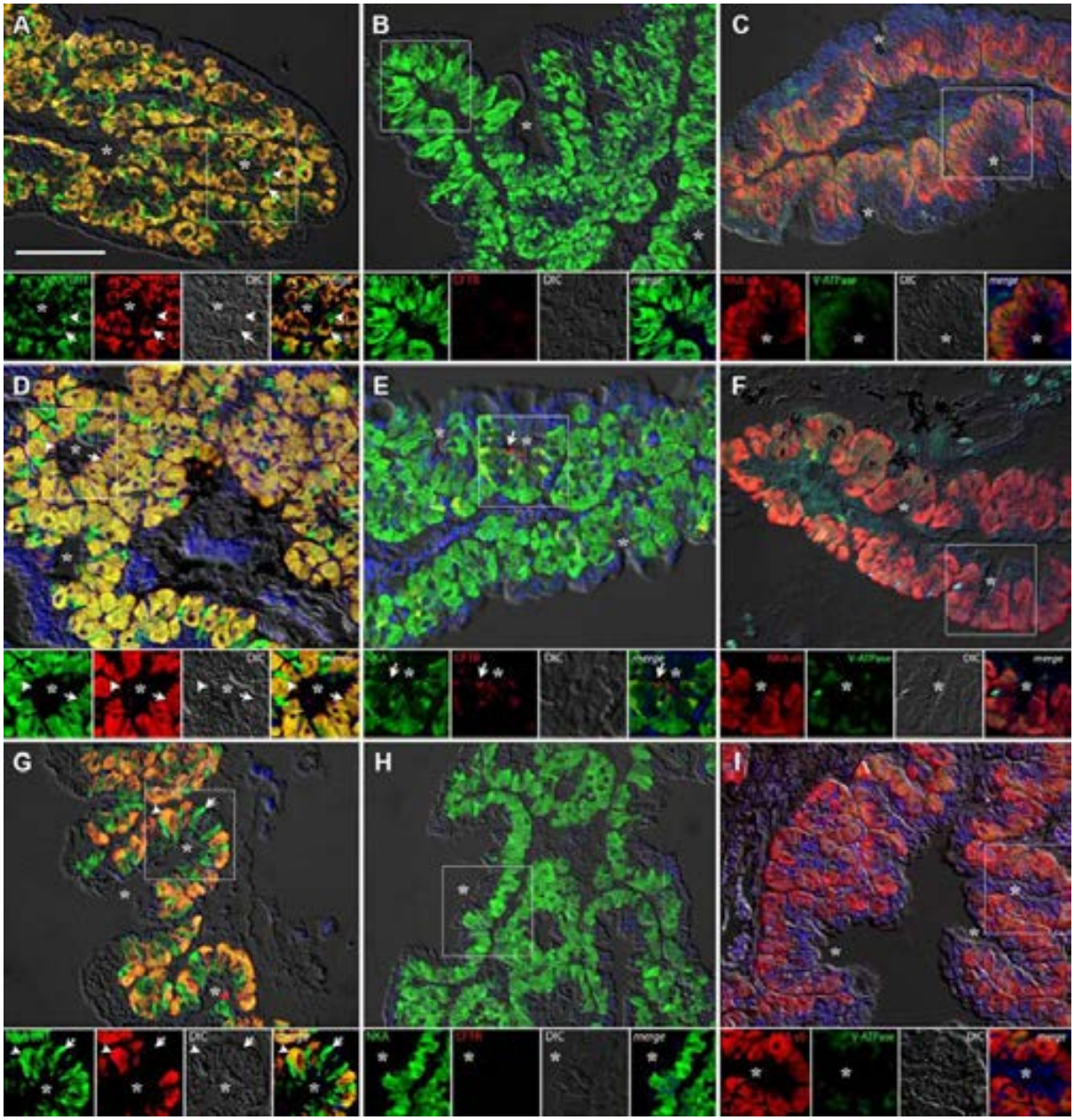

Figure 5. Immunofluorescence localization of Na^+/K^+-ATPase (αR1, green A, D, E, G, H) with NKCC1 (T4, red A, D, G) and CFTR (red, B, E) or Na^+/K^+-ATPase (α5, red C, F, I) with V-ATPase (B2, green C, F, I) in the DO of *P. lineatus*. The *P. lineatus* acclimated in brackish water (BW) 3‰ (a-c), seawater (SW control) 34‰ (d-f) and hypersaline water (HSW) 60‰ (g-i). In A,D,G arrows indicate NKCC1+NKA IR cells and arrowheads NKA only IR cells. In B,E,H, arrows indicate CFTR+NKA IR cells. Asterisks (*) indicate water. See Figure 4 caption for additional information. Scale bar 100 µm.

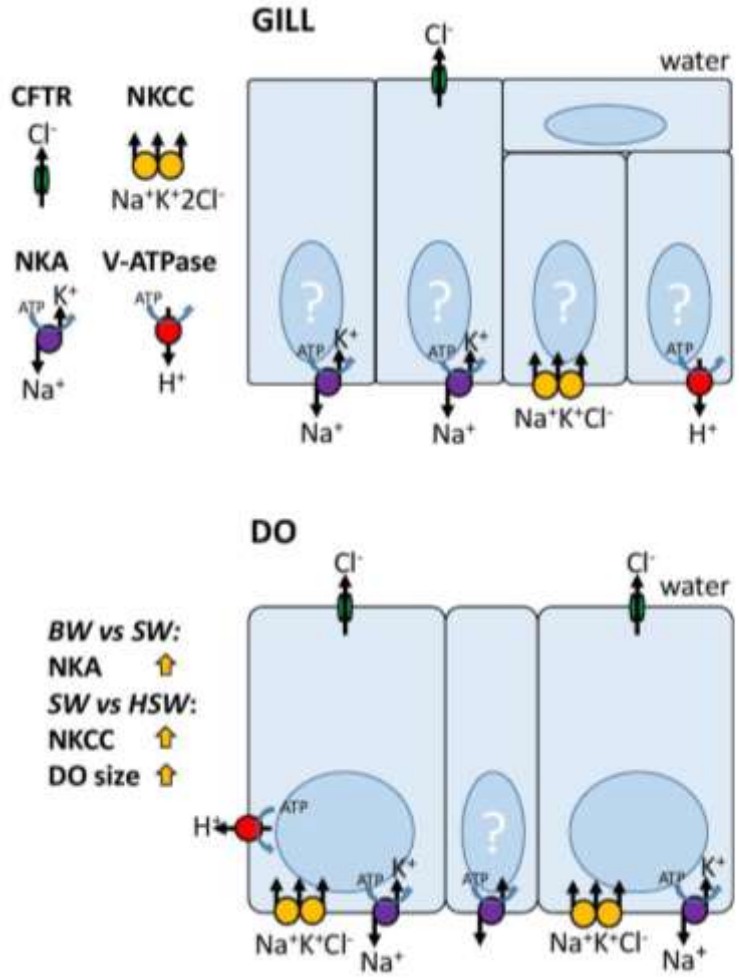

Figure 6. Models for ion transport mechanisms in *P.lineatus* gill, DO and intestine.

2nd International Conference on Oceanography for West Asia

16 , 17 Sept. 2020 Iran. Tehran

Antibacterial activity of muscle wall extracts *Stichopus horrens* sea cucumber of the Chabahar coasts, Iran against some rainbow trout (*Oncorhynchus mykiss*) pathogenic bacteria using disk diffusion and well diffusion methods

Mohammadi Movahed, Mohana[1]; Hosseini, Seyed Abbas [1]; Akbary, Paria [2*]; Hajimoradloo, Abdolmajid [3]; Hedayati, Seyed Ali Akbar [1]

1. Faculty of Fisheries and Environment Sciences, Fisheries and Aquatic Ecology group, Gorgan University of Agricultural, Science and Natural Resources, Gorgan, Iran

2. Chabahar Maritime University, Deparment of Marine Sciences, Fisheries groups

3. Faculty of Fisheries and Environment Sciences, Fisheries and Aquaculture group, Gorgan University of Agricultural, Science and Natural Resources, Gorgan, Iran

*Correspondence email: paria.akbary@gmail.com

Key words: *Sea cucumber, Extract, Antibacterial property, Disk diffusion, Well diffusion*

1. Introduction

Microbial agents are currently one of the most common pathogens in rainbow trout (*Oncorhynchus mykiss*) farms. Therefore, it forces farmers to use antibiotics with different mechanisms to the control and eliminate of bacteria (Soltani et al. 2012). On the other hand, the resistance of pathogenic bacteria to certain antibiotics forces researchers to discover new antibiotics (Lee et al. 2000; Kia and Mehrabi 2013).

In recent years, the role of natural compounds of marine origin is important (Mancini et al. 2007). The term natural compounds is usually used to refer to natural chemicals that have medicinal properties. This term is usually used for secondary metabolites produced by living organisms (Sipkema et al. 2005). Natural compounds found in the marine animals can be used as a rich source of compounds with food use, medicinal, medical, pigment and perfumes (Farjami et al. 2013). Bioactive compounds have been isolated from various animal groups, including corals, crabs, tonics, fish thorns, and sponges (Kijjoa and Pichan 2004).Studies on the biological properties of Echinacea show that most of the chemical compounds with biological properties belong to sea cucumbers (Farjami et al. 2013). The results of studies show that most of these compounds extracted from marine invertebrates have peptide, alkaloid, terpenoid and steroid structures (Datta et al. 2015). So far, numerous researches have been done on the antibacterial activity of different body wall extracts of *parastichopus parvimensis* (Villasin and Pomory 2000), *Actinopyja echimites*, *A. miliaris*, *Holothuria arta* and *H.scabra* (Abraham et al. 2001), *Bohadschia marmorata* (Mokhlesi et al. 2012), *Holothuria leucospilota* (Farjami et al. 2013). Sea cucumbers are a large group of aquatic animals and scattered all over the oceans around the world (Barnes 1987). They usually live near coral reefs or sea grass in warm and shallow water (Yatnita and Syamsudin

2014). Sea cucumbers have a high economic value and the most economical application in East Asia is in the traditional food and pharmaceutical industries (Bordbar et al. 2011).

Due to the antibacterial properties of the secondary metabolites of sea cucumber in this study, antimicrobial effects of ***ethyl acetate, methanol and acetone*** extract of the muscle wall of sea cucumber, *Stichopus horrens* of the Chabahar coasts on some rainbow trout (*Oncorhynchus mykiss*) pathogenic bacteria using both disk diffusion and well diffusion methods

2.Materials and Methods

2.1.Sample collection

Nine live samples of the sea cucumber; *Stichopus horrens*, with mean weight 1690± 12.18 g and mean length 16± 1.89 cm were randomly caught from two locations in Chabahar Bay, southeastern of Iran (25º 16′ N, 60 º 40 ′ E) and (25º 21′ N, 60 º 35 ′ E) in November, 2018 and transferred to the laboratory. Identification of the collected sea cucumber was performed with the help of FAO authentication keys. The visceral organs and Coelomic fluids were discarded. Then the muscle wall of body was cut into 1cm^2 pieces, packed and then kept at -20ºC until extraction (Haug et al. 2002).

2.2. Extraction of *S. horrens*

Preparation of *S.horrens* extracts was carried out according to maceration method (Ridzwan et al. 1995). Briefly, 75 g of frozen specimen was dried in an oven at 45ºC for 2 days, ground and extracted with 200 mL of each of ethyl acetate, methanol and acetone organic solvents for 72h. After shaking for 1 week at 150 rmp, the mixtures were passed through a 45 µm nylon membrane filter and evaporated under vacuum at 40ºC by a rotary evaporator (Heidolph 2002, Germany) and then the collected supernatant of each sample was kept at 4ºC until further analysis.

2.3.Bacterial Strains

The bacterial strains used in the present study were the Gram positive bacteria *Lactococcus garvieae* PTCC1884 and *Streptococcus iniae* PTCC188 and the Gram negative bacteria *Aeromonas hydrophila* and *Yersinia ruckeri* PTCC1887. All culture stocks were grown in Mueller Hinton Broth (MHB; Merck, Germany) at room temperature.

2.4. Determination of antibacterial activity of *S.horrens* extracts by disk diffusion method

The antibacterial activities of *S,horrens* body muscle wall extracts on the tested bacteria, were determined by the disk diffusion method (Villasin and Pomory 2000). For each extract, of 4,8 and 12 mg/mL concentrations were used for providing three disk. After preparation of the suspentions of the tested bacteria using the MCFarland 0.5 standard under a hood, the bacteria strains were inoculated with a swab on a MHB. Then the disks containing the different cincentrations were placed on bacteria culture media and kept in a 25ºC incubator for 2 days. The antibiotics Tetracycline and enrofloxacin (30µg/ mL) were used as a positive control. The zone of the bacterial growth inhibition was measured in mm with a caliper

2.5.Determination of antibacterial activity of *S.horrens* extracts by well diffusion method

The minimum inhibition concentration (MIC) values of *S. horrens* extracts on the above mentioned bacteria were measured using well diffusion method following Thornsberry and McDougal (1983) and Tsai et al. (2007). Briefly, after adjusting of the overnight cultures of the tested bacteria to 1×10^6 colony-forming units (CFU)/Ml, 100 µL of made twofold serial dilutions of each S.horrens extract were added to the well of the sterile 96- well microtiter plates containing 100µL of each the tested bacteria suspention in MHB, then, incubated. In this study, the serial dilutions of each *S.horrens* extract were ranged from 0.019-10 mg/mL. After incubation for 2 days at 25ºC, MIC values were evaluated using a microtitre plate reader (MRP4 plus, Hiperion Co. UK)**.** The MIC value was distinguished as the lowest concentration of the *S. horrens* extract that inhibited bacterial growth. Then, for the measurement of minimum Bactericidal concentration (MBC), 100 µL of those wells that showed no bacterial growth were cultured on MHB and incubated 25ºC for 24 h. The MBC value of *S.horrens* was demonstrated as the lowest concentration of *S. horrens* that decreased the viability of the bacterium to ≥99.9%. (Kang et al. 2011).The tests were done in triplicate.

Statistical analysis

Data were analyzed with SPSS 16.0 software (Armonk, NY, USA) using parametric tests. Significant differences in growth inhibition zones, MIC and MBC values bacteria strains, extract type and the different concentrations of extracts were determined using the One-Way ANOVA at the 5% confidence level using the Duncan Multiple Range Test.

3. Results

3.1. Designation of antibacterial activity of *S. horrens* extracts by paper disc diffusion method

The results given in Table 1 showed that only ethyl acetate extracts of *S. horrens* in the concentrations 8 and 12 mg/mL had an inhibition effect on all of the studied bacteria. This extract on *Y. ruckeri* and *S.iniae* had the most impact with inhibition zones with sizes 12.03 and 12mm respectively. Methanol extracts did not show inhibitory impacts on the tested bacteria except to *Y.ruckri.* Only *Y. ruckeri* and *A. hydrophila* bacteria were sensitive to acetone extracts. Sensitivity of *A. hydrophila* to AE was more than that of *Y. ruckeri.* The results of antibacterial activity of tetracycline and enrofloxacin summarized in Table 2 showed that *A.hydrophila* and *S.iniae* had the most sensitive versus tetracycline and enrofloxacin respectively.

Table 1 Inhibition zones diameter (mm) in the different concentrations of three *Stichopus horrens* extracts, tetracycline and enrofloxacin on all the bacteria under test

Bacteria	Different concentrations of three extracts (mg/mL)										
	Methanol				Acetone				Ethyl acetate		
	4	8	12		4	8	12		4	8	12
Y. ruckeri	-	-	8.16±0.15[a]		-	8.10±0.1[b]	11.10±0.1[b]		-	10±0.10[a]	12.03±0.15[a]
S. iniae	-	-	-		-	-	-		-	8±0.20[b]	12±0.10[a]
A. hydrophila	-	-	-		8.03±0.15[a]	11.16±0.15[a]	13.03±0.15[a]		-	7.10±0.1[c]	8±0.10[c]
L. garvieae	-	-	-		-	-	-		-	5.96±0.15[d]	10±0.10[b]

Values given as mm for the different concentrations of three extracts (means± SD (n=3). Different letters in the same columns indicate significant differences between bacteria ($p < 0.05$). -: not determined

Table 2 Inhibition by tetracycline and enrofloxacin on all the bacteria under test (zone size, mm)

Antibiotic (30µg)	*Bacteria species under test*			
	Y. ruckeri	*S. iniae*	*A. hydrophila*	*L. garvieae*
Tetracycline	18.03 ± 0.15^{b}	7 ± 0.2^{c}	19.03 ± 0.15^{a}	6 ± 0.2^{d}
Enrofloxacin	10 ± 0.2^{c}	17.03 ± 0.15^{a}	7.03 ± 0.15^{d}	16.03 ± 0.15^{b}

Values given as mm for all the studied bacteria (means± SD (n=3). Different letters in the same rows indicate significant differences between bacteria ($p < 0.05$)

3.2.Designation of antibacterial activity of *S. horrens* extracts by microdilution method

The results expressed in Table 3 showed that *S. horrens* extracts exhibited selective antibacterial properties. The best property was recorded with *S. horrens* ethyl acetate extract, with MIC value equal to 0.625 mg/ mL against *S.iniae* and *L. garvieae*. MIC values ranging from 0.626 to 1.25 mg/mL were displayed with acetone extracts respectively against *Y. ruckeri* and *A. hydrophila.* Only methanol extracts of *S. horrens* was effective on *Y.ruckeri* with MIC value equal to 0.625 mg/mL. Ethyl acetate extract of *S. horrens* also illustrated the best range of bactericidal effect with a ratio $\mathrm{MBC/MIC} \leq 4$ gained on four studied bacteria strains.

Table 3 Minimal inhibitory concentration (MIC), minimal bactericidal concentration (MBC) values (mg/mL) and MBC/MIC ratio of three *S. horrens* extracts on all the studied bacteria

Bacteria strains	MIC and MBC values (lg/mL) and MBC/MIC ratio										
	Methanol				Acetone				Ethyl acetate		
	MIC	MBC	MBC/MIC		MIC	MBC	MBC/MIC		MIC	MBC	MBC/MIC
Y. ruckeri	0.625	5	8		0.625	2.5	4		1.25	1.25	1
S. iniae	-	-	-		-	-	-		0.625	1.25	2
A. hydrophila	-	-	-		1.25	2.5	2		2.5	2.5	1
L. garvieae	-	-	-		-	-	-		0.625	2.5	4

not determined

4. Discussion

Microbial agents are one of the pathogens that have a high prevalence in the breeding farms of rainbow trout (*Oncorhynchus mykiss*). The use of natural compounds of marine origin for the prevention and treatment of disease has been considered for various reasons, including increased bacterial resistance to antibiotics and high cost in the breeding farms. The present study was investigated the antibacterial activity of methanol, acetone and ***ethyl acetate*** extracts of the muscle wall of *S.horrens* sea cucumber of the Chabahar coasts on some rainbow trout pathogenic bacteria. The results showed that methanol and acetone extracts had no any effective on the growth inhibition of the Gram positive bacteria *L. garvieae* and *S.iniae*. Also, the most susceptible for *Y. ruckeri, S. iniae, A. hydrophila* and *L. garvieae* was recorded with ethyl acetate, ethyl acetate, acetone and ethyl acetate extracts respectively. Numerous pharmacological and chemical studies on several species of sea cucumber showed these invertebrates contain triterpene tetraglycosides with antibacterial, antifungal and cytotoxic properties (Cuong et al. 2017; Kalinin et al. 2015). Similarity, methanol-acetone extract obtained off the body wall of *Parastichopus parvimensis* sea cucumber of the island of Santa California

was effective on the Gram negative *Escherichia coli* and *Bacillus subtilis* using disk diffusion method (Hirimuthugoda et al. 2006). In the present study, the antibacterial effect of ethyl acetate extract was greater than that of methanol and acetone extracts. Also methanol extracts did not show inhibitory impacts on the tested bacteria except to *Y.ruckri.* This indicates that ethyl acetate is a good solvent for the solubility of bioactive substances in sea cucumber. Unlike ethyl acetate, methanol solvent is not able to isolate the bioactive compounds presented in *S.horrens*. These compounds can damage the sensitive organs of the bacterium by passing through or destroying the walls and membranes and finally prevent the growth of bacteria. One of the important factors caused the antibacterial properties of *S. horrens* extracts is the presence of secondary metabolites such as triterpene –glycosides(Mulyndin and Kovalev 2001). These compounds also increased the production of antibodies, protective effect of the vaccine and stimulated antibacterial resistance in mice against conditional pathogenic Gram-negative microorganisms (Sedov et al. 1990). The antimicrobial potential of these extracts can probably be attributed to the presence of antimicrobial agents such as steroidal saponins (Bordbar et al. 2011). Other metabolites, such as polyunsaturated fatty acids (PUFA) (Svetashev et al. 1991), glycolipids (Vaskovsky et al. 1970), , polyamines (Hamana et al. 1990), carotenoids (Bullock and Dawson 1970) or sterols (Makarieva et al. 1993) may act as bioactive compounds. The antibacterial effect of sea cucumber extracts may be due to the accumulation of several bioactive compounds. Comparing to our study, Mokhlesi et al. (2012) reported that ethyl acetate, aqueous methanol and methanol extracts of *Bohadschia* ***marmorata and*** *Holothuria* ***leucospilota species did not formed the growth inhibition zones on the tested bacteria (e.g.*** *E.coli*, *Salmonella aureus* and *Pseudomonas aeruginosa.* This seems that the sea cucumbers species, extract type and also different concentrations of extracts can be effective on the antibacterial properties. The reason for the difference in the effect of sea cucumbers on different strains of bacteria is due to the different amino acid sequences extracted from them (Shakouri et al. 2017). According to the study of Cimanga et al.(2002), if the diameter of the growth inhibition zone is equal to or more than 15 mm, it is very active, the diameter of the growth inhibition zone is between 10 and 15 mm indicates moderate activity and the diameter of the growth inhibition zone is less than 10 mm, the extract is inactive. In this study, of the studied extracts against bacteria, ethyl acetate extract with moderate activity on *Y. ruckeri*, *S.iniae* and *L.garvieae* bacteria, acetone extract with moderate activity on *A. hydrophila* bactrium and methanol extract were evaluated as an inactive extract. Numerous studies showed that different concentrations of sea cucumbers species extract were effective on antimicrobial properties and by reducing the concentration of the extract, the diameter of the bacterial growth inhibition zone often reduced (Mokhlesi et al. 2012; Omran and Allam 2013; Shakouri et al. 2017), which is in line with the results of our study.

Based on our results, in comparison with other extracts, only ethyl acetate extract showed bacteriostatic effect against *S. iniae* and *L.garvieae* at a concentration of 0.625 mg/ mL. Also, ethyl acetate extract showed bactericidal effect against *S. iniae* and *L.garvieae* at concentrations of 1.25 and 2.5 mg/mL respectively. The investigation of antibacterial properties of sea cucumbers extracts showed that they had the most effect on the Gram positive bacteria (Villasin and Pomory 2000; Nazemi et al. 2014). Similarity, our results showed that ethyl acetate extracts had the most antibacterial effect on the Gram positive bacteria *L.garvieae* and *S.iniae*, and at the lowest concentration led to the death of *S. iniae*.

It seems that different concentrations of the extract, extract type as well as the bacteria strains are effective in forming the growth inhibition zone. This study reveals that ethyl acetate extracts of *S. horrens* displayed the best spectrum of bactericidal effect with a ratio MBC/MIC ≤ 4 obtained on four studied bacteria strains by both disk diffusion and well diffusion. Thus ethyl acetate extract of *S. horrens* with a concentration of 12 mg/g can be used as bioactive compounds to the growth inhibition and finally death of bacteria mentioned in trout farms. Also, the results of this study can provide the basis for further research in the future to isolate the effective ingredients of *S.horrens* sea cucumber and prepare the appropriate drug formulation of the best active ingredient.

References

1. Abraham TJ, Nagarajan J., Shanmugan SA (2001) Antimicrobial substances of potential biomedical importance from Holothurian species. Indian J Mar Sci 31:161-164
2. Barnes RD (1987) Invertebrate zoology. 5th ed. New York: Saunders
3. Bordbar S, Anwar F, Saari N (2011) High-value components and bioactives from sea cucumbers for functional foods--a review. Mar Drugs 9:1761-1805 doi:http://doi:10.3390/md9101761
4. Bullock E, Dawson CJ (1970) Carotenoid Pigments of the *Holothurian Psolus* fabricii Dubenet Koren (the Scarlet psolus).
5. 799–804. Comp Biochem Physio 34 700-804
6. Cimanga KK et al. (2002) Correlation between chemical composition and antibacterial activity of essential oils of some aromatic medicinal plants growing in Democratic Republic of Congo Journal of ethnopharmacology 79:213-220 doi:http://doi.10.1016/S0378-8741(01)00384-1
7. Cuong NX et al. (2017) Cytotoxic triterpene diglycosides from the sea cucumber Stichopus horrens Bioorganic & Medicinal Chemistry Letters 27:2939-2942 doi:https://doi.org/10.1016/j.bmcl.2017.05.003
8. Datta D, Talapatra SN, Swarnakar S (2015) Bioactive Compounds from Marine Invertebrates for Potential Medicines – An Overview International Letters of Natural Sciences 34 doi:http://doi.10.18052/www.scipress.com/ILNS.34.42
9. Ebrahimzadeh M, Nabavi SM, Nabavi SF, Eslami B (2009) Free radical scavenging ability of methanolic extract of Hyoscyamus squarrosus leaves Pharmacologyonline 2:796-802
10. Farjami B, Nematollahi MA, Moradi Y, Irajian G, Nazemi M, Ardebili A, Pournajaf A (2013) Antibacterial activity of the sea cucumber Holothuria leucospilota International Journal of Molecular and Clinical Microbiology 3:225-230
11. Hamana K, Niitsu M, Samejima K, Matsuzaki S (1990) Thermopentamine, a novel linear pentaamine found in Thermus thermophilus FEMS Microbiology Letters 68:27-30 doi:http://doi.10.1111/j.1574-6968.1990.tb04116.x
12. Haug T, Kjuul A, Stensvåg K, Sandsdalen E, Styrvold O (2002) Antibacterial activity in four marine crustacean decapods Fish & shellfish immunology 12:371-385 doi:http://doi.10.1006/fsim.2001.0378

13. Hirimuthugoda N, Chi Z, Ling Z (2006) Probiotics and sea cucumber farming 24

14. Kalinin VI, Avilov SA, Silchenko AS, Stonik VA (2015) Triterpene glycosides of sea cucumbers (Holothuroidea, Echinodermata) as taxonomic markers. Nat Prod Commun 10:21-26 doi:https://doi.org/10.1177/1934578X1501000108

15. Kang C-G, Hah D-S, Kim C-H, Kim Y-H, Kim E, Kim J-S (2011) Evaluation of Antimicrobial Activity of the Methanol Extracts from 8 Traditional Medicinal Plants Toxicological Research 27:31-36 doi:http://doi.10.5487/TR.2011.27.1.031

16. Kia ER, Mehrabi Y (2013) Detection and Identification of Different Streptococcosis Strains in Farmed Rainbow Trout in Boyerahmad and Dena Regions (North South of Iran). World Journal of Fish and Marine Sciences 5:315-321

17. Kijjoa A, Pichan S (2004) Drugs and Cosmetics from the Sea Marine Drugs 2 doi:http:// doi.10.3390/md202073

18. Lee S, Kim S, Oh Y, Lee Y (2000) Characterization of Aeromonas hydrophila isolated from rainbow trouts in Korea The Journal of Microbiology 38:1-7

19. Liu W-H, Ding B, Ruan X-M, Xu H-T, Yang J, Liu S-M (2007) Analysis of free and conjugated phytosterols in tobacco by an improved method using gas chromatography-flame ionization detection Journal of chromatography A 1163:304-311 doi:http://doi.10.1016/j.chroma.2007.06.043

20. Mahmoudi M, Ebrahimzadeh MA, Nabavi SF, Hafezi S, Nabavi SM, Eslami SH (2010) Antiinflammatory and antioxidant activities of gum mastic. European Review for Medical and Pharmacological Sciences 14:765-769

21. Makarieva TN et al. (1993) Biosynthetic studies of marine lipids. 42. Biosynthesis of steroid and triterpenoid metabolites in the sea cucumber Eupentacta fraudatrix Steroids 58:508-517 doi:https://doi.org/10.1016/0039-128X(93)90026-J

22. Mancini I, Defant A, Guella G (2007) Recent Synthesis of Marine Natural Products with Antibacterial Activities Anti-Infective Agents in Medicinal Chemistry 600:17-48 doi:http://doi.10.2174/187152107779314151

23. Mokhlesi A et al. (2012) Biological activities of the sea cucumber Holothuria leucospilota Asian Journal of Animal and Veterinary Advances 7:243-249 doi:http://doi.10.3923/ajava.2012.243.249

24. Mulyndin VA, Kovalev VV (2001) Effects of the Extraction of Internal Organs of the Holothurian Cucumaria japonica on the Indices of Nonspecific Resistance Russian Journal of Marine Biology 27:406-408 doi:http://doi.10.1023/A:1013717907602

25. Nazemi M, Alidoost Salimi M, Alidoost Salimi P, Motallebi A, Jahromi S, Ahmadzadeh O (2014) Antifungal and antibacterial activity of Haliclona sp. from the Persian Gulf, Iran Journal de Mycologie MÃ©dicale/Journal of Medical Mycology 24:220-224 doi:http://doi.10.1016/j.mycmed.2014.03.005

26. Omran NE, Allam NG (2013) Screening of microbial contamination and antimicrobial activity of sea cucumber *Holothuria polii*. Toxicology and Industrial Health 29:944-954 doi: http://doi. 10.1177/0748233712448116.

27. Ridzwan BH, Kaswandi MA, Azman Y, Fuad M (1995) Screening for antibacterial agents in three species of sea cucumbers from coastal areas of Sabah General Pharmacology: The Vascular System 26:1539-1543 doi:https://doi.org/10.1016/0306-3623(95)00041-0

28. Sedov A, Apollonin A, Sevastyanova E (1990) Stimulation of Non-Specific Antibacterial Resistance of Mice Against Conditional Pathogenic Gram-Negative Microorganisms by Triterpene Glycosides. Anti kiiK 1:23-26

29. Shakouri A, Shoushizadeh MR, Nematpour F (2017) Antimicrobial activity of sea Cucumber (*Stichopus variegatus*) body wall extract in Chabahar Bay, Oman Sea. Jundishapur Journal of Natural Pharmaceutical Products 12 1-5 doi:http://doi.10.5812/jjnpp.32422

30. Sipkema D, Franssen MCR, Osinga R, Tramper J, Wijffels RH (2005) Marine Sponges as Pharmacy Marine Biotechnology 7:142 doi:http://doi.10.1007/s10126-004-0405-5

31. Soltani M, Pirali E, Shayan P, Eckert B, Rouholahi S, Sadr SN (2012) Development of a Reverse Line Blot Hybridization method for Detection of some treptococcal/Lactococcal Species, the causative agents of Zoonotic Streptococosis/Lactococosis in farmed fish. Iranian Journal of Microbiology 4:70-74

32. Sun HX, Pan HJ (2005) Immunological adjuvant effect of Glycyrrhiza uralensis saponins on the immune responses to ovalbumin in mice. Vaccine 24:1914-1920 doi:http://doi:10.1016/j.vaccine.2005.10.040

33. Svetashev VI, Levin VS, Cham Ngok L, Do Tuet N (1991) Lipid and fatty acid composition of holothurians from tropical and temperate waters Comparative Biochemistry and Physiology Part B: Comparative Biochemistry 98:489-494 doi:https://doi.org/10.1016/0305-0491(91)90242-6

34. Thornsberry C, McDougal LK (1983) Successful use of broth microdilution in susceptibility tests for methicillin-resistant (heteroresistant) staphylococci. Journal of Clinical Microbiology 18:1084-1091 doi:http:// doi. 10.1128/jcm.18.5.1084-1091.1983

35. Tsai P-J, Tsai T-H, Ho S-C (2007) In vitro inhibitory effects of rosemary extracts on growth and glucosyltransferase activity of Streptococcus sobrinus Food Chemistry 105:311-316 doi:https://doi.org/10.1016/j.foodchem.2006.11.051

36. Vaskovsky VE, Kostetsky EY, Svetaschev VI, Zhukova IG, Smirnova GP (1970) Glycolipids of marine invertebrates Comparative Biochemistry and Physiology 34:163-177 doi:https://doi.org/10.1016/0010-406X(70)90064-2

37. Villasin, Pomory CM (2000) Antibacterial activity of extracts from the body wall of Parastichopus parvimensis(Echinodermata: Holothuroidea) Fish & Shellfish Immunology 10:465-467 doi:https://doi.org/10.1006/fsim.2000.0265

38. Yatnita PC, Syamsudin A (2014) Antibacterial activities of bacterial symbionts of soft corals collected from the water of Wai-Sai Island, Papua. Pharmacia Lett 6:8-13

2nd International Conference on Oceanography for West Asia

16 , 17 Sept. 2020 Iran. Tehran

Identification and discrimination of oil slicks and their advance using radar and optical sensor images

Niazi, Alireza [1]; Mojaradi, Barat [2]; Shabakhti, Naser [3]

1. Master of Marine Structural Engineering, Iran University of Science and Technology (IUST)
2. Ph.D. in Surveying Engineering and faculty member at Iran University of Science and Technology (IUST)
3. Ph.D. in Marine Structural Engineering and faculty member at Iran University of Science and Technology (IUST)

Abstract

The importance and potential of seas and water cannot be underestimated by anyone. Most plant and animal species, and also many fundamental sources of living (e.g. oil and gas) are found in the seas and oceans. Therefore, living organisms must maintain the health of this worthy part of the planet to ensure their survival. In general, oil slicks are prevalent sources of pollution in the oceans and seas. Such slicks are highly endurable with long life, thereby threatening the health of the marine ecosystem. A remarkable measure to diminish this risk is to identify it first. Today, under considerable advancements, remote sensing technology has multiple applications in all kinds of human research and projects. In this work, drawing on radar and optical images, we attempted to identify and discriminate oil slicks. Also, we monitored the advance of these slicks using images taken during two weeks. Ultimately, the results were validated and interpreted.

keywords*: Detection, oil slick motion, remote sensing, radar images*

1. Introduction

Oil spill into the water is a harmful phenomenon and appears with devastating environmental impacts. Therefore, failure to remove oil slicks from the water surface promptly and clean water before reaching the coast will come with disastrous effects. Also, the cost of clearing coastal oil slicks is much more than removing offshore spots [1]. Amongst all the pollutants, oil pollutants are of great influence politically, economically, and scientifically. Oil spills in waters include the unallowed release of oil products into the oceans, natural release of oil wells, marine events, oil release during extraction, and much more [2]. Remote sensing instruments to detect oil slicks include infrared photos and videoes, thermal infrared imaging, aerial laser-stimulated fluorescence (LSF), synthetic aperture radar (SAR), and optical sensors.

Hayes et al. (1992) studied the impact of oil spills on the coastal environment and concluded that these consequences are likely to be substantial in the long term. In particular, constant pollution of the water column and the coastal sediments will cause some problems and irreversible damage to the biodiversity of aquatic ecosystems [3].

The study carried out by Taylor (2002) on crude oil proved that remote sensing can easily detect oil from the background [4].

Alawadi et al. (2007) analyzed and processed the first-order radiometric data obtained from the MADIS sensor to detect and discover oil slicks using remote sensing technology. Then, they matched the results with the location of oil rigs and the route of offshore oil tankers, aiming to improve the accuracy with the identification of oil slicks [5].

Liu et al. (2011) asserted that the spectral reflectance (%) of floating crude oil and kerosene in water depends on the thickness and type of oil layer. Floating crude oil is a thick layer on the surface of the water, and its leading visual features are low reflection and brightness, high absorption capacity, low permeability, and low reflection in visible light [6].

Mityagina et al. (2016) studied look-alike phenomena to identify oil slicks in the Caspian Sea and the Black Sea using Sentinel-1 images. The results confirmed the capacity of this satellite in detecting this phenomenon using appropriate algorithms. Therefore, using images gathered by Sentinel-1 considerably decreases the rate of errors [7].

2. Materials and methods

Many studies have been carried out to identify oil slicks using remote sensing, but there are only limited reports on the detection of oil slick motion (advance) using these images. This study, hence, aims to identify and discriminate the advance (motion) of oil slicks using satellite images.

A distinct region should be studied to discriminate oil slicks. The study area in this study was Cilov-Neft Daşları in the Caspian Sea, which is an industrial village in Baku, Azerbaijan, where the Oil Rocks settlement is located. This oil platform is in the eastern part of the Republic of Azerbaijan, more precisely, 100 km far from Baku.

Sentinel-1 and Sentinel-2 and SNAP software are other tools used in this study, all of which are made available to the public freely by the European Aviation Safety Agency (EASA). Sentinel-1 launched its mission on April 3, 2014. It is a polar-orbiting satellite with a radar imaging capability that can collect and capture phenomena at any time, regardless of weather conditions. This satellite can gather ground information even in the worst weather circumstances. The second series of Sentinel satellites launched their mission on June 23, 2015. Sentinel-2 is a polar-orbiting satellite, and its mission is to capture high-resolution images of phenomena such as water, soil, vegetation, and more. Sentinel-2 holds 13 spectral bands in the visible, infrared, near-infrared, and short-wavelength infrared spectra.

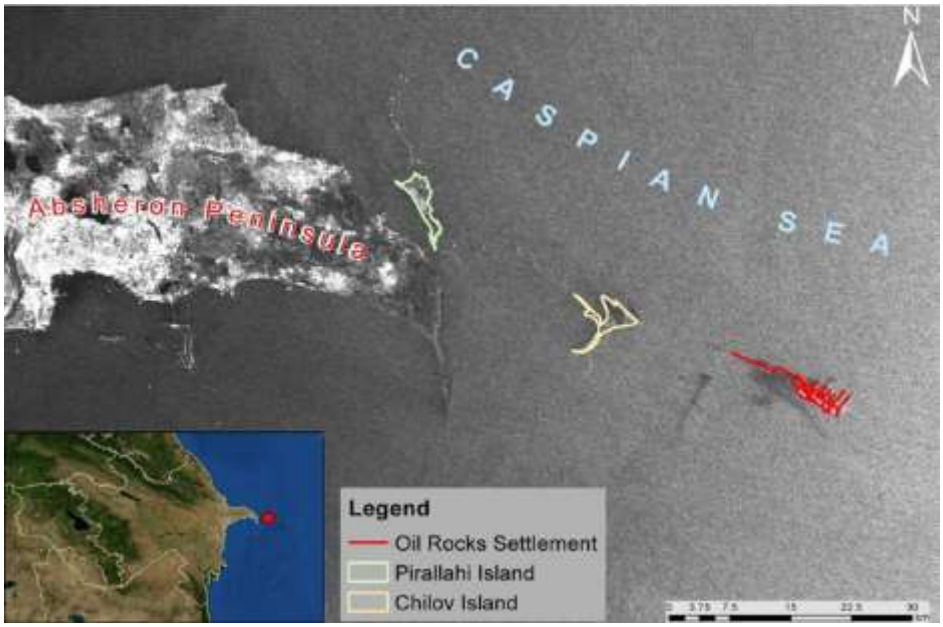

Fig.1. The Oil Rock Settlement in the Republic of Azerbaijan [8]

3. Methodology

The images used in this study are from two optical and radar satellites. Thereby, we need to define two optical and radar analyses for precise examination and processing.

For optical images, we first investigate multiple phenomena of the sea using edge detection algorithms. Oil slicks considerably differ from seawater in reflection and optical and radar properties. Therefore, the first step is to identify phenomena that differ from the sea using the edge detection algorithm. Then geometric and atmospheric corrections are applied if required. Since the pixel accuracy in the bands of Sentinel-2 satellite is different, resampling or aligning the accuracy of band pixels is necessary. For this, the accuracy of all bands is kept equal to study the composition of multiple bands. In the next step, the filtering is applied if required. In this step, the image clouds are filtered to avoid errors in the next operations. The classification of images is the final step, where the oil is separated from the background.

In general, we can produce an image for easier identification of oil slicks, drawing on sufficient data about satellite bands and by designing appropriate band ratios and their combination. For optimal contrast, the use of bands 2, 3, 4, and 8 of the Sentinel-2 satellite gives us band ratios for oil slick recovery. The main band ratios are as follows:

RS1 = (B4 - B3) / B2 (1)

RS2 = B4 / (B3 * B2) (2)

RS3 = B8 / (B3 * B2) (3)

For radar images, the vertical-vertical (VV) band is first chosen for analysis, as the oil slick is more visible in this band. The images obtained are then radio calibrated. This is slightly similar to atmospheric correction in optical images. Images are then revised multiple times. For this, noises are extensively diminished by the combination of spectra. Also, the size of the pixels is reduced if necessary for a better analysis of details. Then, land and coastal images undergo filtering if necessary. In the next step, images undergo a geometric correction. The image is then converted to decibels

(dB) for a better representation of the oil and to achieve a general standard for all images. Finally, the images are classified into two separate categories, and oil is detected and separated from other phenomena by filtering for better transparency.

To study the current motion (advance) we need a specific temporal analysis, which includes a short period where oil slick images are available. For this, optical and radar images were used in the late 8th and early 9th months. From 23 August 2017 to 9 September 2017, three radar images and an optical image were available. The investigation process is as follows:

In Figure 2, the upper part of the slick seems to move (advance). Another part of the slick also seems to be advancing towards Chilov Island. The lower part of the slick seems motionless, as it involves more areas in the more concentrated part. For better understanding, the upper section is separated into three parts. It is marked in the image taken by optical sensors the next day. We can identify the motion of these parts in a single day. Also, using these sections, we estimated the speed of motion, where we found a 10 km advance on average within 19 hours. We estimated this speed by examining several points from the start, end, and inside of these points. According to Fingas [9], the speed of oil motion (advance) under a turbulent current is between 0.5 to 1 m/s. This is equal to 0.5 m in a calm sea. Here, we estimated a speed of 15 cm/s, which is acceptable.

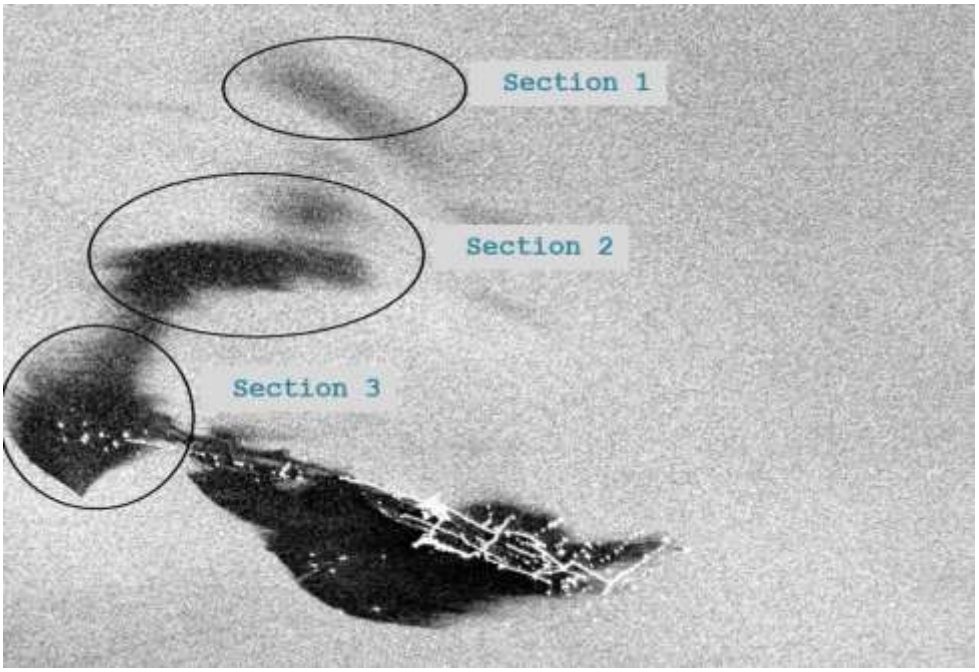

Fig.2. Radar image obtained on 23 August 2017

In Figure 3, the upper part of the slick advances toward the northwest of the Caspian Sea. It crosses the northern part of the Chilov Islands and moves toward the coastal areas of Azerbaijan. The lower part of the slick seems to be motionless and affected by a vortex, which may result from an extensive oil field and its platforms. But the upper part of the slick still advances. The intersection of the motion upstream of the platform and vortices formed around the platform seems to decelerate the movement.

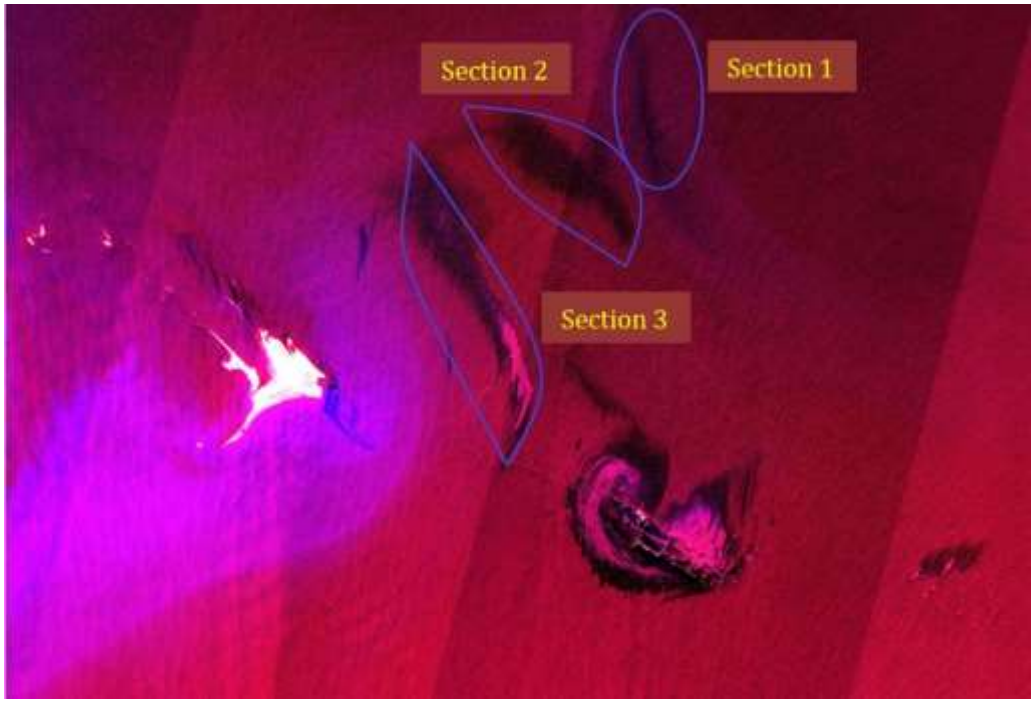

Fig. 3. An optical image taken on 24 August 2017. Sections are illustrated.

Figure 4 illustrates the advance of the northern part of the slick toward the west of the platform. This part is also approaching the coasts of Chiloe Island and the Cape of Azerbaijan. The lower part of the slick is also separating from the platform. Such a separation is in two forms, a vortex to the east and the next vortex to the west. The motion seems to be mainly from westward. In the lower part of the platform, motion is both westward and eastward, whilst in the upper part, the motion is often toward the west. This phenomenon seems to result from the Chiloe Islands, which causes variations in the direction of current.

In Figure 5, like previous figures, the motion is mainly westward. In the northern part of the Chilov Islands, the motion of oil slicks is observed. This slick is much smaller than the previous one, and the current velocity in the north of the island seems to be higher. In the southern part of the island, the traces of the previous slick are observed in the form of a curve, like the previous figure. This indicates the low velocity of the current in the south of the island compared to the north. This is due to the formation of a vortex around the platform, and a cape backside of Chiloe Island. Because the shape of this cape diminishes the speed of current near the cape. Part of this curved slick seems to advance westward from the backside of the island. Another part (the end of the tail) of this slick is also advancing westward.

Fig. 4. A radar image taken on 28 August 2017

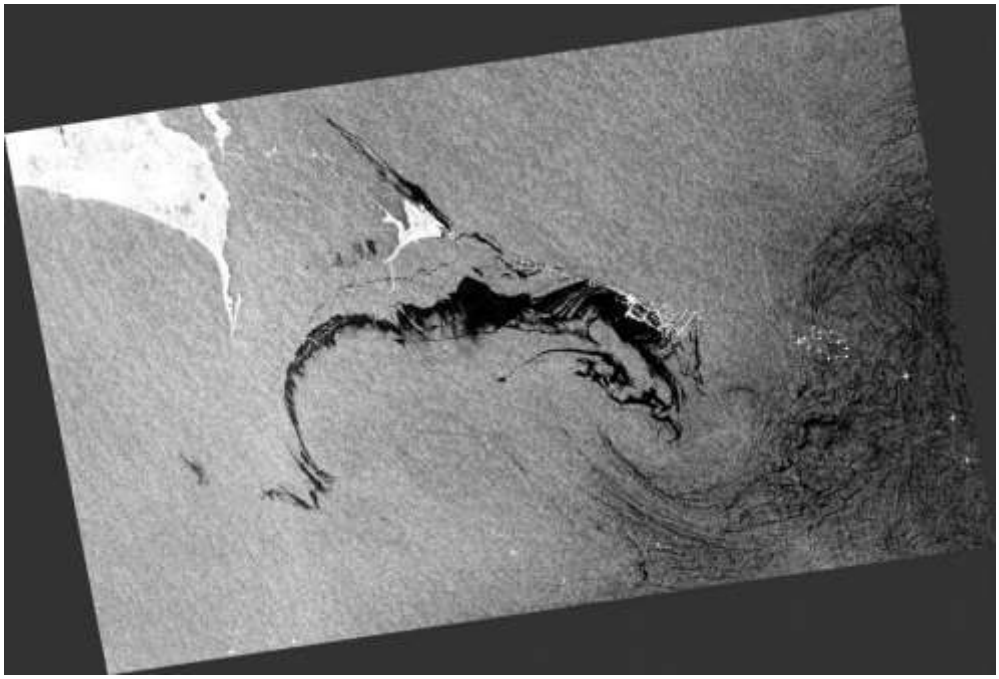

Fig. 5. A radar image taken on 9 September 2017

According to figures and interpretations, it is necessary to confirm the correctness and acceptability of this interpretation of the motion. In other words, the results should be analyzed. For this, we referred to a few months later (in January 2018) when some oil slicks appeared. This month, we attempted to understand if the oil slicks are visible on the beach or not.

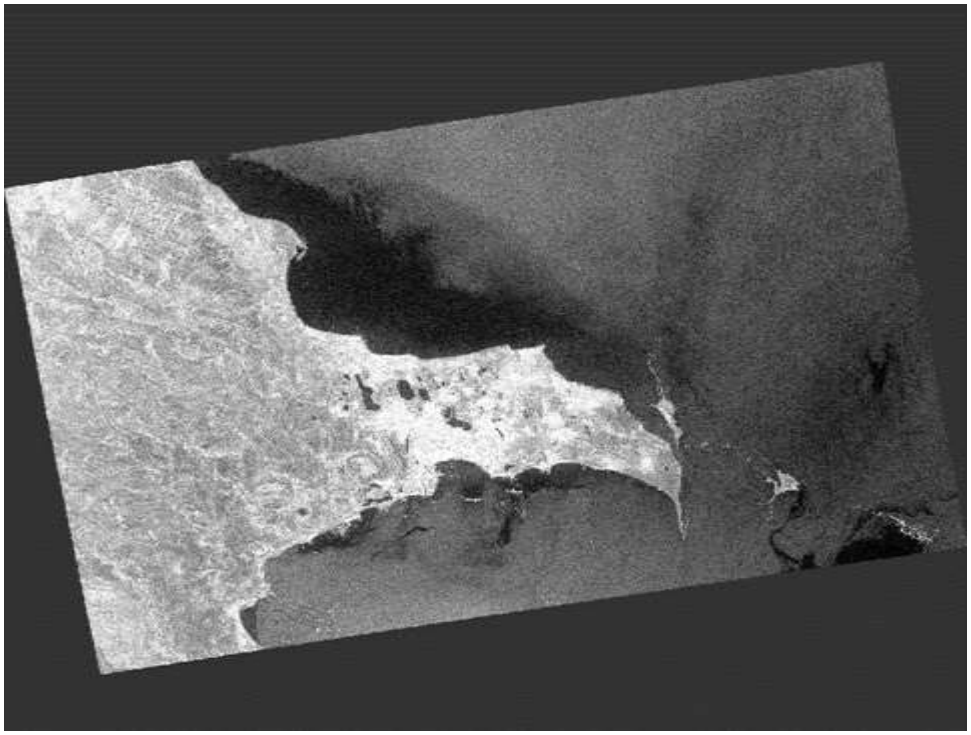

Fig. 6. A radar image of Baku (Azerbaijan) in January 2018

As illustrated, an oil slick appears in the north and south of the cape. In the north part, a greater oil slick is seen, which is due to the predominant current motion westward. Most of the current passes upstream Chilov Island and the cape and reaches the coast of Azerbaijan. This results from the cape's shape with a downward arc and a small cape southward, which causes most of the current to shift toward the north. Some slicks are visible in the southern part of the cape. As mentioned earlier, the slick motion from the south of Chiloe Island is often directed to the south, due to the shape of the island and the cape.

In the next section, the hydrodynamic results are discussed. As reported, the motion is from the northeast to the platform and advances to the west and southwest. Several vortices also appear in the near part of the platform. The results are validated according to Kitazawa and Yang [10], who proposed a numerical model of the Caspian Sea currents. From the results, there is a difference between the currents in the north and south of the Caspian Sea. The investigation of current in August shows a type of motion in the north and south. Kitazawa and Yang stated that the motion in the north is toward the southwest, whilst between the cape, it is almost westward, which is consistent with the results of our study. Also, the prevailing wind motion is from east to west. The effects of wind available in the Central European Database [11] were investigated during the same period, which is consistent with our results.

4. Conclusion

The current motion was discussed in detail in the previous section. From the results, images taken from an area within a short period help us to detect the motion of surface currents. In this study, the current motion was studied in August and September 2017, in the eastern part of Azerbaijan in the Caspian Sea. There are very complex currents in the Caspian Sea, as it is a closed area and various conditions are governing this area. But here, we studied the current in this sea using remote sensing images and with no access to field information and data, and finally reached acceptable

results. In general, the current in this part and these months of the year move from east to west. After hitting the oil platform, the currents form a vortex around the platform due to the large size of this platform and the shape of the platform and its bases. In the northern part, the currents move to the northwest and their speed in these areas is higher than the southern parts. In the southern part, a portion of the current moves from the backside of Chilov Island to the northwest, whilst another part moves to the south of the Cape of Azerbaijan, which is slower than the current in the northern part due to the shape of the cape and Chiloe Island. A summary of the motion interpretation is illustrated in Figure 7. The black part indicates the Oil Rock platform.

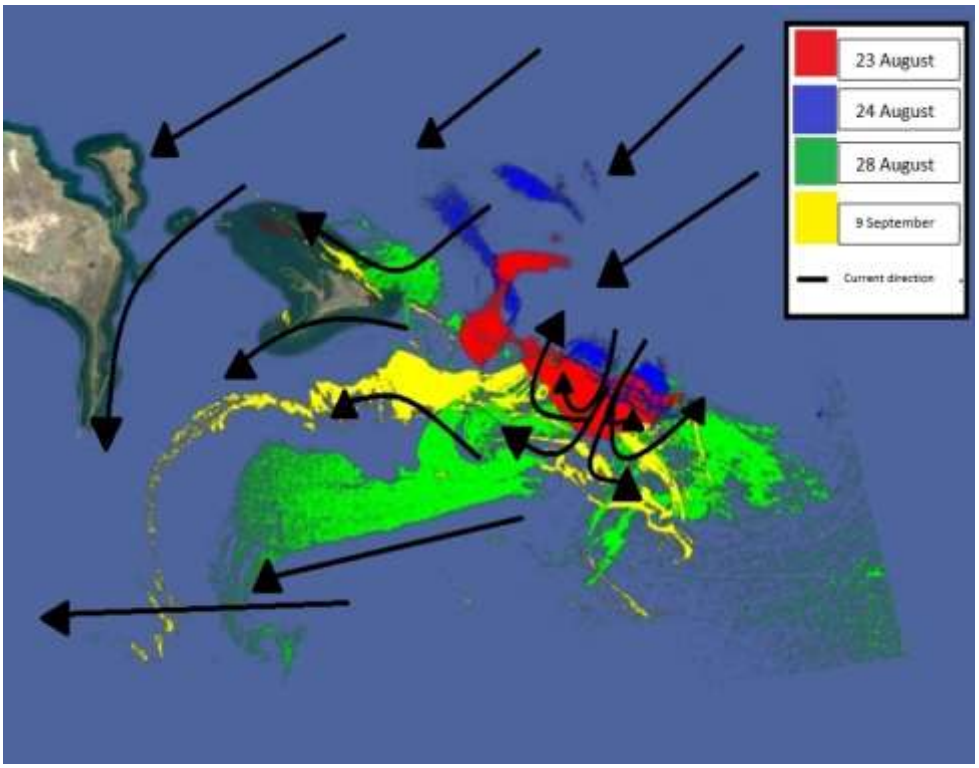

Fig. 7. Surface water currents in the study area

References

1. Columbia/Canada, B., In-Situ Oil Burning Policy and Decision Guidelines., 2001.

2. Annunciado, T., T. Sydenstricker, and S. Amico, Experimental investigation of various vegetable fibers as sorbent materials for oil spills. Marine Pollution Bulletin, (11)50,05p. 1340-1346.

3. Hayes, M.O., Hoff, R., Michel, J., Scholz, D. and Shigenaka, G., 1992. Introduction to coastal habitats and biological resources for oil-spill response (No. PB-92-187590/XAB; HMRAD--92-4). National Oceanic and Atmospheric Administration, Seattle, WA (United States). Coastal Monitoring and Bioeffects Assessment Div.

4. Hu, C., Müller-Karger, F.E., Taylor, C., Myhre, D., Murch, B., Odriozola, A.L. and Godoy, G., 2003. MODIS detects oil spills in Lake Maracaibo, Venezuela. Eos, Transactions American Geophysical Union, 84(33), pp.313-319.

5. Alawadi, F.A., 2011. Detection and classification of oil spills in MODIS satellite imagery (Doctoral dissertation, University of Southampton).

6. LU, Y., CHEN, J., BAO, Y., HAN, W., LI, X., TIAN, Q. and ZHANG, X., 2011. Using HJ-1 satellite CCD data for remote sensing analysis and information extraction in oil spill scenarios. Scientia Sinica Informationis, 41(suppl), pp.193-201.

7. Mityagina M, Lavrova O. 2016. Satellite survey of inner seas: oil pollution in the Black and Caspian Seas. Remote Sens. 8:875 Nicholls JF, Toumi R. 2014. On the lake effects of the Caspian Sea. Q J R Meteorol Soc. 140(681):1399–1408.

8. Bayramov, E., Kada, M. and Buchroithner, M., 2018. Monitoring oil spill hotspots, contamination probability modelling and assessment of coastal impacts in the Caspian Sea using SENTINEL-1, LANDSAT-8, RADARSAT, ENVISAT and ERS satellite sensors. Journal of Operational Oceanography, 11(1), pp.27-43.

9. Fingas, M. Oil Spill Remote Sensing - Scientific Figure on ResearchGate. Available from: https://www.researchgate.net/figure/Landsat-imagery-of-oiled-ice-off-the-east-coast-of-Canada-The-black-lines-in-the-ice-are_fig23_313425652 [accessed 21 Feb, 2019]

10. Kitazawa, D. and Yang, J., 2012. Numerical analysis of water circulation and thermohaline structures in the Caspian Sea. Journal of marine science and technology, 17(2), pp.168-180.

11. https://www.ecmwf.int/ The European Centre for Medium-Range Weather Forecasts.

2nd International Conference on Oceanography for West Asia

16 , 17 Sept. 2020 Iran. Tehran

Assessing the trend of changes in the coastal ecosystems of the Caspian Sea using remote sensing (study area: Miankaleh Wetland - Ashuradeh Island)

Pirali Zefrehei, Ahmad Reza [1*]; Fallah, Maryam [2]; Hedayati, Aliakbar [3]

1. Ph. D, Department of Fisheries and Environmental Sciences, Gorgan University of Agricultural Sciences and Natural Resources (ahmadreza.pirali@gmail.com)

2. Ms.c, Department of Natural Resources, Isfahan University of Technology (maryam.fallah85@gmail.com)

3. Ph. D, Department of Fisheries and Environmental Sciences, Gorgan University of Agricultural Sciences and Natural Resources (hedayati@gau.ac.ir)

Keywords: *Coastline, Landsat, remote sensing, monitoring*

1. Introduction

Understanding the process of change and knowing the evolution of aquatic ecosystems, especially coastal areas, can help to protect and comprehensively manage their future status (Ozesmi and Bauer, 2002). Remote sensing data and satellite imagery in different periods are one of the most reliable and accurate sources for interpreting changes in coastal ecosystems and measuring coastlines (Simon, 2010). Miankaleh Wetland and Ashuradeh Island are located at the southeastern tip of the Caspian Sea and in coordinates 36° 46′ to 36° 57′N and 53° 24′ to 54° 2′E. Fig. (1) shows the position of both ecosystems on the map. Miankaleh Wetland is hydrologically affected by the Caspian Sea and upstream watersheds (Ravanab Consulting Engineers, 2002).

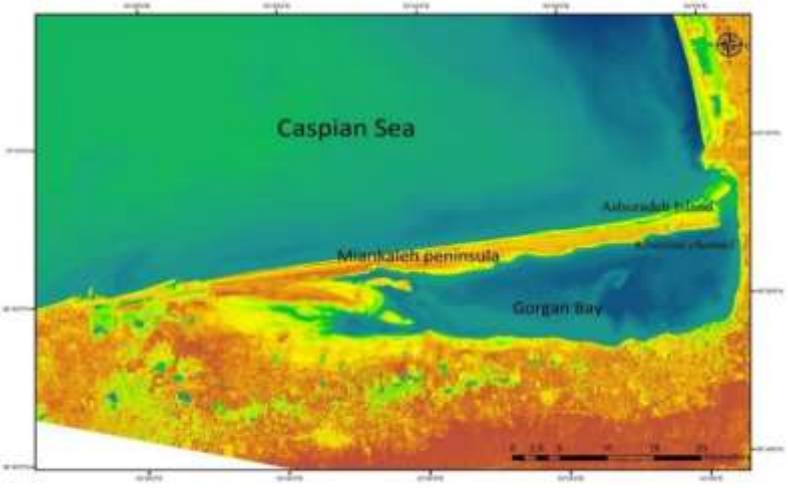

Fig. 1) Location of the ecosystems studied on the map

2. Materials and methods

In this study, using satellite images of TM-5 and OLI-8 related to 1987 and 2018, respectively, the images of periodic changes on the shores of the Caspian Sea in the 29-year were compared and evaluated. High-resolution images were extracted from the "Earthexplorer.usgs.gov" database. After performing the required processing and corrections, the NDWI index was used to separate the water boundary and drought (Ji et al., 2009). G, the green band and the NIR, the infrared band are close. Eq 1:

$$\mathrm{NDWI} = \frac{\mathrm{G} - \mathrm{NIR}}{\mathrm{G} + \mathrm{NIR}}$$

3. Results

The dynamic changes of the coastal ecosystems (Miankaleh Wetland and Ashuradeh Island) during the study period (1988-2018) were shown in Fig. (2). These changes can be seen based on the coastline for review and comparison in Fig. (3).

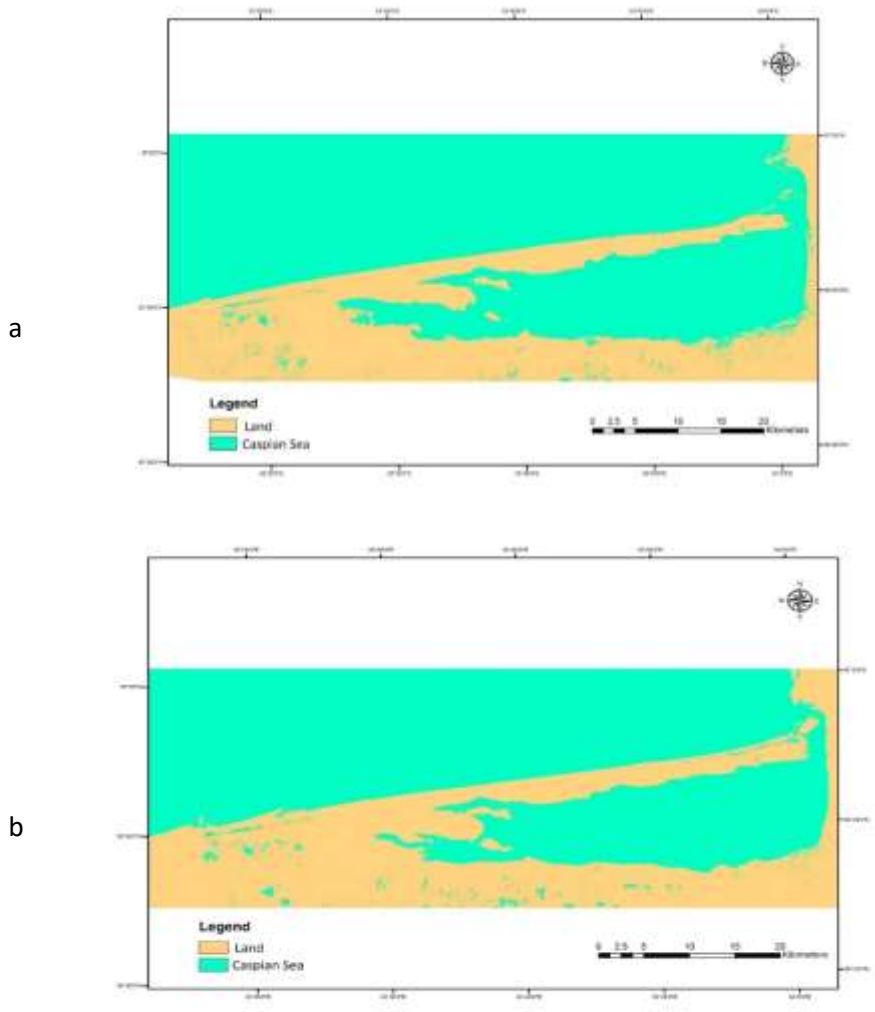

Fig. 2) Miankaleh Wetland and Ashuradeh Island Changes of map, a) 1987, b)2018

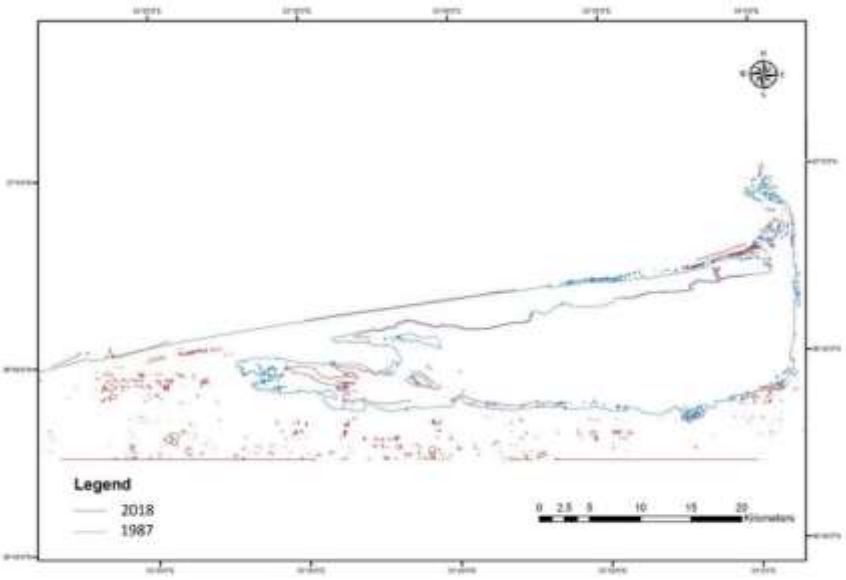

Fig. 3) Coastline changes in the period 1987-2018

Then, to compare the results, the mean water level of the Caspian Sea satellite TOPEX / Jason was used (Fig. 4).

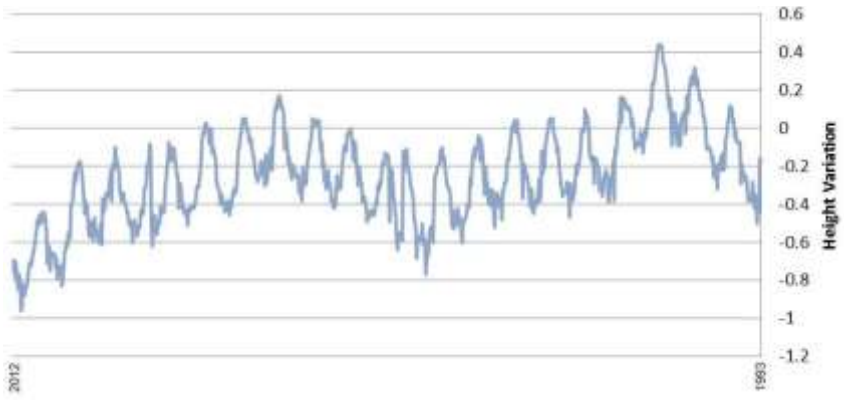

Fig. 4) Changes in the water level of the Caspian Sea recorded by TOPEX / Jason satellite

Quantitative changes in the area by hectare were shown in Fig. 5 during the study period.

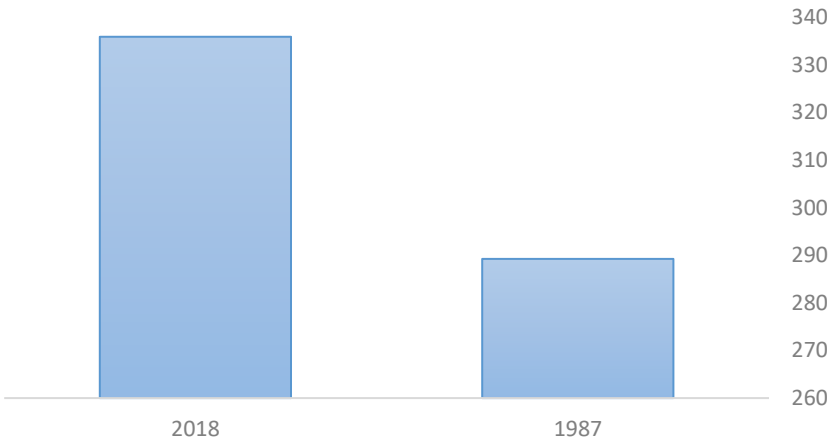

Fig. 5) Area changes per hectare

4. Discussion

The results of the discovery of the coastline generally indicate the water-rise of the arid area of the ecosystems of Miankaleh Wetland and Ashuradeh Island, and in some parts the coast has undergone many changes. Also, the study of the graph of area changes per hectare in the period 1987-2018 shows the same issue (Fig. 5). The study of fluctuations in the Caspian Sea level also corresponds to our results (Fig. 4). In general, the changes that have taken place over the last three decades have, on the one hand, aligned with the Caspian Sea of changes and climate change, and on the other hand, have been the result of uncontrolled human exploitation in these sensitive areas of the Caspian Sea.

References

1. Ravanab Consulting Engineers, 2002, Comprehensive Plan of Miankaleh Protected Area, Volume 1, Environmental Protection Organization
2. Ji, L., Zhang, L., and Wylie, B. 2009: Analysis of dynamic thresholds for the Normalized Difference Water Index. Photogrammetric Engineering & Remote Sensing, 75(11): 1307–1317.
3. Ozesmi, S.L. and Bauer, E.M., 2002. Satellite remote sensing of wetlands. Wetlands Ecology and
4. Management, (10): 381- 402.
5. Simon, P. 2010, Remote Sensing in Geomorphology, Newdelhi, Oxford Book Company.

2nd International Conference on Oceanography for West Asia

16 , 17 Sept. 2020 Iran. Tehran

Assessing the annual changes in the primary production of Choghakhor International Wetland using Landsat and (O.E.C.D)

Pirali Zefrehei, Ahmad Reza [1*]; Hedayati, Aliakbar [2]

1. Ph. D, Department of Fisheries and Environmental Sciences, Gorgan University of Agricultural Sciences and Natural Resources (ahmadreza.pirali@gmail.com)

2. Associate Prof., Department of Fisheries and Environmental Sciences, Gorgan University of Agricultural Sciences and Natural Resources (hedayati@gau.ac.ir)

Abstract

The temporal and spatial distribution pattern of primary production is useful for studying global climate change. In this study, using Landsat images from 1985 to 2017 and their initial processing, the average initial production (based on O.E.C.D) for Choghakhor International Wetland was determined. The results show that the wetland is in terms of chlorophyll-a and secchi disk depth (SDD) in the middle of mesotrophy and towards eutrophication.

Keywords: *primary production, O.E.C.D, Satellite Images*

1. Introduction

Evaluating the pollution of wetlands and lakes is essential for the development and allocation of land use, management, quality monitoring, pollution prevention and biodiversity conservation. One of the most important factors that put wetlands in serious danger and has a very destructive effect on the fauna and flora of the wetland is their enrichment and pollution. Environmental analyzes, especially wetlands, include a wide variety of techniques aimed at determining pollution from land use, environmental monitoring and modeling, and the quality status of wetlands and lakes (Samadi, 2015). Using remote sensing techniques, it is possible to extract water data regionally rather than pointwise (Mueller and Morel, 2002). The aim of this study is to use Landsat images from 1985 to 2017 and their initial processing, the average primary production (based on O.E.C.D) for Choghakhor International Wetland.

2. Materials and methods

Choghakhor International Wetland is located in the suburbs of Chaharmahal and Bakhtiari, Borujen city and Baladaji district, between 50° 52′ to 50° 56′E and 31° 54′ to 31° 56′N (Fig.1) (Ebrahimi and Moshari, 2006). The wetland joined the Ramsar Convention Wetlands List in 2010 (Behrouzi-Rad, 2008).

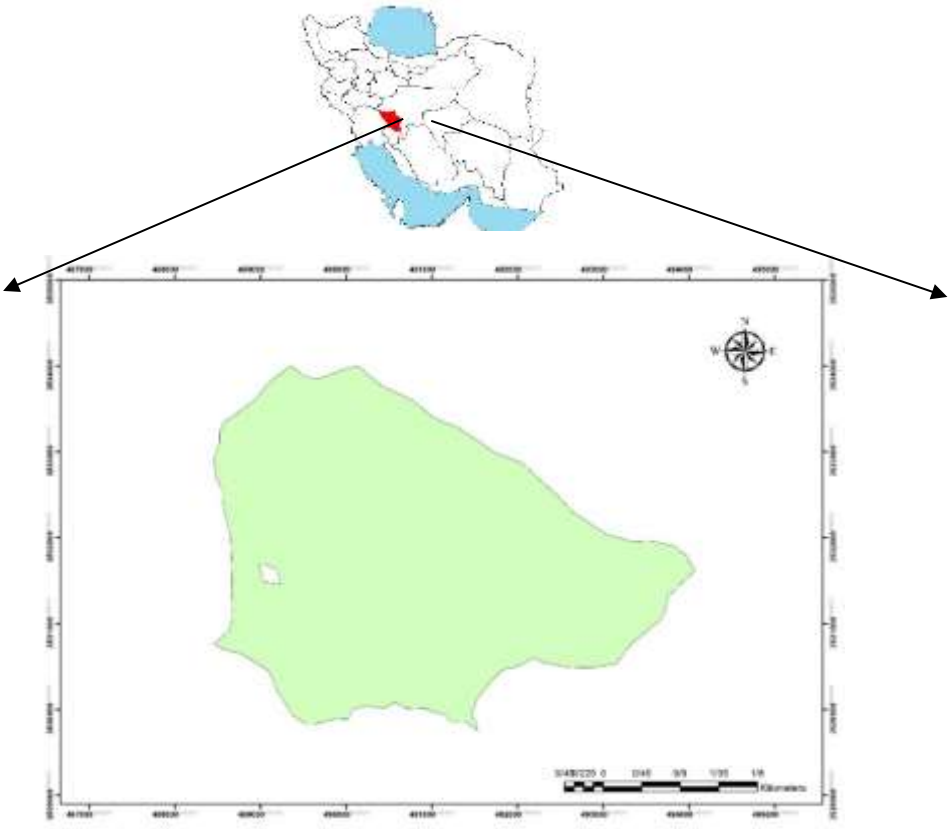

Fig. 1) Map of the study area

Due to the fact that the use of Landsat satellite images is more common in Iran and due to the good time coverage of these images, in this study of images belonging to Landsat 5, 7 and 8 for Choghakhor Wetland in 1985 to 2017 was used. Then, the information layers of parameters were extracted using image processing and algorithms.

In order to apply this indicator in Choghakhor Wetland, first the chlorophyll-a and secchi disk depth (SDD) data of the extraction from the satellite were checked in terms of normality and the data outside the range were removed as discarded data. Then, to determine the probability of different levels of nutritionism and to compare it with the standard curve (O.E.C.D), the normal probability distribution of data (density function of the probability of normal distribution) for each parameter was calculated. Table 1 presents the values of chlorophyll-a and SDD and nutrition levels based on O.E.C.D. All analyzes were performed in R3.4 and Excel, 2016.

Table 1) Average amount of chlorophyll-a and SDD and nutritional levels (O.E.C.D, 1982).

Chl-a (µg/l)			SDD (m)		
Eutro	Meso	Oligo	Eutro	Meso	Oligo
14.3	4.7	1.7	2.45	4.2	9.9

** The µg/l unit is equal to the extraction unit for chlorophyll-a in this study (mg / m3).*

3. Results

Comparison of the normal chlorophyll-a and SDD distribution curves (according to the mean and deviation from the standard of these parameters are drawn in the wetland) can be seen with the standard curve of the above

parameters (O.E.C.D standard) in Fig.2 and 3. The results show that the wetland is in terms of chlorophyll-a and SDD in the middle of mesotrophy and towards eutrophication.

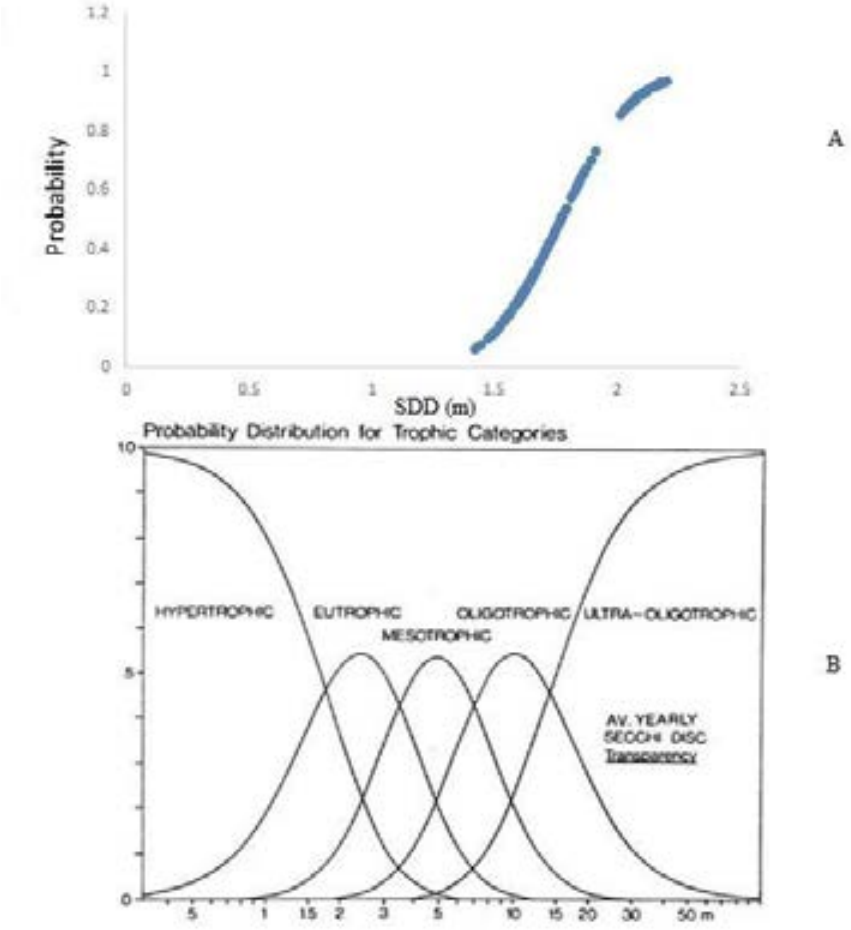

Fig. 2) a) The normal distribution curve of SDD (meter), b) The standard curve (O.E.C.D) of SDD.

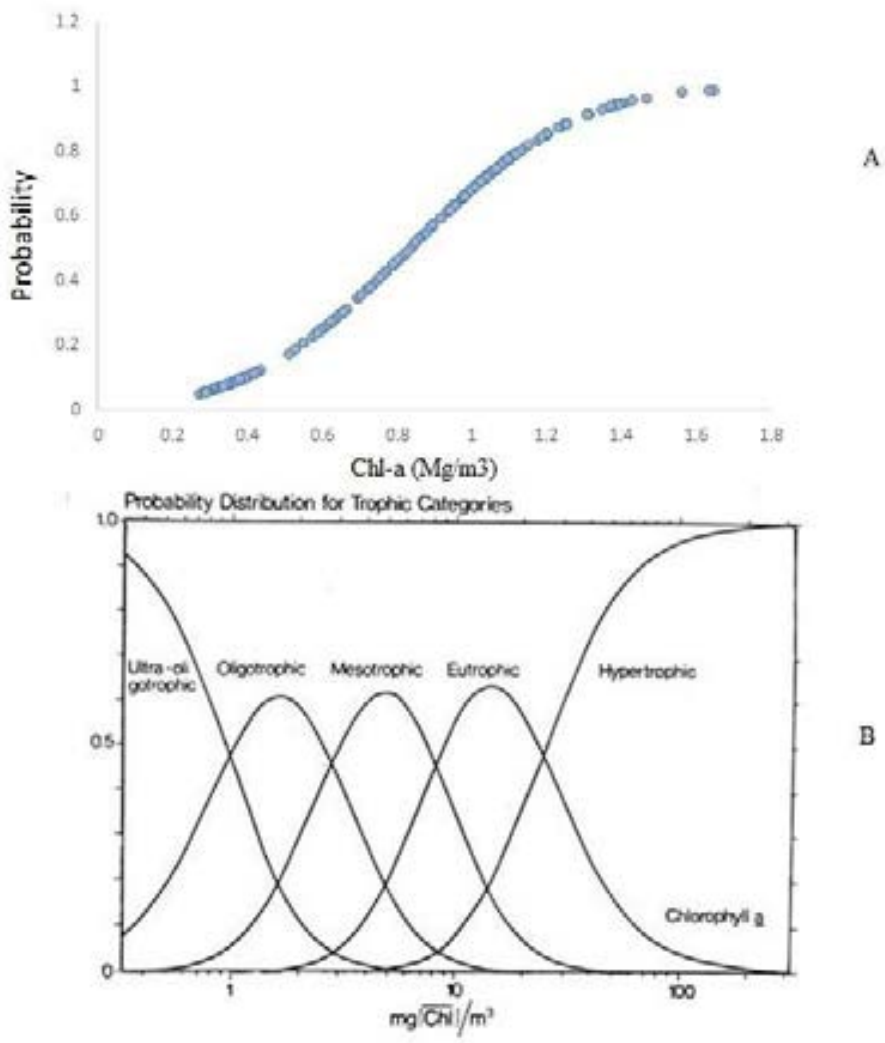

Fig. 3) a) The normal distribution curve of Chlorophyll-a (mg/m3), b) The Standard curve (O.E.C.D) of chlorophyll-a.

4. Discussion

Subsequent changes in chlorophyll-a and SDD levels indicate changes in the number of phytoplankton hams. Today, the population of phytoplankton is heavily influenced by climatic factors such as water temperature and wind. Changes in phytoplankton lead to changes in the life of the aquatic ecosystem that can have economic and food consequences. Therefore, the study of annual changes in primary production is one of the important parameters of fisheries.

References

1. 1-Behrouzi-Rad, B. 2008. Wetlands of Iran. Tehran: National Geographical Organization Publication. [In Persian].
2. 2-Ebrahimi S, Moshari M .2006. Evaluation of the Choghakhor wetland status with the emphasis on environmental management problems. Publications of the Institute of Geophysics, Polish Academy of Sciences; E-6(390):8pp.

3. 3-Mueller, J. L., & Morel, A., 2002, Fundamental Definitions, Relationships and Conventions 56 pp., Greenbelt.

4. 4-Samadi, J. 2015. Survey of Spatial-Temporal Impact of Quantitative and Qualitative of Land Use Wastewaters on Choghakhor Wetland Pollution Using IRWQI Index and Statistical Methods, Iranian Water Resources Research, 11, No. 3, 157-191. In Persian

5. 5-OECD. 1982. *Eutrophication of water*. Monitoring assessment and control, Paris: OECD Publication.

2nd International Conference on Oceanography for West Asia

16 , 17 Sept. 2020 Iran. Tehran

Impacts of salt tectonic on late Holocene relative sea-level changes in the Persian Gulf

Pourkerman, M[1,2*]; Lahijani, H. A. K. [2]; Marriner; N[3]; Morhange, C[1]; Djamali, M[4]; Amjadi, S[2]; Naderi, M[2]

1. Aix Marseille Univ, CNRS, IRD, INRAE, Coll France, CEREGE, Aix-en-Provence, France

2. INIOAS (Iranian National Institute for Oceanography and Atmospheric Sciences), No. 3, Etemad Zadeh St., Fatemi Ave., Tehran, Iran Department example, University example

3. CNRS, ThéMA UMR 6049, Université de Bourgogne Franche-Comté, 32 rue Mégevand, Besançon Cedex, 25030, France

4. Institut Méditerranéen de Biodiversité et d'Ecologie (IMBE/UMR7263), Aix Marseille Université, Avignon Université, CNRS, IRD, IMBE, Technopôle Arbois-Méditerranée, Bât. Villemin, BP 80, F-13545 Aix-en-Provence cedex 04, France

Keywords *Relative sea-level changes, RSL, Persian Gulf, Salt tectonic, late Holocene, geoarchaeology*

1. Introduction

During the early Holocene inundation of the Persian Gulf was happened during 10.5-9.5 kyr BP (Lambeck, 1996) and a Relative sea-level (RSL) highstand of +2 m occurred around 7.1 to 6.89 kyr B.P. (Lambeck, 1996; Lokier et al., 2015). It is possible that inundation of the Persian Gulf led to increased vertical stress of the basin floor that could have reactivated regional salt domes. The salt domes lie in the Hormuz formation and were active before the Zagros folding. The domes were reactivated by subsidence resulting from Zagros tectonic events (Jahani et al., 2007). The distribution of the salt domes is depicted in Figure 1. Deformation of a narrow zone along the Persian Gulf littoral has led to a concentration of domes along the present coast that are classified as active salt domes (zone II) (Jahani et al., 2007). These coastal salt domes could have been reactivated following the displacement of salt to the edge of the area due to basin subsidence resulting from increased vertical stress (Wood et al., 2012).

The rich hydrocarbon resources in the Persian Gulf leads to rapid industry and population development along the coastal zones. Therefore, RSL and coastal uplift are two great risks for the coastal infrastructures. Our knowledge in regard to impacts of salt tectonic on coastal uplift and RSL fluctuations is just limited to handful studies on south of the Persian Gulf. In this study, we employed multidisciplinary geoarchaeological approaches on two important ancient harbours (Siraf and Bataneh) as proxy of shoreline position index during last 2 kyr B.P

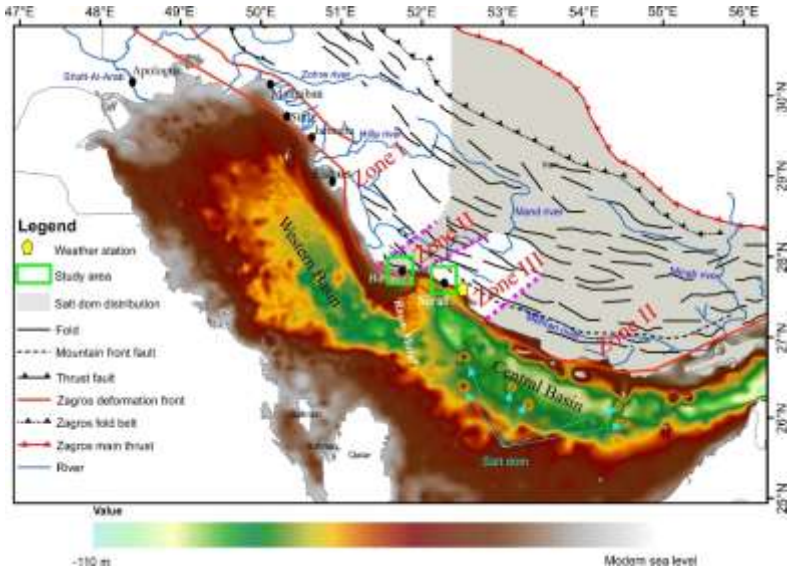

Figure 5) General morphology of the Persian Gulf with the location of some of its ancient harbours and distribution of the salt domes in southern Iran

2. Materials and methods

Two 3-m boreholes were extracted from Siraf and Bataneh water front heritage sites. The cores were leveled using a theodolite in relation to present Mean Sea Level (MSL). After core collection, nondestructive magnetic susceptibility (MS) was measured using a Bartington MS2c 100-mm diameter loop sensor with an MS2 meter at 2 cm resolution (Delile et al., 2014). Subsampling and samples preparation were proceeded according to the Marriner and Morhange (2007); Heiri et al., (2001). Wet sieving was performed using mesh sizes of 2 mm and 63 microns. After processing and oven-drying, the ostracods were picked from 10 g of the >125 µm size fraction and placed on microslides in order to count and identify the species (Marriner et al., 2005). The 14C data were calibrated using Calib version 7.1.0 online version (http://calib.org) and a standard Persian Gulf marine reservoir age (Southon et al., 2002).

The Glacial Isostatic Adjustment (GIA) simulations performed in this work are based on model ICE-6G (VM5a) of Peltier (2012) and Peltier et al. (2015). The Late-Pleistocene-ice-sheets chronology of model ICE-6G (VM5a) was been implemented in the program SELEN4 (Spada and Melini, 2019). SELEN4 solves the Sea-Level Equation by taking into account the horizontal migration of shorelines, for the transition from grounded to floating ice and for the effects of rotational feedback on sea level. The Sea-Level Equation was solved using a pseudo-spectral approach with a spatial resolution corresponding to the maximum harmonic degree lmax=256, on a grid with a spacing of ~40 km.

3. Results

According to the core's facies analysis in Siraf three important Upper shore facies, anthropogenic facies and erosion and accretion facies are recognized and Bataneh cores' facies are classified into four important unites: marine facies, open lagoon with freshwater flux, anthropogenic zone and lagoon.

Reconstructed RSL with ICE-6G (VM5a) model in the Siraf and Bataneh represented that RSL in the Persian Gulf was never fell below present level during the mid to late Holocene (Fig 2).

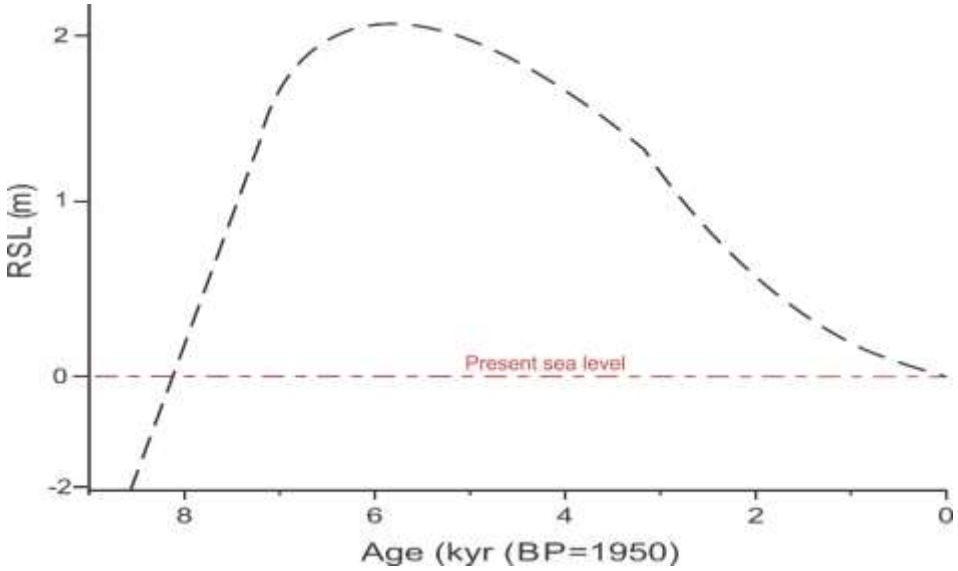

Figure 6) The ICE-6G (VM5a) RSL model graph

4. Discussion and conclusion

Our reconstructed RSL was not correlated with ICE—6G (VM5a) model for the studied sites. Although the model shows a continuous fall since 4 kyr B.P, but, the studied cores were logged three RSL oscillations. Duration between each oscillations was correlated with modeled sea-level position. Increase water column in central basin floor leads to injecting salt from Fars formation into coastal and underwater salt domes. Meanwhile, time interval between lowstand with next highstand were decreased. Concurrent with decreasing sea-level, the oscillation time intervals are changed from 50 years in 1.9 kyr B.P. to 350 year in 1.3 kyr B.P.. Coincide with the oscillations, Bataneh ancient site that is located at south of Darang salt dome recorded cal. 3.7 m uplift.

Previous study on tide gauges was demonstrated that rate of mean sea level raise in the Persian Gulf is 0.7 mm/y more than global rate for the period between 1993 to 2018 (Siddig et al., 2019). Also, the other studies were attested rejuvenation of coastal salt diapirs since Holocene (Jahani et al., 2007). Therefore, according to the results, unique RSL changes in the Persian Gulf put the coastal infrastructures and cities at unpredictable risks of erosion and flooding. So, more studies are required to shed light on Holocene RSL fluctuations and coastal morphology changes in the Persian Gulf.

References

1. Delile, H., Mazzini, I., Blichert-Toft, J., Goiran, J.P., Arnaud-Godet, F., Salomon, F., Albarède, F., 2014. Geochemical investigation of a sediment core from the Trajan basin at Portus, the harbour of ancient Rome. Quat. Sci. Rev. 87, 34–45.

2. Heiri, O., Lotter, A.F., Lemcke, G., (2001). Loss on ignition as a method for estimating organic and carbonate content in sediments: reproducibility and comparability of results. J. Paleolimnol. 25, 101–110.

3. Jahani, S., Callot, J. P., de Lamotte, D. F., Letouzey, J., & Leturmy, P. (2007). The salt diapirs of the eastern Fars Province (Zagros, Iran): A brief outline of their past and present. In Thrust Belts and Foreland Basins (pp. 289-308). Springer, Berlin, Heidelberg.

4. Lambeck, K. (1996). Shoreline reconstructions for the Persian Gulf since the last glacial maximum. Earth and Planetary Science Letters, 142(1-2), 43-57.

5. Lokier, S. W., Bateman, M. D., Larkin, N. R., Rye, P., & Stewart, J. R. (2015). Late Quaternary sea-level changes of the Persian Gulf. Quaternary Research, 84(1), 69-81.

6. Marriner, N., & Morhange, C. (2007). Geoscience of ancient Mediterranean harbours. Earth-Science Reviews, 80(3-4), 137-194.

7. Marriner, N., Morhange, C., Boudagher-Fadel, M., Bourcier, M., & Carbonel, P. (2005). Geoarchaeology of Tyre's ancient northern harbour, Phoenicia. Journal of Archaeological Science, 32(9), 1302-1327.

8. Peltier, W. R., Argus, D., Drummond, R., & Moore, A. W. (2012). Postglacial rebound and current ice loss estimates from space geodesy: the new ICE-6G (VM5a) global model. In AGU Fall Meeting Abstracts.

9. Pourkerman, M., Marriner, N., Morhange, C., Djamali, M., Lahijani, H., Amjadi, S.,... & Naderi, M. (2020). Late Holocene relative sea-level fluctuations and coastal uplift in the Persian Gulf: implications for Bataneh (Najirum) archaeological site, Iran. Unpublished paper.

10. Siddig, N. A., Al-Subhi, A. M., & Alsaafani, M. A. (2019). Tide and mean sea level trend in the west coast of the Persian Gulf from tide gauges and multi-missions satellite altimeter. Oceanologia, 61(4), 401-411.

11. Southon, J., Kashgarian, M., Fontugne, M., Metivier, B., & Yim, W. W. (2002). Marine reservoir corrections for the Indian Ocean and Southeast Asia. Radiocarbon, 44(1), 167-180.

12. Spada, G., & Melini, D. (2019). SELEN4 (SELEN version 4.0): a Fortran program for solving the gravitationally and topographically self-consistent Sea Level Equation in Glacial Isostatic Adjustment modeling. Geoscientific Model Development, 12(12), 5055-5075.

13. Wood, W. W., Bailey, R. M., Hampton, B. A., Kraemer, T. F., Lu, Z., Clark, D. W. James, R.H. and Al Ramadan, K. (2012). Rapid late Pleistocene/Holocene uplift and coastal evolution of the southern Persian Gulf. Quaternary Research, 77(2), 215-220.

2nd International Conference on Oceanography for West Asia

16 , 17 Sept. 2020 Iran. Tehran

The effect of copper bioaccumulation on filtration rate of zebra mussel (*Dreissena polymorpha)* from Anzali Wetland- Caspian Sea

Rahnama, Reza [1*]; Javanshir, Arash [2]; Hamzehpour, Ali [1]; Darvish Bastami, Kazem [1]

1. Iranian National Institute for Oceanography and Atmospheric Science (INIOAS).

2. Department of Fisheries and Environment, Faculty of Natural Resources, University of Tehran, Tehran/ Iran

***** Corresponding author, email: reza.rah@inio.ac.ir

1. Introduction

Natively the zebra mussel *Dreissena polymorpha* inhabits parts of western Russia near the Caspian Sea and the Ural River. Zebra mussel is highly abundant in the Anzali wetland in south Caspian Sea basin. Zebra mussel is an important link in the aquatic food chain: it accelerates the circulation of organic compounds by filtering large amounts of phytoplankton from the water (Stanczykowska, 1987). This mussel forms the main source of food for some benthivorous fish, such as roach *Rutilus rutilus* (Prejs *et al*., 1990; Bleeker *et al*., 1992). As a filter feeder, *Dreissena* filters inert particles and phytoplankton from the water column, but nearly 100% of the particles >1 mm, cannot be filtered because those are too big for *Dreissena*. In freshwater ecosystems with great density of *D. polymorpha*, concentrations of phytoplankton decreased, and it is one of the main problems for planktonivorous fishes. Effects of pollutants on this mussel can affect on the food chain in freshwater ecosystems (Kraak *et al*., 1991). One of the main pollutants of water ecosystems are metals. Metals affect freshwater and marine bivalves such as *D. polymorpha*. The filtration rate is reduced (Watling, 1981; Grace *et al*., 1987), the animals keep their shells closed for longer periods of time (Salanki *et al*., 1989), they produce less byssus threads (Bleeker *et al*., 1992), and their heart rate is lower (Grace *et al*., 1987). All these cases affected the filtration rate of mussels. Metals can be divided into two groups: the essential (e.g., Cu, Zn) and the non-essential metals (e.g., Cd, Pb). Essential metals are used in small amounts by animals as components of proteins and enzymes (Simkiss, 1982). Most animals are able to regulate the concentration of these metals in their body up to a certain ambient water concentration, which above this concentration, metals accumulated and toxic effects may occur. Non-essential metals do not play any biological role. These metals are, therefore, potentially toxic at low concentration (Amiard *et al*., 1987). In this study the sub-lethal effect of the essential metal copper on the filtration rate of *D. polymorpha* sampled from the Anzali wetland in the south Caspian Sea region was investigated in order to better understand

the impact of this metal on the food chain. After the filtration experiments the copper concentrations in the mussels were determined, with the expectation that copper could be regulated by zebra mussel.

2. Materials and methods

The mussels were sampled from relatively unpolluted area in the Anzali wetland (march, 2007). They were picked up from the stems of aquatic plants *Fragmites* sp. After collection, they were carried to the laboratory and the acclimation period (14 days) was realized by using a plastic aquarium, containing 10 L of filtered fresh water (0.45 mm) from the sample site.

After this period, mussels were sorted by length and only the ranges between 17 and 23 mm were taken. The average length did not differ between treatments. The exposure to copper consisted of five treatments of 5, 15, 25, 50 and 70 $\mu g.L^{-1}$ that were made up using a stock solution of 1000 $mg.L^{-1}$ $CuCl_2$ (Kraak *et al*., 1992, 1999). Six plastic aquariums were used to conduct the experiment. One used as control (0 $\mu g.L^{-1}$). Volume of each treatment was 10 L and each of them contained a group of 25 specimens. Copper was added to the aquaria at the beginning of the experiments. Mussels in each treatment were exposed to copper for 48 hours, during which they were starved. After this period, water samples were taken from each treatment and the concentrations of Cu were analyzed by furnace atomic adsorption spectrometer (FAAS, Perkin Elmer 1100B), in order to determine the actual concentrations of copper to which the animals were exposed during the experiments. After 48 hours, algae *Chlorella* spp. (20,000 $cells.mL^{-1}$) was added. Filtration rate was measured from the differences of algae concentration at each sampling time. For a period of 100 minutes, every 10 minutes, 2 mL of water from each aquarium was taken. The algal concentrations in the water samples were measured using a Coulter Counter (Model ZI). The filtration rate was calculated from the decrease in algal concentration, according to Jørgensen's formula (Jørgensen, 1990):

$$Fr = \frac{V}{W\,T} Ln \frac{C_0}{C_t}$$

Where Fr = indicates filtration rate in $mL.gdw^{-1}.min^{-1}$, V = volume of the solution (10,000 mL), W = dry weight of mussels in grams, T = duration of the experiment in minutes, and C_0 and C_t represent the algal concentration in the beginning and at the end of exposure time.

During the experiment the mussels were continuously aerated and always saturated with oxygen. The water temperature was kept constant at 25°C using a water heater, the hardness was 88.96 $mgCaO.L^{-1}$ and the pH was 8.16. Filtration was measured when 90% of the mussels opened their inhalant and exhalent siphons, which usually happened during the first minute after algae had been added to the treatments.

After the filtration experiments the soft tissues of five mussels from each aquarium were analyzed for their copper concentration. The antero–posterior lengths were measured, and also their soft tissue dry weight was determined

with oven temperature at 60°C for 24 hours (Klerks *et al*., 1997; Pessatti *et al*., 2002; Rahnama *et al*., 2010, 2001). The soft tissues (1 gram) were digested in 5 mL concentrated HNO_3 with 2 mL distilled water added. After refluxing for 4 hours at 120°C, 2 mL of H_2O_2 (30%, Fisher certified grade) was added and heating was continued for an additional 2 hours after cooling. The tissue digest was filtered using glass-fiber filters and brought up to volume 25 mL using 0.4 M HNO_3. The samples were analyzed for copper by furnace atomic adsorption spectrometer (FAAS, Perkin Elmer 1100B). The detection limit in the samples was 0.5 $\mu g.L^{-1}$. The accuracy of analytical procedure was evaluated using standard reference material (LUTS-1 National Research Council, Canada). Recovery value of metal analysis was 98%.

3. Results

During the experiment in control and copper treatments no mussels died. (Figure 1) shows the filtration rates of *D. polymorpha* exposed to control and five Cu treatments (5, 15, 25, 50 and 70 $\mu g.L^{-1}$). As mentioned in the figure, at two high concentrations of copper component (50 and 70 $\mu g.L^{-1}$) the filtration rates decreased compared to low concentrations and both of them followed the same pattern. Also, filtration rates of mussels in treatments of 5, 15, 25 $\mu g.L^{-1}$ showed same pattern as control without pollutant. Filtration rates increased visibly 50-60 minutes after the beginning of the exposure. At very low densities mussels start to clear slowly compared to high densities.

Comparison of mean values of mussel's filtration rates in control and Cu treatments showed insignificant differences ($p> 0.05$) except for two concentrations of 50 and 70 $\mu g.L^{-1}$ ($p<0.05$) (Figure 2). The mean value of filtration rate in control mussels is about 25 ± 2 $mL.gdw^{-1}.min^{-1}$. At a concentration of 5 $\mu g.L^{-1}$ filtration rate is 24 ± 2 $mL.gdw^{-1}.min^{-1}$, at 15 $\mu g.L^{-1}$ filtration rate is 22 ± 2 $mL.gdw^{-1}.min^{-1}$, at 25 $\mu g.L^{-1}$ filtration rate is 21 ± 1 $mL.gdw^{-1}.min^{-1}$. While, at concentrations of 50 and 70 $\mu g.L^{-1}$ filtration rates respectively were about 11 ± 1 $mL.gdw^{-1}.min^{-1}$ and 9 ± 1 $mL.gdw^{-1}.min^{-1}$.

If the mean values of mussel's filtration rates presented as percentages compared to control mussel's filtration rate, at a concentration of 5 $\mu g.L^{-1}$, the filtration rate was closely near to control (98%). Also, in treatments of 15 and 25 $\mu g.L^{-1}$, filtration rates were close to control (92 and 88% of control, respectively). But, at concentration of 50 and 70 $\mu g.L^{-1}$, filtration rates of *D. polymorpha* decreased respectively about 44 and 36% of the control mussels.

The low percentage of two high Cu treatments suggests that, there is a limit of filtering activity controlled by concentration of pollutant in its experimental environment. (Figure 3) shows the decrease in copper content of water in each treatment after 48 hours of mussels' exposure. Most reduction of copper in the water at concentration of (70 $\mu g.L^{-1}$) and lowest reduction were observed at concentration of (5 $\mu g.L^{-1}$). Absorbed metal in the tissue of mussels was also related to initial concentration in its ambient water. As shown in (Figure 4), the copper concentrations in the mussel's tissue plotted against the Cu concentrations in the water. Assimilated concentration

increased when Cu concentration in water increased. All assimilated copper concentrations of the exposed mussels differed significantly ($p<0.05$).

References

1. Amiard, J.C., C. Amiard-Triquet, B. Berthet and C. Metayer, 1987. Comparative study of the patterns of bioaccumulation of essential (Cu, Zn) and non-essential (Cd, Pb) trace metals in various estuarine and coastal organisms. J. Exp. Mar. Biol. Ecol. 106: 73-89.

2. Bleeker, E.A.J., M.H.S. Kraak and C.Davids, 1992. Ecotoxicity of lead to the zebra mussel *Dreissena polymorpha*, Pallas. Hydrobiol. Bull. 25: 233-236.

3. Davids, C. 1964. The influence of suspensions of microorganisms of different concentrations on the pumping and retention of food by the mussel (*Mytilus edulis* L.). Neth. J. Sea Res. 2: 233-49.

4. Grace, A.L. and L.F. Gainey Jr, 1987. The effects of Cu on the heart rate and filtration rate of *Mytilus edulis*. Mar. Pollut. Bull.18: 87-91.

5. Jørgensen, C.B. 1990. Bivalve filter feeding: Hydrodynamics, bioenergetics, physiology and ecology. Fredensborg: Olsen & Olsen.

6. Klerks, P.L., Peter C. Fraleigh, and Jay E. Lawniczak, 1997. Effects of the exotic zebra mussel *(Dreissena polymorpha*) on metal cycling in Lake Erie. Can. J. Fish. Aquat. Sci. 54: 1630-1638.

7. Kraak, M.H.S., M.C.Th. Scholten, W.H.M. Peeters and W.Chr. De kock, 1991. Biomonitoring of heavy metals in the western European rivers Rhine and Meuse using the freshwater mussel *Dreissena polymorpha*. Environ. Pollut. 74: 101-114.

8. Kraak, M.H.S., D. Lavy, W.H.M. Peeters and C. Davids, 1992. Chronic ecotoxicity of copper and cadmium to the zebra mussel *Dreissena polymorpha*. Arch. Environ. Contam. Toxicol. 23: 363-369.

9. Kraak, M.H.S., S.C. Stuijfzand, W. Admiral, 1999. Short-term ecotoxicity of a mixture of five metals to the zebra mussel *Dreissena polymorpha*. Bull. Environ. Contam. Toxicol. 63: 805-812.

10. Lecoeur, S., B. Videmann, and Ph. Berny, 2004. Evaluation of metallothionein as a biomarker of single and combined Cd/Cu exposure in *Dreissena polymorpha*. Environ Res. 94: 184-191.

11. Lobel, P.B., Mogie. P, Wright. D.A, Wu BL, 1982. Metal accumulation in four mollusks. Mar. Pollut. Bull. 13: 170-174.

12. Okumus, I., Bascinar, N., Özkan, M., 2002. The Effects of Phytoplankton Concentration, Size of Mussel and Water Temperature on Feed Consumption and Filtration Rate of the Mediterranean Mussel (*Mytilus galloprovincialis* Lmk). Turk. J. Zool. 26: 167-172.

13. Pessatti, M.L., Resgalla, J.R., C. Reis Fo, R.W. Kuhen, J. Salomao, L.C. and Pontana, J.D., 2002. Variability of filtration and food assimilation rates, respiratory activity and multixenobiotic resistance (MXR) mechanism in the mussel *Perna perna* under lead influence. Braz. J. Biol. 62: 651-656.

14. Prejs, A., K. Lewandowski and A. Stanczykowska-Piotrowska, 1990. Size-selective predation by roach (*Rutilus rutilus*) on zebra mussel (*Dreissena polymorpha*): field studies. Oecologia, 83: 378-384.

15. Rahnama, R., Javanshir, A., Mashinchian, A., 2010. The effects of lead bioaccumulation on filtration rate of zebra mussel (*Dreissena polymorpha*) from Anzali wetland-Caspian Sea. Toxicol. Environ. Chem. 92: 107-114. doi: 10.1080/02772240902744444.

16. Rahnama, R., Javanshir, A., Mashinchian, A., 2011. The effects of lead bioaccumulation on condition indices of zebra mussel (*Dreissena polymorpha*) from Anzali wetland-Caspian Sea. Turk. J. Fish. Aquat. Sci. 2011, doi: 10.4194/1303-2712-v11_4_09.

17. Rainbow, P.S., White, S.L, 1989. Comparative strategies of heavy metal accumulation by crustaceans: zinc, copper and cadmium in a decapod, an amphipod and a barnacle. Hydrobiolgia. 174: 245-262.

18. Salanki, J. and K.V. Balogh, 1989. Physiological background for using freshwater mussel in monitoring copper and lead pollution. Hydrobiolgia. 188/189: 445-454.

2nd International Conference on Oceanography for West Asia

16 , 17 Sept. 2020 Iran. Tehran

On a collection of ghost shrimps (Crustacea, Decapoda) from the Persian Gulf and Gulf of Oman (Persian Gulf Explorer)

Sepahvand, Vahid [1*]; Momtazi, Farzaneh [1]

1. Department of Marine Biological Sciences, Iranian National Institute for Oceanography and Atmospheric Science (INIOAS), Tehran, Iran

Abstract

During the Persian Gulf Explorer Crouse in April-May 2019 yielded several specimens of ghost shrimps. They are belong to four genera and three families including: Eucalliacidae(Andamancalliax sp), Eucalliacidae(Caviallianassa sp), Callianassidae , Gourretia qeshmensis Sepahvand, Rastegar-Pouyani and Momtazi, 2016 , Aqaballianassa ehsani Sepahvand, Tudge and Momtazi, 2018). With these new records, 27 species of these shrimps are now known in the Persian Gulf fauna.

Keywords: *Persian Gulf Explorer, Ghost shrimps, Macroinvertebrates, Biodiversity*

1. Introduction

The substrate of Persian Gulf and Gulf of Oman is composed of different habitats, such as sandy-mud, muddy, sandy, rocky and muddy-sand dominated by mollusk shells and fragments. These diverse habitats provide suitable environment for a wide variety of burrowing organisms, especially mud shrimps.

The Persian Gulf benthic ghost shrimps (mud shrimps) fauna is still poorly understood, but efforts to improve knowledge of its taxonomic composition and zoogeographic affinities have met with significant success (Sepahvand *et al.,* 2013, Sepahvand & Tudge 2019).

The first comprehensive study on burrowing shrimps of the Persian Gulf and Gulf of Oman was carried out by Sepahvand *et al.*, (2013) which documented 13 species in this group of cryptic decapods. Sakai (2002; 2005) and Dworschak (2009) reported species of burrowing shrimps from the Persian Gulf but recently Sepahvand *et al.,* (2015; 2016; 2018a, b) have identified more species, using molecular and morphological approaches.

2. Material and methods

The Persian Gulf Explorer (1901) was down in 45 stations in transects parallel to coastal line during April-May 2019. Sampling was done by box corer from soft substrate in the Persian Gulf Explorer Cruise. Three subsamples were studied. All biological samples were washed over a 500 µm sieve and sorted under a stereomicroscope. Extracted fauna was

transferred to 70% ethanol and identified. Thalassinidean shrimps were subsequently accessioned at the Iranian National Institute for Oceanography Collection (INIOC).

3. Results

The species reported herein are currently classified as follows:

Infraorder Axiidea

Family Callianassidae Dana, 1852

Genus *Aqaballianassa* Poore, Dworschak, Robles, Mantelatto & Felder, 2019

Aqaballianassa ehsani (Sepahvand, Tudge and Momtazi, 2018)

Material: Gulf of Oman, Iran, Station T10S2, Latitude: 25.2237454, Longitude: 59.1107001, Depth: 150m.

Remarks : The material of the present study is well agree with previous description of *Aqaballianassa ehsani* . In the present study *A. ehsani* was found in the subtidal waters of the Gulf of Oman. However Sepahvand et al 2018, reported this species from the intertidal waters.

Genus *Caviallianassa* Poore, Dworschak, Robles, Mantelatto & Felder, 2019

Caviallianassa sp Fig1. E-H

Material**:** Persian Gulf, Iran, Station T5S4, Latitude: 25.5747848, Longitude: 53.7012269, Depth: 38m.

Remarks: The present specimens from the Persian Gulf agree well with Komai & Fujiwara 2012 description except for the large chelipeds and maxiliped3. This is a first report of Caviallianassa genus from the northwestern in the Indian Ocean and also third species of this genus around the world.

Family Ctenochelidae Manning & Felder, 1991

Genus *Gourretia* de Saint Laurent, 1973

Gourretia qeshmensis Sepahvand, Rastegar-Pouyani and Momtazi, 2016

Material**:** Strait of Hormuz**,** Persian Gulf, Iran, Station: T7S3, Latitude: 26.8461569, Longitude: 56.4408207, Depth: 56m.

Remarks:

This species was reported by Sepahvand *et al.,* 2016, from strait of Hurmuz , Persian Gulf and the specimens in the present study agree well with Sepahvand's *et al.,* 2016 drawings except for the number of spines on the Ischium of large chelipeds.

Family Eucalliacinae Manning & Felder, 1991

Genus *Andamancalliax* Sakai, 2011

Andamancalliax sp Fig 1. A-D

Material**:** Persian Gulf, Iran, Station T5S4, Latitude: 25.5747848, Longitude: 53.7012269, Depth: 38m.

Remarks:

The *Andamancalliax* was established by Sakai (2011) and Poore *et al*., (2019) recognize and confirmed it. The specimens of the present study with the following character states strongly assign to the *Andamancalliax* genus: maxilliped 3 ischium and merus narrow, more than twice as long as wide at their articulation; ischium with strong proximal lobe on lower margin, wider proximally than distally. Major cheliped broad, minor cheliped narrower, with long fingers. *Andamancalliax* sp is the first member of *Andamancalliax* described from Iranian subtidal waters and can be differentiated by a large cheliped with a ventro-proximal spine on the merus. Also the specimens of the present study recorded the second species of *Andamncalliax* genus around the world.

4. Discussion and conclusion

The present study shows that ghost shrimps are associated with different habitat types and were found only in five out of 50 stations. Despite several attempts, no mud shrimps were found along the entire coast and continental shelf and subtidal waters of the northeast Persian Gulf (including Khuzestan and the eastern part of Bushehr Provinces) possibly due to the degraded nature of the habitat including dominance of very soft sediments, higher salinity or pollution. For the pollution, several studies revealed that the heavy metal concentrations in the northern Persian Gulf including Bushehr and Khuzestan Provinces are higher than that of other regions of Persian Gulf (see Diagomanolin et al., 2004; Pourang et al., 2005; Karbasi et al., 2005; Dehghan-Madiseh et al., 2009; Kazemi et al., 2011). This is mainly due to oil pollution and other anthropogenic impacts.

Figure 1. *Andamancalliax*, A-D, A: large cheliped inner view. B: small cheliped outer View. C: telson and uropod, dorsal view. D: maxiliped 3 outer view. *Caviallianassa*, E-H, E: large cheliped outer view. F: ischium-merus of large cheliped, G: small cheliped outer view., H: telson dorsal view. Scale bar: 1mm

References:

1. Manning, R.B., and Felder, D.L. 1991. Revision of the American Callianassidae (Crustacea: Decapoda: Thalassinidea). Proceedings of the Biological Society of Washington 104: 764– 792.

2. Poore, G. C. B., Dworschak, P. C., Robles, R., Mantelatto, F. L. and Felder, D. L. (2019). A new classification of Callianassidae and related families (Crustacea: Decapoda: Axiidea) derived from a molecular phylogeny with morphological support. *Memoirs of Museum Victoria*, 78, 73–146.

3. Sepahvand, V., Sari, A., Salehi, H., Nabavi, S. M. B. and Ghorbanzadeh, S. G. (2013). Littoral mud shrimps (Decapoda: Gebiidea & Axiidea) of the Persian Gulf and Gulf of Oman, Iran. *Journal of the Marine Biological Association of the United Kingdom,* 93 (4), 999–1008.

4. Saint Laurent, M. de 1973. Sur la systématique et la phylogénie des Thalassinidea: définition des familles des Callianassidae et des Upogebiidae et diagnose de cinq genres nouveaux. *Comptes Rendus Hebdomadaires de Séances de l'Académie des Sciences, Paris*. 277, 513–516.

2nd International Conference on Oceanography for West Asia

16 , 17 Sept. 2020 Iran. Tehran

Assessment and Source Identification of parent and mono-methylated PAH pollution in the sediments of Chabahar Bay

Seyed Hashtroudi, Mehri [1]*; Mehdinia, Ali [1]; Aghadadashi, Vahid [1]; Sheijooni Fumani, Neda [1]

1. Ocean Sciences Department, Iranian National Institute for Oceanography and Atmospheric Science

* hashroudi@inio.ac.ir

Keywords: *PAHs, Sediment, Chabahar Bay, Diagnostic ratio*

1. Introduction

Identification and measurement of Polycyclic Aromatic Hydrocarbons (PAHs) which are one of the main groups of persistent organic pollutants (POPs) have been of great interest in the last 40 years. They can be originated from both anthrapogenic and natural sources. According to their high hydrophilicity, PAHs tends to be deposited on bottom sediments (shilla *et al.*, 2019). The negative impact of PAHs on the health of aquatic life and humans and their potential carcinogenicity has been well documented (Duben 2010, Balcıoğlu, 2016). Generally, the 16 approved EPA priority parent PAHs have been measured by now, mostly because of their easier commercial availibiliy, but in the recent years the topic of the correct analysis of alkyl PAHs has also received increasing attention for some reasons including mounting evidence that their toxic potential may easily surpass that of the parent compounds. Chabahar Bay with its crenulated shape is the largest bay in bordering Oman Sea and is located in the south east of Iran. Since Chabahar is the closest and best access point of Iran to the Indian Ocean, it is the focal point for development of the eastern part of the country through economical and industrial activities. All these activities make the Bay prone to increase of different pollution including PAH pollution. In continuation of our previous study (Seyed Hashtroudi & Aghadadashi, 2018), we report here the current state of the Chabahar Gulf in terms of pollution to16 PAH compounds and their 6 mono-methylated derivatives along with their source identification.

2. Materials and methods

A total of 21 stations were selected for our study including 16 stations in the coastal area, 3 stations in the Bay entrance and 3 stations in the middle portion of the Bay. Table 1. shows the geographical coordinates of sampling sites.

Table 1. Coordinates of sampling sites

Station	X	Y	Station	X	Y	Station	X	Y
1	60.6063	25.3963	8	60.6038	25.2699	15	60.4335	25.4153
2	60.6028	25.3566	9	60.4902	25.4377	16	60.4604	25.3987
3	60.6105	25.3127	10	60.4909	25.4241	17	60.4047	25.3709
4	60.5431	25.4192	11	60.5085	25.3811	18	60.437	25.3671
5	60.5835	25.3933	12	60.523	25.3391	19	60.464	25.3311
6	60.5859	25.342	13	60.5383	25.2975	20	60.484	25.3016
7	60.594	25.3098	14	60.5528	25.2623	21	60.4941	25.2671

The sampling was performed in triplicate using a van veen grab sampler in Nov. 2016 and the (0-5 cm) sediments were collected in pre-cleaned aluminum containers and kept in freezer. The deep frozen sediments were dried using a benchtop freezedryer (OPERON, Korea). The triplicate samples in each station were mixed, homogenized and sieved through 250 µm sieve and 21 subsamples were obtained. Extraction of the PAHs from sediments was done according to MOOPAM guidelines (MOOPAM, 1999). Briefly, 4g of the sediment was spiked with proper amount of surrogate standards (i.e naphthalene-*d8*, antherancene-*d10*, chrysene-*d12* and perylene-*d12)* and the extractions were performed using a laboratory microwave oven (Ethos 1, Milestone, Italy) with a mixture of *n*-hexane-acetone (1:1, v/v) as the extraction solvent in 150 °C for 20 min. The silica gel-alumina cleanup method was applied to the extracts and the final extracts were treated with acid-activated copper to remove elemental sulfur, avoiding sulfur interference in GC-MS. The analysis of the samples was performed by an Agilent Gas chromatography-mass spectrometry system (GC–MS), model 6890N GC equipped with a 5973 mass detector while adding p-terphenyl-*d14* as the injection standard just prior to injection. 16 parent PAH from naphthalene to Indeno(1,2,3,cd)pyrene and 6 methyl-PAHs including 1-methyl naphthalene, 2-methyl naphthalene, 1-methyl phenanthrene, 2-methyl phenanthrene, 3-methyl phenanthrene and 9-methyl phenanthrene were measured.

3. Results and discussion

The stations were selected to show an estimate of the overall pollution status of the study area. Figure 1 shows the obtained amount of PAHs in each stations in terms of parent PAHs (16 EPA PAHs) and 6 methylated PAHs. The concentration of total PAHs ranges from 7.8 to 273.5 ng/g with an average of 102.9 ng/g. The estimation shows that the PAHs with methyl derivatives make up about 25% of the total PAH concentrations which were frequently ignored by now in spite of their importance. As it could be seen, station 21, 16, 12, 14 and 8 are the most polluted stations, respectively and the least polluted stations are stations 6, 10 and 18. Station 21, 14 and 8 are located in the entrance of the bay and station 12 in the middle portion of the Bay. Taking all the finding into consideration and compared to our previous report in 2006, it seems that the Chabahar Bay is still low to moderate polluted (Baumard *et al.*, 1998). The Bay status is healthier than Busher which is in the pollution category of medium to high (Aghadadashi *et al.*, 2016) or Jinhae Bay in Korea which is low to high polluted (Yim et al., 2014).

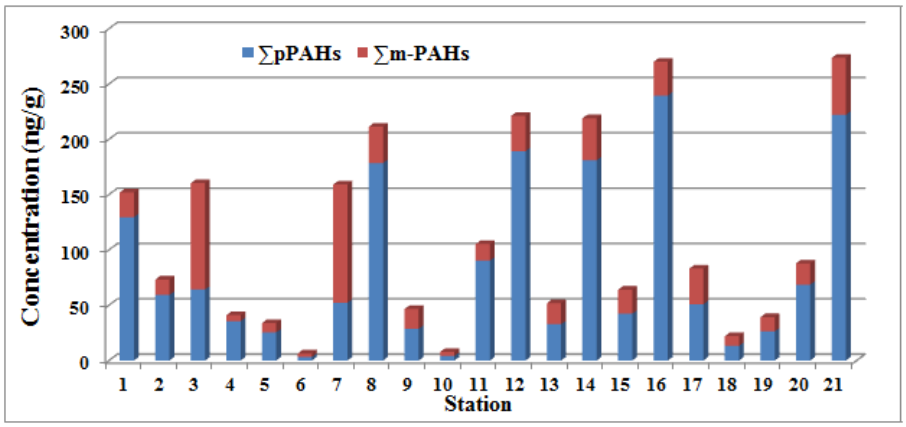

Fig. 1 A comparison of total parent PAHs (Σp-PAHs) and methylated PAHs (Σm-PAH)

Fig. 2 shows the abundance of each PAH in the whole studied area. It seems that low molecular weight (LMW) PAHs are dominant in the whole region. Naphthalen and its methyl derivatives, phenantherene and fluoranthene have the highest measured values.

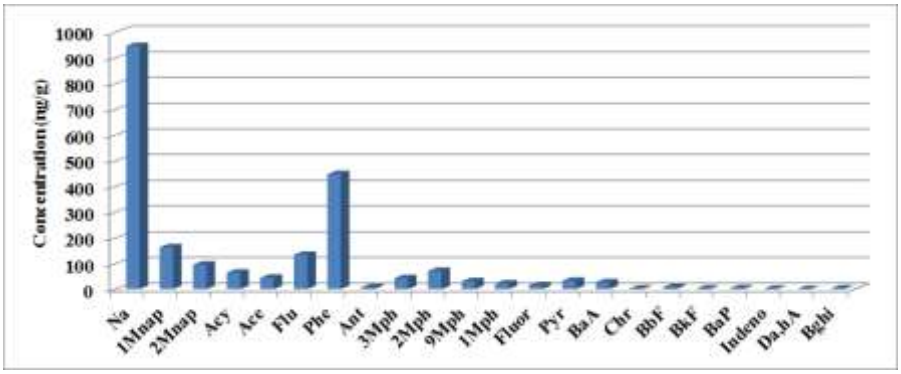

Fig. 2 Total Concentration of each PAH in the sampling location

The main emission sources of PAHs are combustion processes or spills of crude oil or its products. There are different diagnostic ratios of selected hydrocarbons which can suggest the source of PAH emission and propose the possible transport pathway prior to their final deposition in sediments. The origin of PAHs may also affect their ageing in the sediment, which in consequence may alter their mobility. So, it seems important to know the origin of PAH compounds. Estimation of some some ratio such as Phenanthrene/anthracene, Fluoranthene/Pyrene and low molecular weight/high molecular weight (LMW/HMW) shows that the PAHs in the Chabahar Bay mainly originate from the direct seepage of crude oil.

In conclusion, due to approval of the strategic plan for the development of Makran region, a regular and continuous monitoring of pollution including PAHs in the region provides the required valid information for the policy maker to set guidelines to achieve a sustainable and environmentally friendly development of the region.

References:

1. Andersson, J.T. and Achten, C., 2015. Time to say goodbye to the 16 EPA PAHs? Toward an up-to-date use of PACs for environmental purposes. *Polycyclic Aromatic Compounds*, *35*(2-4), pp.330-354., *35*(2-4), 330-354.

2. Balcıoğlu, E.B., 2016. Potential effects of polycyclic aromatic hydrocarbons (PAHs) in marine foods on human health: a critical review. *Toxin Reviews*, *35*(3-4), pp.98-105.

3. Baumard, P., Budzinski, H., Garrigues, P.H., Sorbe, J.C., Burgeot, T. and Bellocq, J., 1998. Concentrations of PAHs (polycyclic aromatic hydrocarbons) in various marine organisms in relation to those in sediments and to trophic level. *Marine pollution bulletin*, *36*(12), pp.951-960.

4. Douben, P.E. ed., 2003. *PAHs: an ecotoxicological perspective*. John Wiley & Sons.

5. Moopam, A., 2012. Manual of oceanographic observation and pollution analysis. regional or-ganization for the protection of Marine Environment (ROPME), Kuwait.

6. Seyed Hashtroudi, M. and Aghadadashi, V., 2018. Sediment-associated polycyclic aromatic hydrocarbons and potential eco-hazards in Chabahar Bay, Iran. *Marine pollution bulletin*, *129*(2), pp.875-883.

7. Shilla, D., Pajala, G., Routh, J., Dario, M. and Kristoffersson, P., 2019. Trophodynamics and biomagnification of trace metals in aquatic food webs: The case of Rufiji estuary in Tanzania. *Applied geochemistry*, *100*, pp.160-168.

8. Yim, U.H., Hong, S.H., Ha, S.Y., Han, G.M., An, J.G., Kim, N.S., Lim, D.I., Choi, H.W. and Shim, W.J., 2014. Source-and region-specific distribution of polycyclic aromatic hydrocarbons in sediments from Jinhae Bay, Korea. Science of the total environment, 470, pp.1485-1493.

2nd International Conference on Oceanography for West Asia

16 , 17 Sept. 2020 Iran. Tehran

Wave Characteristics in the Northern Coasts of Persian Gulf

Shafieefar, Mehdi [1]; Rezaee Mazyak, Ahmad [2]; Khosravi, Mohammadreza [2*]

1. Civil Engineering Faculty, Tarbiat Modares University
2. Ports and Marine Structures Department, Pars Geometry Consultants

Keywords: *ECMWF, Wave characteristics, Persian Gulf*

1. Introduction

The results of global models as a source of data can be used to simulate local waves in coastal areas. Before applying these models, their results should be compared with the measurement data in the study area. One of the most important global models is the ECMWF model. Khosravi et al evaluated the quality of the results of this model in the Makran coast area [1]. Wave simulations have been carried out on the shores of Bushehr province as part of Mapna desalination plant project. In this project, the characteristics of the waves were measured in the study area for 2 months. In this paper, after evaluating the ECMWF model results with the measured data and assuring its quality, the local wave simulation is performed using the ECMWF global model results as the model boundary.

Study Area

The current study area is located in the east of Boushehr Bay which is in the northern coasts of Persian Gulf.

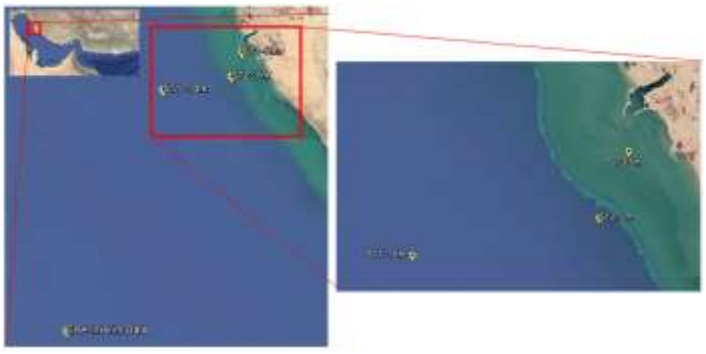

Figure1. Study area and measurement stations

2. Materials and methods

The characteristics of waves were measured in MAPNA seawater desalination project. The distance from each station to the coast and the measurement period are presented in Table 1. In addition, the location of the stations is shown in Figure 1. As seen in Figure 2, the maximum wave height at stations 1, 2 and 3 is 2, 1.3 and 1.8 m, respectively. Also, the average peak wave period at these stations is 3.5 seconds and the dominant direction is northwest (300 degrees).

Table1. Characteristics of measurement stations

Station No.	Depth (m.CD)	Distance from Coast (Km)	Date
1	10	5	03/18/2019-05/11/2019
2	7	2	05/14/2019-06/22/2019
3	5	0.85	03/18/2019-06/22/2019

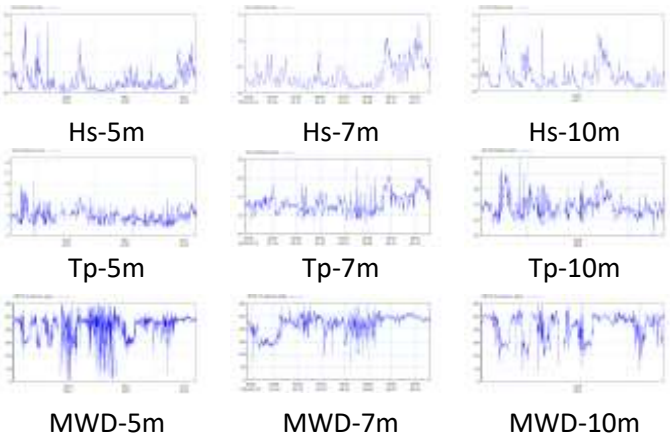

Figure2. Wave characteristics at measurement station

The European Centre for Medium-Range Weather Forecasts (ECMWF) operates one of the largest supercomputer complexes in Europe and the world's largest archive of numerical weather prediction data. ERA-Interim is a reanalysis of the global atmosphere covering the data-rich period since 1979 and continuing in real time. As ERA-Interim continues forward in time, updates of the archive will take place on a monthly basis [2].

Due to the lack of up-to-date data on the northern coasts of the Persian Gulf, using ECMWF results as boundary data in local models can be helpful. Accordingly, the quality of these data on the northern coast of the Persian Gulf has been evaluated with measurement data at station1.The correlation coefficient indicates that the oscillations of the waves are well simulated. The BIAS parameter, which is approximately 0.12 m, indicates that the difference between the model results and the measurement data is not high, but is overestimate. The RMSE parameter shows the spreading of the model result in comparison with measured data is about 30 percent. The comparison between measured data and ERA-Interim results shows in Figure 3.

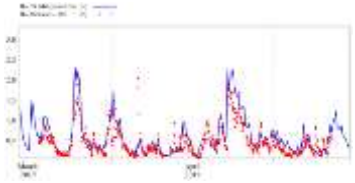
(Significant wave height)

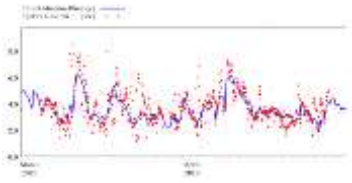
(Peak wave period)

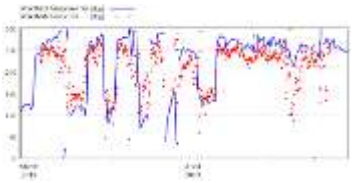
(Mean wave direction)

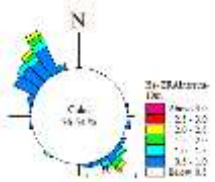

(wave rose-ERA-Interim)

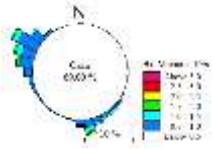

(wave rose- Measure)

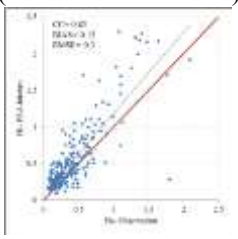
(Scatter plot)

Figure3. Evaluating of ERA-Interim model

Model Setup

Calculating the significant wave height with different return periods is one of the most important steps in designing a seawater desalination plant. Hence the simulation of the waves has been carried out in the MAPNA desalination project. In the first step, the results of the ERA-Interim model were used as boundaries. Secondly, the computational grid and effective parameters for simulating waves such as White Capping, Bottom Friction, and Wave breaking were determined. Accordingly, the mesh grid was defined by 1214 nodes and 2060 elements. Also, the values considered for the parameters are given in Table 2.

Table2. Calibration Parameters

Parameter	Value
White Capping	Dissipation Coefficient, Cdis = 4.5 Dissipation Coefficient, Delta= 0.5
Bottom Friction	Nikuradse Roughness, k_n= 0.002
Wave Breaking	Gamma Data= 0.8

Comparison of model results with measurement data at stations 2 and 3 shows that the modeling performed by using ECMWF data as boundaries is of good quality. The results of the model are slightly overestimated; however the wave oscillations are well simulated. The RMSE parameter at both stations is about 0.25, indicating that the dispersion of the modeling results is about 25% compared to the measurement data. Also, the difference between the average of the model results and the average of the measured data is approximately 0.15 m.

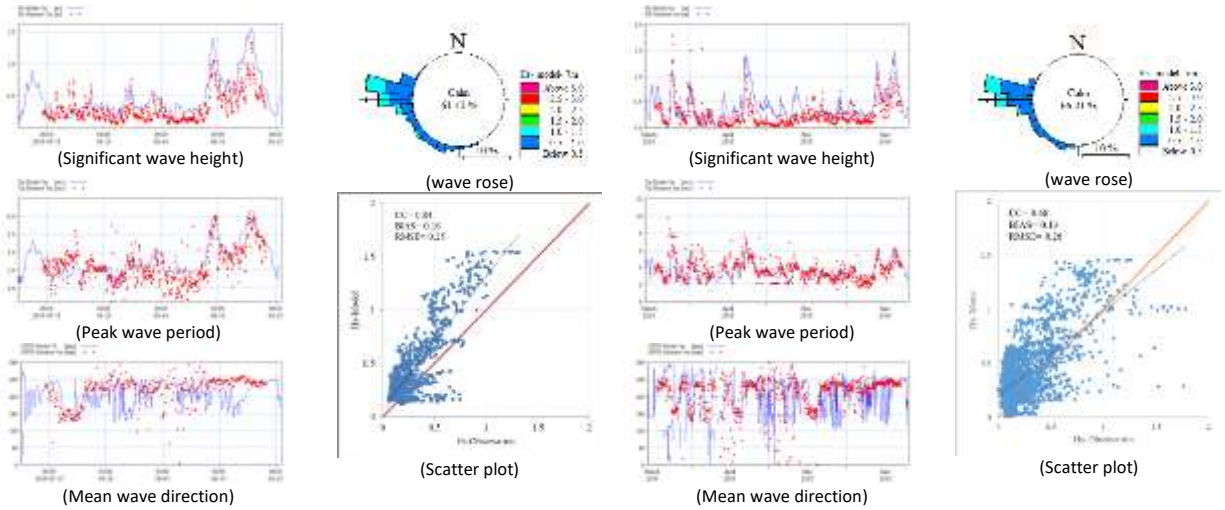

Figure4. Result of model at station 2 and 3

3. Conclusion

Due to the lack of up-to-date data on the Iranian coasts of the Persian Gulf, the results of the ECMWF model have been evaluated in this area. First of all, the measured data at a distance of 5 km from the coast are evaluated with the results of the model and after assuring the quality of the data the simulation is done. Based on the modeling results, it can be said that the ECMWF model results are of good quality for use in local modeling in the northern coasts of the Persian Gulf.

References

1. Mohammadreza Khosravi, Mohammad Bagheri, Mohammadhosein Nemati, Mehdi Shafieefar, Aghil Hajmomeni, Ahmad Rezaee Mazyak, “The Wind-Wave Climate of the Makran Coastlines(A: appraising of ERA-Interim results),”First International Conference on oceanography for West Asia, Tehran, Iran, 2017.

2. Paul Berrisford, The ERA-Interim Archive, European Centre for Medium Range Weather Forecasts, United Kingdom, 2011.

2nd International Conference on Oceanography for West Asia

16 , 17 Sept. 2020 Iran. Tehran

Extraction of coastlines from satellite images using sub-pixel algorithms Case study: Parts of Hormozgan coast

Tilkoo, Alireza [1]; Siadatmousavi, Seyed Mostafa [2] ; Mojaradi Barat [3]

1. Civil Engineering Department, Shahrood University of Technology, alirezatilkoo@gmail.com
2. Civil Engineering Department, Iran University of Science and Technology, Siadatmousavi@iust.ac.ir
3. Civil Engineering Department, Iran University of Science and Technology, mojaradi@iust.ac.ir

Abstract

Coastal environments are always under the pressure of natural processes such as erosion, sedimentation, natural disasters as well as human projects. These threats have made coastal areas a priority for coastline monitoring and sustainable coastal management programs. In this paper, algorithms for separating water and land boundaries as well as new sub-pixel methods are presented with the aim of dividing large pixels (with low resolution and spatial accuracy) into smaller pixels and creating a classified map with better spatial resolution. Different water identification indices and machine learning algorithms were investigated, and two models of Spatial Attraction Models were implemented. Results showed that the Sub-pixel / Sub-pixel Spatial Attraction Model had more capacity in providing higher resolution and precision, while provided 10% reduction in error when compared with observations. To skill assess these two methods, the difference in areas created by each method compared to the reference shoreline (high resolution aerial image) was computed. Also, in order to accurately evaluate and show the high accuracy of sub-pixel algorithms, the results of these algorithms should be examined by conventional classification methods. The creation of such models is proposed to support integrated coastal management in the Persian Gulf region for future studies.

Keywords *subpixel algorithms, shoreline, spatial attraction model, machine learning algorithms*

1. Introduction

Coastal areas are critical and very complex environments; thus, various geophysical parameters must be continuously monitored. Nowadays, the use of spectral indices has gained more attention because they are considered as less restrictive and more reproducible methods, particularly for applications on a broad or global scales (Aires et al., 2017; Pekel, Cottam, Gorelick, & Belward, 2016). A variety of spectral indices have been developed recently to track surface water areas using satellite imagery (Jones, 2015; Lefebvre et al., 2019; McFeeters, 1996).

Due to the advances in remote sensing science and GIS, integrated techniques have been proposed to extract coastlines with different resolutions. In general, super resolution methods, first introduced by Atkinson in 1997(Atkinson, 1997), produce sub-pixel-level classification maps. Such algorithms are based on the spatial dependence within adjacent pixels (Sánchez-García, Balaguer-Beser, Almonacid-Caballer, & Pardo-Pascual, 2019; Xiong et al., 2018).

The nature of the real landscape and the process of obtaining information is complex because many mixed pixels exist in remote sensing images, which leads to difficulties in image inspection as well as its use (Nguyen, Atkinson, & Lewis, 2005). Assigning mixed pixels to a single class would result in loss of some information, which is not appropriate. Soft classifications estimate the proportion of each class within mixed pixels; these methods includes the fuzzy c-means classifier (Dewi & Bijker, 2019), decision tree (Poortinga et al., 2019), random forest (Zhou, Liu, & Zhang, 2019), and support vector machine (Elnabwy et al., 2020; Navale & Haldar, 2019). However, machine learning algorithms

fails to identify the location of these classes in each pixel. Therefore, sub-pixel mapping or sub-pixel placement has been proposed as a way to remedy this problem (Wang, Zhang, Hao, & Wang, 2019).

These methods reduce the potential errors of spectral mixing. Generally Speaking, Spatial Attraction Models solve an inverse, illpossessed problem, because minimal image information is not sufficient to achieve the spatial distribution of groups on a subpixel scale (Song, Zhong, Ma, & Feng, 2019; Wang, Zhang, Zhang, et al., 2019). Spatial algorithms were introduced by creating functions between subpixels and pixels based on the theory of spatial dependence. In the SPSAM[1] model, attraction occurs between sub-pixels of the central pixel and eight adjacent pixels, but in the SSSAM[2] model, this occurs for sub-pixels and adjacent sub-pixels.(P. Wang & Wang, 2017; Q. Wang, Wang, & Liu, 2012). In this paper, the water spectral index and soft classifier were used along with spatial attraction models. A detailed description of spatial attraction algorithms is provided in Section 2.

2. Materials and methods

The images used in this study are Landsat satellite images with a spatial resolution of 30 meters. Initially, the spatial resolution of images are increased to 15 meters using one of the methods of combining satellite images with the panchromatic band of Landsat multispectral images. Combining images at the pixel level is the most common level of image integration and is used to improve image quality for visual interpretation. GS[3] algorithm has been used to increase spatial resolution. Then, to reduce amount of the post calculations in MATLAB software processing, a smaller portion of the images were selected.

[1] Subpixel/Pixel Spatial Attraction Model
[2] Subpixel/Subpixel Spatial Attraction Model
[3] Gram-Schmidt spectral sharpening

The Modified Normalized Difference Water Index (MNDWI) spectral index was used to extract coastlines. Land cover ratios must be determined by one of the soft classification methods. The support vector machine (SVM) classification method was employed which is a supervised learning system based on recent advancements in statistical learning theory. SVM was developed for binary classification. A number of studies have focused on the mathematical relationships for SVMs. It requires a dataset for training phase. In this study, according to the purpose of extracting the coastline, the selection of two training areas (ROI) is sufficient. Spatial attraction algorithms are applied to these areas. In the following, each of these two algorithms is presented briefly.

2.1 SPSAM Classification

In a subpixel/spatial attraction model (SPSAM), the attraction between each subpixel in pixels of coarse resolution and its neighboring pixels is calculated to determine the subpixel spatial distribution of each class (Q. Wang et al., 2012). Assumptions of this approach is as follows: the model acts on the basis of fraction values in neighboring pixels relative to subpixels in a central pixel. A subpixel can only be attractted by pixels around the center pixel (which includes the subpixel); as a result, the maximum of eight neighboring pixels can be considered for attraction, and the rest of pixels are too far to be attracted (Mertens, De Baets, Verbeke, & De Wulf, 2006). The formulas of this method are:

$$SD_{cf} = \sum_{k=1}^{N_A} \omega_k F_c(P_k) \qquad (1)$$

$$D_{c.ij} = \sum_{k=1}^{N_A} \omega_k F_c(P_k) = \sum_{k=1}^{N_A} \frac{F_c(P_k)}{d_k} \qquad (2)$$

where SD_{cf} is the measure of spatial dependence of class c to subpixel pf, N_A is the number of neighboring pixels, ω_k is the weight of spatial dependence, $F_c(P_k)$ is the proportion of the kth neighbor pixel P_k to class c, and d_k is the Euclidean distance between geometric centers of subpixel p_{ij} and its neighbor pixel P_k.

2.2 SSSAM Classification

In the SPSAM method, the subpixels of each neighbor of the central pixel were considered to be the central points of the neighboring pixel. Then the spatial attraction for the class c is calculated for the subpixel p_{ij} from each neighboring pixel as the attractor between the p_{ij} center and its neighbor center. Clearly, this description of attraction is not always correct because the subpixels of the internal pixel may not be entirely close to the central point. Instead, they may be located at a corner or near to a boundary of that pixel so that each pixel cannot be considered as a point (Q. Wang et al., 2012). In SSSAM method, the spatial attraction of each neighboring pixel is the sum of the attraction between the center p_{ij} and the center of each subpixel in the neighboring pixel. Suppose p_m is a subpixel within P_k, and d_m is the Euclidean distance between geometric centers of subpixels p_{ij} and p_m; then the SD_{cf} can be calculated as (L. Wang, Wang, & Liu, 2011) :

$$SD_{cf} = \sum_{k=1}^{N_A} \omega_k F_c(P_k) = \sum_{k=1}^{N_A} \omega_k \frac{F_c(P_k)S^2}{S^2} = \frac{1}{S^2} \sum_{m=1}^{N_A S^2} \omega_k x_{cm} = \frac{1}{S^2} \sum_{m=1}^{N_A S^2} \frac{x_{cm}}{d_m} \qquad (3)$$

Mixed pixel P_{ab} in the coarse low resolution image (i.e. fraction image) is selected. Attractions for subpixels within P_{ab} caused by each class from neighbors are calculated according to equation (3). The subpixels with the highest attraction values are allocated to the corresponding class. The flowchart of the research process is given in Figure 1.

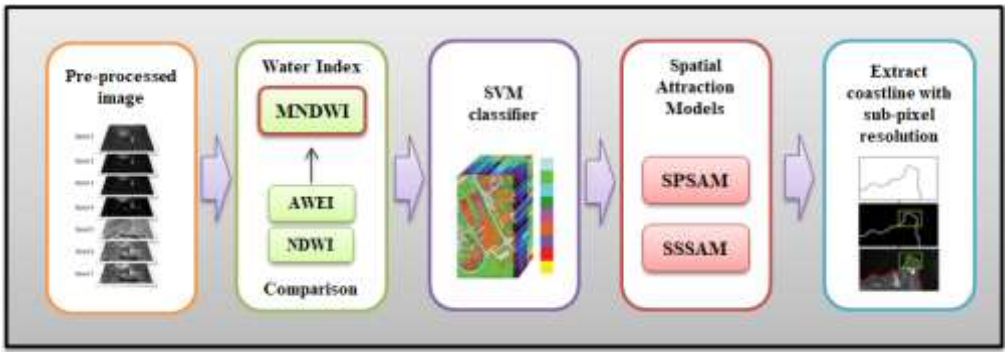

Figure 1. Flowchart of the proposed methodology for extraction coastlines

3. Results

In this research, three spatial subsets have been cut from Landsat satellite imagery from rocky areas of Hormozgan province close to Bonod and Tobon coasts. It should be noted that the choice of rocky parts of the coastal areas has been made to ignore tidal changes. To evaluate the accuracy of the methods in extracting the coastline, the difference between the areas created between the estimated coastline from each method and the reference coastline should be calculated. It is important to note that the drawing lines on the raster vector are hard to classify without smoothing, and the reference shoreline is drawn using aerial images with a pixel accuracy of 20 cm. It is clear that the method, which provides a smaller total area, has better accuracy in extracting coastlines. Due to the limited number of pages of the article, the results of one area are displayed (area 2). Figure 2 shows the three parts of area 2 with reference lines (aerial photographs) and the estimated coastline from each method.

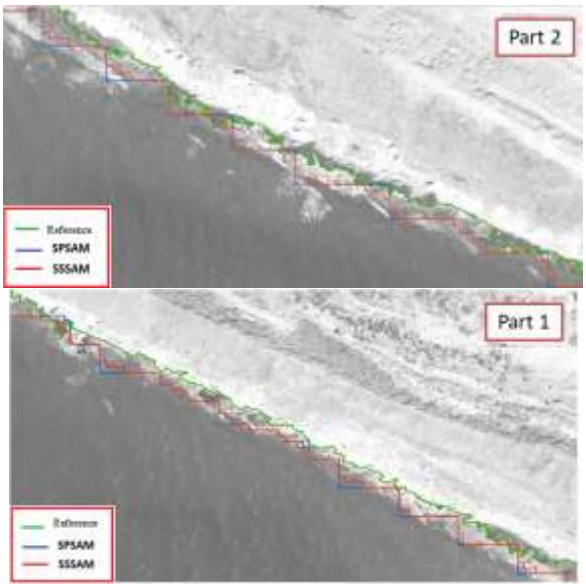

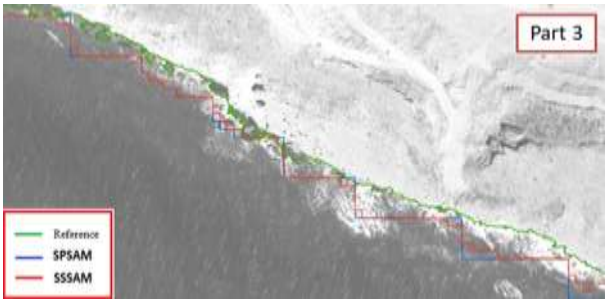

Figure 2. There are 3 parts of area 2 with a rocky part and close to the coasts of Bonoud, The colors are green, blue, and red, respectively, for the shoreline, the reference extracted from the aerial image, and the output of the SPSAM and SSSAM methods.

4. Discussion and conclusion

According to the error index for 3 study areas, the SSSAM method outperformed SPSAM method. The SPSAM method makes more mistakes due to the fact that it considers only the central values of the adjacent pixels and ignores the values of the corners. In contrast, in SSSAM method, these values are considered. The total area difference of the SSSAM method is less than the SPSAM method (Table 1). From the ratio of the obtained areas, the reduction of the error of the second method can be estimated as ~10%.

Table 1: Differences in areas for each method and the reference shoreline (area 2)

Methods	Total areas (m^2)
SPSAM	5577.29
SSSAM	5189.57

It should be noted that better results occurred when appropriate water spectral index and better classifier were used. In the latest research on the extraction of water bodies and between types of spectral indices, the combination of SVM classification with MNDWI index has achieved the best results among related techniques with desirable spatial and spectral quality. For this reason, this technique was used in this study. Table 2 shows the comparison between the Support Vector Machine (SVM) with the results of two sub-pixel algorithms on area 3.

Table 2: Comparison between methods on area 3

Methods	Total areas (m^2)
SPSAM	3386.29
SSSAM	3593.67
Support Vector Machine	4471.62

References

1. Aires, F., Miolane, L., Prigent, C., Pham, B., Fluet-Chouinard, E., Lehner, B., & Papa, F. (2017). A global dynamic long-term inundation extent dataset at high spatial resolution derived through downscaling of satellite observations. *Journal of Hydrometeorology, 18*(5), 1305-1325.

2. Atkinson, P. M. (1997). Mapping sub-pixel boundaries from remotely sensed images. *Innovations in GIS, 4*, 166-180.

3. Dewi, R. S., & Bijker, W. (2019). Dynamics of shoreline changes in the coastal region of Sayung, Indonesia. *The Egyptian Journal of Remote Sensing and Space Science*.

4. Elnabwy, M. T., Elbeltagi, E., El Banna, M. M., Elshikh, M. M., Motawa, I., & Kaloop, M. R. (2020). An Approach Based on Landsat Images for Shoreline Monitoring to Support Integrated Coastal Management—A Case Study, Ezbet Elborg, Nile Delta, Egypt. *ISPRS International Journal of Geo-Information, 9*(4), 199.

5. Jones, J. W. (2015). Efficient wetland surface water detection and monitoring via landsat: Comparison with in situ data from the everglades depth estimation network. *Remote sensing, 7*(9), 12503-12538.

6. Lefebvre, G., Davranche, A., Willm, L., Campagna, J., Redmond, L., Merle, C., . . . Poulin, B. (2019). Introducing WIW for detecting the presence of Water In Wetlands with Landsat and Sentinel satellites. *Remote sensing, 11*(19), 2210.

7. McFeeters, S. K. (1996). The use of the Normalized Difference Water Index (NDWI) in the delineation of open water features. *International Journal of Remote Sensing, 17*(7), 1425-1432.

8. Mertens, K. C., De Baets, B., Verbeke, L. P., & De Wulf, R. R. (2006). A sub-pixel mapping algorithm based on sub-pixel/pixel spatial attraction models. *International Journal of Remote Sensing, 27*(15), 3293-3310.

9. Navale, A., & Haldar, D. (2019). Evaluation of machine learning algorithms to Sentinel SAR data. *Spatial Information Research*, 1-11.

10. Nguyen, M. Q., Atkinson, P. M., & Lewis, H. G. (2005). Superresolution mapping using a Hopfield neural network with LIDAR data. *IEEE Geoscience and Remote Sensing Letters, 2*(3), 366-370.

11. Pekel, J.-F., Cottam, A., Gorelick, N., & Belward, A. S. (2016). High-resolution mapping of global surface water and its long-term changes. *Nature, 540*(7633), 418-422.

12. Poortinga, A., Tenneson, K., Shapiro, A., Nquyen, Q., San Aung, K., Chishtie, F., & Saah, D. (2019). Mapping plantations in Myanmar by fusing landsat-8, sentinel-2 and sentinel-1 data along with systematic error quantification. *Remote sensing, 11*(7), 831.

13. Sánchez-García, E., Balaguer-Beser, Á., Almonacid-Caballer, J., & Pardo-Pascual, J. E. (2019). A new adaptive image interpolation method to define the shoreline at sub-pixel level. *Remote sensing, 11*(16), 1880.

14. Song, M., Zhong, Y., Ma, A., & Feng, R. (2019). Multiobjective sparse subpixel mapping for remote sensing imagery. *IEEE Transactions on Geoscience and Remote Sensing, 57*(7), 4490-4508.

15. Wang, L., Wang, Q., & Liu, D. (2011). *Sub-pixel mapping based on sub-pixel to sub-pixel spatial attraction model.* Paper presented at the Geoscience and Remote Sensing Symposium (IGARSS), 2011 IEEE International.

16. Wang, P., & Wang, L. (2017). Soft-then-hard super-resolution mapping based on a spatial attraction model with multiscale sub-pixel shifted images. *International Journal of Remote Sensing, 38*(15), 4303-4326.

17. Wang, P., Zhang, G., Hao, S., & Wang, L. (2019). Improving remote sensing image super-resolution mapping based on the spatial attraction model by utilizing the pansharpening technique. *Remote sensing, 11*(3), 247.

18. Wang, P., Zhang, L., Zhang, G., Bi, H., Dalla Mura, M., & Chanussot, J. (2019). Superresolution land cover mapping based on pixel-, subpixel-, and superpixel-scale spatial dependence with pansharpening technique. *IEEE Journal of Selected Topics in Applied Earth Observations and Remote Sensing, 12*(10), 4082-4098.

19. Wang, Q., Wang, L., & Liu, D. (2012). Integration of spatial attractions between and within pixels for sub-pixel mapping. *Journal of Systems Engineering and Electronics, 23*(2), 293-303.

20. Xiong, L., Deng, R., Li, J., Liu, X., Qin, Y., Liang, Y., & Liu, Y. (2018). Subpixel surface water extraction (SSWE) using Landsat 8 OLI data. *Water, 10*(5), 653.

21. Zhou, X., Liu, X., & Zhang, Z. (2019). *Automatic Extraction of Lakes on the Qinghai-Tibet Plateau from Sentinel-1 SAR Images.* Paper presented at the 2019 SAR in Big Data Era (BIGSARDATA).

2nd International Conference on Oceanography for West Asia

16 , 17 Sept. 2020 Iran. Tehran

The effects of weaning strategies on survival and growth of yellowfin seabream larvae (*Acanthopagrus latus*)

Torfi Mozanzadeh, Mansour [1,2,3]; Nafisi Bahabadi, Mahmoud [2,3]; Morshedi, Vahid [3]; Agh, Naser [4]

1. South Iran Aquaculture Research Centre, Iranian Fisheries Science Institute (IFSRI), Agricultural Research Education and Extension organization (AREEO), Ahwaz, Iran

2. Department of Fisheries and Biology, Persian Gulf Research Institute, Persian Gulf University, Bushehr, Iran

3. Department of Fisheries and Aquaculture, Faculty of Marine Science and Technology, Persian Gulf University, Bushehr, Iran

4. Artemia and Aquatic Research Institute, Urmia University, Urmia, Iran

*Corresponding author: M.torfi@areeo.ac.ir; Mansour.torfi@gmail.com (Mansour Torfi Mozanzadeh)

Keywords: *Alkaline phosphatase, leucine-alanine peptidase, live food, Sparidae, stress resistance*

A 30-day trial was conducted to evaluate the effects of different weaning strategies on growth and survival of yellowfin seabream larvae (*Acanthopagrus latus*). Eight feeding strategies were carried out by applying different combinations of two sizes (75 and 150 µm) of a microdiet (MD) (Skretting® GemmaMicro®) and live food (LF) including super small type marine rotifer (*Brachionus rotundiformis*) and *Artemia* metanauplii in triplicate (Three tanks per each treatment) including (A): 100 LF: larvae fed only live food (100%) including rotifers and *Artemia* metanauplii from 2 to 30 dph; (B): 75LF-25MD: 25% of the amount of live food in 100LF treatment was replaced with MD from 2 to 30 dph; (C): 50LF-50MD: 50% of the amount of live food in 100LF treatment was replaced with MD from 2 to 30 dph; (D): 25LF-75MD: 75% of the amount of live food in 100LF treatment was replaced with MD from 2 to 30 dph; (E): 100 MD: larvae fed only on MD (100%) from 2 to 30 dph; (F): Sudden weaning: Co-feeding of MD with rotifers from 2 to 5 dph followed by feeding only with MD from 6 to 30 dph; (G): Early weaning: Co-feeding of MD with rotifers from 10 dph to 14 dph followed by feeding only with MD from 15 to 30 dph and (H): Late weaning: Co-feeding of MD with rotifers and *Artemia* metanaupli from 12 dph to 20 dph followed by feeding only with MD from 21 to 30 dph. The amount of supplied MD were fixed between 0.4 to 2.0 g $tank^{-1}$ day^{-1} from 2 to 30 dph according to the larval developmental stage. At the end of the trial larvae in E (10.5 ± 3.5) and F (16.9 ± 4.8) groups

had the least survival rate, but A (51.8 ± 10.7), B (54.7 ± 4.5) and C (56.2 ± 4.0) groups showed the greatest survival rate and the other treatments demonstrated intermediate values (Fig. 1). At the end of the trial 30 days post hatch (DPH), larvae from A, B, C and H had the greatest total length and wet weight values. Furthermore, gradual replacement of LF with MD over 50% in D and E groups reduced total length and wet weight in *A. latus* larvae. Moreover, application of sudden or early weaning strategies also remarkably compromised total length and wet weight of larvae compared to the late weaning strategy ($P < 0.05$). The results of the present study demonstrated that replacement of 50% of LF with MD and application of late weaning strategies did not compromise growth and survival in *A. latus* larvae.

United Nations
Educational, Scientific and
Cultural Organization

Intergovernmental
Oceanographic
Commission

RCOWA

2nd International Conference on
Oceanography for West Asia 2020

دومین کنفرانس بین المللی اقیانوس شناسی غرب آسیا

16 - 17 Sep. 2020 ۲۶ و ۲۷ شهریور ۱۳۹۹